

**Key Words:** Distribution  
Coefficient, Geochemistry,  
Performance Assessment,  
Solubility Concentration  
Limits, Special Analysis

**Retention: Permanent**

## **Geochemical Data Package for Performance Assessment Calculations Related to the Savannah River Site**

**Daniel I. Kaplan**

March 15, 2010

Savannah River National Laboratory  
Savannah River Nuclear Solutions  
Aiken, SC 29808

---

Prepared for the U.S. Department of Energy under  
contract number DE-AC09-08SR22470.



**DISCLAIMER**

This work was prepared under an agreement with and funded by the U.S. Government. Neither the U.S. Government or its employees, nor any of its contractors, subcontractors or their employees, makes any express or implied:

1. warranty or assumes any legal liability for the accuracy, completeness, or for the use or results of such use of any information, product, or process disclosed; or
2. representation that such use or results of such use would not infringe privately owned rights; or
3. endorsement or recommendation of any specifically identified commercial product, process, or service.

Any views and opinions of authors expressed in this work do not necessarily state or reflect those of the United States Government, or its contractors, or subcontractors.

**Printed in the United States of America**

**Prepared For  
U.S. Department of Energy**

**Key Words:** Special  
Analysis, Distribution  
Coefficient, Performance  
Assessment, Geochemistry,  
Solubility Concentration  
Limits

**Retention: Permanent**

## **Geochemical Data Package for Performance Assessment Calculations Related to the Savannah River Site**

**Daniel I. Kaplan**

March 15, 2010

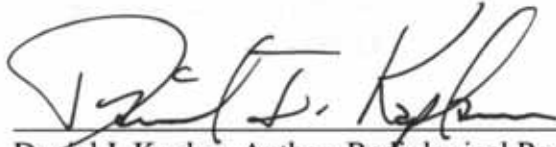
Savannah River National Laboratory  
Savannah River Nuclear Solutions  
Aiken, SC 29808

---

Prepared for the U.S. Department of Energy under  
contract number DE-AC09-08SR22470.



## REVIEWS AND APPROVALS




---

 Daniel I. Kaplan, Author, Radiological Performance Assessment

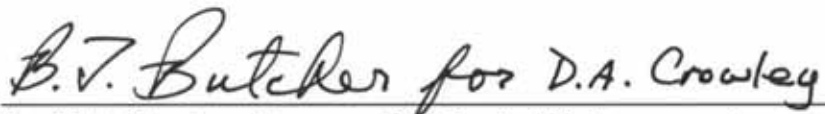
 3/24/2010  
 Date




---

 Kimberly P. Crapse, Design Check, Separation Science Programs

 3/24/2010  
 Date




---

 David A. Crowley, Manager, Radiological Performance Assessment

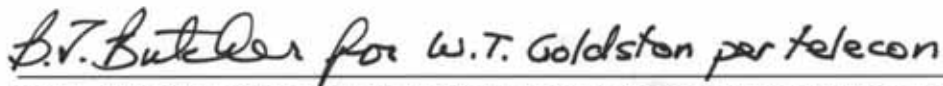
 3/24/2010  
 Date




---

 Sharon L. Marra, Manager, E&CPT Research Programs

 3/24/10  
 Date




---

 W. T. Goldston, Customer, Regulatory Integration and Business Management

 3/24/2010  
 Date


## Table of Contents

1.0	Executive Summary .....	14
2.0	Objective and Scope .....	16
3.0	Philosophy and Assumptions.....	17
3.1	Theoretical Distribution Coefficients, Empirical Distribution Coefficients, and their Relation to Retardation Factors .....	17
3.2	Solubility Constraints.....	21
3.3	Overview of Mechanistic Complexation Models .....	23
3.4	Unique Conditions Resulting in Enhanced Contaminant Transport of Radionuclides. 25	
3.4.1	Cellulose Degradation Products .....	25
3.4.2	Colloid-Facilitated Transport of Contaminants .....	27
4.0	Conceptual Geochemical Model.....	29
4.1	Sediments.....	31
4.1.1	Clayey Sediment Environment .....	32
4.1.2	Sandy Sediment Environment .....	34
4.1.3	Cellulose-Degradation-Product (CDP) Impacted Clayey Sediment, Environment.. 34	
4.1.4	CDP-Impacted Sandy Sediment Environment .....	39
4.2	Cementitious Materials .....	39
4.2.1	Young Cementitious Solids (1 <sup>st</sup> Stage) Environment.....	40
4.2.2	Moderately-aged Cementitious Solids (2 <sup>nd</sup> Stage) Environment.....	41
4.2.3	Aged Cementitious Solids (3 <sup>rd</sup> Stage) Environment.....	42
4.2.4	Cementitious Leachate Impacted Clayey Sediment Environment .....	42
4.2.5	Cementitious Leachate Impacted Sandy Sediment Environment.....	46
4.2.6	Cementitious Leachate Impacted and CDP-Impacted Sediment Environments .....	46
4.3	Reducing Cementitious Materials.....	47
4.3.1	Young Reducing Cementitious Solids (1 <sup>st</sup> Stage) Environment.....	50
4.3.2	Moderately-aged Reducing Cementitious Solids (2 <sup>nd</sup> Stage) Environment .....	50
4.3.3	Aged Reducing Cementitious Solids (3 <sup>rd</sup> Stage) Environment .....	50
4.4	Radionuclide Leaching from Waste Materials .....	50
4.5	Radionuclide Leaching from Special Waste Forms.....	51
4.6	Geochemical Parameters' Ranges and Distributions.....	51
5.0	Waste Facilities Descriptions: Assignment of Geochemical Environments and Types of Constants to Use in Simulations .....	53
5.1	Slit and Engineered Trenches .....	54
5.2	Low-Activity Waste (LAW) Vaults.....	58
5.3	Components-in-Grout Trenches.....	61
5.4	Intermediate-Level Vault .....	64
5.5	Naval Reactor Component Disposal Areas.....	67
5.6	TRU Pad Disposal Unit .....	70
5.7	Saltstone Disposal Facility.....	72
5.8	Radioactive Waste Tanks.....	75
6.0	Data Tables .....	78
7.0	Future Research and Data Needs .....	111

8.0	References.....	113
9.0	Appendix A: Additional Information Regarding Cellulose -Degradation-Product Correction Factors For $K_d$ Values .....	126
9.1	Selected Data Sets from Kaplan and Serkiz (2004) “Influence of Dissolved Organic Carbon and pH on Contaminant Sorption to Sediment” .....	127
10.0	Appendix B: Cement Lifespan.....	143
11.0	Appendix C: Influence of Cementitious Leachate on Sediment Buffering Capacity.....	145
12.0	Appendix D: Additional Information Regarding Range and Distribution of $K_d$ Values in SRS Subsurface Sediments.....	148
12.1	Selected Data Sets from Grogan et al. (2008) “Distribution of Sorption Coefficients ( $K_d$ Values) in the SRS Subsurface Environment” .....	149
12.2	Distribution of Tc $K_d$ Values in an SRS Borehole .....	152
13.0	Appendix E: Spectroscopic Evidence of the Reduction of Tc(VII) to Tc(IV) by Cementitious Material Containing SRS Slag.....	157
14.0	Appendix F: Total Organic Carbon Concentrations in the Old Low Level Waste Burial Grounds.....	166

## List of Tables

Table 1. Calculated Leachate Chemical Compositions During the Three Stages of Cement Degradation. For Comparison, the Chemical Composition of an SRS Groundwater. ....	43
Table 2. Cementitious Leachate Impact Factors (Eq. 8) Generated from Data from the "Geochemistry Data Package for the Vadose Zone in the Single-Shell Tank Waste Management Areas at the Hanford Site" (Cantrell et al. 2007). ....	45
Table 3. Description of Whether Cellulose Degradation Products (CDP) is Present and if Reducing and Oxidizing Cementitious Materials were used During the Construction of the Disposal Unit/Facility. ....	47
Table 4. Slit Trenches: Conceptual Geochemical Model of Features and Parameters (See Figure 8). ....	57
Table 5. LAW Vault: Conceptual Geochemical Model of Features and Parameters (See Figure 11). ....	60
Table 6. Components-in-Grout Trenches: Conceptual Geochemical Model of Features and Parameters (Figure 13). ....	63
Table 7. Intermediate-Level Vault: Conceptual Geochemical Model of Features and Parameters (Figure 15). <sup>(a)</sup> ....	66
Table 8. Naval Reactor Component Disposal Areas: Conceptual Geochemical Model Features and Parameters (See Figure 17). ....	69
Table 9. TRU PAD-1: Conceptual Geochemical Model of Features and Parameters (See Figure 19). ....	71
Table 10. Saltstone Facility: Conceptual Geochemical Model of Features and Parameters (See Figure 20 and Figure 21). ....	74
Table 11. Closed Radioactive Waste Tanks: Conceptual Geochemical Model of Features and Parameters (See Figure 22 and Figure 23). ....	77
Table 12. Radionuclides of Interest and Their Assumed Oxidation States or Speciation Under Varying Environments. ....	79
Table 13. Look-up Table of Various Sediment $K_d$ Values: Best $K_d$ Values, $K_d$ (CDP) Values, Cement Leachate with CDP $K_d$ Values, Cement Leachate Impact Factors, and Cellulose Degradation Product Correction Factor. ....	80
Table 14. Look-up Table of Concrete $K_d$ Values and Apparent Solubility Values Under Oxidizing and Reducing Conditions. ....	82
Table 15. Special Waste Form $K_d$ Values (mL/g) Under Ambient and Cementitious Leachate Environments. ....	84
Table 16. Distribution Coefficients ( $K_d$ values, mL/g): Sandy Sediment Layer (<25 wt-% silt + clay) and Clay Sediment Layer (25 to 45 wt-% silt + clay). ....	85
Table 17. Distribution Coefficients ( $K_d$ values, mL/g): Oxidizing Cementitious Solids. ....	93
Table 18. Distribution Coefficients ( $K_d$ values, mL/g): Reducing Cementitious Solids. ....	98
Table 19. Apparent Solubility Concentration Limits (mol/L) for Oxidizing Cementitious Solids. ....	100
Table 20. Apparent Solubility Concentration Limits (mol/L) for Reducing Cementitious Solids. ....	103
Table 21. Cellulose Degradation Product Correction Factors ( $f_{CDP}$ ). ....	105
Table 22. Cementitious Leachate Impact Factors, $f_{CementLeach}$ (Eq. 6). ....	107

Table 23. <i>Kd</i> Values for Environments Impacted by CDP and Cementitious Leachate, <i>Kd</i> <sub>CDP_CemLeach</sub> .....	109
Table 24. Ni <i>Kd</i> Values (mL/g).....	130
Table 25. Sr <i>Kd</i> Values (mL/g).....	132
Table 26. Ce <i>Kd</i> Values (mL/g).....	134
Table 27. Eu <i>Kd</i> Values (mL/g).....	136
Table 28. Zr <i>Kd</i> Values (mL/g).....	138
Table 29. Th <i>Kd</i> Values (mL/g).....	140
Table 30. CDP Correction Factors Based on <i>Kd</i> Values Measured in the pH 3.9 or 5.3 Sandy Sediment System.....	141
Table 31. Cellulose-degradation-products Correction Factors, <i>f</i> <sub>CDP</sub> , for <i>Kd</i> Values. ....	142
Table 32. Summary Statistics of <i>Kd</i> Values (Grogan et al. 2008).....	150
Table 33. Distribution Test Results and 95-Percentile Ranges for Tc <i>Kd</i> Values.....	154
Table 34. Total organic carbon concentrations is well near and beneath the Low Level Waste Burial Ground. (Data from McIntyre and Wilhite 1987; DPST-87-762). Data used to established concentration to use in CDP concentrations in E-Area applications. ....	167

## List of Figures

Figure 1. Effect of aqueous metal ( $M_{aq}$ ) and solid metal ( $M_{solid}$ ) concentrations on distribution coefficients ( $Kd$ ) and solubility product. Point "A" identifies the solubility concentration limit. ....	22
Figure 2. Comparison of sediment desorption data (this study) from a lysimeter containing SRS sediment and Pu (referred to as "This Study") and a Pu(V)/PuO <sub>2</sub> (am) 0.4 M NaClO <sub>4</sub> system (no sediment present, 0.0018- $\mu$ m filtrates; Rai et al. (2001) (taken from Kaplan et al. 2006b)). Y-axis represents Pu concentrations in porewater solutions. ....	23
Figure 3. Example of an actual borehole profile in E-Area demonstrating the tendency for sediments with a more clayey texture to exist in the Upper Vadose Zone, whereas sediments with a sandier texture exist in the Lower Vadose and Aquifer Zones (Well BGO-3A, Grogan et al. 2008; Grogan et al. 2010). ....	33
Figure 4. Examples of waste disposed in the Low Level Waste Burial Ground. Note the disposal of cellulose degradation products similar to present waste disposal in E-Area Slit Trenches presented in Figure 9. ....	37
Figure 5. Eu $Kd$ values as a function of pH and SR-NOM concentrations in clayey (top) and sandy (bottom) sediments (all $Kd$ values >20,000 mL/g are greater-than values). ....	38
Figure 6. Conceptual model used by Bradbury and Sarott (1995) describing the influence of exchange cycles (X-axis) on pH and the designated Stages (or regions) (Atkinson et al. 1988). ....	40
Figure 7. Consumption of slag reduction potential by diffusing dissolved oxygen in infiltrating water into the Saltstone Facility (Kaplan and Hang 2003). Results from Lukens et al. (2005) is also presented (value corrected for diffusion from four sides). ....	49
Figure 8. Schematic representation of the geochemical conceptual model of a Slit and Engineered Trench Units. Not shown is a multilayered-closure cap that will be added above these units during Post-Institutional Control. ....	54
Figure 9. E-Area Slit Trench Facility showing a range of waste materials. Also note the red clayey sediment, characteristic of the upper sediment strata. ....	55
Figure 10. Engineered Trench: (top) aerial view and (bottom) close up of metal containers holding low level waste (WSRC 2008). ....	56
Figure 11. Schematic representation of the geochemical conceptual model of the Low-Activity Waste Vault. Not shown is a multilayered-closure cap that will be added above the vault during Post-Institutional Control. ....	58
Figure 12. Low Activity Waste (LAW) Vault: (top) exterior view and (bottom) interior view (WSRC 2008). ....	59
Figure 13. Schematic representation of the geochemical conceptual model of a Components-in-Grout Trenches. Not shown is a multilayered-closure cap that will be added above the vault during Post-Institutional Control. ....	61
Figure 14. Sequence of steps in the disposing of waste as Components in Grout (CIG; WSRC 2008). ....	62
Figure 15. Schematic representation of the geochemical conceptual model of the Intermediate-Level Vault Facility. Not shown is a multilayered-closure cap that will be added above the vault during Post-Institutional Control. ....	64

Figure 16. Intermediate-Level Vaults: (top left) aerial photo graph with roof off of one cell; (top right) waste components cemented within a partially filled cell; (bottom) cross-sectional diagram of unit (WSRC 2008).	65
Figure 17. Schematic representation of the geochemical conceptual model of the Naval Reactor Component Disposal Areas. Not shown is a multilayered-closure cap that will be added above the pads during Post-Institutional Control. See Table 8 for facility description and Figure 18 for photographs of the facility.	67
Figure 18. (Top) Photo showing partially covered naval reactor components of various sizes. Earth and a clay cap will be mounded over naval reactor waste prior to final disposal. There are two such facilities, the “old” (two top photos) and “new” (bottom photo) facilities. (Bottom) Naval reactor component before it is placed in the disposal area (WSRC 2008).	68
Figure 19. Schematic representation of the geochemical conceptual model of the TRU PAD-1. Not shown is a multilayered-closure cap that will be added above the pads during Post-Institutional Control. See Table 9 for facility description.	70
Figure 20. Schematic representation of the geochemical conceptual model of the Saltstone Facility. Not shown is a multilayered-closure cap that will be added above the Saltstone Facility during Post-Institutional Control. See Table 10 for facility description.	72
Figure 21. (Top) Saltstone disposal facility (SDF) Vault 1 and 4 (photograph taken December 1, 2002). Metal roofs shown over Vault 1 Cells D and E have been removed from the vault. (Bottom) Cross sectional diagram of Vault 1 (WSRC 2008).	73
Figure 22. Schematic representation of the geochemical conceptual model of the Radioactive Waste Tank Closure Concept. See Table 11 for facility description (Bottom figure taken from Buice et al. 2005).	75
Figure 23. Examples of Radioactive Waste Tank construction. Top Left: 17-cm concrete basemat pads; Top Right: Carbon steel liners; Bottom Left: Tank concrete walls (note relative scale of tanks compared to men on scaffolding (photos from Buice et al. 2005).	76
Figure 24. Final pH vs. targeted SR-NOM concentration of no-sediment control samples (2 observations for each mean and standard deviation).	127
Figure 25. Cs <i>Kd</i> values as a function of pH and SR-NOM concentrations in clayey (top) and sandy (bottom) sediments.	128
Figure 26. Ni <i>Kd</i> values as a function of pH and SR-NOM concentrations in clayey (top) and sandy (bottom) sediments.	129
Figure 27. Sr <i>Kd</i> values as a function of pH and SR-NOM concentrations in clayey (top) and sandy (bottom) sediments.	131
Figure 28. Ce <i>Kd</i> values as a function of pH and SR-NOM concentrations in clayey (top) and sandy (bottom) sediments (all <i>Kd</i> values >25,000 mL/g are greater-than values).	133
Figure 29. Eu <i>Kd</i> values as a function of pH and SR-NOM concentrations in clayey (top) and sandy (bottom) sediments (all <i>Kd</i> values >20,000 mL/g are greater-than values).	135
Figure 30. Zr <i>Kd</i> values as a function of pH and SR-NOM concentrations in clayey (top) and sandy (bottom) sediments.	137
Figure 31. Th <i>Kd</i> values as a function of pH and SR-NOM concentrations in clayey (top) and sandy (bottom) sediments.	139
Figure 32. Titration of two sediments collected from the SRS subsurface environment (4-g soil: 25 mL aqueous; constant ionic strength = 0.01 M, 0.02 M NaCl, distilled water, and 0.005 M NaCl).	147

Figure 33. Log-normal fit of  $Kd$  values for a)  $^{109}\text{Cd}$ , b)  $^{137}\text{Cs}$ , c)  $^{57}\text{Co}$ , d)  $^{60}\text{Co}$ , e)  $^{85}\text{Sr}$ , and f)  $^{88}\text{Y}$  (Grogan et al. 2009). ..... 149

Figure 34. Average Tc  $Kd$  (mL/g) vs. depth below ground surface (0 ft) in Upper Vadose, Lower Vadose and Aquifer Zone. .... 152

Figure 35. Normal quantile plot, outlier box plot, and distribution functions for Tc  $Kds$  for the entire core, Upper Vadose Zone, Lower Vadose Zone, and Aquifer (Kaplan et al. 2008b). ..... 153

Figure 36. Map of wells used to collect total organic carbon data at LLW Burial Ground. Outline shows plumes from 1971 solvent spill and plume generated near decontamination station. .... 169

## Acronyms

CDP	Cellulose degradation products
CIG	Components-in-Grout
CLSM	Controlled Low Strength Material
CSH	Calcium-silicate-hydrate
DOC	Dissolved organic carbon
IDF	Intergraded Disposal Facility
ILV	Intermediate Level Vault
LAW	Low Activity Waste
<i>K<sub>d</sub></i>	Distribution coefficient
MWCO	Molecular weight cut-off
PA	Performance Assessment
SA	Special Analysis
SRNL	Savannah River National Laboratory
SRS	Savannah River Site
TRU	Transuranic

## Elements

Ac	Actinium	Fr	Francium	Rn	Radon
Ag	Silver	Gd	Gadolinium	Sb	Antimony
Al	Aluminum	3-H	Tritium	Se	Selenium
Am	Americium	Hg	Mercury	Sm	Samarium
Ar	Argon	I	Iodine	Sn	Tin
As	Arsenic	K	Potassium	Sr	Strontium
At	Astatine	Kr	Krypton	Tc	Technetium
Ba	Barium	Lu	Lutetium	Th	Thorium
Bi	Bismuth	Mn	Manganese	Tl	Thallium
Bk	Berkelium	Mo	Molybdenum	U	Uranium
C	Carbon	N	Nitrogen	Y	Yttrium
Ca	Calcium	Na	Sodium	Zn	Zinc
Cd	Cadmium	Nb	Niobium	Zr	Zirconium
Ce	Cerium	Ni	Nickel		
Cf	Californium	Np	Neptunium		
Cl	Chlorine	Pa	Protactinium		
Cm	Curium	Pb	Lead		
Co	Cobalt	Po	Polonium		
Cr	Chromium	Pt	Platinum		
Cs	Cesium	Pu	Plutonium		
Eu	Europium	Ra	Radium		
F	Fluorine	Rb	Rubidium		
Fe	Iron	Re	Rhenium		

## 1.0 EXECUTIVE SUMMARY

The Savannah River Site disposes of low-activity radioactive waste within subsurface-engineered facilities. One of the tools used to establish the capacity of a given site to safely store radioactive waste (*i.e.*, that a site does not exceed its Waste Acceptance Criteria) is the Performance Assessment (PA). The objective of this document is to provide the geochemical values for the PA calculations. This work is being conducted as part of the on-going maintenance program that permits the PA to periodically update existing calculations when new data becomes available.

Because application of values without full understanding of their original purpose may lead to misuse, this document also provides the geochemical conceptual model, the approach used for selecting the values, the justification for selecting data, and the assumptions made to assure that the conceptual and numerical geochemical models are reasonably conservative (*i.e.*, reflect conditions that will tend to predict the maximum risk to the hypothetical recipient). This document provides >1030 input parameters for geochemical parameters describing transport processes for 64 elements (>130 radioisotopes) potentially occurring within nine subsurface disposal or tank closure areas (Slit Trenches, Engineered Trenches, Low Activity Waste (LAW) Vault, Intermediate Level (ILV) Vaults, TRU-Pad-1, Naval Reactor Component Disposal Areas, Components-in-Grout Trenches, Saltstone Facility, and Closed Liquid Waste Tanks).

This work builds upon earlier PA geochemical data compilations (McDowell-Boyer et al. 2000; Kaplan 2007). The primary changes compared to the most recent geochemical data package (Kaplan 2007) are:

- The inclusion of information about  $Kd$  distributions (normal, log-normal), means, and 95 percentile ranges based on recent field measurements (Grogan et al. 2008; Grogan et al. 2010; Kaplan et al. 2008b) to address needs for stochastic modeling. Related, it no longer provides the “*reasonably conservative*” parameter, which was based on professional judgment. This latter parameter was replaced with the statistically defined lower 95-percentile limit.
- The addition of a section that provides  $Kd$  values of special waste forms. These waste forms, which include exchange resins and activated carbon, are highly specialized waste streams and possess unique sorption properties that are difficult to estimate from the literature. They were measured in the laboratory using site-specific materials and appropriate leaching solutions.
- The inclusion of a new Environment, or geochemical zone, called the Cementitious Leachate Impacted Sediment, to account for the influence that the leachate from cementitious materials have on sorption properties in underlying vadose zone sediments. Cementitious porewater is highly basic (pH >12) and has a high ionic strength ( $10^{-2}$  molar) for much of the lifespan of cement, and as such it can influence the sorption of many radionuclides. Previously we had accounted for the impact of the cementitious aqueous phase in estimating radionuclide sorption ( $Kd$  and solubility values) within, but not beneath the cementitious materials.
- Assumption related to the implementation of the cellulose degradation product (CDP) correction factors (factors that account for enhanced mobility due to the complexation of radionuclides by organics, thereby reducing the tendency for the radionuclides to sorb to the sediment) were altered from “conservative” in the last data package (Kaplan 2007) to “best estimate” in this data page. Overall, the “best estimate” CDP-impacted  $Kd$  values are higher than “conservative” values; this is generally favorable for the groundwater pathway. Additionally, a surface complexation and component additivity model dealing with CDP, pH and europium was recently published (Kaplan et al. 2010) and the approach, not the details, is described as an example of a more robust approach for dealing with this complex geochemical system.

- There were several new sorption studies also conducted and these results were incorporated into the report, resulting in changes in recommended  $Kd$  and solubility values. These reports include:
  - Iodine, Np, Pu, and Tc sorption studies on SRS cementitious materials under oxidizing and reducing conditions, which established much higher Np and Pu  $Kd$  values (Lilley et al. 2009),
  - Np sorption studies on SRS sediments under oxidizing and reducing conditions and in the presence of natural organic matter, which measured SRS clayey sediment Np(V)  $Kd$  values for the first time and demonstrated that the SRS sediments have little tendency to reduce Np(V) to the less mobile species Np(IV) (Miller et al. 2009)
  - Am, Cd, Ce, Co, Cs, Hg, I, Np, Pu, Pa, Sn, Sr, Tc, U, and Y sorption studies with both oxidizing and reducing cementitious materials, which provided a large number of site-specific  $Kd$  values (Kaplan and Coates 2007; Kaplan et al. 2008b),
  - Tc sediment sorption and  $Kd$  distribution studies, which greatly increased the number of SRS Tc  $Kd$  values and clearly demonstrated that Tc sorbed to SRS sediments and data also provided a distribution for stochastic modeling (Kaplan et al. 2008b),

The changes that have the greatest potential implication to performance assessments and special analyses are tabulated below. Two common risk drivers, I and Tc, both have significantly increased sediment  $Kd$  values. But in cement-leachate impacted vadose zone sediments, such as beneath a cement vault, the  $Kd$  values decrease, such that,  $Kd_{CementLeach}$  for I is 0.0 and 0.1 mL/g for sandy and clayey sediments, respectively, and for Tc it is 0.1 and 0.2 mL/g for sandy and clayey sediments, respectively. The solubilities of Np and Pu in SRS cementitious materials were measured to be very low, i.e., the  $Kd$  values were very high.

Rad	Geochemical Data Source	Sand $Kd$	Clay $Kd$	Oxidizing Cement $Kd$			Reducing Cement $Kd$			$f_{CementLeach}^{(c)}$ Cement-leachate impact factor
				1 <sup>st</sup> Stage, Young	2 <sup>nd</sup> Stage, Middle	3 <sup>rd</sup> Stage, Old	1 <sup>st</sup> Stage, Young	2 <sup>nd</sup> Stage, Middle	3 <sup>rd</sup> Stage, Old	
<b>I</b>	Kaplan 2007	0	0.6	8	20	0	8	20	0	
	This document	<b>0.3</b>	<b>0.9</b>	8	15	4	5	9	<b>4</b>	<b>0.1</b>
<b>Np</b>	Kaplan 2007	0.6	35	2000	2000	200	2000	2000	200	
	This document	<b>3</b>	<b>9</b>	<b>10,000<sup>(a)</sup></b>	<b>10,000<sup>(a)</sup></b>	<b>5000</b>	<b>10,000<sup>(a)</sup></b>	<b>10,000<sup>(a)</sup></b>	<b>5000</b>	1.5
<b>Ra</b>	Kaplan 2007	5	17	100	100	70	100	100	70	
	This document	5	17	100	100	70	0.5	3	20	3.0
<b>Pu</b>	Kaplan 2007	270	5900	5000	5000	500	5000	5000	500	
	This document	290	5970	<b>10,000<sup>(b)</sup></b>	<b>10,000<sup>(b)</sup></b>	<b>2000</b>	<b>10,000<sup>(b)</sup></b>	<b>10,000<sup>(b)</sup></b>	<b>2000</b>	2.0
<b>Sr</b>	Kaplan 2007	5	17	1	1	0.8	1	1	0.8	
	This document	5	17	15	15	5	15	15	5	3.0
<b>Tc</b>	Kaplan 2007	0.1	0.2	0	0	0	5000	5000	5000	
	This document	<b>0.6</b>	<b>1.8</b>	0.8	0.8	0.5	5000	5000	<b>1000</b>	<b>0.1</b>
<b>U</b>	Kaplan 2007	200	300	1000	1000	70	5000	5000	5000	
	This document	200	300	250	250	70	2500	2500	2500	3.0

<sup>(a)</sup> Np sorption best represented by a solubility value of 1e-13 M under reducing conditions and 1e-12 under oxidizing conditions.

<sup>(b)</sup> Sorption best represented by an apparent solubility value of 1e-12 M under oxidizing and reducing conditions.

<sup>(c)</sup> Cement-leachate impact factors,  $f_{CementLeach}$ , are used in the vadose zone beneath cementitious structures, such as cement vaults or cement-filled tanks, to adjust  $Kd$  values to account for the influence of cementitious leachate on radionuclide sorption to sediments.  $Kd_{CementLeach} = Kd \times f_{CementLeach}$ . Guidance is provided in this document on when and how deep in the vadose zone to apply the Cement-leachate impacted  $Kd$  value, which is new to the SRS PA with this document.

As part of the PA maintenance plan, future program needs were identified, including developing a reactive transport code for certain aspects of the PA, continued research in colloid-facilitated transport, measuring ranges and distributions of cementitious materials, and measuring radionuclide sorption in the presence of cementitious leachate.

## 2.0 OBJECTIVE AND SCOPE

The objectives of this document are to explain the following as they relate to performance assessment's (PAs) conducted at the Savannah River Site (SRS):

1. the geochemical conceptual model,
2. the approach used to select values for the numerical parameters of these conceptual models,
3. the assumptions made to assure that the conceptual and numerical models are reasonable,
4. the recommended geochemical input values for the PA and justification for their selection, and
5. identification of critical data needs.

The scope of this document follows.

1. To provide geochemical input values for PA modeling of the:
  - Slit Trenches,
  - Engineered Trenches,
  - Low Activity Waste (LAW) Vault,
  - Intermediate Level (ILV) Vault,
  - TRU-Pad-1,
  - Naval Reactor Component Disposal Areas,
  - Components-in-Grout Trenches,
  - Saltstone Disposal Facility, and
  - Closed Liquid Waste Tanks.
2. To provide geochemical input values for PA modeling of the radioactive and the stable isotopes of the following 64 elements: Ac, Ag, Al, Am, Ar, As, At, Ba, Bi, Bk, C, Ca, Cd, Ce, Cf, Cl, Cr, Cm, Co, Cs, Cu, Eu, F, Fe, Fr, Gd, <sup>3</sup>H, Hg, I, K, Kr, Lu, Mn, Mo, N (as NO<sub>3</sub><sup>-</sup> and NO<sub>2</sub><sup>-</sup>) Na, Nb, Ni, Np, Pa, Pb, Pd, Po, Pu, Pt, Ra, Rb, Re, Rn, Sb, Se, Sm, Sn, Sr, Tc, Te, Th, Tl, U, Y, Zn, and Zr.
3. The duration of interest varies between calculations but is commonly 1000 years, 10,000 years, or until the maximum dose is obtained. Thus, if geochemical conditions are expected to change with time, such as redox conditions, appropriate adjustments to the geochemical conceptual and numerical models must also be made.

### 3.0 PHILOSOPHY AND ASSUMPTIONS

The basic philosophy of the geochemistry applied to the PA was to utilize mechanistic studies under controlled experimental conditions to provide the paradigms for the conceptual models and empirical studies to provide input values to help quantify these conceptual models. Radionuclide partitioning between the aqueous and solid phases was described using the distribution coefficient,  $Kd$  value, and the solubility concentration limit. A series of look-up tables were prepared containing these parameters that vary with the type of porous media (*e.g.*, sandy sediment, clayey sediment, cementitious material), the presence of strong complexing ligands in the groundwater (*e.g.*, cellulose degradation products), and in the case of cementitious materials, the age of the solid and the presence or absence of slag (a strong reducing agent).

The basic philosophy underpinning the geochemistry modeling was to utilize mechanistic studies to provide conceptual models and empirical studies to provide input values for these conceptual models.

Section 3.1 contains a description of the differences between the theoretical and empirical distribution coefficients and their relation to the retardation factor, a parameter in reactive transport models that describes geochemical interactions. Section 3.1 is followed by a description of solubility constraints and how they differ from distribution coefficients (Section 3.2). Importantly, it was decided not to employ more mechanistic surface complexation models, which are discussed in Section 3.3. While the PA has employed such models to describe limited data sets (Serkiz and Kaplan 2006), their application to the large heterogeneous systems described in the various PAs would not be appropriate at this time due to the large amount of input data required.

#### 3.1 Theoretical Distribution Coefficients, Empirical Distribution Coefficients, and their Relation to Retardation Factors

Coupled reactive-transport modeling seeks to integrate groundwater flow with transport of contaminants by fluid-sediment interactions to create a model capable of predicting spatial and temporal distribution of contaminants. The typical approach is to establish parameters describing fluid-sediment interactions based on the literature, or preferably based on site-specific measurements. The fluid-sediment interactions may consist of adsorption-desorption, ion exchange, and precipitation-dissolution reactions. Some models consider these reactions separately. However, the most common approach is to incorporate all of these reactions into one  $Kd$  value. The  $Kd$  value is the simplest construct describing contaminant sorption<sup>1</sup> to sediments. It is the ratio of the contaminant concentration sorbed to the solid phase divided by the contaminant concentration in the liquid surrounding the solid phase (Equation 1):

---

<sup>1</sup> Sorption in this text is defined to include all processes that remove solutes from the aqueous phase, including, adsorption, absorption, partitioning into the organic matter, complexation, precipitation, and co-precipitation. These terms are described in detail by Sposito (1989).

$$Kd = \frac{C_{solid}}{C_{liquid}}, \quad (1)$$

where  $C_{solid}$  (mol g<sup>-1</sup>) and  $C_{liquid}$  (mol mL<sup>-1</sup>) are the concentration in the solid and liquid phases, respectively. It is important to note that sorption, as expressed by  $Kd$  values, is normalized by mass, and not volume, as transport modelers use, or surface area, as surface chemist use. First and foremost, it is assumed that steady state is achieved and that kinetic is not an issue. Sorption kinetics is typically not an issue for groundwater flow rates that generally do not exceed cm per day, thereby providing long aqueous/solid phase contact times.

Contaminant transport modelers commonly use  $Kd$  values to account for chemical interactions between the contaminant and the porous media. The  $Kd$  value is used to define the retardation factor, ( $R_f$ , unitless) which is the ratio of the average linear velocity of water ( $v_w$ , m s<sup>-1</sup>) divided by the average linear velocity of the contaminant ( $v_c$ , m s<sup>-1</sup>). For water saturated systems, the  $Kd$  value is related to the  $R_f$  by the bulk density ( $\rho_b$ , g cm<sup>-3</sup>) and the porosity ( $\eta$ , cm<sup>3</sup> cm<sup>-3</sup>) as follows (Valocchi 1984, Bower 1991):

$$R_f = \frac{v_w}{v_c} = \left( 1 + \frac{Kd\rho_b}{\eta} \right). \quad (2)$$

The bulk density and porosity terms in Equation 2 convert the mass-normalized  $Kd$  value into a volume-normalized value. Note that for partially saturated sediments, such as in the vadose zone, the porosity term,  $\eta$ , is replaced by the volumetric water content of the vadose zone sediments.

The theoretical distribution coefficient is a thermodynamic construct. It is the ratio of the concentration of a species reversibly adsorbed/exchanged to surface sites divided by the concentration of the species in the surrounding solution. Using uranyl as an example, the definition of a species-specific  $Kd$  as a thermodynamic construct ( $Kd_{thermo}$ ) is:

$$Kd_{thermo} = \frac{X \equiv UO_2^{2+}}{UO_2^{2+}} \quad (3)$$

where  $X \equiv UO_2^{2+}$  is the activity of the uranyl species reversibly adsorbed to a specific surface site X, and  $UO_2^{2+}$  is the activity of dissolved “free” uranyl species at equilibrium with the surface site X. Among the many assumptions underpinning  $Kd_{thermo}$  is that adsorption is instantaneous, fully reversible (*i.e.*, the rate of adsorption is equal to the rate of desorption), linear (*i.e.*, the proportional adsorption of a contaminant is not influenced by the aqueous contaminant concentration) and the presence of adsorbed species does not influence subsequent adsorption of other dissolved species. Thus, a single distribution coefficient is used to represent both sorption and desorption of each contaminant species for a specific adsorbent (solid phase with one type of surface site) and for a specific macro solution chemical composition.

However, in order to apply the  $Kd$  construct to contaminant transport and performance assessment calculations, the definition of the construct is relaxed. The definition needs to be relaxed for several reasons. In natural systems, a multitude of different types of sorption sites and aqueous species exists. For example, Sposito (1989; pg. 69) calculated that a typical soil solution can easily contain 100 to 200 different soluble complexes.

Also, it is very difficult to measure the thermodynamic activity of individual chemical species on the adsorbents' surfaces. Furthermore, the measurement of thermodynamic activities of dissolved species is rarely performed and, as mentioned in discussion of Equation 3, for adsorbates on solids, no techniques exist for the measurement of their thermodynamic activity. The parameters that can be readily measured are the total contaminant concentration or radionuclide activity (not to be confused with thermodynamic activity) as opposed to the concentration/radioactivity of each individual species. Thus, the  $Kd_{thermo}$  construct, as defined in Equation 3, requires differentiating and quantifying each type of surface site and each solution species. Additionally, spatial variability of the surface sites and groundwater chemistry in natural systems cannot practicably be characterized to the degree necessary for the full implementation of species' specific sorption models, such as the triple layer surface complexation model (see reviews by Kent et al. 1988 and Jenne 1998).

The empirical definition of the  $Kd$  value becomes the ratio of the concentration of the complete suite of species, the sum of the total concentration of all species that include the contaminant of interest, sorbed by an assemblage of surface sites, divided by the sum of the total concentration of all species in solution. Again, using uranyl as an example, the definition of the thermodynamic  $Kd$  construct would be for a simple system that contained three U(VI) species [ $UO_2^{2+}$ ,  $UO_2(OH)^+$ , and  $UO_2(OH)_2^0$ ]:

$$Kd_{therm} = \frac{\sum \text{Adsorbed U Species}}{\sum \text{Dissolved U Species}} = \frac{X\equiv UO_2^{2+} + X\equiv UO_2(OH)^+ + X\equiv UO_2(OH)_2^0}{UO_2^{2+} + UO_2(OH)^+ + UO_2(OH)_2^0} \quad (4)$$

where  $X\equiv$  is an average sorbent site (more than one sorbent site-type is expected in nature). The numerator and denominator in Equation 4 are summed over contaminant species sorbed as well as sorbent sites. The "empirical"  $Kd$  equation would be:

$$Kd_{empirical} = \frac{\text{total U(VI) on solid}}{\text{total U(VI) in solution}} \quad (5)$$

In an attempt to distinguish  $Kd_{thermo}$  from  $Kd_{empirical}$ , researchers, especially in Europe, referred to the latter term as  $Rd$  (e.g., Bradbury and Sarott 1995). This is rarely used any longer, and  $Kd_{empirical}$  is referred to simply as  $Kd$ , as is done in this text.

An important limitation of the  $Kd_{empirical}$  is that it in theory describes a very limited set of conditions. It describes sorption for a specific contaminant, specific soil solution (e.g., pH, dissolved organic matter, Eh, etc.) and soil solid phase properties (e.g., cation exchange capacity, clay content, soil organic matter, etc.). Again, this definition is relaxed when it is used in contaminant transport calculations.

Among the reasons for selecting the “empirical”  $Kd$  construct for the PA, as exemplified by Equation 5, are

- 1) the bulk of the existing sorption literature on radionuclide sorption, especially at SRS can be classified as “empirical”  $Kd$  values,
- 2) under the expected low concentrations of the contaminants in the far field, sorption can be considered to be independent of contaminant concentration and, therefore,  $Kd$  is a constant for a given contaminant/geological material/water composition combination under identical (geo)chemical conditions,
- 3)  $Kd$  can be used directly in all PA transport codes, and
- 4) perhaps most importantly, there is presently no thermodynamically-based conceptual model or numerical code that is robust enough to predict accurately the degree of radionuclide adsorption by natural sediments (see below).

By using site-specific materials, namely sediments or cementitious materials and groundwater from disposal areas, it is possible to gather directly relevant data and not to rely on extrapolation from other sediment and aqueous systems reported in the literature. The problem with the rigorous thermodynamic species approach is that there is presently no numerical or conceptual model developed that is sufficiently robust to predict accurately the degree of radionuclide adsorption by natural sediment (Sposito 1984, Westall 1994, Westall 1986, Wang et al. 1997, Davis et al. 1998). However, mechanistic models provide the necessary paradigms upon which technically defensible “empirical”  $Kd$  values must be based. For most of the data used in the PA geochemical data package, sorption experiments have been conducted with site-specific sediment and site-specific groundwater, which also resembles natural vadose-zone porewaters.

Mechanistic models, although impractical for PA purposes, provide the necessary paradigms upon which “empirical”  $Kd$  values must be based.

Another aspect of the  $Kd$  construct that is typically relaxed when used in contaminant transport calculations is the chemical process that it describes. As pointed out earlier, Equation 3 implies an adsorption or exchange reaction that is reversible. The laboratory  $Kd$  measured with complex natural sediments and perhaps complex natural groundwater solutes, often reflect not only adsorption and exchange reactions, but also absorption, specific or somewhat irreversible adsorption, surface complexation, and varying degrees of (co)precipitation reactions. Identifying the processes that govern radionuclide chemical behavior is the single most important task necessary for estimating  $Kd$  values for a PA. Once the dominant geochemical process is identified for a specific geological and chemical environment, the range of relevant “empirical”  $Kd$  values can be narrowed. Radionuclide geochemical processes have been ascertained primarily through experiments in which a key parameter is systematically varied, *e.g.*, suspension pH or radionuclide concentration. The trends displayed during these experiments provide key information regarding

Identifying the processes that govern radionuclide chemical behavior is the single most important task necessary for estimating  $Kd$  values. Once the dominant geochemical process is identified for a specific set of environmental conditions, the range of reasonable values for the “empirical”  $Kd$  parameter can be narrowed.

radionuclide behavior and also shed light on which processes may be controlling the radionuclide interaction between the solid and liquid.

The importance of first identifying the dominant geochemical process affecting radionuclide concentrations in the mobile aqueous phase can be illustrated through an experiment conducted by Kaplan et al. (1998a). In this experiment, as the pH of a sediment-groundwater slurries was increased from pH 8 to 10, U(VI)- $Kd$  values gradually increased from 1.3 to 3.5 mL/g. Above pH 10.5 the amount of U(VI) removed from the aqueous phase increased by >500 fold. The initial increase in  $Kd$  between pH 8 and 10 was attributed to increased cation exchange capacity of the sediment. That is, the number of pH-dependent adsorption sites in the natural sediment, which attract cations, increased as the pH increased. The latter more dramatic increase was attributed to (co)precipitation of U(VI) with carbonate solid phases. These conclusions were supported by independent solubility calculations. What we learn from this particular study is much more than simply the magnitude of the  $Kd$  value that should be used as an input parameter to a PA; we gain a plausible explanation of the processes governing U(VI) removal from solution. As this example illustrates, changes in the dominant chemical processes may account for an appreciable amount of variability in derived  $Kd$  values under different geochemical conditions.

### 3.2 Solubility Constraints

In addition to the  $Kd$  construct, the solubility product,  $k_{sp}$ , (mol/L or M,) (both thermodynamically and empirically based) are used to describe radionuclide geochemical behavior in a disposal site. A  $k_{sp}$  is used for conditions where the concentrations of the radionuclides are believed to exceed the solubility of an assumed solubility-controlling mineral phase. The selection of controlling solid phases for SRS PA activities was based on laboratory experiments, calculations, and the literature. Once the solid phase was selected, the upper limit of radionuclide concentration was calculated with the appropriate background electrolyte composition. If the background electrolyte composition remained essentially constant, then the solubility product was assumed to also be nearly constant. This has led some transport modelers to refer to solubility products as constants but in reality the solubility product  $k_{sp}$ , varies with solution chemistry.

When radionuclide concentrations exceed the solubility limit for some mineral, precipitation can be expected and subsequent radionuclide aqueous concentrations and behavior is controlled by solubility. At concentrations below the solubility product (Point A in Figure 1), the radionuclide concentration will be controlled by the “empirical”  $Kd$  construct.

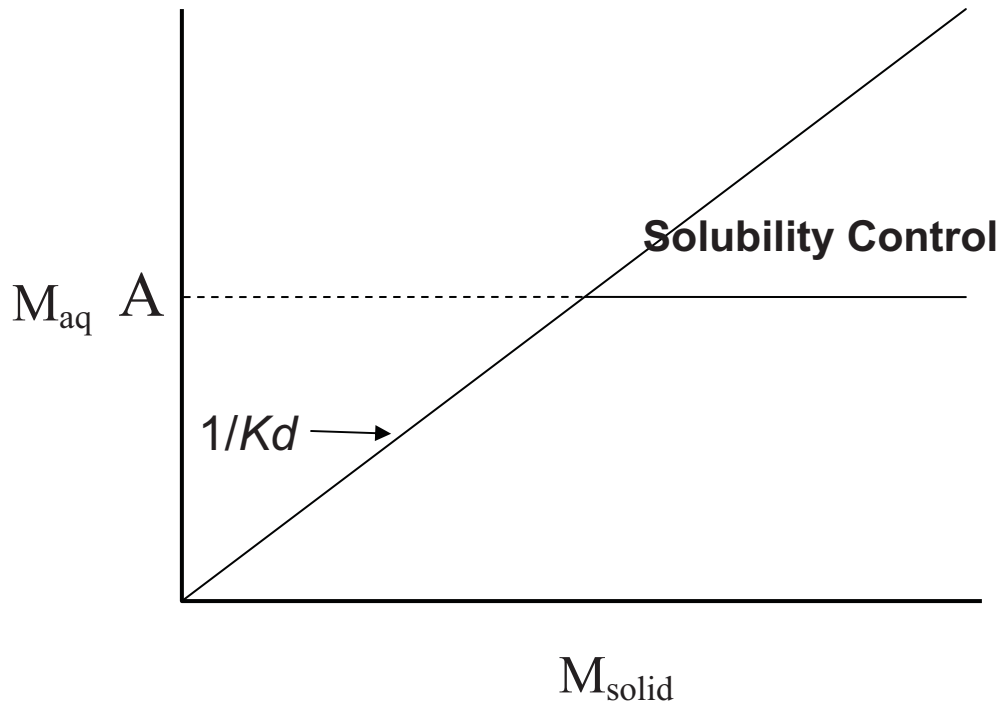


**Figure 1.** Effect of aqueous metal ( $M_{aq}$ ) and solid metal ( $M_{solid}$ ) concentrations on distribution coefficients ( $Kd$ ) and solubility product. Point "A" identifies the solubility concentration limit.

When the solubility-controlling solid could not be identified but empirical solubility tests indicated that some unidentified phase was controlling solution concentration, then an empirical solubility relationship was used. An example of this is presented in Figure 2. Figure 2 presents data from Kaplan et al. (2006b) showing the desorption of Pu from a lysimeter which had been in contact with the Pu for 24 years. The Pu was originally placed in the lysimeter as dissolved  $Pu^{IV}(NO_3)_4$  dried on a filter. In this batch test, portions of the lysimeter sediment were put in suspensions of varying pH and permitted to equilibrate.

The total equilibrated Pu solution concentrations were compared to data from Rai et al. (2001), showing  $PuO_{2(am)}$  solubility (more specifically, this phase oxidizing to Pu(V) and then solubilizing). The study by Rai et al. (2001) was conducted in the absence of sediment, simply an aqueous phase and the Pu solid phase. The main point to take from Figure 2 is that the two data sets behave very similarly with respect to pH, except that they are offset by a constant amount. Based on this and other data presented in the paper, Kaplan et al. (2006b) suggested that porewater Pu concentrations in SRS sediments are largely controlled by solubility. In this example, the solubility controlling phase is not known, and adsorption along with solubility is likely controlling the total aqueous Pu concentrations. Thus, an apparent or empirical solubility term may be appropriate to describe such data.

When the controlling solid could not be identified but empirical solubility tests indicate that some phase was controlling solution concentration, then an empirical solubility relation was constructed.

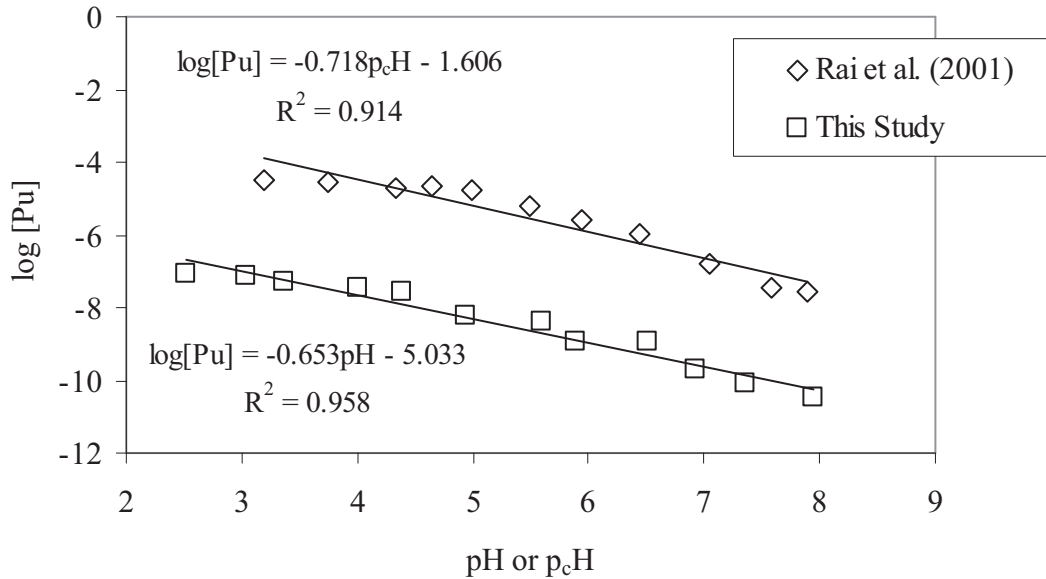


**Figure 2.** Comparison of sediment desorption data (this study) from a lysimeter containing SRS sediment and Pu (referred to as “This Study”) and a Pu(V)/PuO<sub>2</sub>(am) 0.4 M NaClO<sub>4</sub> system (no sediment present, 0.0018- $\mu$ m filtrates; Rai et al. (2001) (taken from Kaplan et al. 2006b)). Y-axis represents Pu concentrations in porewater solutions.

Finally, in some cases, the empirical solubility concentration limit data may be simplified as a constant concentration limit. This is especially true for the PA because little site/waste form/engineered barrier solubility work has been performed that identifies the solubility-controlling solids. It is also true that for short-lived radionuclides, the regulatory limits are usually far lower than the solubility limits. For example, the solubility limit for Ra-228 ( $t_{1/2} = 5.7$  yr) as RaSO<sub>4</sub> is several orders of magnitude greater than any regulatory limit. For these short-lived constituents solubility limits rarely come into play.

### 3.3 Overview of Mechanistic Complexation Models

Mechanistic models explicitly accommodate the dependency of  $Kd$  values, or other sorption values, on contaminant concentration, competing ion concentrations, pH-dependent surface charge on the adsorbent, and solute species distribution. Incorporating mechanistic, or semi-mechanistic, concepts into models is attempted because the models become more robust and, perhaps more importantly, from the standpoint of the PA, scientifically defensible. There are several mechanistic models that can describe solute adsorption; some are accurate only under limited environmental conditions (Sposito 1984). For instance, the Stern model is a better model for describing adsorption of inner-sphere complexes, whereas the Gouy-Chapman model is a better model for describing outer-sphere or diffuse-swarm adsorption (Sposito 1984, Westall 1986). The complexity of installing these models into existing transport codes that are favored for complete disposal system performance assessment and the diversity of SRS waste leachate/sediment/contaminant combinations of interest would require a data collection effort more intense and costly than is likely to be available. A brief description of the state of the science is presented below. References to

excellent review articles have been included in the discussion to provide the interested reader with additional information.

Experimental data on interactions at the mineral-electrolyte interface can be represented mathematically through two different approaches: 1) empirical models and 2) mechanistic models. An empirical model can be defined as a mathematical description of the experimental data without any particular theoretical basis. For example, the  $K_d$ , Freundlich isotherm, Langmuir isotherm, Langmuir Two-Surface Isotherm, and Competitive Langmuir are considered empirical models by this definition (Sposito 1984). Mechanistic models refer to models based on thermodynamic concepts such as reactions described by mass action laws and material balance equations. Four of the most commonly used mechanistic models include the Helmholtz, Gouy-Chapman, Stern, and Triple Layer models (Sposito 1984). The empirical models are often mathematically simpler than mechanistic models and are suitable for characterizing sets of experimental data with a few adjustable parameters, or for interpolating between data points. On the other hand, mechanistic models contribute to an understanding of the chemistry at the interface and are often used for describing data from complex multi-component systems for which the mathematical formulation (*i.e.*, functional relations) for an empirical model might not be obvious. Mechanistic models can also be used for interpolation and characterization of data sets in terms of a few adjustable parameters. However, mechanistic models are often mathematically more complicated than empirical relationships. Adjustable parameters are required for both mechanistic and empirical models, but not for the  $K_d$  model.

Several mechanistic models have been proposed; however, their application to complex natural sediments is not resolved (Westall and Hohl 1980, Sposito 1984, Westall 1986, Davis and Kent 1990, Sposito 1989, Schindler and Sposito 1991). Any complete mechanistic description of chemical reactions at the mineral-electrolyte interface must include a description of the electrical double layer. While this fact has been recognized for years, a satisfactory description of the double layer at the mineral-electrolyte interface still does not exist.

Part of the difficulty of characterizing this interface stems from the fact that natural mineral surfaces are very irregular and non-homogeneous. They consist of many different micro-crystalline structures that exhibit quite different chemical properties when exposed to solutions. Thus, examination of the surface by virtually any experimental method yields only averaged characteristics of the surface and the interface. Parson (1982) discussed the surface chemistry of single crystals of pure metals and showed that the potential of zero charge of different crystal faces of the same pure metal can differ by over 400 mV. For an oxide surface, this difference was calculated by Westall (1986) to be energetically equivalent to a variation in the zero-point-of-charge of more than six pH units. This example indicated that an observable microscopic property of a polycrystalline surface might be the result of a combination of widely different microscopic properties and characterization of these surfaces will remain somewhat operational in nature.

Another fundamental problem encountered in characterizing reactions at the mineral-electrolyte interface is the coupling between electrostatic and chemical interactions, which makes it difficult to distinguish between their effects. Westall and Hohl (1980) have shown that many models for reactions at the mineral-electrolyte interface are indeterminate in this regard.

Mechanistic or surface-complexation models were originally designed to describe well-defined systems of little or no heterogeneity, a far cry from natural sediments. One method of addressing heterogeneous systems is an empirical approach that Davis et al. (1998) and Davis et al. (2004) refer to as the generalized composite approach. In this approach experimental data on site soils are fitted to various stoichiometric sorption reactions and model formulations based on reaction scheme simplicity and goodness-of-fit (Herbelin and Westall, 1999). This avoids the necessity of detailed mineralogical characterization required in the more general approach that Davis et al. (1998) and Davis et al. (2004) call the “component additivity” approach. It is also important to note that the authors of this approach do not assign specific binding sites (*e.g.*, Fe-oxide “B” sites or planar kaolinite sites) to the solid phases.

Data collection to support the generalized composite approach requires experimental determination of surface complexation under all mineralogical and chemical conditions expected within a plume. The resulting data permits calculating semi-empirical geochemical sorption parameters that can then be used to describe contaminant sorption for a wide range of environmental conditions at the study site. Less site-specific data is required to support the component additivity approach and this approach can simulate changing conditions more realistically than the generalized composite approach. For example, if a phase is predicted to precipitate (or disappear) in the future it cannot be accounted for in the generalized composite approach, whereas this can be incorporated into the component additivity approach. The inclusion of these geochemical models into the PA is an eventual goal and studies are presently underway to accomplish this goal (Serkiz and Kaplan 2006). One recent successful application of this modeling approach has been with Eu (an analogue for trivalent radionuclides), natural organic matter (an analogue for cellulosic degradation products), and SRS sediment (Kaplan et al. 2010). The value this brings, albeit is still quite limited in scope, is that a wide range of environmental conditions, in this case, soil type, pH, and natural organic matter concentrations, can be modeled, a far more robust description than a Eu *K<sub>d</sub>* construct.

A recent application of the component additivity approach and generalized surface complexation model provided a much more robust description than the *K<sub>d</sub>* construct (Kaplan et al. 2009).

### 3.4 Unique Conditions Resulting in Enhanced Contaminant Transport of Radionuclides

#### 3.4.1 Cellulose Degradation Products

Cellulosic materials (*e.g.*, wood, paper, and cardboard products) readily degrade in the environment to form cellulose degradation products (CDP) in both the solid and dissolved (*i.e.*, dissolved organic carbon; DOC) phases. Natural organic matter can greatly influence the speciation and mobility of nonradioactive elements (Perdue and Gjessing 1990, Thurman 1985, Stumm and Morgan 1981) and radioactive elements (Choppin 1989, Allard et al. 1989, Fairhurst et al. 1995; and Ledin et al. 1994). Co-disposal of radionuclides with cellulosic materials is, therefore, expected to influence nuclide fate and transport in the subsurface (Serne et al. 1993). The disposal and degradation of wood products in the E-Area Slit Trenches and the Engineered

Trenches are a source of organic matter that is expected to influence radionuclide fate and transport.

A modest amount of research has been conducted to evaluate the effect of CDP on radionuclide sorption to SRS sediments (Serkiz and Myers 1996, Serkiz et al. 1998, Serkiz et al. 1999, Kaplan and Serkiz 2004, Serkiz and Kaplan 2006, and Kaplan and Serkiz 2006). Initial studies were strictly calculations describing radionuclide sorption in the presence of CDP using available literature and limited SRS site-specific data (Serkiz and Myers 1996). This initial modeling used published stability constants for reactions between low molecular-weight acids (*i.e.*, citric acid and EDTA) and radionuclides to approximate behavior of CDP. Laboratory studies with U(VI) and Eu(III) were conducted and their results were introduced into numerical models (Serkiz et al. 1998, Serkiz et al. 1999). These elements, along with Cs data, were then used as analogues to generate recommended *Kd* values for use with a wide range of elements (Serkiz 2000).

Most recently, Kaplan and Serkiz (2004) conducted a full-factorial study evaluating the influence of varying concentrations of organic C (using fulvic acid as a surrogate for CDP), and pH on the sorption of monovalent cations ( $K^+$  and  $Cs^+$ ), divalent cations ( $Ni^{2+}$  and  $Sr^{2+}$ ), trivalent cations ( $Ce^{3+}$  and  $Eu^{3+}$ ) and tetravalent cations ( $Th^{4+}$  and  $Zr^{4+}$ ). Analogues were matched to ~30 radionuclides based on similarities in periodicity and chemical properties and a look-up table of CDP-impacted *Kd* values were created as a function of soil type (sandy and clayey), pH and organic carbon content. This data was later modeled using a first-principles approach to provide a mechanistic geochemical understanding of the processes controlling the radionuclide-sediment-CDP system (Serkiz and Kaplan 2006a). An interesting aspect of this data was that it showed that at low to moderate CDP concentrations, the sorption of several radionuclides actually increased due to the sorption of the organic matter to the sediment, which increased the sediment's sorption capacity for the radionuclides. Furthermore, this effect existed only at low pH levels (pH <7), where some organic C sorbed to the sediment and did not remain in the aqueous phase. At higher pH values, the dissolved C remained in solution and acted as a ligand to complex the radionuclide, preventing it from sorbing to the sediment. This trend was true for some but not all radionuclides. CDP constituents are subject to further biodegradation as they migrate in a plume. In some cases, the enhanced migration may be a transitory effect. For example, 1) the CDP may undergo microbial degradation or 2) even though the common cations (Na, Ca, and Mg) form less strong complexes with the low molecular weight organic acids and fulvic acid with time and distance, they will out-compete the stronger but less concentrated radionuclide to form complexes with the CDP.

Kaplan and Serkiz (2006b) conducted sediment sorption tests with perrhenate ( $ReO_4^-$ , as an analogue for pertechnetate,  $TcO_4^-$ ), selenate ( $SeO_4^{2-}$ ), and iodide (I) and CDP. Iodide did not sorb to the sediments. Perrhenate sorbed at very low concentrations and was inversely related to pH and was not influenced by fulvic acid concentration additions. Selenate sorbed very strongly to the sediment; the *Kd* values were >1040 mL/g for the sandy and clayey sediments at most pH and fulvic acid concentrations.

### 3.4.2 Colloid-Facilitated Transport of Contaminants

**Introduction:** Contaminant transport is traditionally modeled in a two-phase system: a mobile aqueous phase and an immobile solid phase. Over the last 15 years, there has been an increasing awareness of a third phase, a mobile solid phase, or colloidal phase. Mobile colloids consist of organic and/or inorganic submicron-particles that move with groundwater flow. When radionuclides are associated with colloids, the net effect is that radionuclides can move faster through the system than would be predicted without including colloids. This mode of contaminant transport has recently come to the forefront because of the discovery of Pu on colloids 1.3 km from their source at the Nevada Test Site (Kersting et al. 1999). Reviews of colloid-facilitated transport of contaminants have been presented by McCarthy and Degueudre (1993), McCarthy and Zachara (1989), and most recently by Kretzschmar and Schafer (2006).

Mobile colloid formation is commonly described as a three-step process: genesis, stabilization, and transport. Colloid genesis describes how the submicron particles are formed in groundwater. Stabilization describes how the colloids are brought into suspension, which is a function of the colloid and groundwater composition and water flow forces. Transport describes how the suspended colloids move through the porous media or are retained by physical forces (such as diffusion, straining, or gravitational settling) or physicochemical attraction to the matrix.

Regarding the first step, colloid genesis, there is little doubt that radionuclide-bearing colloids will be generated at the E-Area and Z-Area disposal sites. Ramsay (1988) presented strong evidence for the existence of colloid particles in glass and cement leachate and provided an in-depth review of the various types of colloids that can/may exist (e.g., glass fragments, precipitation products, geological materials, secondary phases formed from glass leachate). However, it is not clear whether environmental conditions at the SRS are conducive for colloid stabilization and subsequent transport.

Field studies of colloid facilitated transport of Pu have been studied on the SRS by two groups, the University of Georgia/SRNL (Kaplan et al. 1994)<sup>2</sup> and Woods Hole Oceanographic Institution (Dai et al. 2002). Together their results indicate little or perhaps no colloidal transport of Pu occurs. Kaplan *et al.* (1994) measured Pu associated with a filterable fraction in groundwater recovered in F-Area, near the E-Area burial grounds and the Saltstone disposal facility. This filterable fraction was presumed to be a colloidal fraction based on specialized low flow collection and filtering techniques. Very little Pu was found in association with colloids, 0.003 pCi/L <sup>239/240</sup>Pu. To put this concentration in perspective, the Maximum Contaminant Level (MCL) for <sup>239/240</sup>Pu is 15 pCi/L (Federal Register, Vol. 65, No. 236, December 2, 2000); thus the amount found associated with colloids was 5000 time less than the MCL. Even though these are small amounts, the point of studying Pu at this site is that 1) Pu can be detected, 2) it has a known source (more on this below), and 3) the study

Pu transport is enhanced by colloids at the SRS. However, the Pu concentration is extremely low, <5000 time below the drinking water standard. We study Pu in this system because it provides a good tracer from a well defined source from a very well characterized system (F-Area).

<sup>2</sup> Kaplan et al. (1994) also detected Th, U, Am, Cm and Ra on colloids, and the fraction of radionuclides associated with colloids increased as: Pu > Th > U > Am = Cm > Ra.

site is a very well characterized with >200 wells and >20 years of groundwater monitoring history.

The percentage of Pu retained by filters, increased as the pH of the plume increased, which was also coincidental with distance from the point source. Inversely, the percentage of Pu that passed through the smallest membrane, 500 molecular weight cutoff (MWCO; ~0.5 nm) decreased with distance from the point source. The ratio between the Pu concentration of colloids in well water and liquid in the source zone did not change in a systematic manner with distance (or pH) in the field (Kaplan et al. 1994).

Dai et al. (2002) also conducted a colloid study in F-Area and concluded that colloids were not involved in Pu transport. The difference between these two results, Kaplan et al. (1994) reporting little colloidal Pu and Dai et al. (2002) reporting no colloidal Pu, may be attributed to the latter sampling some eight years later in a somewhat more basic pH plume and to significant differences in sampling and analytical techniques. Dai et al. (2002) used more sensitive analytical methods but larger molecular weight cut-off membranes (permitted larger particles to pass through (1000 MWCO (~1 nm)) to separate colloidal from the dissolved fractions than those used by Kaplan et al. (1994; 500 MWCO, (~0.7nm)).

Woods Hole Oceanographic Institution and the SRNL returned to F-Area in 2004 to characterize changes in Pu oxidation states and Pu association with colloids in groundwater samples collected six years earlier (Buessler et al. 2009). They reported small concentrations of Pu associated with colloids. The percentage of Pu associated with colloids, 1 to 23%, was less than that reported by Kaplan et al. (1994), 28 to 100%, but was more than that reported by Dai et al. (2002), 0 to 10%. They concluded that Pu moved primarily in the dissolved state (and in the higher Pu oxidation states). They reported that colloidal Pu increased systematically with decreases in redox conditions. They observed greater dynamic shifts in Pu speciation, colloid association, and transport in groundwater on both seasonal and decadal time scales and over short field spatial scales than commonly believed.

**Colloid Model:** Modeling colloid facilitated transport of radionuclides in the SRS subsurface environment is greatly hindered by the paucity of data on the subject. Measurements presented by Kaplan et al. (1994), Dai et al. (2002), and Buessler et al. (2009) were conducted in the F-Area Seepage Basin plume, which is very acidic, pH 3 to 5.5 (background). As such it does not reflect conditions expected in any of the PA scenarios. In fact, if anything, plumes of interest to SRS PAs will likely have a background or alkaline pH due to the common use of cementitious engineered barriers (Section 5.0). Given this important caveat, the Pu concentration carried by colloids, based on F-Area results, were thousands of times below the MCL (15 pCi/L), even though an estimated 7,000,000,000 pCi of <sup>239/240</sup>Pu was disposed in the seepage basins. At higher pH systems than that of F-Area, it is likely that colloids would play a greater role in transporting contaminants. It is difficult to determine to what extent more mobile colloids would exist in the various plumes of interest to the PA. If the number of colloids increases by a couple orders of magnitude above that detected in F-Area, it is likely that the groundwater concentration of strongly sorbing contaminants, like Pu, Ac, Am, Cm, Eu, or Th, would increase due to the rise of their association with colloids. It is not clear that this increase would necessarily result in exceeding MCL limits.

Kaplan (2006b) conducted a series of colloid dispersion experiments using SRS sediments as a function of ionic strength (the amount of salts in solution), pH, and soil type. pH values had a significant effect on the dispersion of five SRS sediments. At background sediment pH values (pH 4.2 to 5.9), there was minimal tendency for clays to disperse. As the pH was increased, there was generally a critical pH above which dispersion occurred sharply. This critical pH was between 5.7 and 6.2. These findings have implications to the Low-Level waste disposal systems where cementitious materials are present. Cementitious materials will likely elevated pH conditions above ambient levels. However, cementitious materials also create leachates that have chemical properties that resist colloid dispersion, namely they have higher ionic strengths and greater divalent cation concentrations than typical Savannah River Site groundwaters. (Divalent cations tend to flocculate suspensions, whereas monovalent cations tend to be more dispersing.) Future studies are planned to address the specific impact of cementitious leachate on colloid dispersion properties. Perhaps more importantly, there is need for the development of a site-specific conceptual model that would take into consideration potential mobile colloid generation induced by pH changes propagated by ionic strength and pH changes induced by cementitious leachate. Although a great deal was learned from the F-area plume (pH 3 to 4.5), it is imperative to transfer that knowledge to an elevated pH scenario (pH 5 to 9).

#### 4.0 CONCEPTUAL GEOCHEMICAL MODEL

To facilitate modeling the wide range of chemical conditions needed for performance assessment and composite analyses on the SRS, 12 Environments were established. These conceptualized Environments account for important geochemical parameters influencing radionuclide sorption within a particular setting. As such, the Environments provide general descriptions of important aqueous and mineralogical environmental parameters influencing radionuclide interaction with the solid phase. Following is a list of each Environment and a reference to the section in which they are described in more detail:

1. Clayey Sediment (described in more detail in Section 4.1.1),
2. Sandy Sediment (Section 4.1.2),
3. Cellulose-degradation Produce (CDP) Impacted Clayey Sediment (Section 4.1.3),
4. CDP-Impacted Sandy Sediment (Section 4.1.4),
5. Young Cementitious Solids (Section 4.2.1),

*Environments* are conceptualized subsurface settings with defined aqueous, mineralogical, and solid phase properties that influence radionuclide sorption.

6. Moderately-aged Cementitious Solids (Section 4.2.2),
7. Aged Cementitious Solids (Section 4.2.3),
8. Cementitious-Leachate Impacted Sandy Sediment (Section 4.2.4),
9. Cementitious-Leachate Impacted Clayey Sediment (Section 4.2.5),
10. Cementitious-Leachate and CDP Impacted Sediments (Section 4.2.6),
11. Young Reducing Cementitious Solids (Section 4.3.1),
12. Moderately-aged Reducing Cementitious Solids (Section 4.3.2),
13. Aged Reducing Cementitious Solids (Section 4.3.3),
14. General Waste Forms (Section 4.4), and
15. Special Waste Forms (Section 4.5).

For each Environment, 62  $Kd$  values and/or apparent solubility values are provided. For each element and Environment a “best,” “minimum,” and “maximum” estimate of the  $Kd$  values and/or apparent solubility concentration limits are provided.<sup>4</sup> The “best” estimates are presented to provide guidance on what the most likely  $Kd$  values and apparent solubility concentration limits are for a given condition. These values are based primarily on some central value of the literature, SRS site-specific experimental data, or on expert judgment.

Ideally, all input data would be derived from experiments conducted under the appropriate Environment. For example, much of the Clayey Sediment and Sandy Sediment  $Kd$  data was, in fact, derived from sorption experiments conducted with site-specific sediments. Where site specific data was not available, chemical analogues were used. For example, no site-specific sorption data is available for Fr (francium) and Rb (rubidium), however, a great deal of SRS sediment sorption data is available for Cs. Cesium behaves chemically very similarly to Fr and Rb, all three elements are in Group 1A in the periodic chart, have a +1 valence, form weak complexes, and exist in groundwater primarily as an uncomplexed monovalent free ion. For that reason, Fr and Rb  $Kd$  values were approximated, using the measured Cs  $Kd$  values. Where site specific data and reasonable analogues were not available, literature values were used. Careful selection of these literature values was required to make sure that the experimental conditions used to generate the  $Kd$  values were appropriate for SRS conditions. Professional opinion and geochemistry experience were used where non-site-specific data were available and where possible experimental evidence was provided to support technical judgment. “Literature  $Kd$  values” are viewed as having a lower pedigree than those  $Kd$  values derived from site specific conditions.

In summary, a ranking of the priority for selecting  $Kd$  values and apparent solubility concentration limits follow:

---

<sup>4</sup> In the previous versions of this document (Kaplan 2007), a “reasonably conservative” value was provided. This term was replaced with the “minimum” value, which has a different definition. The “reasonably conservative” term represent lower-bounding values that take into consideration the range of physical, chemical, and mineralogical conditions that often lead to enhanced radionuclide migration. The “reasonably conservative” value was ideally based on the lower limit of multiple  $Kd$  value measurements or the upper limit of solubility measurements. In the absence of sufficient data, the “reasonably conservative” value was based on an assumed range of values, using the “Best” value as the central point in the range. For large values ( $Kd$  or solubility concentration limits  $\geq 1000$  mL/g), a range of an order of magnitude was used and for small  $Kd$  values or solubility concentration limits, a range of two fold was used.

1. Site-specific measured data,
2. literature experimental data, and
3. technical judgment.

The “minimum” and “maximum” estimates were based on experimental work conducted by Grogan et al. (2008)<sup>5</sup> and Kaplan et al. (2009). In these data, *Kd* distributions and the 95% confidence levels were estimated in 27 E-Area subsurface sediments for monovalent, divalent, trivalent and tetravalent radionuclide cations and  $\text{TcO}_4^-$ . The “minimum” and the “maximum” were set to the estimates of the lower and upper boundaries of the 95% confidence limits, respectively (discussed in Section 4.6).

The low level radioactive waste has several different forms and as a result there are several different types of facilities to dispose of this waste. They include paper, plastics, wood, cloth, spent ion exchange resins, metal, concrete debris, and glass. The degree to which the various radionuclides sorb to each material is largely unknown. Therefore, the simplifying assumption was made that unless waste-form specific data was measured (discussed in Section 4.5), the extent that a radionuclide sorbs to the waste form was assumed to be similar to the extent that the radionuclide sorbs to the solid phase immediately in contact with the waste. Radionuclide leaching from waste materials is discussed in Section 4.4.

Unless waste-form specific data is available, the extent that a radionuclide sorbs to the waste form will be set equal to the extent that the radionuclide sorbs to the solid phase (sediment or cement) immediately in contact with the waste.

## 4.1 Sediments

The subsurface environment beneath and near the waste units in E- and Z-Areas are assumed to consist of two primary geological strata. This simplification of the subsurface is taken from Phifer et al. (2006) and was based on particle-size distribution data and observations of several borehole specimens made in the E-Area subsurface environment. Phifer et al. (2006) describe the upper strata as extending about 7 m below the surface and having a finer texture than the lower strata, which may extend some 27 m below ground surface. The upper layer has been referred to as the Upper Vadose Zone, whereas the lower zone includes both the Lower Vadose Zone and the Aquifer Zone. The water table in E- and Z-Area is approximately 15 to 25 m below the ground surface. Additional information regarding the surface aquifer, the groundwater monitoring well program, and groundwater communication between the unconfined and confined aquifers may be found in McDowell-Boyer et al. (2000). An example of the texture of an E-Area borehole, delineating the Upper and Lower Vadose Zone and the Aquifer Zone is presented in Figure 3.

There were unique sorption values for a Clayey Sediment and a Sandy Sediment Environments, meant to represent the Upper Vadose Zone and Lower Vadose/Aquifer Zones, respectively. As mentioned above, site-specific data were used whenever possible. However,

<sup>5</sup> A manuscript using some of the data generated in Grogan et al (2008) is presently in review: Grogan, K, R. A. Fjeld, D. I. Kaplan, T. DeVol, and J. D. Coates. 2010. Distributions of Radionuclide Sorption Coefficients ( $K_d$ ) in Subsurface Sediments and Their Implications to Transport. Journal of Environmental Radioactivity. (In Review).

where site-specific data were lacking, literature-derived data were used. Also important to note is that the data provided in the data look-up table in Section 5.0 is broken down for each of the 12 Environments. The extent that environmental conditions deviate from their “ideal” descriptions in this section, compromise the applicability of the selected data values. For example, the *Kd* values provided for a Sandy Sediment Environment or a Clay Sediment Environment would not be especially applicable for a wetland because the “ideal” description is for a subsurface sediment with a much lower organic matter content than for a typical wetland.

#### **4.1.1 Clayey Sediment Environment**

The Clayey Sediment Environment was conceptualized as a subsurface sediment containing a clay and silt content 25 to 45 wt-%, the mineralogy composed primarily of kaolinite, hydroxyl-interlayered vermiculite, quartz, gibbsite, goethite, and hematite (most notable about its mineralogy is that it contains very low concentrations of 2:1 clays, such as smectites and vermiculites); organic matter concentration is low (<0.01 wt-%); pH is 5.5; and the sediment is covered with Fe-oxides, giving it a reddish color.

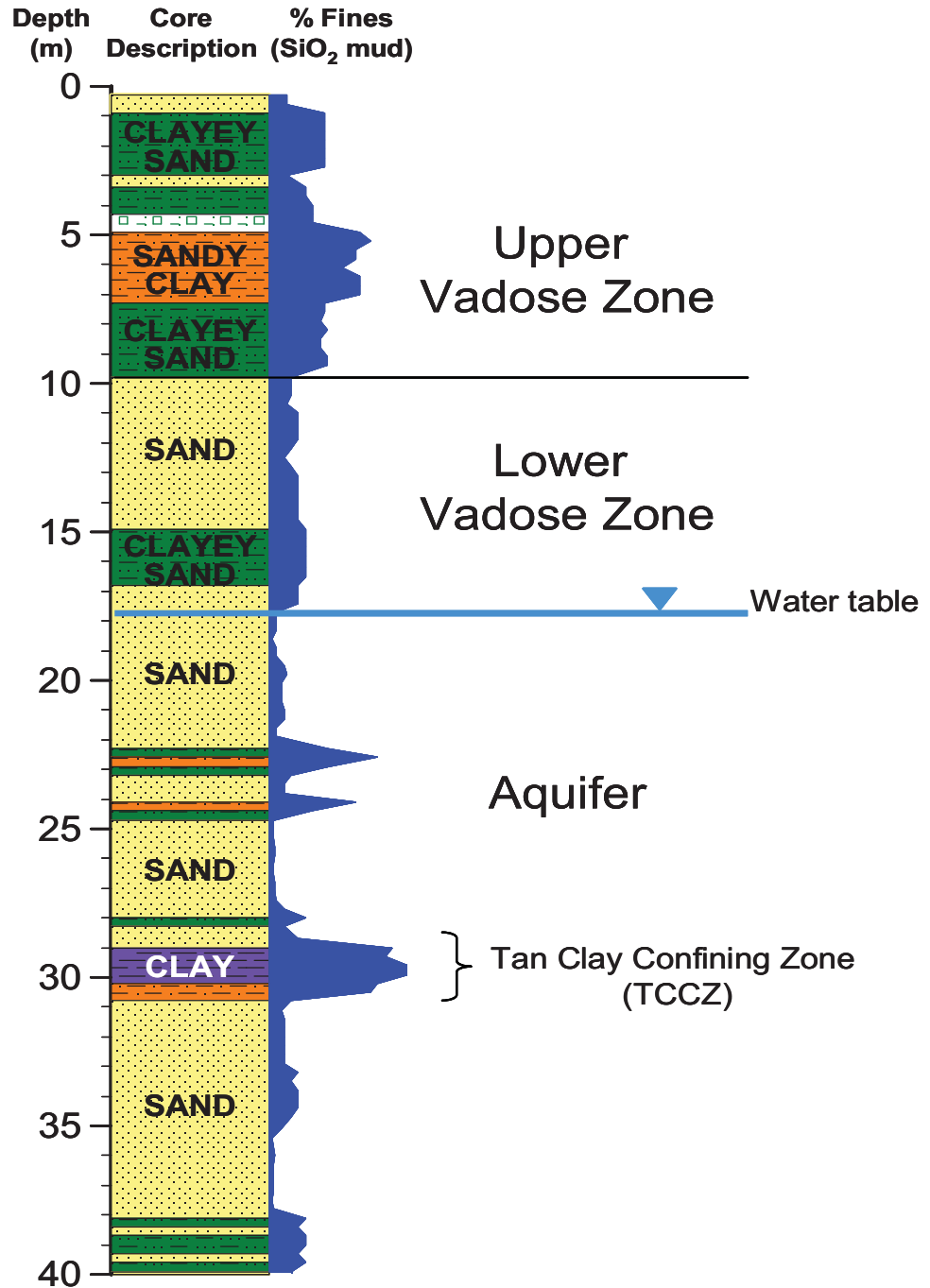


**Figure 3.** Example of an actual borehole profile in E-Area demonstrating the tendency for sediments with a more clayey texture to exist in the Upper Vadose Zone, whereas sediments with a sandier texture exist in the Lower Vadose and Aquifer Zones (Well BGO-3A, Grogan et al. 2008; Grogan et al. 2010).

#### 4.1.2 Sandy Sediment Environment

The Sandy Sediment Environment was conceptualized to have identical properties as the Clayey Sediment except the clay and silt content was <25 wt-%. Most of the sorption experiments from which data was considered for the look-up tables came from sandy sediments with clay and silt concentrations appreciably <25 wt-%, closer to 8 to 12%. The pH is 5.5, there is low organic matter concentrations, and the sediment tends to have a yellowish color derived from Fe-oxide coatings (most noticeably, goethite).

#### 4.1.3 Cellulose-Degradation-Product (CDP) Impacted Clayey Sediment, Environment

The CDP-Impacted Clayey Sediment Environment contains relatively high concentrations of CDP relative to background conditions of the Clayey Sediment Environment (Section 4.1.1). CDP will influence the tendency of radionuclides to sorb to sediments, and therefore to move away from the buried waste. Several laboratory studies and surface complexation models have been conducted to evaluate this phenomenon (Serkiz et al. 1998, Serkiz et al. 1999, Kaplan and Serkiz 2004, Serkiz and Kaplan 2006; Kaplan et al. 2010). From these studies, the amount of sediment clay content, pH, organic C content, contact time, and order of addition were evaluated. CDP-Correction Factors,  $f_{CDP,pH,C}$ , were estimated from this work that varied as a function of pH and organic carbon content:

$$f_{CDP,pH,C} = \frac{Kd_{CDP,pH,C=x}}{Kd_{pH,C=0}} \quad (6)$$

As is the case with all  $Kd$  values,  $f_{CDP,pH,C}$  values are also very sediment specific. The numerator,  $Kd_{pH,C=x}$ , is a measure of the radionuclide  $Kd$  value with a sediment at a given pH and organic carbon content dissolved in the solution. The denominator,  $Kd_{pH,C=0}$  is a measure of the radionuclide  $Kd$  value with the same sediment and the same pH, but without any cellulose degradation products present in the solution. The CDP-correction factor was used to calculate a CDP-corrected  $Kd$  value,  $Kd_{CDP}$ :

$$Kd_{CDP} = f_{CDP} \times Kd. \quad (7)$$

For the purposes of this document, the  $Kd$  values used to calculate  $Kd_{CDP}$  were calculated by multiplying the  $Kd$  values in Table 13 by the  $f_{CDP,pH,C}$  values presented in Table 21 (the later were taken from Table 14 in Serkiz and Kaplan (2006) and Table 7 in Kaplan and Serkiz (2006)).

Overall, it is important to realize that CDP generally increased  $Kd$  values at low CDP concentrations, and it was not until much greater concentrations that  $Kd$  values decreased.

The experimental work included monovalent ( $Cs^+$ ), divalent ( $Ni^{2+}$ , and  $Sr^{2+}$ ), trivalent ( $Ce^{3+}$  and  $Eu^{3+}$ ) and tetravalent ( $Zr^{4+}$  and  $Th^{4+}$ ) cations and anions (iodide, perrhenate, and selenate) at three pH and 5 organic C concentrations (Kaplan et and Serkiz 2004; Kaplan and Serkiz 2006).

A detailed description of the application of surface complexation speciation modeling of Eu sorption to SRS sediments in the presence of CDP as a function of pH is presented by Kaplan et al. 2010. The sorption results for these specific species were then applied as analogues to provide estimates of how other radionuclides with similar chemical properties may behave. The laboratory results were consistent with expected results based on considerations of the relative strengths of ligand bonds between radionuclides and organic matter, versus organic matter-sediment surface bonds, versus radionuclide-sediment surface bonds. An example of the data showing Eu sorption to clayey and sandy SRS sediment is provided in Figure 5. Additional data of other radionuclides is presented in Section 9.0: Appendix A: Additional Information Regarding Cellulose -Degradation-Product Correction Factors For  $K_d$  Values. In some cases an increase in dissolved organic C concentrations resulted in a systematic decrease in  $K_d$  values. In other cases, the presence of dissolved cellulosic materials resulted in an increase in  $K_d$  values at low organic C concentrations ( $\leq 95$  mg C/L) and a decrease in  $K_d$  values at highest organic C concentration (222 mg C/L; except for Cs). This occurred because the organic carbon partitioned onto the sediment surfaces and increased the sorption capacity of the sediment (which has a relatively very poor sorption capacity, a cation exchange capacity of SRS sediment is commonly between 1 and 3 meq/100 g).

Overall, it is important to realize that CDP generally increased  $K_d$  values at low CDP concentrations, and it was not until much greater concentrations that  $K_d$  values decreased.

The  $K_{dCDP}$  will be employed as long as cellulosic degradation materials emanate from the waste. For each waste source containing CDP (see Table 3 for a list of disposal units that contain CDP), the total amount of CDP (in units of mass of organic carbon) will need to be estimated. The conceptual model underlying the reactive transport models will release carbon into the groundwater from the CDP at a constant concentration (rate) of **5 mg/L C** until all the carbon in the CDP is exhausted. This value is based on an average of 5.2 mg/L TOC estimated from 158 field total organic carbon (TOC) measurements taken in groundwater samples collected from near or beneath the Low-Level Waste Burial Grounds between October 1982 and June 1985 (Ryan 1983 and reviewed in McIntyre and Wilhite 1987). Because there are few, if any, TOC measurements from beneath the E-Area Slit Trenches, this is an ideal analogue site because it received CDP waste in a similar capacity and purpose as E-Area and it is located in an adjoining field site, as close as 70 m from some of the Slit Trenches (Figure 4). The 5 mg/L value represents the average concentration expected in the entire source term. As such, the average groundwater TOC value measured under the Low-Level Waste Burial Grounds provides an ideal analogue site in terms of similarity of type of waste, sediment moisture content (the primary control on microbial activity that regulates CDP degradation rate), type of sediment, and waste handling practices. Conceptually, the TOC concentrations are expected to be extremely high, several hundred mg/L within centimeters of the aging cellulosic source, such as paper, but the concentrations are expected to quickly dilute as it gets further away from this source, such as in the middle of disposed concrete rubble piles. The 158 TOC samples provided a volume averaging that was

It was previously assumed that CDP would leach from the source terms at a constant rate of 95 mg/L. This rate was selected to produce the general lowest set of  $K_d$  values. The best estimate is now believed to be 5 mg/L C CDP based on data collected from an adjoining site on the SRS. This results in CDP impact factors that do not lower the  $K_d$  values greatly.

collected close to the buried waste at the LLW Burial Sites offer excellent insight as to TOC concentrations close to the source.

Short-term laboratory leach experiments with various solids containing the precursors to CDPs can create a wide range of organic C concentration in solution depending on the solid to liquid ratio, types of solids used, and age of suspension (Serkiz et al. 1998, Serne et al. 1993). To provide some context, a 20 mg/L organic C solution has a slight yellow color to it. A 95 mg/L organic C solution is highly colored and produces a translucent yellowish-orange solution.

All  $f_{\text{CDP}}$  values will be taken from experimental data generated at 20 mg/L (no 5 mg/L C experimental data is available) (Kaplan and Serkiz 2004, Table 14; Kaplan and Serkiz, Table 7).



**Figure 4.** Examples of waste disposed in the Low Level Waste Burial Ground. Note the disposal of cellulose degradation products similar to present waste disposal in E-Area Slit Trenches presented in Figure 9.

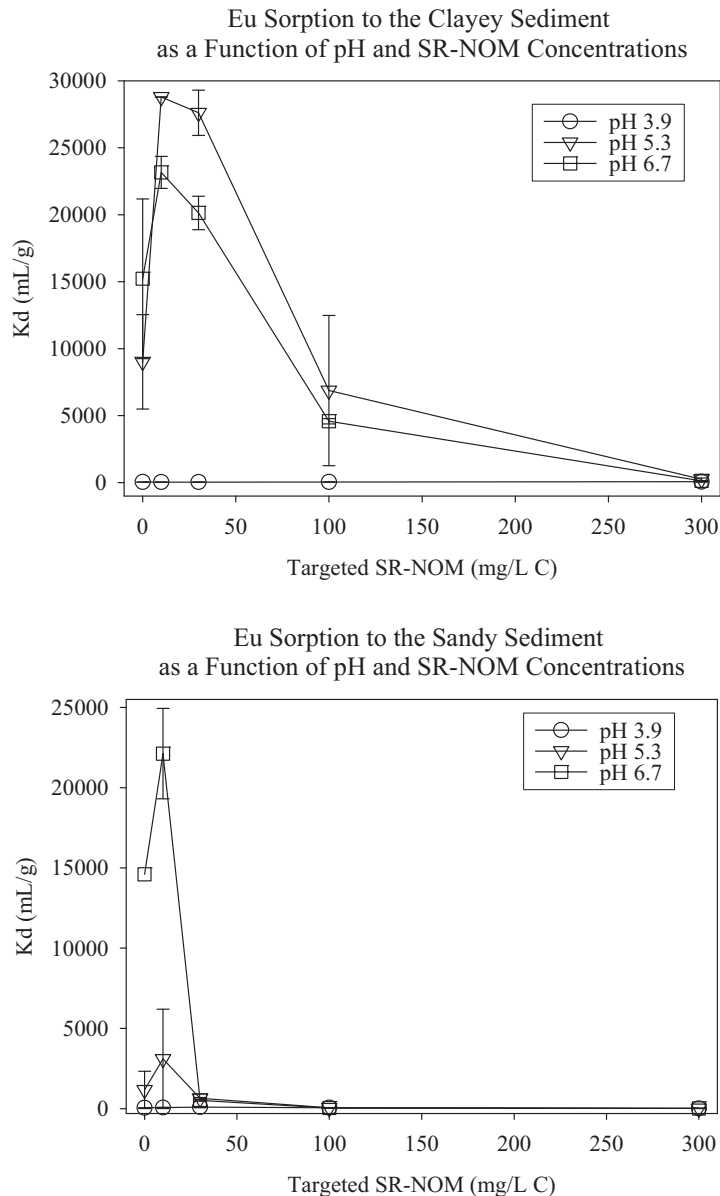


**Figure 5.** Eu  $K_d$  values as a function of pH and SR-NOM concentrations in clayey (top) and sandy (bottom) sediments (all  $K_d$  values  $>20,000$  mL/g are greater-than values).

Kaplan and Serkiz (2006) conducted CDP-corrected  $K_d$  measurements with  $\text{TcO}_4^-$  (pertechnetate),  $\text{SeO}_4^{2-}$  (selenate), and I (iodide). Using fulvic acid as an analogue for CDP, and perrhenate ( $\text{ReO}_4^-$ ) as an analogue for  $\text{TcO}_4^-$ , they concluded that CDP- $K_d$  I values for I and Tc will not differ from non-CDP-impacted  $K_d$  values. Selenate sorbed very strongly to the sediment; the  $K_d$  value was  $>1040$  mL/g for the sand and clay sediments at most pH and fulvic acid concentrations. In the sandy sediment, but generally not in the clayey sediment, as the fulvic

acid concentrations increased, the selenate  $Kd$  values decreased. These are the first  $\text{SeO}_4^{2-}$  sorption tests using SRS sediments; therefore they provide site specific values for both CDP and regular conditions.

As mentioned briefly above, more sophisticated modeling of the influence of CDP on Eu sorption to SRS sediments has been developed using surface complexation modeling, component additivity model, and thermodynamic calculations (Kaplan et al. 2010). This model is more dynamic and robust than the simple  $Kd$  approach presented here, being applicable to a wide range of dissolved organic carbon contents (CDP), 0 to 200 mg/L C, and pH levels 4 to 7. However, it is modeling intensive and we do not have enough input parameters for all 55 radionuclides of interest for the PA.

#### 4.1.4 CDP-Impacted Sandy Sediment Environment

The CDP-Impacted Sandy Sediment Environment contains relatively high dissolved organic matter relative to the Sandy Sediment Environment (Section 4.1.2).  $Kd$  values are calculated the same way as those used in the CDP-Impacted Clayey Sediment Environment except instead of using  $Kd$  values for a Clayey Sediment Environment, values for a Sandy Sediment Environment are used (Section 4.1.3).

## 4.2 Cementitious Materials

The conceptual model used to describe radionuclide geochemistry in cementitious environments was taken from Bradbury and Sarott (1995). They described three types of physicochemical environments, or stages, that all cements and cementitious materials progress through as they age (Figure 6). As such, these three stages represent the progression that all types of cementitious materials would undergo as they age. The duration of each stage is controlled by how much pore water (and to some extent the water chemical composition) passes through the cement, thereby promoting cement degradation; as can be seen by the exchange cycles, or pore volumes, the X-axis of Figure 6.

Cementitious materials are assumed to progress through three stages as they age. Each stage has unique physical, mineralogical, and chemical properties, resulting in unique  $Kd$  and/or solubility concentration limits for each stage.

The advantage of using Figure 6 and the concept of exchange cycles is that it is generic in nature. Once flow models have been established for a specific facility, the exchange cycles for that facility can be quantified. Facilities with more concrete will have larger exchange cycles than those with less concrete.

Development of this conceptual model was based on laboratory studies as well as on natural analogue and ancient cement/concrete characterization studies. One of the key aqueous parameters used to identify when one stage ended and the next one started was pH (Figure 6). The pH changes are the result of mineralogical transformations that occur as the cement ages. The cement solids present in each stage are assumed to have unique sorption properties and for this reason, unique  $Kd$  values and solubility concentration limits were assigned to the cement solids in each stage. A brief description of each of the three stages is described below in

Sections 4.2.1 through 4.2.3, while a more detailed discussion is presented in Bradbury and Sarott (1995) and Krupka and Serne (1998). Unique  $K_d$  values and solubility concentration limits for oxidizing and reducing cementitious materials is provided (Section 5.0). Reducing cements are used to enhance the immobilization of certain redox-sensitive radionuclides, such as Tc, U, and Np, and are created by adding blast-furnace slag to the cement mixture. Because no SRS site-specific sorption data were identified for cementitious materials, the values included in the look-up tables came entirely from the literature (Table 17 through Table 20).

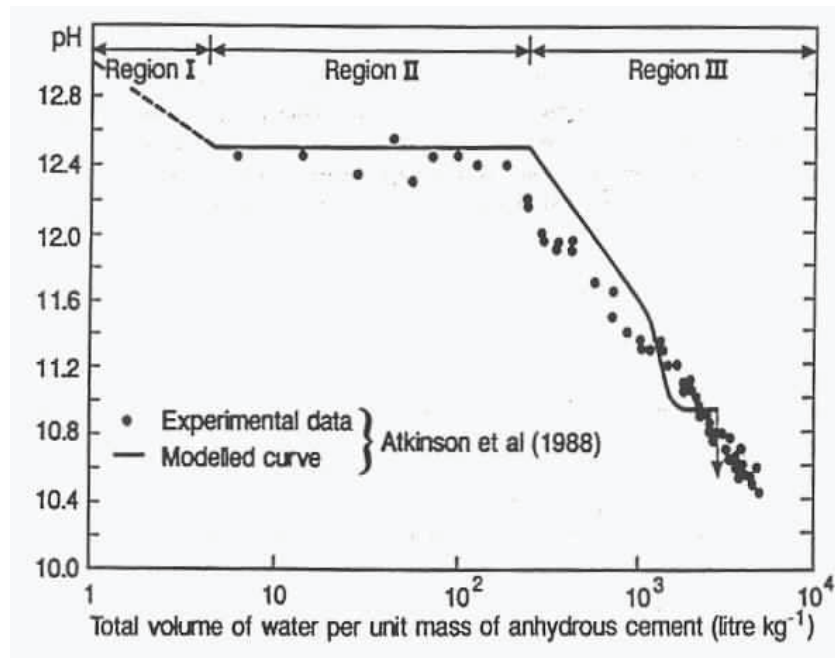


Figure 6. Conceptual model used by Bradbury and Sarott (1995) describing the influence of exchange cycles (X-axis) on pH and the designated Stages (or regions) (Atkinson et al. 1988).

#### 4.2.1 Young Cementitious Solids (1<sup>st</sup> Stage) Environment

The Young Cementitious Solids Environment of the 1<sup>st</sup> Stage occurs immediately after the cement hardens and infiltrating water passes through it. The cement porewater is characterized as having a high pH (>12), high ionic strength, and high concentrations of potassium and sodium. The high concentrations of these monovalent cations result from the dissolution of alkali impurities in the clinker phases. Hydration continues during the 1<sup>st</sup> Stage with the formation of calcium-silicate-hydrate gels (a common shorthand for this gel is C-S-H, which is a CaO-SiO<sub>2</sub>-H<sub>2</sub>O amorphous material that hardens and constitutes “cement”) and Portlandite [Ca(OH)<sub>2</sub>]. The composition of the cement pore fluid is at equilibrium with Portlandite during this time.

Based on the modeling estimates provided by Berner (1992), the 1<sup>st</sup> Stage may last between 1 and 100 exchange cycles. An exchange cycle, or cycle, is a unitless parameter that represents the

cement pore volume, *i.e.*, the length of time it takes for a pore volume to pass through a cementitious system. This in turn can be quickly converted into units of time once the water travel rate through a specific cementitious facility is established. Unfortunately, assuming a low exchange cycle value for this stage may be conservative for some elements, such as Pb, while not conservative for other elements that tend to form precipitates at high pH values (*i.e.*, have high *Kd* values and low solubility concentration limits). Therefore, it was assumed that the 1<sup>st</sup> Stage lasts 50 exchange cycles for SRS relevant scenarios.<sup>6</sup>

For a calculation related to Pb leaching from a Components-in-Grout Trenches, Kaplan and Myers (2001) assumed the 1<sup>st</sup> Stage was 70 exchange cycles (not 50 exchange cycles as recommended here). Because this is the stage in which the lead solubility was at its highest, producing the highest dissolved lead concentrations<sup>7</sup>, a conservative assumption would be to assume the stage lasts 100 cycles. However, because diffusion is an important chemical process influencing the leachate chemistry, the low ionic strength and low inorganic carbon concentration of SRS groundwater will likely limit the concrete/cement aging process occurring during this stage, thereby lengthening the duration of this stage. Carbonate reacts with Ca from the calcium-silicate-hydrate gel (CHS) to promote degradation. Another reason for selecting 70 cycles for the duration of the 1<sup>st</sup> Stage was for convenience. The PA for the E-Area LLW Facility assumed the concrete infiltration rate was 4 cm/yr for the first 1050-years; 70 cycles corresponds to 1050 years (assuming 60-cm thick concrete/cycle, 4-cm/yr) (Kaplan and Myers 2001).<sup>8</sup>

#### 4.2.2 Moderately-aged Cementitious Solids (2<sup>nd</sup> Stage) Environment

During this stage, the soluble salts of the alkali metals are all dissolved and washed out of the cement solids. The pH of the cement pore water is controlled at a value of ~12 by the solubility of portlandite. The calcium-silicate-hydrate gel and portlandite are the major solid phases present. The 2<sup>nd</sup> Stage may last for a long time, and its duration depends on how much water percolates through the system and the mass of cement present in the concrete structure. The total dissolved calcium is 20 mM, the pH is strongly buffered at pH ~12, and the silica concentration is very low, <0.03 mM/L. The flux of water must dissolve all the slightly soluble portlandite before the leachate chemistry changes.

Concrete in the 2<sup>nd</sup> Stage binds most radionuclides relatively strongly, and the porewater buffered at pH ~12. It is anticipated to last 500 exchange cycles (pore volumes).

Berner (1992) determined that the 2<sup>nd</sup> Stage lasts between 100 and 1000 cycles. According to the Bradbury and Sarott (1995) and adopted here, most radionuclides have higher *Kd* values and solubility concentration limits in the 2<sup>nd</sup> Stage than in the 3<sup>rd</sup> Stage. Therefore, a lower 2<sup>nd</sup> Stage

<sup>6</sup> This value of 50 exchange cycles or pore volumes is a recommended value if a project-specific value is not calculated using a reactive transport model. For example, for calculations associated with the SRS Liquid Waste Tanks Closure PA, a reactive transport model was using based a site specific data to estimate transitions between Stages 1, 2 and 3 (Denham 2009)

<sup>7</sup> Based on thermodynamic calculations presented in Kaplan and Myers (2001), as the pH increases from 12.2 to 12.8, the solubility of  $\text{Pb}(\text{OH})_{2(\text{solid})}$  sharply increases and the concentration of  $\text{Pb}(\text{OH})_{4}^{2-}(\text{aq})$  increases. At pH 12.8, all of the Pb solid was total dissolved.

<sup>8</sup> 70 exchange cycles x 60-cm cement/exchange cycle x 1/4 yr/cm = 1050 years

lifespan is conservative. The 2<sup>nd</sup> Stage  $Kd$  values and solubility concentrations limits are generally higher lower than those in the 1<sup>st</sup> Stage, except in the case where cation exchange is the predominant sorption mechanism, in which case the  $Kd$  in the 1<sup>st</sup> Stage will be lower due to high salt concentrations in the porewater. Taking into consideration the slow dissolving attribute of the low-carbonate SRS groundwater when in contact with cementitious solids, an exchange cycle of 500 cycles was assumed.

#### 4.2.3 Aged Cementitious Solids (3<sup>rd</sup> Stage) Environment

In the 3<sup>rd</sup> Stage, the portlandite has been fully dissolved/reacted and the solubility or reactions of calcium-silicate-hydrate gel with the infiltrating water controls the pH of the cement porewater/leachate (Figure 6). The calcium-silicate-hydrate gel starts to dissolve incongruently<sup>9</sup> with a continual decrease in pH until it reaches the pH of the background sediment, pH 5.5. At the end of this evolution, the 3<sup>rd</sup> Stage can be conceptualized as leaving only silica (SiO<sub>2</sub>) as the solubility control for the pore water pH. The ionic strength of the cement leachate during this period is relatively low and its pH drops to ~10 and lower over long times. Solution calcium concentrations decrease to 1- to 5-mM and silica concentrations increases to 2- to 6-mM. At very high cycle numbers, other sparingly soluble solids, such as brucite [Mg(OH)<sub>2</sub>], may buffer the solution pH and dissolved cation concentrations.

Concrete in the 3<sup>rd</sup> Stage binds radionuclides the least, and the porewater buffered by the CSH gel at pH10 to 5.5, SRS background pH. It is anticipated to last 7000 exchange cycles (pore volumes).

Berner (1992) suggested that the duration of the 3<sup>rd</sup> Stage is between 1000 and 10,000 cycles. Because SRS groundwater is low in carbonate concentrations, a longer duration for this stage would be appropriate; a “lifetime” of 7000 cycles was selected for the SRS PA calculations. A discussion of estimating the longevity of concrete in the subsurface, with an example of how environmental conditions at SRS are favorable because of low dissolved carbonate concentrations, is presented in Appendix B: Cement Lifespan.

#### 4.2.4 Cementitious Leachate Impacted Clayey Sediment Environment

Cement porewater contains moderate levels of dissolved solids, resulting in the chemistry of the water altering once it passes through it. Demonstrating this point under SRS conditions, Dr. Miles Denham (SRNL, personal communications) conducted thermodynamic simulations passing SRS groundwater through concrete as it degraded through three successive idealized phases: Stage I when Portlandite is the dominant phase controlling solid phase dissolution; Stage II when calcium-silicate-hydroxide (CSH) gel is the dominant phase; and Stage III, when calcite is the dominant phase (Table 1). The most important point to take away from this table is that the pH and ionic strength (*i.e.*, the porewater’s salt content) during the two early stages of cement aging, Stages I and II, are very different from the background SRS Groundwater. The leachates have a much higher pH and ionic strength. Such background solutions increase

<sup>9</sup> Incongruent dissolution is dissolution to give dissolved material in different proportions from those in the original solid.

sorption via promoting precipitation, *e.g.*,  $\text{UO}_2^{2+}$  (Kaplan et al. 1998), and in other cases decreasing sorption via competing for sorption sites (Kaplan et al. 1998; Cantrell et al. 2007). For example, using Hanford sediment Kaplan et al. (1998) showed that Se had  $Kd$  values of 6 mL/g under natural groundwater conditions (pH 8.1). When the ionic strength was increased the  $Kd$  values decreased ( $Kd = 4.11$  at 1 M  $\text{NaClO}_4$ ) or when the pH was increased the  $Kd$  values decreased ( $Kd = 0.04$  at pH 11.9), suggesting that anionic competition, likely hydroxide or carbonate, and/or anion exchange capacity was involved in the desorption process. Neither  $\text{I}^-$  nor  $\text{TcO}_4^-$  sorbed occurred in the Hanford sediment under natural conditions or when the pH was increased to pH 12.

**Table 1.** Calculated Leachate Chemical Compositions During the Three Stages of Cement Degradation. For Comparison, the Chemical Composition of an SRS Groundwater.

	Cementitious Leachate – Stage I <sup>(a)</sup>	Cementitious Leachate – Stage II <sup>(b)</sup>	Cementitious Leachate – Stage III <sup>(c)</sup>	SRS Groundwater <sup>(d)</sup>
pH	12.37	11.14	9.56	5.79
Eh (V)	0.49	0.56	0.66	0.33
Ionic Strength	4.6e-2	8.2e-3	7.0e-4	3.0e-4
$\text{Al}^{3+}$ (mol/L)	2.19e-5	1.05e-7	1.323e-5	3.33e-5
$\text{Ca}^{2+}$ (mol/L)	1.83e-2	2.92e-3	1.43e-4	1.01e-5
$\text{Cl}^-$ (mol/L)	2.64e-4	2.65e-4	2.65e-4	7.65e-5
$\text{Fe}^3$ (mol/L)	6.87e-10	3.63e-11	1.70e-12	9.93e-7
$\text{HCO}_3^-$ (mol/L)	4.59e-6	6.90e-6	1.81e-4	
$\text{Mg}^{2+}$ (mol/L)	1.04e-8	2.16e-5	4.99e-5	2.92e-5
$\text{Na}^+$ (mol/L)	1.33e-4	1.33e-4	1.33e-4	1.20e-4
$\text{SO}_4^{2-}$ (mol/L)	5.16e-5	2.08e-6	2.08e-6	6.41e-5
$\text{SiO}_2^-$ (mol/L)	1.29e-3	2.95e-3	~0	1.69e-4
<sup>(a)</sup> Stage I solid phase (Portlandite dominant) was modeled consisting of 50-g hematite, 176-g ettringite, 669-g Ca-silica-hydrate phase, 13-g hydrotalcite, 171-g C4AH13 phase, 138-g Portlandite, and 1-g calcite; 110 pore volumes. <sup>(b)</sup> Stage II solid phase (CSH dominant) was modeled consisting of 51-g hematite, 366-g CSH, 17-g hydrotalcite, and 6-g calcite; 1143 pore volumes. <sup>(c)</sup> Stage III solid phase (Calcite dominant) was modeled consisting of 52-g hematite, 19-g hydrotalcite and 7-g calcite; 2380 pore volumes. <sup>(d)</sup> Uncontaminated groundwater on the SRS, Well No P19D. <sup>(e)</sup> Calculations by Dr. Miles Denham (SRNL).				

The influence of cementitious-leachates on uranyl sorption to Hanford sediment was found to gradually increase from 1.07 to 2.22 mL/g as the pH increased from 8.3 to 9.3 (Kaplan et al. 1998). At  $\text{pH} \geq 10.3$ , precipitation occurred and the  $Kd$  value increased suddenly to  $>400$  mL/g; the precipitation did not occur unless the sediment was present, suggesting the mechanism was heterogeneous (as opposed to homogeneous) precipitation. Thus, in the cementitious leachate impacted environment at the Hanford Site, they use in their PAs much higher  $Kd$  values, 100

mL/g, than under ambient, 0.2 mL/g (Cantrell et al., 2007; Cementitious Leachate Sediment Value: Waste Chemistry/Source Category 6: IDF Cementitious Waste High Impact, Table 3.2, Page 3.10. Ambient value: Waste Chemistry/Source Category 4: Low Organic/Sow Salt/Near Neutral, Table 3.2, Page 3.9).

In Appendix C: Influence of Cementitious Leachate on Sediment Buffering Capacity, calculations are presented that demonstrate that the hydroxides emanating from the pH 11/ionic strength  $10^{-2}$  cementitious leachate during Stages I and II of concrete degradation will likely overwhelm the buffering capacity of SRS subsurface sediments. This high ionic strength plume will be dominated by hydroxides and  $\text{Ca}^{2+}$  (Table 1). In this calculation, a 1-m high cementitious slab would be expected to alter the buffering capacity all the way down to the water table during the early stages of concrete aging (Stage I). The altered chemistry would remain during the first two stages of the PA. Once this high pH front reached the aquifer it would be rapidly diluted and likely have negligible influence on subsequent radionuclide sorption.

Cementitious Leachate-Impacted Clayey Sediment Environment is defined as a Clayey Sediment Environment between a cementitious waste form and the aquifer. This Environment will have a nominal pH of 10.5 and an elevated ionic strength  $>10$  mM dominated by hydroxide and  $\text{Ca}^{2+}$  ions. At this writing there have been no suitable site-specific studies conducted for  $Kd$  values for these conditions. Early guidance will rely on measured differences between cementitious-leachate impacted and non-impacted  $Kd$  values for the Hanford PAs (Cantrell et al. 2007). Cementitious Leachate Impact Factors,  $f_{\text{CementLeach}}$ , will be created from the Hanford data based on Eq. 8:

Cementitious Leachate-Impacted Clayey Sediment Environment is defined as a Clayey Sediment Environment between a cementitious waste form and the aquifer: pH of 11 and elevated ionic strength 10 mM.

$$f_{\text{CementLeach}} = \frac{Kd_{\text{CementLeach}}}{Kd} \quad (8)$$

where  $Kd_{\text{CementLeach}}$  and  $Kd$  are the  $Kd$  values measured under cementitious-leachate and natural groundwater conditions, respectively. To calculate SRS  $Kd_{\text{CementLeach}}$  values to use in SRS PAs, Eq. 8 is reorganized:

$$Kd_{\text{CementLeach}} = f_{\text{CementLeach}} \times Kd \quad (9)$$

Clearly, the use of Eq. 8 and 9 are far from ideal, but they are intended to provide provisional guidance until laboratory measurements can be made using site-specific materials.

**Table 2.** Cementitious Leachate Impact Factors (Eq. 8) Generated from Data from the "Geochemistry Data Package for the Vadose Zone in the Single-Shell Tank Waste Management Areas at the Hanford Site" (Cantrell et al. 2007).

Radio-nuclide	Hanford Ground water <sup>(a)</sup> Best $Kd$	Hanford IDF Cementitious Waste <sup>(b)</sup> Intermediate Impact Sand – Best $Kd$	Cementitious Leachate Impact Factor, $f_{CementLeach}$ <sup>(c)</sup> (Unitless)	Suggested $f_{CementLeach}$ (Unitless)	Comments
H	0	0	NA	1	
Tc	0	0	NA	0.1	High pH will greatly reduce anion exchange capacity. Furthermore, high ionic strength will promote desorption of ion that are weakly sorbed. Unlike Hanford sediment, SRS sediments tend to sorb anions, such as $TcO_4^-$ .
Cl	0	0	NA	0.1	Similar chemistry as Tc.
I	0.2	0.2	1	0.1	Using Hanford sediment, Kaplan et al. (1998) showed that I $Kd$ decreased from 0.22 mL/g at pH 8.1 to 0.01 mL/g at pH 9.9.
U	0.8	1	1.25	5	The Hanford recommended value (3 <sup>rd</sup> column) suggests the authors believe that sorption and not precipitation occurs under these conditions. Kaplan et al. (1998) reported uranyl precipitation under mildly cementitious environments, at pH $\geq 10.3$ . pH will be $\geq 10.3$ in this plume and therefore much larger $Kd$ values are recommended here.
Se	5	7	1.4	1.4	
Np	10	15	1.5	1.5	
C	0	5	NA	5	
Sr	2.2	14	6.4	3	Cantrell et al. (2007) did not comment on why the Sr $Kd$ increased. Co-precipitation as Sr, Ca-carbonate is not expected, but perhaps some have occurred in microenvironments. <i>A priori</i> it was anticipated that Sr exchange would occur resulting in lower $Kd$ values.
Cs	2000	2000	1	1	
Pu	600	150	0.25	2	In cementitious environments, pH 7 solubility of Pu is $10^{-5}$ . Above the pH of 9, the solubility of Pu drops to $10^{-10}$ M (Ewart et al. 1992).
Eu	200	300	1.5	1.5	

<sup>(a)</sup> Page 3.9, Table 3.2 Cantrell et al. 2007.  
<sup>(b)</sup> Table 3.10, Table 3.2 Cantrell et al. 2007. Selected "Intermediate Impact" and not "High Impact" because the former is more conservative with respect to the groundwater scenario (lower  $Kd$  values, and over the course of multiple ages (Stage I, Stage II, and Stage III). It was through that "intermediate impact" would be more representative than "high impact" over the entire age of the facility. IDF = Intergraded Disposal Facility  
<sup>(c)</sup> Equation 8.

#### 4.2.5 Cementitious Leachate Impacted Sandy Sediment Environment

The Cementitious Leachate Impacted Sandy Sediment Environment is similar to the Cementitious Leachate Impacted Clayey Sediment Environment discussed above (Section 4.2.4) except it is for the lower Sandy Sediment Environment that exists between cementitious waste forms and the aquifer.  $Kd$  values for this Environment are created in the same manner as above, namely, through the use of Equations 8 and 9, and through the use of Table 2. Again, this is to provide early guidance until appropriate measurements can be made, as described in Section 7.0 Future Research and Data Needs.

#### 4.2.6 Cementitious Leachate Impacted and CDP-Impacted Sediment Environments

Many Environments within and beneath waste units that use concrete as an engineered barrier contain cellulosic materials, such as the Low Activity Waste Vault (Table 3). As such, the mobility of radionuclides will be influenced by both the cementitious chemistry and the cellulose degradation products (CDP) chemistry. There has been little research conducted evaluating radionuclide sorption to sediments in the presence of CDP (or natural organic matter) in a cementitious aqueous system. CDP sorbs to sediments at low pHs (<pH~7). Below this pH, the elevated CDP sorption to the sediment surface promotes radionuclide sorption to the sediment surfaces, increasing  $Kd$  values (Kaplan et al. 2010). As the pH increases above 7, CDP sorption decreases and consequently, radionuclide  $Kd$  values generally decrease. Between pH 10 and 12.5, it is not clear what happens to radionuclide  $Kd$  values in this ternary system. Presumably those radionuclides whose aqueous concentrations are strongly controlled by solubility, (e.g., trivalent, Pu, Np, and U; Table 19 and Table 20) their concentration will be primarily controlled by solubility and not by the presence or absence of CDP. Conversely, those radionuclides that form strong complexes to CDP, but do not have solubility constraints, that is, almost all other radionuclides, their concentrations in Environments impacted by cementitious leachate and CDP may be thought of being primarily controlled by CDP. Given this logic, the following rules were made for assigning  $Kd$  values in Cementitious Leachate Impacted and CDP-Impacted Sediment Environments:

In this *Environment*, trivalent, tetravalent, and other radionuclides that tend to be sparingly soluble under cementitious environments have  $Kd$  values that are impacted by cement leachate impact factor.  $Kd$  values for all other elements are impacted by the CDP impact factor in this Environment.

- $Kd_{CementLeach}$  (Solubility  $<10^{-6}$  M; Table 19 and Table 20) or Solubility Values: Ac, Al, Am, Bk, Bi, Ce, Cf, Cm, Eu, Fe, Gd, Lu, Sm, Y, Ag, Co, Cd, Cu, Hg, Ni, Pb, Pd, Po, Pt, Sn, Zn, Np, Pa, Pu, Pu(III/IV), Th, Zr, U (for reducing cement: Tc, Re and Cr)
- $Kd_{CDP}$  (Solubility  $>10^{-6}$  M; Table 19 and Table 20):  $^3\text{H}$ , Ar, As, At, Cl, Cr, Cs, F, Fr, I, K, Kr, Mn, Mo, N, Na, Nb, Pu(V/VI), Rb, Re, Rn, Sb, Se, Tc(VII), Te, Tl, C, Ra, Ba, Ca, and Sr.

Apparent solubility concentration or  $Kd$  value, whichever maintains the lower aqueous concentration, will be used for the first category. Therefore, the  $Kd$  or solubility values will be taken from either  $Kd_{CDP}$  or  $Kd_{CementLeach}$  data sets. It is recommended in Section 7.0 “Future Research and Data Needs” that research be conducted to address this important data need. These  $Kd$  values are summarized in Table 13 and Table 23.

**Table 3.** Description of Whether Cellulose Degradation Products (CDP) is Present and if Reducing and Oxidizing Cementitious Materials were used During the Construction of the Disposal Unit/Facility.

Disposal Unit	CDP <sup>(a)</sup>	Constructed with Reducing Cementitious Materials <sup>(b)</sup>	Constructed with Oxidizing Cementitious Materials
Slit Trenches	Yes	No	No
Engineered Trenches	Yes	No	No
Low-Activity-Waste Vault	Yes	Yes	Yes
Components-in-Grout Trench	Yes	No	Yes
Intermediate Level Vault	Yes	Yes	Yes
Naval Reactor Component Disposal Areas	Yes	No	No
TRU-Waste Pad	Yes	No	Yes
Saltstone Facility	No	Yes	Yes

<sup>(a)</sup> Cellulose degradation products are released from wood, cardboard, and paper products. The amount of cellulosic materials contained in each of these disposal facilities is expected to vary greatly. Consequently the duration that CDP-correct  $Kd$  values will be used prior to using simple  $Kd$  values will also vary greatly between facilities.

<sup>(b)</sup> Reducing cementitious materials contain slag to create the reducing environment for immobilizing redox-sensitive radionuclides, such as Tc and Pu.

### 4.3 Reducing Cementitious Materials

Some cementitious materials have blast-furnace slag included in their formulations to promote the reductive precipitation of the radionuclide with sulfide, thus reducing the tendency of the radionuclides to leach from the solid waste form. Experimentation has shown that leaching of Cr and Tc was effectively reduced to a level that enabled all projected salt solution compositions to be processed into a non-hazardous solid waste (MMES 1992). Long-term lysimeter studies have shown that the addition of slag into the Saltstone formulation essentially stopped <sup>99</sup>Tc leaching, but did not reduce nitrate leaching (MMES 1992). In addition to the blast-furnace slag creating a low redox status (*i.e.*, low reduction potential, which has been measured with an Eh meter), it also tends to raise the concentration of sulfides in the porewater. The net effect is that numerous metals precipitate out of solution as a result of reductive precipitation (the result

For purposes of the Saltstone PA, a “shrinking core model” is assumed with the outer layer growing becoming oxidized and growing in size towards the core. Additional calculations need to be conducted to determine the duration of the reducing environment of the Intermediate Level Vault.

of lower the Eh) and/or due to the complexation with sulfides (a strong precipitating moiety. Tc, is an example of a radionuclide that undergoes both reduction from Tc(VII) to Tc(IV) and forms insoluble precipitates with sulfides to form  $Tc_2S_7$  (Lukens et al. 2005). Other radionuclides immobilized in the presences of blast-furnace slag include U and Np.

In the past, the interaction of oxidation of the reducing saltstone and release of Tc was based on laboratory measurements and two-dimensional reactive transport calculations (Kaplan and Hang 2003). It was calculated that ~16% of the saltstone reduction capacity would be consumed after 213,000 years (Figure 7). For purposes of comparison, two additional calculations, based on entirely different assumptions, were discussed. The first calculation conducted by Lukens et al. (2005), based on spectroscopy considerations (sans diffusion or aqueous transport considerations), yielded nearly identical results as above. The second calculation conducted as a first approximation and using unrealistically high groundwater flow rates, concluded that the Z-Area saltstone waste form will maintain a reducing environment for more than 10,000 years (Kaplan and Hang 2003). Obtaining similar conclusions by three extremely different types of calculations and sets of assumptions provides additional credence to the conclusion that the Z-Area saltstone will maintain a reducing environment in excess of 10,000 years.

In the past it was assumed for the Saltstone PA, that reducing cementitious materials maintained much of their reducing environments for the entire PA scenario, 10,000 years. In the future, as the oxidation front moves through the reducing grout the Tc(IV) will be instantly oxidized to Tc(VII), resulting in the solubility concentration limits and ( $Kd$  value) changing in a manner that will release Tc into the aqueous phase with the oxidizing front. In the case of Tc, the aqueous Tc concentration will be initially controlled within the reducing Saltstone by solubility to  $10^{-10}$  M (170 pCi/L; note that the Maximum Contaminant Level (MCL) is 900 pCi/L). But once the oxidizing front reaches the Saltstone, that particular node will have a  $Kd$  of 0 mL/g. (Additionally, the influence of cracking as a function of time will be integrated into the transport of oxygenated water.)

A related report deals with estimating the duration of the reduction capacity within a high-level waste tank (Kaplan et al. 2005). This report does not contain any new experimental data but demonstrates the application of the reduction data to a set of very different environmental conditions.

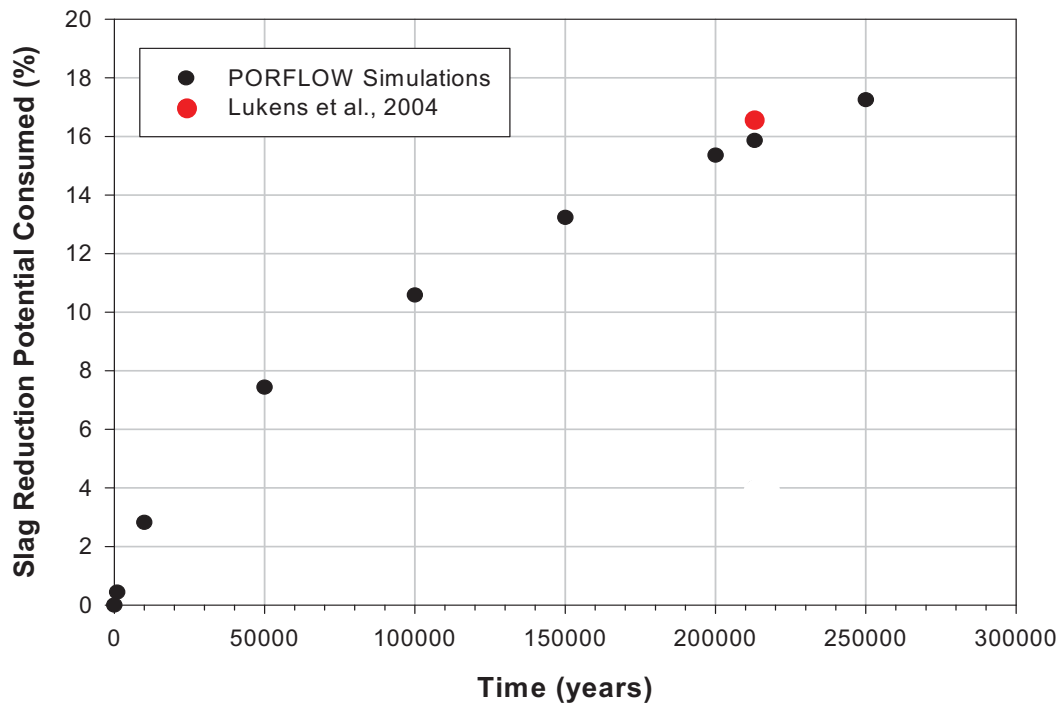


**Figure 7.** Consumption of slag reduction potential by diffusing dissolved oxygen in infiltrating water into the Saltstone Facility (Kaplan and Hang 2003). Results from Lukens et al. (2005) is also presented (value corrected for diffusion from four sides).

Kaplan et al. (2008b) conducted some additional reduction capacity measurements. They measured the reduction capacity of Vault 2 concrete (a simulant of the vault walls within which the Saltstone will be poured),<sup>10</sup> DDA simulated Saltstone, blast furnace slag (which is used as an ingredient in the previous two samples), and a 50-yr-old SRS concrete. The Saltstone that contained 23 wt-% slag had the same reduction capacity as the pure slag. The Vault 2 concrete, which contains only 10 wt-% slag, had about 25% the reduction capacity of 100% slag. The cause for the greater than expected reduction capacity in the Saltstone and Vault 2 concrete is not known, but may be attributed to these materials having semi-conductor properties, permitting them to transfer electrons to the water/solid interface to create a reducing environment. Alternatively, the slag may have greater surface areas when it is hydrated and combined with cementitious materials, thereby creating greater opportunity for electrons to move to and from the slag. So when Kaplan et al. (2005) tested it in the pure form (neat), it may not have hydrated to the extent that it would have in a pH 12 system and in the process, it had a much lower surface area and ability to transfer electrons to the surface. Other explanations are offered by Kaplan et al. (2008b). Clearly, additional work is required to understand not only the capacity, but the electrical process by which the system is maintained in a reducing condition. A finite reduction capacity was measured in the SRS sediment and in regular Portland cement, albeit much less, 20 times less than that measured in the Saltstone.

<sup>10</sup> The Saltstone vault walls contain (lbs/yd<sup>3</sup>) 201 cement, 268 slag, 45 silica fume, 156 fly ash 911 sand 1850 aggregate and 31 gal/yd<sup>3</sup> water.

#### 4.3.1 Young Reducing Cementitious Solids (1<sup>st</sup> Stage) Environment

This Environment is conceptually identically to that of the Young Cementitious Solids (1<sup>st</sup> Stage) Environment (Section 4.2.1) except that it contains reducing slag. The reducing slag, as discussed above creates a reducing environment that promotes the reduction of several radionuclides, including Pu and Tc. It has its own  $Kd$  and solubility values in look up tables.

#### 4.3.2 Moderately-aged Reducing Cementitious Solids (2<sup>nd</sup> Stage) Environment

This Environment is conceptually identically to that of the Moderately-aged Cementitious Solids (2<sup>nd</sup> Stage) Environment (Section 4.2.2) except it contains reducing slag. It has its own  $Kd$  and solubility values in look up tables.

#### 4.3.3 Aged Reducing Cementitious Solids (3<sup>rd</sup> Stage) Environment

This Environment is conceptually identically to that of the Moderately-aged Cementitious Solids (3<sup>rd</sup> Stage) Environment (Section 4.2.3) except it contains reducing slag. It has its own  $Kd$  and solubility values in look up tables.

### 4.4 Radionuclide Leaching from Waste Materials

There are a large number of different types of solid phases that are disposed within the various E-Area facilities, especially, in the trenches. They include paper, plastics, wood, cloth, spent ion exchange resins, metal, concrete debris, and glass. The degree to which the various radionuclides sorb to each material is largely unknown. Therefore, the following simplifying assumption was made. Unless waste-form specific data is available (Section 4.5), the extent that a radionuclide sorbs to the waste form is assumed to be similar to the extent that the radionuclide sorbs to the solid phase immediately in contact with the waste. For example, the leaching rate of Th associated with paper disposed in the Slit Trench Facility will be calculated using the Th  $Kd$  value reported in the Clayey Sediment look-up table. The Clayey Sediment is the solid phase in contact with the waste. The leaching rate of Th associated with paper disposed in the cementitious Low Activity Waste (LAW) Vaults will be calculated using the Th  $Kd$  value reported in the Cementitious Leachate Impacted Clayey Sediment Environment look-up table.

Unless waste-form specific data is available, the extent that a radionuclide sorbs to the waste form will be set equal to the extent that the radionuclide sorbs to the solid phase (sediment or cement) immediately in contact with the waste.

#### 4.5 Radionuclide Leaching from Special Waste Forms

There are some, not many, waste-specific  $Kd$  values and solubility concentration limits, especially for anions sorbing to anionic resins (*e.g.*, Kaplan and Serkiz 2000). The extent that radionuclides desorb from waste can be estimated through the use of  $Kd$  values and solubility concentration values. The use of these parameters to estimate desorption, is simply the reverse of adsorption. One of the assumption of the  $Kd$  construct is that it is fully reversible, meaning that adsorption occurs at the same rate as desorption. The list of special waste forms (Table 15) is certainly not a complete list but rather of list of waste that desorption  $Kd$  values were measured, most commonly because the PA needed to quantify the strong sorbing capacity of the waste form.

When special waste forms are located in an area where cellulose degradation products (CDP) are present, CDP-correction factors should be used along with the appropriate  $Kd$  values (Table 15; see sections 4.1.3 and 4.1.4).

#### 4.6 Geochemical Parameters' Ranges and Distributions

Associated with the “best”  $Kd$  and apparent solubility values are parameters that address the expected variability associated with these parameters. The range and distribution of Am, Cd, Cs, Ce, Co, Hg, Sr, Sn, Tc, and Y  $Kd$  values were measured in 27 sediment (triplicate measurements resulting in 81  $Kd$  measurements per element; 810  $Kd$  measurements in total) collected from the subsurface vadose and aquifer zones of E-Area. The statistical ranges and distributions of these  $Kd$  values were reported in Grogan et al. (2008) and Kaplan et al. (2008). Implication of the distributions and a depiction of the results of these normal and log-normal distributions are presented in Grogan et al. (2010) and the  $Kd$  data sets fitted to log-normal distributions are presented in Appendix D.

The conclusions of this study can be summarized as follows:

The 95-percentile range and type of distributions assigned to radionuclide  $Kd$  values should be assigned based on the following general rules. These general rules were derived from the measurements described in Grogan et al (2008), some geochemical/geological consideration, and parsimony.

- The results indicated that the distributions of  $Kd$  values were most closely log-normally distributed for the entire 27-sample taken from a well borehole from E-Area.
- The 95% confidence level for the mean  $Kd$  was twice the mean in the Aquifer Zone (16.5 to 30.3m depth – Sandy Sediment Environment), equal to the mean for the Upper Vadose Zone (3.3 to 9.8 m depth – Clayey Sediment Environment), and half the mean for the Lower Vadose Zone (9.8 to 16.5 m depth – Sandy Sediment Environment).
- The distribution of  $Kd$  values was log normal in the Upper Vadose Zone and Aquifer Zone, and normal in the Lower Vadose Zone.

Based on these findings, the  $Kd$  distributions and ranges were estimated for each of the various Environments. No data are presently available regarding the ranges and distribution of

$Kd$  values in cementitious environments or for solubility values, so they were assumed to be similar to the  $Kd$  values measured in the sediments. Future research is intended to actually measure these ranges and distributions in site specific cementitious materials.

All distributions were assumed to be log-normal based on Grogan et al. (2008) and Kaplan et al. (2009).

For the Sandy Sediment Environments (and the Cementitious Leachate Impacted), which is the dominant type of Environment in the Aquifer and Lower Vadose Zones, it was assumed that the 95% confidence level for the mean  $Kd$  was 1.5 times the mean, which is a combination of the recommended multiplying factors for the Aquifer Zone and the Lower Vadose Zone. This would result in a calculation for the minimum (“Min”) and maximum (“Max”) values of the ranges as follows:

$$\text{“Min”} = Kd - (1.5 * 0.5 * Kd) = 0.25 * Kd \quad (\text{Eq. 10})$$

$$\text{“Max”} = Kd + (1.5 * 0.5 * Kd) = 1.75 * Kd \quad (\text{Eq. 11})$$

For the Clayey Sediment Environments (and the Cementitious Leachate Impacted), which is the dominant type of Environment in the Upper Vadose Zone, it was assumed that the 95% confidence level for the mean  $Kd$  value was 1.0 times the mean, which corresponds to the value recommended by Grogan et al. (2008) for the Upper Vadose Zone. This would result in a calculation for the minimum (“Min”) and maximum (“Max”) values of the ranges as follows:

$$\text{“Min”} = Kd - (1.0 * 0.5 * Kd) = 0.5 * Kd \quad (\text{Eq. 12})$$

$$\text{“Max”} = Kd + (1.0 * 0.5 * Kd) = 1.5 * Kd \quad (\text{Eq. 13})$$

For cementitious Environments, the range was assumed to be the same as for sediments. Equations 1 and 2 for the Sandy Sediment Environments were used to calculate the range for cementitious Environments (*i.e.*, a 95% confidence level of 1.5 times the mean).

## 5.0 WASTE FACILITIES DESCRIPTIONS: ASSIGNMENT OF GEOCHEMICAL ENVIRONMENTS AND TYPES OF CONSTANTS TO USE IN SIMULATIONS

The purpose of this section is to describe the key features of the waste units and facilities and to assign geochemical Environments. More specifically, this section describes the geochemical conceptual model of how to model waste facilities by assigning Environments to various materials around the various facilities. For each facility, there is a schematic, followed by a table containing the conceptual geochemical materials (*e.g.*, concrete, reducing concrete, sandy sediment) of the facility and the associated parameters used to describe the radionuclide as it interacts with these features. At the end of this section, are the various look-up tables containing the  $Kd$  values and solubility concentration limits. The schematic and description of the geochemical materials for each disposal facility are:

- Slit and Engineered Trenches (Figure 8, Figure 10 and Table 4),
- Low Activity Waste (LAW) Vault (Figure 11, Figure 12 and Table 5),
- Components-in-Grout Trenches (Figure 13, Figure 14 and Table 6),
- Intermediate Level (ILV) Vault (Figure 15, Figure 16 and Table 7),
- Naval Reactor Component Disposal Areas (Figure 17, Figure 18 and Table 8),
- TRU-Pad-1 (Figure 19, and Table 9),
- Saltstone Disposal Facility (Figure 20, Figure 21 and Table 10), and
- Radioactive Waste Tank (Figure 22, Figure 23 and Table 11).

## 5.1 Slit and Engineered Trenches

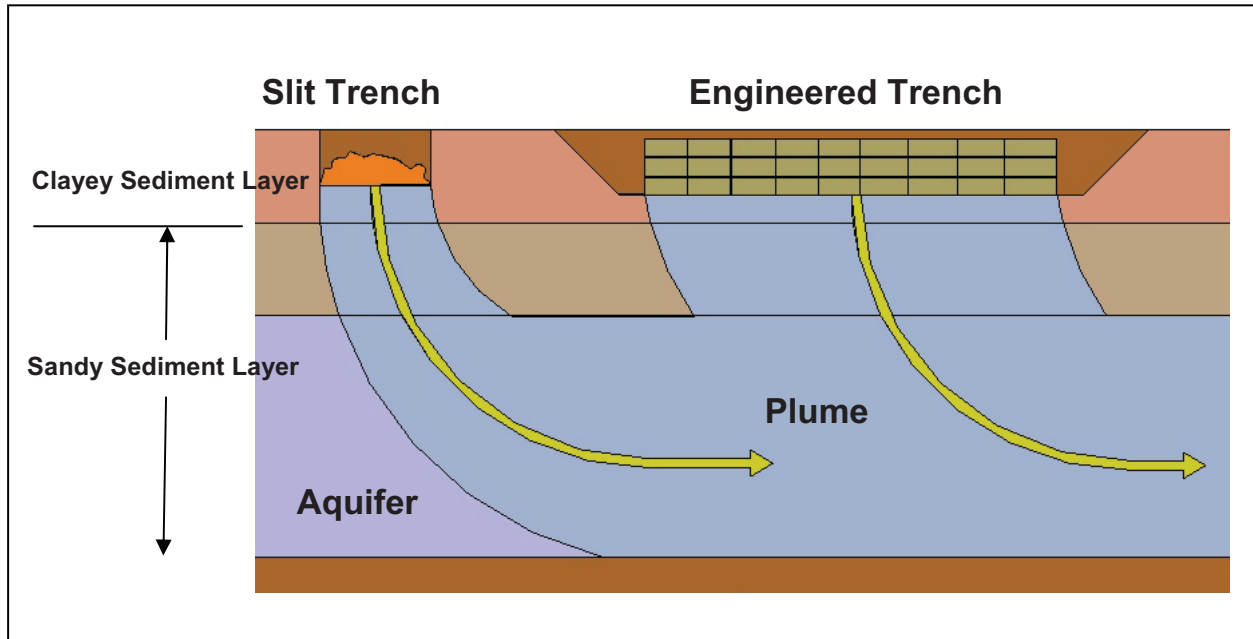


Figure 8. Schematic representation of the geochemical conceptual model of a Slit and Engineered Trench Units. Not shown is a multilayered-closure cap that will be added above these units during Post-Institutional Control.



Figure 9. E-Area Slit Trench Facility showing a range of waste materials. Also note the red clayey sediment, characteristic of the upper sediment strata.



Figure 10. Engineered Trench: (top) aerial view and (bottom) close up of metal containers holding low level waste (WSRC 2008).

**Table 4.** Slit Trenches: Conceptual Geochemical Model of Features and Parameters (See Figure 8).

Solid Phases	Aqueous Phase	Geochemical Parameter
Waste Zone <sup>(a)</sup>	SRS ground water: pH 5.5, ionic strength $10^{-4}$ <sup>11</sup> , except for trace levels of radionuclide concentrations and CDPs (Table 1)	Initially use Clayey Sediment $Kd_{CDP}$ until all the CDP <sup>(b)</sup> has leached from the Waste Zone. Then use Clayey Sediment $Kd$ . Will assume waste has characteristics of Clayey Sediment, the nearest solid phase to the Waste Zone. No cementitious materials are included as engineered barriers.
Clayey Sediment: Upper Vadose Zone	As above.	Initially use Clayey Sediment $Kd_{CDP}$ until all the CDP <sup>(b)</sup> has leached from the Waste Zone. Then use Clayey Sediment $Kd$ .
Sandy Sediment: Lower Vadose Zone	As above.	Initially use Sandy Sediment $Kd_{CDP}$ until all the CDP <sup>(b)</sup> has leached from the Waste Zone. Then use Sandy Sediment $Kd$ .
Sandy Sediment: Aquifer Zone	As above	Same as immediately above.
<p><sup>(a)</sup> Slit Trenches are approximately 6-m x 6-m x 200-m and receive a wide range of materials that contain, for example, very low concentrations of radioactivity, including from environmental restoration and building decommissioning. The Engineered Trenches are about 218-m long by 50-m wide and 7-m depth and received similar types of waste materials as the Slit Trenches. All waste from the Engineered Trenches is placed in metal boxes (e.g., B-25 boxes) that are stacked on top of each other.</p> <p><sup>(b)</sup> <math>Kd_{CDP} = Kd</math> for cellulose degradation products.</p>		

<sup>11</sup> Ionic strength of a solution is a measure of the amount of ionic species in solutions and is proportional to the salt content. Its influence on radionuclide sorption is complex and non-linear. In simple cation exchange systems, as described by  $Kd$  values, an increase in ionic strength results in greater desorption, and this general rule holds true in most natural environments. Above a critical concentration, and depending on the ions in solution, precipitation may occur.

## 5.2 Low-Activity Waste (LAW) Vaults

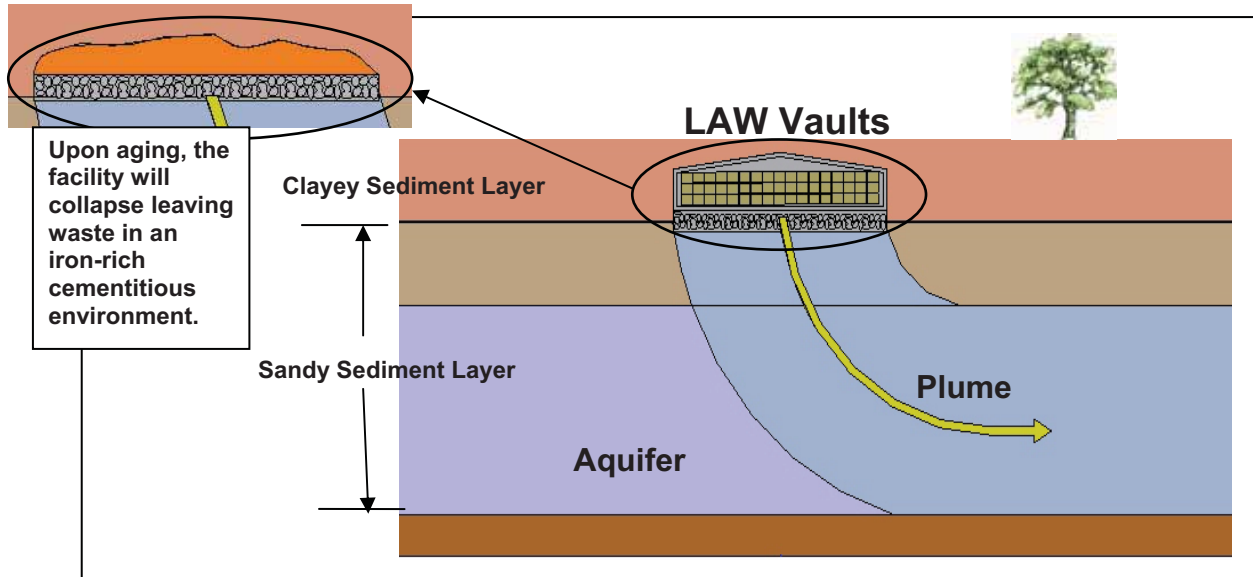


**Figure 11.** Schematic representation of the geochemical conceptual model of the Low-Activity Waste Vault. Not shown is a multilayered-closure cap that will be added above the vault during Post-Institutional Control.

Exterior View



Interior View

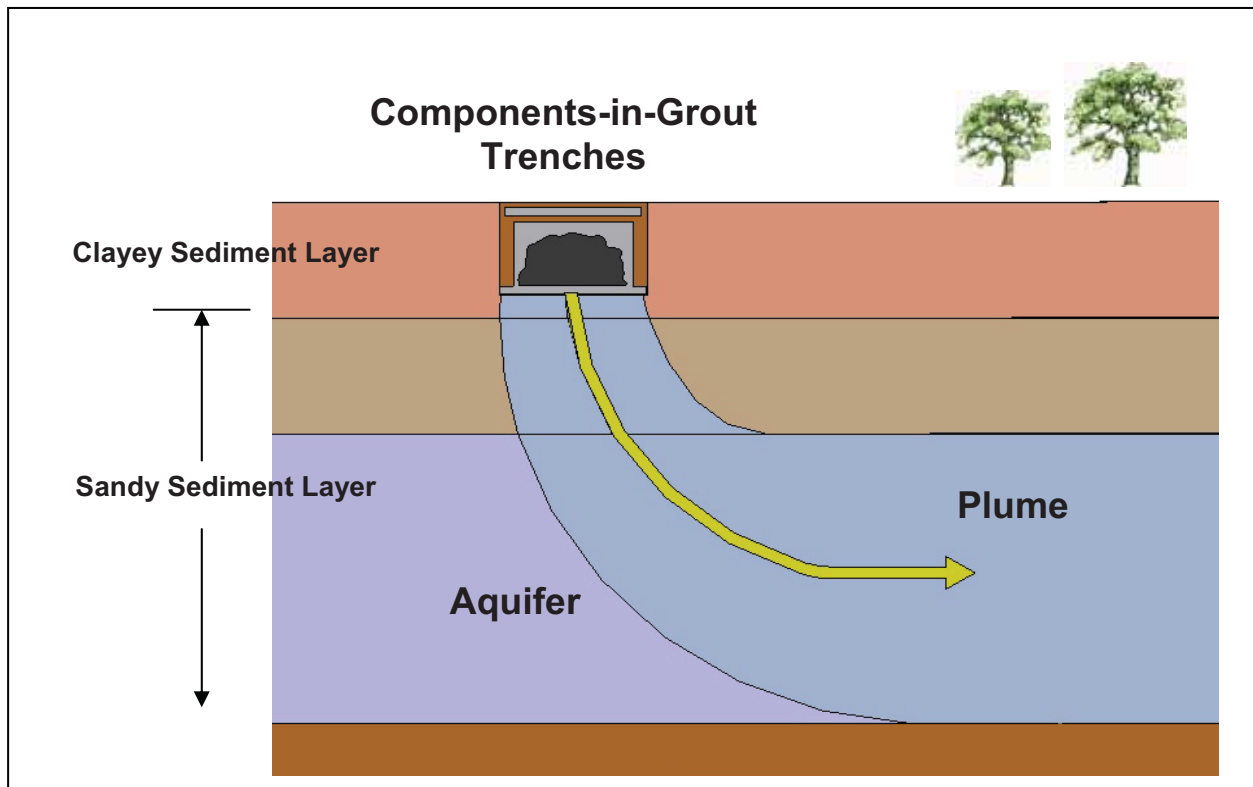


Figure 12. Low Activity Waste (LAW) Vault: (top) exterior view and (bottom) interior view (WSRC 2008).

**Table 5.** LAW Vault: Conceptual Geochemical Model of Features and Parameters (See Figure 11).

Solid Phases	Aqueous Phase	Geochemical Parameter
Waste Zone <sup>(a)</sup> : Aged metal boxes (B-25 boxes) containing waste. Over time the boxes rust and release radionuclides. Eventually concrete vault structure and B-25 boxes collapse leaving waste in an Fe-rich cementitious environment.	Concrete leachate enters metal boxes or into collapsed rusted iron rubble. This is a cementitious leachate impacted aqueous phase (elevated pH and ionic strength; Table 1).	Use cementitious leachate impacted clayey sediment $Kd$ ; $Kd_{CementLeach}$ . Clayey sediments on the SRS are typically red in color as a result of containing Fe-oxide coatings. These Fe-oxides coatings will provide a conservative (less abundant) approximation of pure Fe-oxides. <sup>(b)</sup>
Concrete: concrete roof, walls, and floor.	Cementitious Impacted Leachate: Three general types of concrete leachate chemistries controlled by different aged solid phases: elevated pH and ionic strength (Table 1; Figure 6).	Use reducing cement $Kd$ or apparent solubility concentrations for the three cement ages.
Crushed stone: used beneath LAW Vault facility. <sup>(c)</sup>	Cementitious (as above).	See footnote (c).
Clayey Sediment: Upper Vadose Zone	Cementitious (as above).	Use cementitious leachate impacted clayey $Kd$ values; $Kd_{CementLeach}$ .
Sandy Sediment: Lower Vadose Zone	Cementitious (as above).	Use cementitious leachate impacted sandy $Kd$ values; $Kd_{CementLeach}$ for sandy sediment.
Sandy Sediment: Aquifer Zone	Cementitious leachate pore water gets diluted with typical SRS groundwater and the aqueous phase takes on the properties of the latter: pH 5.8 and ionic strength $10^{-4}$ , except for trace levels of radionuclide concentrations and CDPs (Table 1)	Initially use Sandy Sediment $Kd_{CDP}$ until all the CDP <sup>(d)</sup> has leached from the Waste Zone. Then use Sandy Sediment $Kd$ .
<p><sup>(a)</sup> This waste contains greater radioactivity than the waste disposed in the Slit Trenches. Some cellulosic materials will be disposed in the vaults. Waste is placed in large metal boxes (B-25 and B-12 boxes) which are stacked and stored in large concrete vaults. The vault consists of concrete roof, walls, and floor, which are generally about 1-ft thick.</p> <p><sup>(b)</sup> As noted in Section 4.2.6, in the presence of cementitious leachate and the influence of CDP on radionuclide sorption will not be accounted for.</p> <p><sup>(c)</sup> A 1.1-m layer of crushed stone exists immediately beneath the concrete floor of the LAW Vault. It has not been included in previous PA modeling efforts, because it was believed that this layer would become "silted in" within a relatively short period of time. For this same reason, it is not included in the conceptual geochemical model of this disposal site and will be modeled as behaving like the Clayey Sediment: Upper Vadose Zone.</p> <p><sup>(d)</sup> <math>Kd_{CDP} = Kd</math> for cellulose degradation products.</p>		

### 5.3 Components-in-Grout Trenches



**Figure 13.** Schematic representation of the geochemical conceptual model of a Components-in-Grout Trenches. Not shown is a multilayered-closure cap that will be added above the vault during Post-Institutional Control.

Emplacement of Bottom Foot of Grout



Component Emplacement



Grouting Sides of Segment



Initial Waste Layer Encapsulated



Top of Grout



4-Foot of Clean Soil Cover

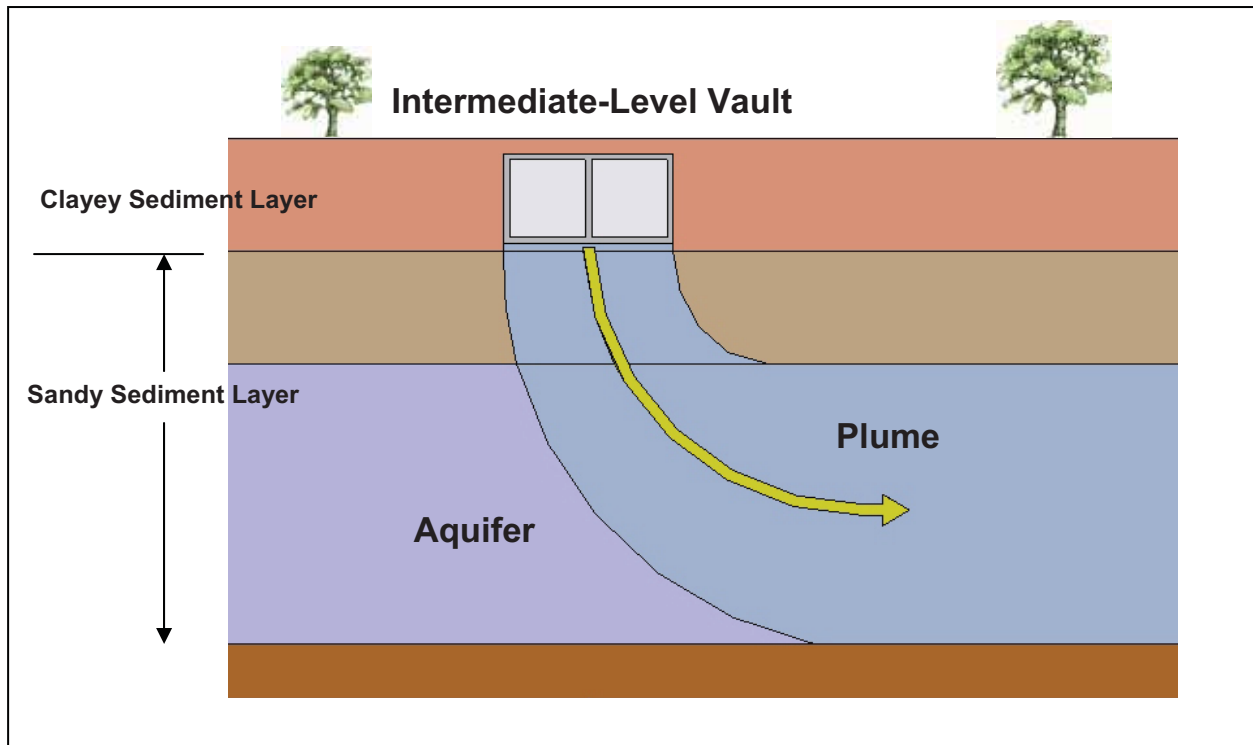


Figure 14. Sequence of steps in the disposing of waste as Components in Grout (CIG; WSRC 2008).

**Table 6.** Components-in-Grout Trenches: Conceptual Geochemical Model of Features and Parameters (Figure 13).

Solid Phases	Aqueous Phase	Geochemical Parameter
Waste Zone <sup>(a)</sup>	Cementitious Impacted Leachate: Three general types of concrete leachate chemistries controlled by different aged solid phases: elevated pH and ionic strength (Table 1; Figure 6).	Oxidizing concrete $Kd$ or Oxidizing concrete solubility concentration limits
Concrete: 0.3-m-thick concrete/grout walls & floor of trench, concrete/grout poured over waste to encapsulate waste.	Cementitious (as above)	Oxidizing concrete $Kd$ or Oxidizing concrete solubility concentration limits
Clayey Sediment: Upper Vadose Zone	Cementitious (as above).	Use cementitious leachate impacted clayey $Kd$ values; $Kd_{CementLeach}$
Sandy Sediment: Lower Vadose Zone	Cementitious (as above).	Use cementitious leachate impacted sandy $Kd$ values; $Kd_{CementLeach}$ for sandy sediment.
Sandy Sediment: Aquifer Zone	Cementitious leachate pore water gets diluted with typical SRS groundwater and the aqueous phase takes on the properties of the latter: pH 5.8, ionic strength $10^{-4}$ , trace levels of radionuclide concentrations and CDPs.	Initially use Sandy Sediment $Kd_{CDP}$ until all the CDP <sup>(d)</sup> has leached from the Waste Zone. Then use Sandy Sediment $Kd$ .
<p><sup>(a)</sup> This waste is too bulky and too large to place in the Low-Activity Waste Vault or the Intermediate Level Vault and contains more radioactivity than the waste that is placed in Slit Trenches. A trench is excavated to act as a form, a 1-ft grout floor is poured, and the waste is placed in the floor, ~1-ft of grout is poured over the waste, and then sediment backfill is added to fill the trench. A reinforced concrete slab is installed over new Components-in-Grout trench for support of the final closure cap. It is expected that negligible cellulosic material is included in this waste.</p> <p><sup>(b)</sup> <math>Kd_{CDP} = Kd</math> for cellulose degradation products.</p>		

## 5.4 Intermediate-Level Vault



**Figure 15.** Schematic representation of the geochemical conceptual model of the Intermediate-Level Vault Facility. Not shown is a multilayered-closure cap that will be added above the vault during Post-Institutional Control.

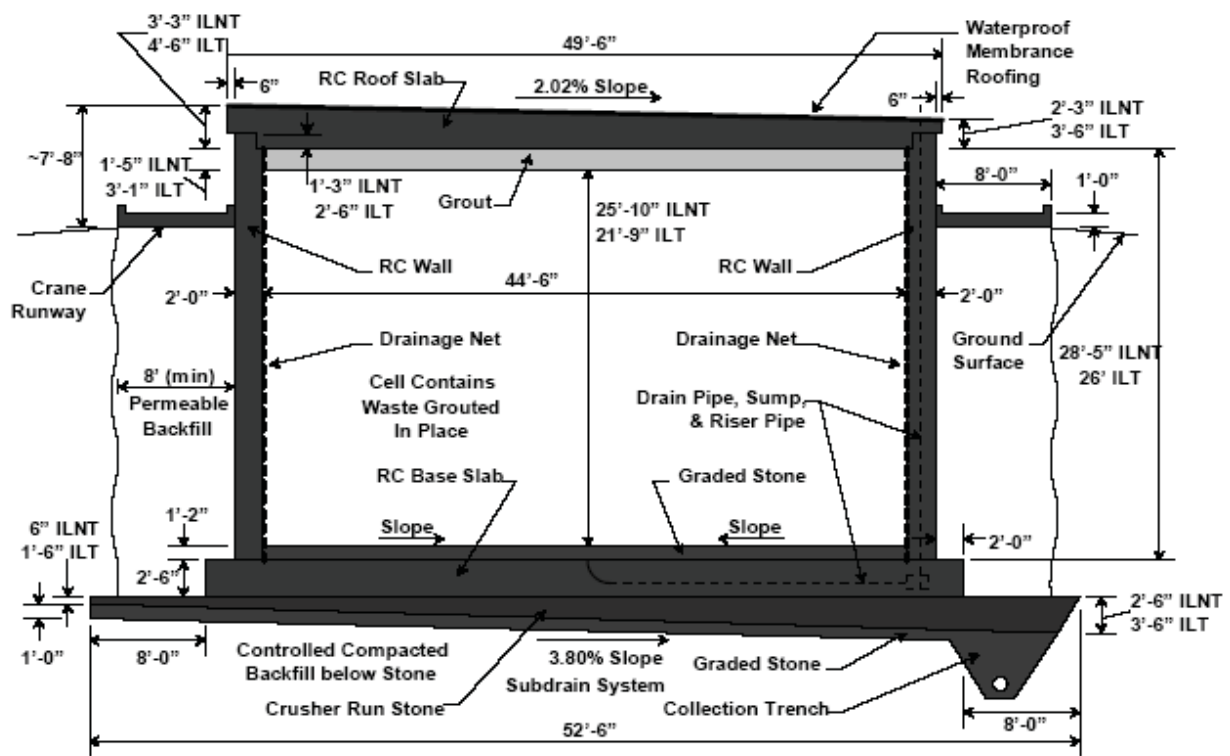
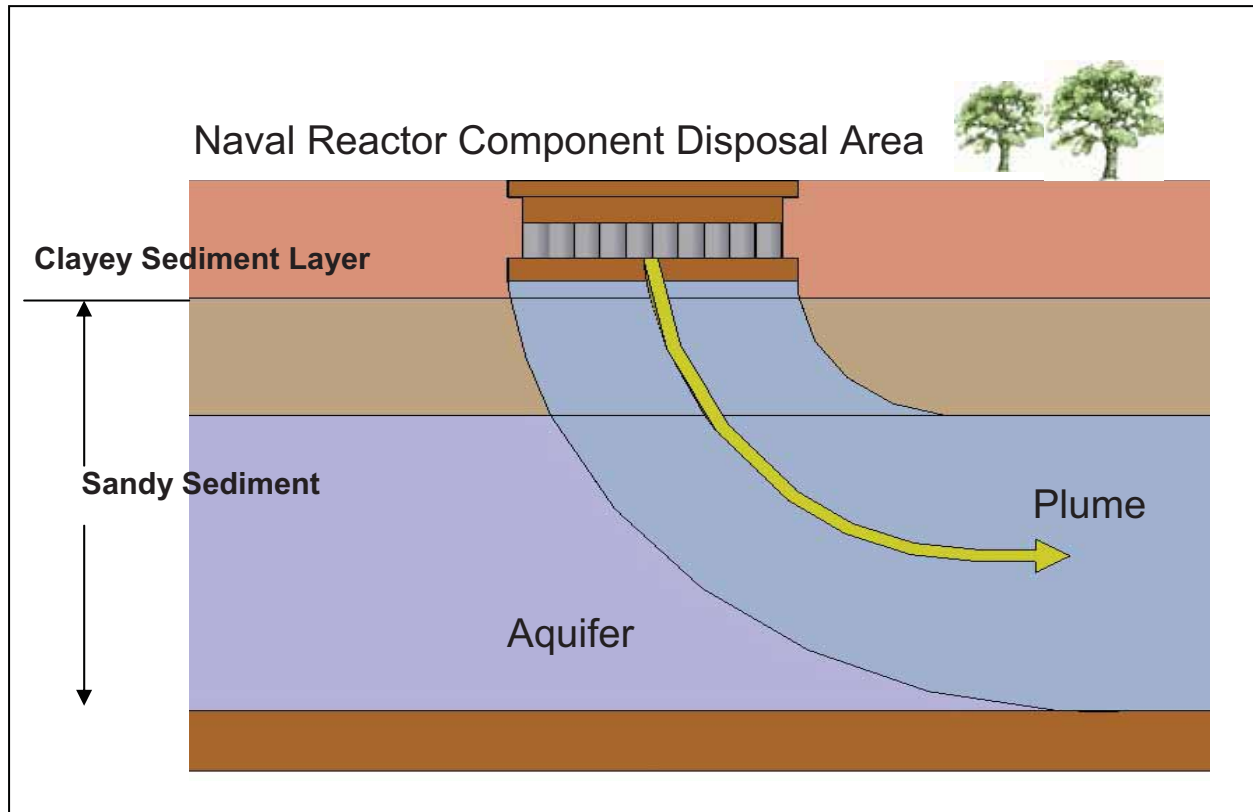


Figure 16. Intermediate-Level Vaults: (top left) aerial photo graph with roof off of one cell; (top right) waste components cemented within a partially filled cell; (bottom) cross-sectional diagram of unit (WSRC 2008).

**Table 7.** Intermediate-Level Vault: Conceptual Geochemical Model of Features and Parameters (Figure 15).<sup>(a)</sup>

Solid Phases	Aqueous Phase	Geochemical Parameter
Waste Zone <sup>(a)</sup>	The closure plan does not presently specify the type of material to use between the buried casks (Phifer et al. 2009). Depends on whether a cementitious or sediment material is used. Most likely candidate materials are CLSM and sediment/sand, the former is a slightly cementitious material.	Reducing concrete $Kd$ & reducing concrete solubility concentration limits <sup>(c)</sup>
Reducing concrete <sup>(c)</sup> : Slag added to concrete used in floor and walls. Roof truss steel structure will be replaced with reducing concrete.	Reducing Cementitious Environment: (as immediately above)	Reducing concrete $Kd$ & reducing concrete solubility concentration limits <sup>(b)</sup>
Clayey Sediment: Upper Vadose Zone	Cementitious or sediment (please see above).	Use cementitious leachate impacted clayey $Kd$ values; $Kd_{CementLeach}$ .
Sandy Sediment: Lower Vadose Zone	Cementitious (as above).	Use cementitious leachate impacted sandy $Kd$ values; $Kd_{CementLeach}$ for sandy sediment.
Sandy Sediment: Aquifer Zone	Cementitious leachate pore water gets diluted with typical SRS groundwater and the aqueous phase takes on the properties of the latter: pH 5.8, ionic strength $10^{-4}$ , trace levels of radionuclide concentrations and CDPs.	Initially use Sandy Sediment $Kd_{CDP}$ until all the CDP <sup>(d)</sup> has leached from the Waste Zone. Then use Sandy Sediment $Kd$ .
<p><sup>(a)</sup> This waste contains more radioactivity than Slit- and Engineered-Trench waste and LAW Vaults. It is placed in the vault in layers and is grouted in place. The facility includes Intermediate-Level Non-Tritium Vault and the Intermediate-Level Tritium Vault. The latter is used for disposal and storage of tritium-bearing waste packed in 10-gallon drums, spent tritium extraction crucibles, and tritium job control waste. Other forms of waste not listed are also present. Void space between casks may be appropriately filled with 1) Controlled Low-Strength Material (CLSM) or flowable fill or 2) sand or sediment.</p> <p><sup>(b)</sup> Some oxidizing concrete may have been used to anchor B-25 metal waste containers as reducing concrete or CLSM was added to cover waste within vault, but a majority of the cementitious material contains slag.</p> <p><sup>(c)</sup> Reducing cementitious materials are those that contain slag and change the pore water chemistry sufficiently to require unique geochemical parameters (see Section 4.3).</p> <p><sup>(d)</sup> <math>Kd_{CDP} = Kd</math> for cellulose degradation products.</p>		

## 5.5 Naval Reactor Component Disposal Areas



**Figure 17.** Schematic representation of the geochemical conceptual model of the Naval Reactor Component Disposal Areas. Not shown is a multilayered-closure cap that will be added above the pads during Post-Institutional Control. See Table 8 for facility description and Figure 18 for photographs of the facility.



Figure 18. (Top) Photo showing partially covered naval reactor components of various sizes. Earth and a clay cap will be mounded over naval reactor waste prior to final disposal. There are two such facilities, the “old” (two top photos) and “new” (bottom photo) facilities. (Bottom) Naval reactor component before it is placed in the disposal area (WSRC 2008).

**Table 8.** Naval Reactor Component Disposal Areas: Conceptual Geochemical Model Features and Parameters (See Figure 17).

Solid Phases	Aqueous Phase	Geochemical Parameter <sup>(b)</sup>
Waste Zone: Activated metal waste. It is assumed that the metal waste will rust to form Fe-oxides and that the radionuclides will sorb to these Fe-oxides. <sup>(a)</sup>	SRS ground water: pH 5.5, ionic strength $10^{-4}$ <sup>12</sup> , except for trace levels of radionuclide concentrations and CDPs (Table 1)	Initially use Clayey Sediment <i>Kd</i> .
Clayey Sediment: Upper Vadose Zone	As above.	Use Clayey Sediment <i>Kd</i> .
Sandy Sediment: Lower Vadose Zone	As above.	Use Sandy Sediment <i>Kd</i> .
Sandy Sediment: Aquifer Zone	As above	Same as immediately above.
<p><sup>(a)</sup> This waste contains large pieces of activated metal naval reactor components encased in heavily shielded shipping containers. There are two Naval Reactor Component Disposal Areas. The casks are placed on an earthen pad and will be covered with a minimum of 4.1 m of backfill and a moisture barrier (clay, gravel, and geotextile fabric layers). There are negligible amounts of cellulosic materials included amongst this waste.</p> <p><sup>(b)</sup> To pack in the naval reactor casks in the subsurface, an unspecified suitable solid has been mandated. The solid could be sand, backfill sediment, or cementitious material (Phifer et al. 2009). If the latter is used, than cementitious impacted <i>Kd</i> values should be used throughout each Environment.</p>		

<sup>12</sup> Ionic strength of a solution is a measure of the amount of ionic species in solutions and is proportional to the salt content. Its influence on radionuclide sorption is complex and non-linear. In simple cation exchange systems, as described by *Kd* values, an increase in ionic strength results in greater desorption, and this general rule holds true in most natural environments. Above a critical concentration, and depending on the ions in solution, precipitation may occur.

## 5.6 TRU Pad Disposal Unit

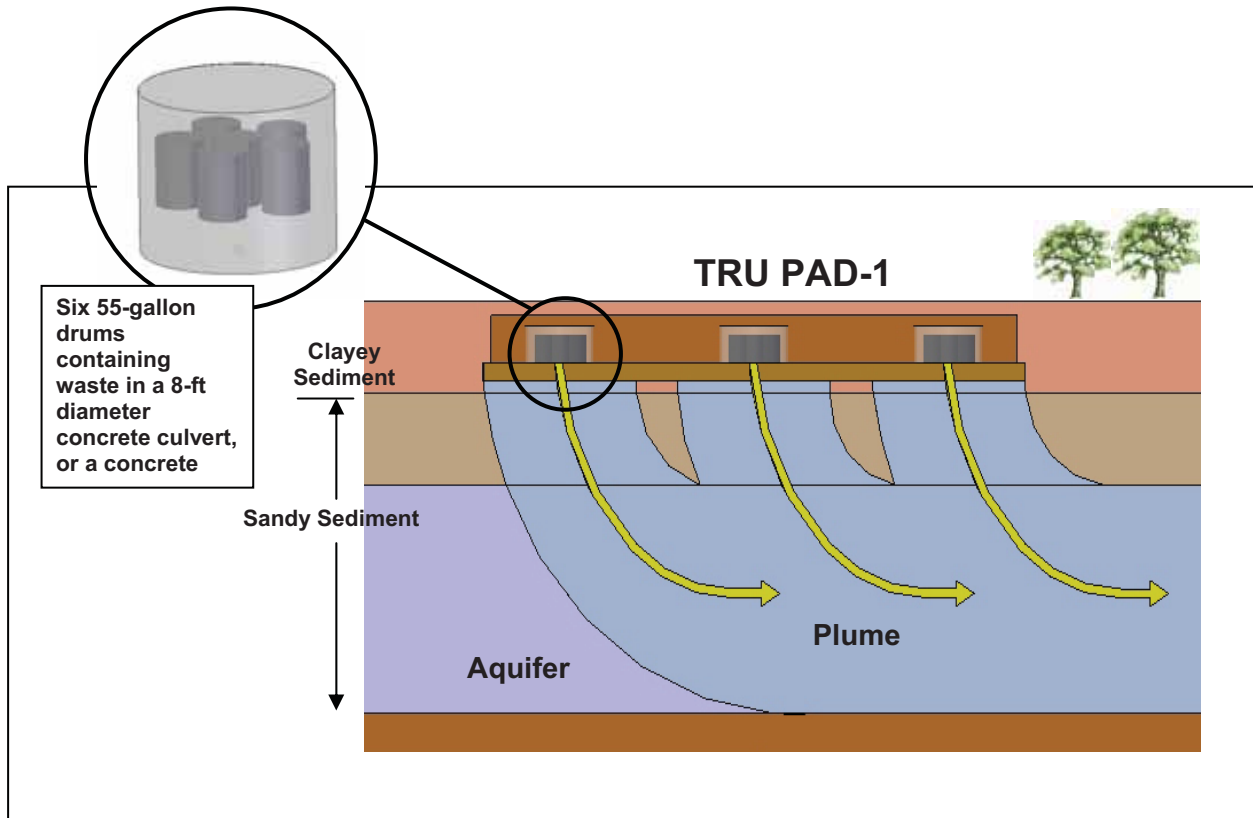


**Figure 19.** Schematic representation of the geochemical conceptual model of the TRU PAD-1. Not shown is a multilayered-closure cap that will be added above the pads during Post-Institutional Control. See Table 9 for facility description.

**Table 9.** TRU PAD-1: Conceptual Geochemical Model of Features and Parameters (See Figure 19).

Solid Phases	Aqueous Phase	Geochemical Parameter
Waste Zone <sup>(a)</sup>	Oxidizing Concrete: Three types of concrete leachate chemistries controlled by different aged solid phases: young concrete leachate pH ~12, then pH 10.5, final pH 5.5 (Figure 6); higher in ionic strength than SRS groundwater	Oxidizing Concrete <i>Kd</i> or Oxidizing Concrete solubility concentration limits. <i>Kd<sub>CDP</sub></i> are necessary because job waste is included in waste zone.
Concrete: 1-ft-thick concrete/grout walls & floor of trench, concrete/grout poured over waste to encapsulate waste.	Oxidizing Concrete (as immediately above)	Oxidizing Concrete <i>Kd</i> or Oxidizing Concrete solubility concentration limits
Clayey Sediment: Upper Vadose Zone	Cementitious (as above).	Use cementitious leachate impacted clayey <i>Kd</i> values; <i>Kd<sub>CementLeach</sub></i>
Sandy Sediment: Lower Vadose Zone	Cementitious (as above).	Use cementitious leachate impacted sandy <i>Kd</i> values; <i>Kd<sub>CementLeach</sub></i> for sandy sediment.
Sandy Sediment: Aquifer Zone	Cementitious leachate pore water gets diluted with typical SRS groundwater and the aqueous phase takes on the properties of the latter: pH 5.8, ionic strength $10^{-4}$ , trace levels of radionuclide concentrations and CDPs.	Initially use Sandy Sediment <i>Kd<sub>CDP</sub></i> until all the CDP <sup>(b)</sup> has leached from the Waste Zone. Then use Sandy Sediment <i>Kd</i> .
<p><sup>(a)</sup> This waste form includes six 55-gallon drums that are placed in an 8-ft-diameter concrete culvert or concrete box. The drums will be arranged with one drum in the middle and the remaining five surrounding it. Concrete will be poured between the drums to hold them in the culvert or concrete box. Approximately 2 ft of concrete will be poured between the outside of the drums and the inside of the culvert/box. The waste-containing concrete culverts/boxes will be placed on a concrete pad and will be covered with a minimum of 4.1 m of backfill and a moisture barrier (clay, gravel, and geotextile fabric layers).</p> <p><sup>(b)</sup> Some protective clothing and a small amount of cellulosic material is included in this waste, thus CDP-<i>Kd</i> values need to be applied for the appropriate length of time, as discussed in section 3.4.1 (<i>Kd<sub>CDP</sub></i> = <i>Kd</i> for cellulose degradation products).</p>		

## 5.7 Saltstone Disposal Facility

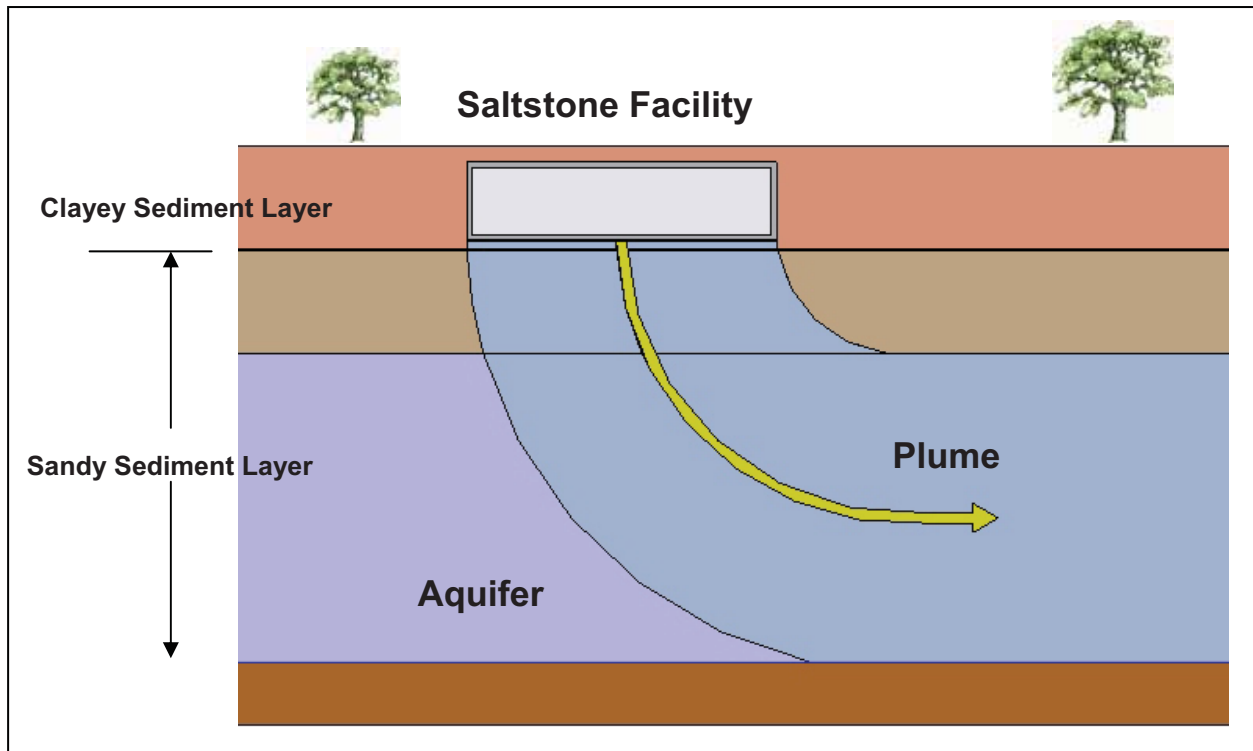


**Figure 20.** Schematic representation of the geochemical conceptual model of the Saltstone Facility. Not shown is a multilayered-closure cap that will be added above the Saltstone Facility during Post-Institutional Control. See Table 10 for facility description.

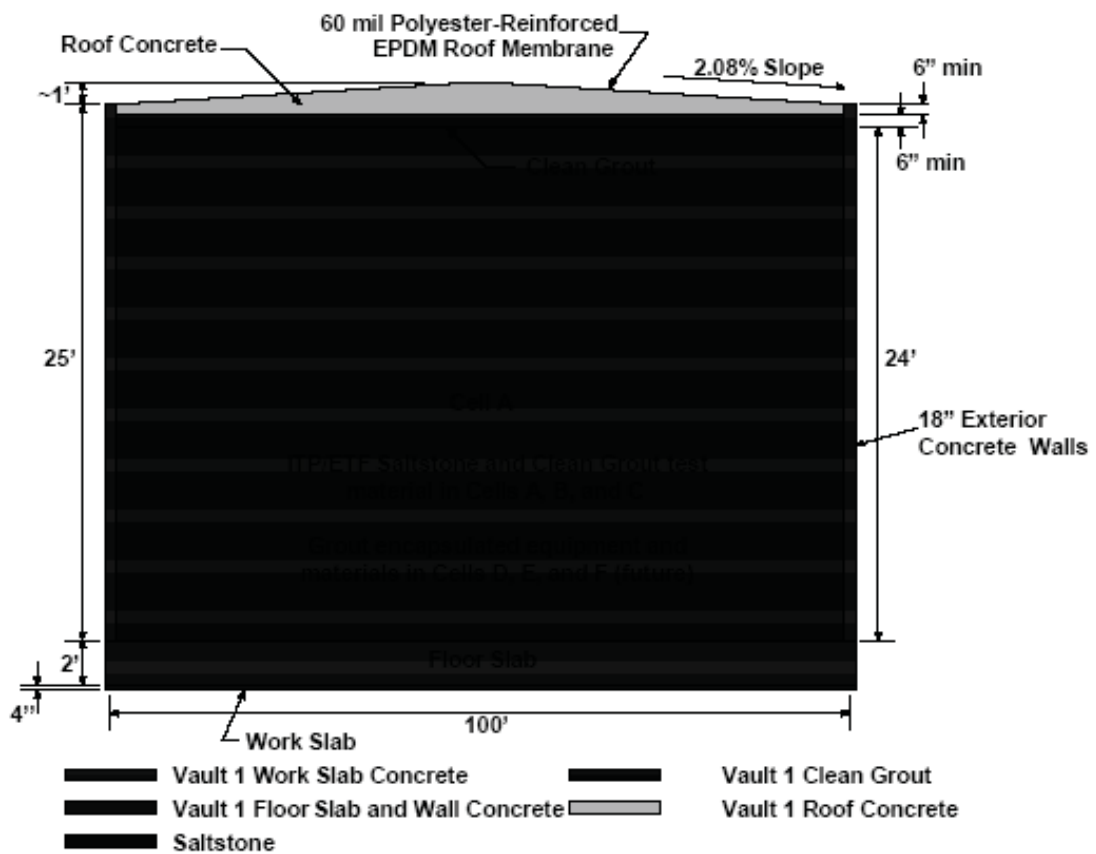
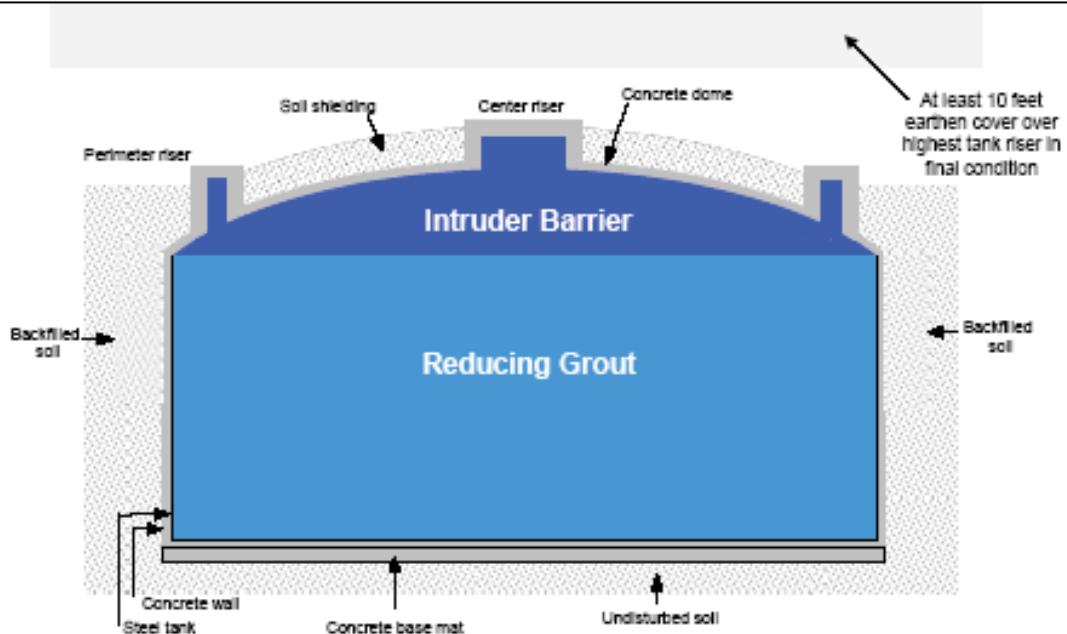
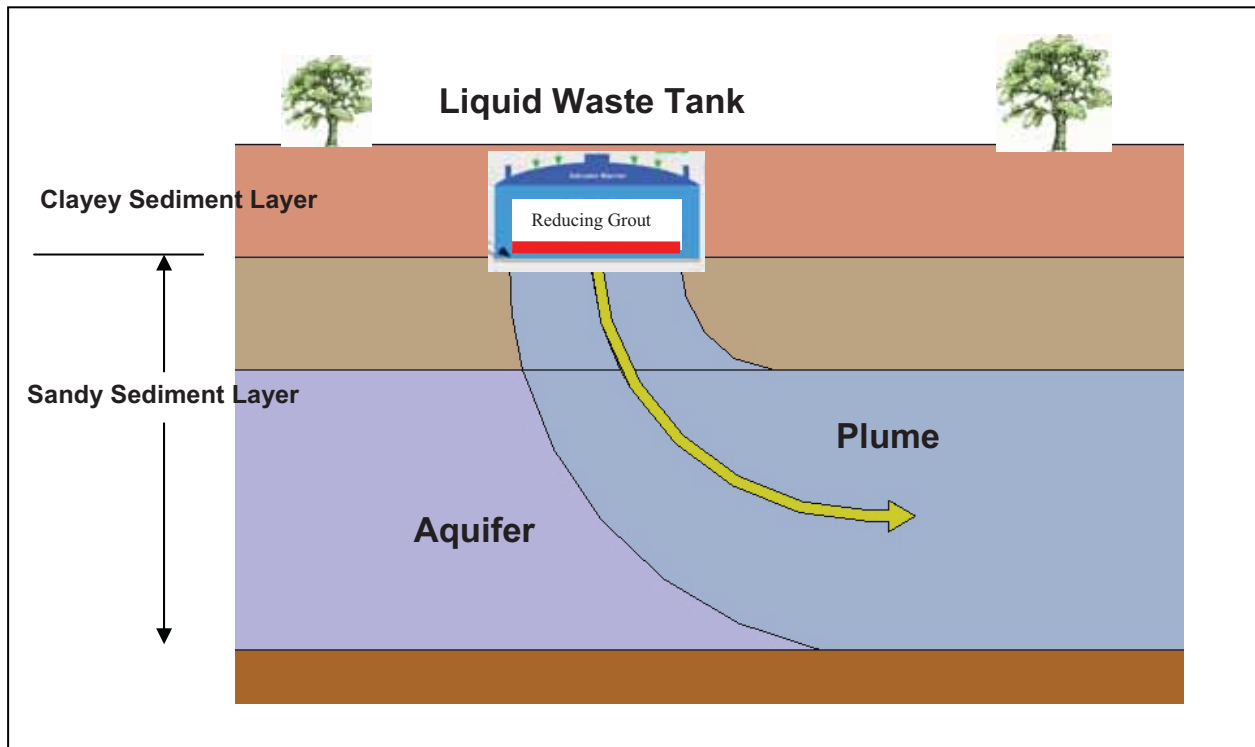


Figure 21. (Top) Saltstone disposal facility (SDF) Vault 1 and 4 (photograph taken December 1, 2002). Metal roofs shown over Vault 1 Cells D and E have been removed from the vault. (Bottom) Cross sectional diagram of Vault 1 (WSRC 2008).

**Table 10.** Saltstone Facility: Conceptual Geochemical Model of Features and Parameters (See Figure 20 and Figure 21).

<b>Solid Phases</b>	<b>Aqueous Phase</b>	<b>Geochemical Parameter</b>
Waste Zone <sup>(a)</sup>	Reducing Cementitious <sup>(c)</sup> : Three types of concrete leachate chemistries controlled by different aged solid phases: young concrete leachate pH ~12, then pH 10.5, final pH 5.5 (Figure 6); generally higher in ionic strength than SRS groundwater. Leachate will contain sulfides released from slag (Angus and Glasser 1985).	Reducing Concrete <i>Kd</i> or Reducing Concrete solubility concentration limits <sup>(b)</sup>
Reducing Concrete <sup>(c)</sup> : 1-ft-thick concrete/grout walls and 2-ft thick floor of vault.	Reducing Concrete (as immediately above)	Reducing Concrete <i>Kd</i> or Reducing Concrete solubility concentration limits <sup>(b)</sup>
Clayey Sediment: Upper Vadose Zone	Cementitious (as above).	Use cementitious leachate impacted clayey <i>Kd</i> values; <i>Kd<sub>CementLeach</sub></i> .
Sandy Sediment: Lower Vadose Zone	Cementitious (as above).	Use cementitious leachate impacted sandy <i>Kd</i> values; <i>Kd<sub>CementLeach</sub></i> for sandy sediment.
Sandy Sediment: Aquifer Zone	Cementitious leachate pore water gets diluted with typical SRS groundwater and the aqueous phase takes on the properties of the latter: pH 5.8, ionic strength $10^{-4}$ , trace levels of radionuclide concentrations and CDPs.	Initially use Sandy Sediment <i>Kd<sub>CDP</sub></i> until all the CDP <sup>(d)</sup> has leached from the Waste Zone. Then use Sandy Sediment <i>Kd</i> .
<p><sup>(a)</sup> The Saltstone contains blast-furnace slag (a strong reducing agent). The dimensions of the vaults vary; some are rectangular, while others are cylindrical.</p> <p><sup>(b)</sup> Kaplan and Hang (2003) estimated that reducing conditions in the Saltstone facility will exist for an extremely long time. They calculated that after 10,000 years, &lt;3% of the total reduction capacity of the Saltstone waste had been oxidized. Therefore, to assume that reducing condition exist during the entire duration of the PA simulation is acceptable (See Section 4.3). Additional research needs to be conducted in this area and is proposed in Section 7.0.</p> <p><sup>(c)</sup> Reducing cementitious materials are those that contain slag and change the pore water chemistry sufficiently to require unique geochemical parameters (see Section 4.3).</p>		

5.8 Radioactive Waste Tanks



[NOT TO SCALE]

**Figure 22.** Schematic representation of the geochemical conceptual model of the Radioactive Waste Tank Closure Concept. See Table 11 for facility description (Bottom figure taken from Buice et al. 2005).



**Figure 23.** Examples of Radioactive Waste Tank construction. Top Left: 17-cm concrete basemat pads; Top Right: Carbon steel liners; Bottom Left: Tank concrete walls (note relative scale of tanks compared to men on scaffolding (photos from Buice et al. 2005).

**Table 11.** Closed Radioactive Waste Tanks: Conceptual Geochemical Model of Features and Parameters (See Figure 22 and Figure 23).

Solid Phases	Aqueous Phase	Geochemical Parameter
Waste Zone <sup>(a)</sup>	Reducing Cementitious Leachate <sup>(b)</sup> : The rad waste consists typically of a thin layer (averaging 1.2 to 2 cm thick) existing on bottom of tank, ranging from ~0.3 cm for most of the bottom to ~4.5 cm along the edges. It is covered with reducing grout. Three types of concrete leachate chemistries controlled by different aged solid phases: young concrete leachate pH ~12, then pH 10.5, final pH 5.5; generally higher in ionic strength than SRS groundwater. Leachate will contain sulfides released from slag (Angus and Glasser 1985).	Reducing Concrete <i>Kd</i> or Reducing Concrete solubility concentration limits <sup>(b)(c)</sup>
Basemat Concrete: 18-cm-thick concrete basemat thick floor.	Reducing Cementitious Leachate: we model as if the aqueous phase is a reducing leachate because essentially all the water will originate from the closed tank above	Reducing Concrete <i>Kd</i> or Reducing Concrete solubility concentration limits <sup>(b)</sup>
Clayey Sediment: Upper Vadose Zone	Oxidized Cementitious Leachate: Oxidized cementitious leachate with three types of water chemistries, as described above.	Use cementitious leachate impacted clayey <i>Kd</i> values; $Kd_{CementLeach}$
Sandy Sediment: Lower Vadose Zone	Oxidized Cementitious Leachate:	Use cementitious leachate impacted sandy <i>Kd</i> values; $Kd_{CementLeach}$ for sandy sediment.
Sandy Sediment: Aquifer Zone	Cementitious leachate pore water gets diluted with typical SRS groundwater and the aqueous phase takes on the properties of the latter: pH 5.8, ionic strength $10^{-4}$ , trace levels of radionuclide concentrations.	Use Sandy Sediment <i>Kd</i> .
<p><sup>(a)</sup> Release of contaminants from the Contamination Zone is described by Denham (2009). In this model, radionuclides are solubility controlled.</p> <p><sup>(b)</sup> Reducing cementitious materials are those that contain slag and change the pore water chemistry sufficiently to require unique geochemical parameters (see Section 4.3).</p> <p><sup>(c)</sup> This table is not applicable for all tanks. The intruder barrier would not have to be treated differently than the grout.</p>		

## 6.0 DATA TABLES

A number of data tables are presented in the section based on the conceptual models presented in Section 4.0. The first three are look-up tables that assembled to make it easy to find values quickly. The remaining tables provide supporting information.

- Table 13. Look-up Table of Various Sediment *Kd* Values: Best *Kd* Values, *Kd* (CDP) Values, Cement Leachate with CDP *Kd* Values, Cement Leachate Impact Factors, and Cellulose Degradation Product Correction Factor.
- Table 14. Look-up Table of Concrete *Kd* Values and Apparent Solubility Values Under Oxidizing and Reducing Conditions.
- Table 15. Special Waste Form *Kd Values* (mL/g) Under Ambient and Cementitious Leachate Environments.
- Table 16. Distribution Coefficients (*Kd* values, mL/g): Sandy Sediment Layer (<25 wt-% silt + clay) and Clay Sediment Layer (25 to 45 wt-% silt + clay)
- Table 17. Distribution Coefficients (*Kd* values, mL/g): Oxidizing Cementitious Solids
- Table 18. Distribution Coefficients (*Kd* values, mL/g): Reducing Cementitious Solids
- Table 19. Apparent Solubility Concentration Limits (mol/L) for Oxidizing Cementitious Solids
- Table 20. Apparent Solubility Concentration Limits (mol/L) for Reducing Cementitious Solids

For the look-up tables, a “best” value and a “minimum” and “maximum” value are provided. The “minimum” and “maximum” values, as discussed in Section 4.6, represent the limits of the 95% range of expected *Kd* values. These estimates are based on generalized rules that are site specific and vary with sediment type, clay or sand (rules defining ranges of cement sorption values are identical to those for sand).

**Table 12.** Radionuclides of Interest and Their Assumed Oxidation States or Speciation Under Varying Environments.

	Chemical Grouping <sup>(b)</sup>	Sandy Sediment, Clayey Sediment, Cementitious Leachate Impacted Sandy/Clayey Sediment, CDP Impacted Sandy/Clayey Sediment	Oxidizing Cement	Reducing Cement
tritium (T)		HTO	HTO, OH <sup>-</sup>	HTO, OH <sup>-</sup>
Inorganic C		CO <sub>3</sub> <sup>2-</sup> , HCO <sub>3</sub> <sup>-</sup>	CO <sub>3</sub> <sup>2-</sup> , HCO <sub>3</sub> <sup>-</sup>	CO <sub>3</sub> <sup>2-</sup> , HCO <sub>3</sub> <sup>-</sup>
Ag, Tl	Monovalent soft metal	+1	+1	+1
Al	Trivalent metal	+3	+3	+3
As, Sb	Divalent Oxyanion	XO <sub>4</sub> <sup>2-</sup>	+5	+3
Co, Cd, Ni, Pt	Divalent Transition	+2	+2	+2
Cr		CrO <sub>4</sub> <sup>2-</sup>	+6	+3
Cu			+2	+1
Fe		Fe <sup>+3</sup>	+3	+2
Mn			+4	+2
Mo			+6	+4
N		NO <sub>3</sub> <sup>-</sup> /NO <sub>2</sub> <sup>-</sup>	+5/+3	-3
Se, Te	VIB Elements	XO <sub>4</sub> <sup>2-</sup> , XO <sub>3</sub> <sup>2-(c)</sup>	XO <sub>4</sub> <sup>2-</sup> , XO <sub>3</sub> <sup>2-</sup>	XO <sub>3</sub> <sup>2-</sup>
Kr, Rn, Ar	Noble Gas	0	0	0
Sr, Ra, Ba, Ca	Alkali-earth metals	+2	+2	+2
Zr, Th	Group VI Elements	+4	+4	+4
Nb		Nb(OH) <sub>6</sub> <sup>-</sup>	Nb(OH) <sub>6</sub> <sup>-</sup>	Nb(OH) <sub>4</sub> <sup>-(a)</sup>
Tc, Re	XO <sub>4</sub> <sup>-(c)</sup>	XO <sub>4</sub> <sup>-</sup>	XO <sub>4</sub> <sup>-</sup>	X <sup>4+</sup>
Sn		+4	+4	+4
Cl, F, I, At	VIIB, Halides	-1	-1	-1
Cs, Fr, K, Na, Rb	Alkali metal	+1	+1	+1
Ac, Am, Bk, Bi, Ce, Cf, Cm, Eu, Gd, Lu, Sm, Y	Trivalent Actinides & Rare Earth Elements	+3	+3	+3
Hg, Pb, Po,	Soft, divalent cation	+2	+2	+2
U		UO <sub>2</sub> <sup>2+</sup>	UO <sub>2</sub> <sup>2+</sup>	U <sup>4+</sup>
Np, Pa		XO <sub>3</sub> <sup>-(c)</sup>	XO <sub>3</sub> <sup>-</sup>	X <sup>4+</sup>
Pu		Pu <sup>VI</sup> O <sub>2</sub> <sup>2+</sup> , Pu <sup>V</sup> O <sub>2</sub> <sup>+</sup> , colloid	Pu <sup>VI</sup> O <sub>2</sub> <sup>2+</sup> , Pu <sup>V</sup> O <sub>2</sub> <sup>+</sup> , colloid	Pu <sup>4+</sup> , colloid

<sup>(a)</sup> Nb likely exists as Nb(III) under reducing conditions, but little sorption data is available for this species (Baes and Mesmer 1976).

<sup>(b)</sup> These groupings of radionuclides will be used in the following *Kd* and solubility limit value tables in the absence of experimental data. These groupings are based on basic chemical considerations including periodicity and basic aqueous chemical properties.

<sup>(c)</sup> X = generic metal

Table 13. Look-up Table of Various Sediment *Kd* Values: Best *Kd* Values, *Kd* (CDP) Values, Cement Leachate with CDP *Kd* Values, Cement Leachate with CDP *Kd* Values, Cement Leachate with CDP Impact Factors, and Cellulose Degradation Product Correction Factor.

Rad	Best Sand <i>Kd</i> (mL/g)	Best Clay <i>Kd</i> (mL/g)	Best Sand <i>Kd</i> (CemLeach) (mL/g)	Best Clay <i>Kd</i> (CemLeach) (mL/g)	Best Sand <i>Kd</i> (CDP) (mL/g)	Best Clay <i>Kd</i> (CDP) (mL/g)	Best Cement Leachate with CDP Sand <i>Kd</i> (mL/g)	Best Cement Leachate with CDP Clay <i>Kd</i> (mL/g)	Cement Leachate Impact Factor, f(CemLeach) (unitless)	Sand Cellulose Degradation Product Correction Factor f(CDP) (unitless)	Clay Cellulose Degradation Product Correction Factor f(CDP) (unitless)	Correction Factor or f(CemLeach) for Best cement leachate with CDP Sand <i>Kd</i> (unitless)	Correction Factor f(CemLeach) or f(CemLeach) for Best cement leachate with CDP Clay <i>Kd</i> (unitless)
Ac	1100	8500	1650	12750	605	4675	1650	12750	1.5	0.55	0.55	1.5	1.5
Ag	60	150	192	480	60	150	192	480	3.2	1	1	3.2	3.2
Al	1300	1300	1950	1950	715	715	1950	1950	1.5	0.55	0.55	1.5	1.5
Am	1100	8500	1650	12750	605	4675	1650	12750	1.5	0.55	0.55	1.5	1.5
Ar	0	0	0	0	0	0	0	0	1	1	1	1	1
As	100	200	140	280	100	200	100	200	1.4	1	1	1	1
At	0.3	0.9	0.0	0.1	0.3	0.9	0.3	0.9	0.1	1	1	1	1
Ba	5	17	15	51	5	17	5	17	3	1	1	1	1
Bi	1100	8500	1650	12750	605	4675	1650	12750	1.5	0.55	0.55	1.5	1.5
Bk	1100	8500	1650	12750	605	4675	1650	12750	1.5	0.55	0.55	1.5	1.5
C	10	400	50	2000	10	400	10	400	5	1	1	1	1
Ca	5	17	15	51	5	17	5	17	3	1	1	1	1
Cd	15	30	45	90	15	30	45	90	3	1	1	3	3
Ce	1100	8500	1650	12750	605	4675	1650	12750	1.5	0.55	0.55	1.5	1.5
Cf	1100	8500	1650	12750	605	4675	1650	12750	1.5	0.55	0.55	1.5	1.5
Cl	0	0	0	0	0	0	0	0	0.1	1	1	1	1
Cm	1100	8500	1650	12750	605	4675	1650	12750	1.5	0.55	0.55	1.5	1.5
Co	40	100	128	320	40	100	128	320	3.2	1	1	3.2	3.2
Cr	4	10	6	14	4	10	4	10	1.4	1	1	1	1
Cs	10	50	10	50	10	50	10	50	1	1	1	1	1
Cu	50	70	160	224	50	70	160	224	3.2	1	1	3.2	3.2
Eu	1100	8500	1650	12750	605	4675	1650	12750	1.5	0.55	0.55	1.5	1.5
F	0	0	0	0	0	0	0	0	0.1	1	1	1	1
Fe	200	400	300	600	110	220	300	600	1.5	0.55	0.55	1.5	1.5
Fr	10	50	10	50	10	50	10	50	1	1	1	1	1
Gd	1100	8500	1650	12750	605	4675	1650	12750	1.5	0.55	0.55	1.5	1.5
H	0	0	0	0	0	0	0	0	1	1	1	1	1
Hg	800	1000	2560	3200	800	1000	2560	3200	3.2	1	1	3.2	3.2
I	0.3	0.9	0.0	0.1	0.3	0.9	0.3	0.9	0.1	1	1	1	1
K	5	25	5	25	5	25	5	25	1	1	1	1	1
Kr	0	0	0	0	0	0	0	0	1	1	1	1	1

Rad	Best Sand Kd (mL/g)	Best Clay Kd (mL/g)	Best Sand Kd (CemLech) (mL/g)	Best Clay Kd (CemLech) (mL/g)	Best Sand Kd (CDP) (mL/g)	Best Clay Kd (CDP) (mL/g)	Best Cement Leachate with CDP Sand Kd (mL/g)	Best Cement Leachate with CDP Clay Kd (mL/g)	Cement Leachate Impact Factor, f(CemLech) (unitless)	Sand Cellulose Degradation Product Correction Factor f(CDP) (unitless)	Clay Cellulose Degradation Product Correction Factor f(CDP) (unitless)	Correction Factor f(CDP) or f(CemLech) for Best cement leachate with CDP Clay Kd (unitless)	Correction Factor f(CDP) or f(CemLech) for Best cement leachate with CDP Sand Kd (unitless)
Lu	1100	8500	1650	12750	605	4675	1650	12750	1.5	0.55	0.55	1.5	1.5
Mn	15	200	21	280	15	200	15	200	1.4	1	1	1	1
Mo	1000	1000	1400	1400	1000	1000	1000	1000	1.4	1	1	1	1
N	0	0	0	0	0	0	0	0	0.1	1	1	1	1
Na	5	25	5	25	5	25	5	25	1	1	1	1	1
Nb	0	0	0	0	0	0	0	0	1.4	0.2	1	0.2	1
Ni	7	30	22	96	7	30	22.4	96	3.2	1	1	3.2	3.2
Np	3	9	5	14	3	9	5	14	1.5	1	1	1.5	1.5
Pa	3	9	5	14	3	9	5	14	1.5	1	1	1.5	1.5
Pb	2000	5000	6400	16000	2000	5000	6400	16000	3.2	1	1	3.2	3.2
Pd	7	30	22	96	7	30	22	96	3.2	1	1	3.2	3.2
Po	2000	5000	4000	10000	2000	5000	4000	10000	2	1	1	2	2
Pt	7	30	22	96	7	30	22.4	96	3.2	1	1	3.2	3.2
Pu(combo)	290	5950	580	11900	290	5950	580	11900	2	1	1	2	2
Pu(III/IV)	300	6000	600	12000	300	6000	600	12000	2	1	1	2	2
Pu(V/VI)	16	5000	32	10000	16	5000	16	5000	2	1	1	1	1
Ra	5	17	15	51	5	17	5	17	3	1	1	1	1
Rb	10	50	10	50	10	50	10	50	1	1	1	1	1
Re	0.6	1.8	0.1	0.2	0.6	1.8	0.6	1.8	0.1	1	1	1	1
Rn	0	0	0	0	0	0	0	0	1	1	1	1	1
Sb	2500	2500	3500	3500	2500	2500	2500	2500	1.4	1	1	1	1
Se	1000	1000	1400	1400	1000	1000	1000	1000	1.4	1	1	1	1
Sm	1100	8500	1650	12750	605	4675	1650	12750	1.5	0.55	0.55	1.5	1.5
Sn	2000	5000	6000	15000	2000	5000	6000	15000	3	1	1	3	3
Sr	5	17	15	51	5	17	5	17	3	1	1	1	1
Tc	0.6	1.8	0.1	0.2	0.6	1.8	0.6	1.8	0.1	1	1	1	1
Te	1000	1000	1400	1400	1000	1000	1000	1000	1.4	1	1	1	1
Th	900	2000	1800	4000	900	2000	1800	4000	2	1	1	2	2
Tl	10	50	10	50	10	50	10	50	1	1	1	1	1
U	200	300	600	900	200	300	600	900	3	1	1	3	3
Y	1100	8500	1650	12750	605	4675	1650	12750	1.5	0.55	0.55	1.5	1.5
Zn	15	30	45	90	15	30	45	90	3	1	1	3	3
Zr	900	2000	1800	4000	900	2000	1800	4000	2	1	1	2	2

**Table 14.** Look-up Table of Concrete *Kd* Values and Apparent Solubility Values Under Oxidizing and Reducing Conditions.

Rad	Best Oxidizing Cement <i>Kd</i> Young	Best Oxidizing Cement <i>Kd</i> Middle	Best Oxidizing Cement <i>Kd</i> Old	Best Reducing Cement <i>Kd</i> Young	Best Reducing Cement <i>Kd</i> Middle	Best Reducing Cement <i>Kd</i> Old	Oxidizing Apparent Solubility Young (10e-x)	Oxidizing Apparent Solubility Middle (10e-x)	Oxidizing Apparent Solubility Old (10e-x)	Reducing Apparent Solubility Young (10e-x)	Reducing Apparent Solubility Middle (10e-x)	Reducing Apparent Solubility Old (10e-x)
Ac	6000	6000	600	7000	7000	1000	-11	-8	-7	-11	-8	-7
Ag	4000	4000	400	5000	5000	1000	-7	-7	-6	-7	-7	-6
Al	6000	6000	600	7000	7000	1000	-11	-8	-7	-11	-8	-7
Am	6000	6000	600	7000	7000	1000	-11	-8	-7	-11	-8	-7
Ar	0	0	0	0	0	0	NA	NA	NA	NA	NA	NA
As	1000	1000	100	1000	1000	100	NA	NA	NA	NA	NA	NA
At	8	15	4	5	9	4	NA	NA	NA	NA	NA	NA
Ba	100	100	70	100	100	70	-5	-5	NA	-5	-5	NA
Bi	6000	6000	600	7000	7000	1000	-11	-8	-7	-11	-8	-7
Bk	6000	6000	600	7000	7000	1000	-11	-8	-7	-11	-8	-7
C	3000	3000	300	3000	3000	300	-6	-4	-4	-6	-4	-4
Ca	15	15	5	15	15	5	-5	-5	NA	-5	-5	NA
Cd	4000	4000	400	5000	5000	1000	-7	-7	-6	-7	-7	-6
Ce	6000	6000	600	7000	7000	1000	-11	-8	-7	-11	-8	-7
Cf	6000	6000	600	7000	7000	1000	-11	-8	-7	-11	-8	-7
Cl	10	10	1	10	10	1	NA	NA	NA	NA	NA	NA
Cm	6000	6000	600	7000	7000	1000	-11	-8	-7	-11	-8	-7
Co	4000	4000	400	5000	5000	2000	-7	-7	-6	-7	-7	-6
Cr	10	10	1	1000	1000	1000	NA	NA	NA	-7	-7	-6
Cs	2	20	10	2	20	10	NA	NA	NA	NA	NA	NA
Cu	4000	4000	400	5000	5000	2000	-7	-7	-6	-7	-7	-6
Eu	6000	6000	600	7000	7000	1000	-11	-8	-7	-11	-8	-7
F	10	10	1	10	10	1	NA	NA	NA	NA	NA	NA
Fe	6000	6000	600	7000	7000	1000	-11	-8	-7	-11	-8	-7
Fr	2	20	10	2	20	10	NA	NA	NA	NA	NA	NA
Gd	6000	6000	600	7000	7000	1000	-11	-8	-7	-11	-8	-7
H	0	0	0	0	0	0	NA	NA	NA	NA	NA	NA
Hg	300	300	100	5000	5000	2000	-7	-7	6	-7	-7	6
I	8	15	4	5	9	4	NA	NA	NA	NA	NA	NA
K	2	20	10	2	20	10	NA	NA	NA	NA	NA	NA
Kr	0	0	0	0	0	0	NA	NA	NA	NA	NA	NA

Rad	Best Oxidizing Cement Kd Young	Best Oxidizing Cement Kd Middle	Best Oxidizing Cement Kd Old	Best Reducing Cement Kd Young	Best Reducing Cement Kd Middle	Best Reducing Cement Kd Old	OXIDIZING Apparent Solubility Young (10e-x)	OXIDIZING Apparent Solubility Middle (10e-x)	OXIDIZING Apparent Solubility Old (10e-x)	REDUCING Apparent Solubility Young (10e-x)	REDUCING Apparent Solubility Middle (10e-x)	REDUCING Apparent Solubility Old (10e-x)
Lu	6000	6000	600	7000	7000	1000	-11	-8	-7	-11	-8	-7
Mn	100	100	10	100	100	10	NA	NA	NA	NA	NA	NA
Mo	300	300	150	300	300	150	NA	NA	NA	NA	NA	NA
N	10	10	1	10	10	1	NA	NA	NA	NA	NA	NA
Na	0.5	1	0.5	0.5	1	0.5	NA	NA	NA	NA	NA	NA
Nb	1000	1000	500	1000	1000	500	NA	NA	NA	NA	NA	NA
Ni	4000	4000	400	4000	4000	400	-7	-7	-6	-7	-7	-6
Np	10000	10000	5000	10000	10000	5000	-13	-13	-7	-13	-13	-5
Pa	10000	10000	5000	10000	10000	5000	-13	-13	-7	-13	-13	-5
Pb	300	300	100	500	500	250	-7	-7	-6	-7	-7	-6
Pd	4000	4000	400	4000	4000	400	-7	-7	-6	-7	-7	-6
Po	300	300	100	5000	5000	500	-7	-7	-6	-7	-7	-6
Pt	4000	4000	400	5000	5000	2000	-7	-7	-6	-7	-7	-6
Pu(combo)	10000	10000	2000	10000	10000	2000	-12	-12	-7	-12	-12	-9
Pu(III/IV)	10000	10000	2000	10000	10000	2000	-12	-12	-7	-12	-12	-9
Pu(V/VI)	1000	1000	100	1000	1000	100	NA	NA	NA	NA	NA	NA
Ra	100	100	70	100	100	70	-6	-6	-6	-6	-6	-6
Rb	2	20	10	2	20	10	NA	NA	NA	NA	NA	NA
Re	0.8	0.8	0.5	5000	5000	1000	NA	NA	NA	-10	-10	-6
Rn	0	0	0	0	0	0	NA	NA	NA	NA	NA	NA
Sb	1000	1000	100	1000	1000	100	NA	NA	NA	NA	NA	NA
Se	300	300	150	300	300	150	NA	NA	NA	NA	NA	NA
Sm	6000	6000	600	7000	7000	1000	-11	-8	-7	-11	-8	-7
Sn	4000	4000	2000	5000	5000	500	-7	-7	-6	-7	-7	-6
Sr	15	15	5	15	15	5	-5	-5	NA	-5	-5	NA
Tc	0.8	0.8	0.5	5000	5000	1000	NA	NA	NA	-10	-10	-6
Te	300	300	150	300	300	150	NA	NA	NA	NA	NA	NA
Th	10000	10000	2000	5000	5000	500	-12	-12	-7	-12	-12	-7
Tl	2	20	10	2	20	10	NA	NA	NA	NA	NA	NA
U	250	250	70	2500	2500	2500	5E-06	5E-05	-6	-6	-7	-7
Y	6000	6000	600	7000	7000	1000	-11	-8	-7	-11	-8	-7
Zn	4000	4000	400	5000	5000	2000	-7	-7	-6	-7	-7	-6
Zr	10000	10000	2000	5000	5000	500	-12	-12	-7	-12	-12	-7

**Table 15.** Special Waste Form  $K_d$  Values (mL/g) Under Ambient and Cementitious Leachate Environments.

Radio-nuclide	Waste Form	$K_d$ When Waste is Disposed in Sediment (mL/g)	$K_d$ When Waste is Disposed in Concrete (mL/g)	References	SRS Document No.
I-129	F-Area Activated C	132,500	880	Kaplan and Serkiz 2000	WSRC-TR-2000-00308
I-129	H-Area Activated C	58,100	320	Kaplan and Serkiz 2000	WSRC-TR-2000-00308
I-129	F-Area CG-8	50	3	Kaplan and Serkiz 2000	WSRC-TR-2000-00308
I-129	H-Area CG-8	380	100	Kaplan and Serkiz 2000	WSRC-TR-2000-00308
I-129	H-Area Filtercake	650	630	Kaplan and Serkiz 2000	WSRC-TR-2000-00308
I-129	H-Area Dowex 21K	15,600	1980	Kaplan and Serkiz 2000	WSRC-TR-2000-00308
I-129	F-WTU Dowex 21K	6,800	2,800	Kaplan et al. 1999	WSRC-TR-1999-00270
I-129	ETF Carbon	7,400	600	Kaplan et al. 1999	WSRC-TR-1999-00270
I-129	EDF GT-73	10,000	3,100	Kaplan et al. 1999	WSRC-TR-1999-00270
I-129	K&L Disassembly Basin Facilities Resins <sup>(a)</sup>	3700 <sup>(b)</sup>	3700 <sup>(b)</sup>	Kaplan and Coffey 2002	WSRC-TR-2002-00349
I-129	SIR-1200	5900	5800	Kaplan 2001	WSRC-TR-2001-00346
I-129	F-Area Ground Water Treatment Unit Filtercake	56.9	13.9	Kaplan and Iverson 1999	WSRC-TR-2001-00253
C-14	K&L Disassembly Basin Facilities Resins <sup>(a)</sup>	240	140	Kaplan and Coffey 2002	WSRC-TR-2002-00349
Tc-99	K&L Disassembly Basin Facilities Resins <sup>(a)</sup>	680 <sup>(b)</sup>	810 <sup>(b)</sup>	Kaplan and Coffey 2002	WSRC-TR-2002-00349

<sup>(a)</sup> This is a mixed bed of resins, including a 42:58 cation:anion mass ratio of the cation resin CG-8, and the anion resin SBG-1. The tests were conducted, as was the case with the other measurements in this table, with spent resin, i.e., resin that had been used in production, actual waste resin that would be disposed.

<sup>(b)</sup> These were originally measured as “greater than” values.

**Table 16.** Distribution Coefficients ( $K_d$  values, mL/g): Sandy Sediment Layer (<25 wt-% silt + clay) and Clay Sediment Layer (25 to 45 wt-% silt + clay)

Radio-nuclide	Sandy Sedi-ment	Clayey Sedi-ment	Comments/References <sup>(a)</sup>
Ar, <sup>3</sup> H, Kr, Rn,	0	0	<u>Tritium &amp; Noble Gases:</u> No sorption experiments were found to have been conducted on SRS sediments or other sediments with these elements. Tritium is assumed to be water species and the inert noble gases should also not interact with the sediments.
Cl, Nb, N (nitrate, nitrite), F	0	0	<u>Anions:</u> Unless site specific data is available, assume that anions do not sorb to SRS sediments.
Cr	4	10	Seaman et al. (32) measured Cr(VI) sorption to SRS vadose sediments in batch and column studies. Fe-oxide existing at below the zero point of charge (pH ~8) were responsible for much of the sorption.
Ac, Am, Bi, Bk, Ce Cf, Cm, Eu, Gd, Lu, Sm, Y	1100	8500	<u>Trivalent Cations:</u> Kaplan and Serkiz (2004) reported that SRS sandy sediment Ce(III) $K_d = 1220 \pm 1040$ mL/g at pH 5.3; SRS clayey sediment Ce(III) $K_d = 8697 \pm 4980$ mL/g at pH 5.3 (Ce(III) is being used here as a chemical analogue for the trivalent radionuclides of interest). Kaplan and Serkiz (2004) reported SRS sandy sediment Eu(III) $K_d = 1168 \pm 1159$ mL/g at pH 5.3; SRS clayey sediment Eu(III) $K_d = 9020 \pm 3526$ mL/g at pH 5.3. Both trivalent cations had very similar $K_d$ values for a given sediment. Grogan et al (29) measured Y $K_d$ values in 27 SRS sediments collected from the SRS subsurface. Most of the $K_d$ values were "greater-than values;" that exceeded 3000 mL/g.
Al	1300	1300	Crapse et al. (31; Figure 33 and Table 4) made in situ measurements of Al solubility in a wide pH range from sediments collected from D-Area. At pH 3.18, Al porewater concentrations were at a maximum of 276,300 ppb, and then the concentration decreased to ~10 ppb at pH 7, and then at higher pH levels the Al concentrations started to rise again. At the pH of interest for the hypothetical Sandy and Clayey sediment, pH 5.5, the Al concentrations (solubility) were ~300 ppb. A comparable $K_d$ value was 1300 mL/g (Al-solid = 402 ppm [Table 25 in Crapse et al. (31) Al-liquid = 0.3ppm [Fig. 33 and Table 5 in Crapse et al. 31]). Theoretically, Al sorption is actually quite large in alkaline environments. Assumed species: Low pH: $Al^{3+}$ , $Al(OH)^{2+}$ , $Al(OH)_3$ , <sup>0</sup> High pH: $Al(OH)_4^-$ , $Al(OH)_4^{2-}$ .
Fe	200	400	Knox and Kaplan (35) measured Fe $K_d$ values of a subsurface sediment collected from TNX on the SRS. They conducted a sorption isotherm ( $K_d$ as a function of dissolved Fe concentrations at ambient pH levels, pH 5.8. They noted a rather flat response of $K_d$ to $Fe_{aq}$ concentrations from 0.1 to 0.21 $\mu$ g/L; above this concentration Fe precipitation obviously occurred because the $K_d$ values increased precipitously. The Fe $K_d$ values at the low concentrations were 400 mL/g.
Inorganic C	10	400	No inorganic C sorption data related to SRS sediments was found in the literature. C is assumed to exist primarily as $HCO_3^-$ and $CO_2$ -gas. The $K_d$ construct does not describe any speciation of gases. Consideration of $CO_2$ -gas will require a special analysis and some site-specific measurements. In the aqueous phase, C is anticipated to exist as an anion, and little sorption is expected. Little carbonate exists in the upper aquifers of the SRS due to the low pH. Roberts and Kaplan (30) found that $^{14}C$ -carbonate sorption to sediments was not a steady state process and that even after 6 months $^{14}C$ -carbonate sorption to SRS sediments had not come to steady state. $K_d$ values in a sandy sediment were 1.50 mL/g after 1 day and 8.64 mL/g after

Radio-nuclide	Sandy Sedi-ment	Clayey Sedi-ment	Comments/References <sup>(a)</sup>
Cs, Fr, Rb, Tl	10	50	<p>6 months. Similarly, <math>K_d</math> values in a subsurface clayey sediment were 27.6 mL/g after 1 day and &gt;372 after 6 months. Again, it was not established that the <math>K_d</math> values would not continue to increase had the contact time been extended.</p> <p><u>Monovalent (Group 1A)</u>: Hoeffner (1985) reported that Cs sorption to SRS sediments is very pH dependent. Under ambient conditions, <math>K_d</math> values = 410 mL/g. Bibler and Marson (1992) reported Cs <math>K_d</math> values for: an E-Area sediment (TF1, 40-60 mesh) of 34 mL/g, a second E-area sediment (TF2, 40-60 mesh) of 37 mL/g, and an ETF sediment of 7 to 8 mL/g. It should be noted that had the entire soil been used, including the &lt;40 mesh fraction, that the <math>K_d</math> values would be larger. Johnson (1995; Figure 5-18) reported Cs <math>K_d</math> values of 800 mL/g in aged samples with initial Cs concentrations of 1e-8 MCs at pH 5. In field observations (squeezed porewater out of aquifer sediment), he measured a <math>K_d</math> of 29 mL/g at pH 5. Johnson (1995; Figure 5-17), using subsurface F-area sediments, showed that the Cs sorption to SRS sediments was very pH dependent and that there was a steep increase in sorption from pH 4.2 to 6.4, between which the <math>K_d</math> increased from about 5 to 95 mL/g. At pH 5.5 the <math>K_d</math> values ranged from 20 to 35 mL/g. Findley (1998) conducted sequential extraction studies and reported that field contaminated sediments did not desorb Cs until extremely harsh acids were used, whereas in lab tests where Cs was added during adsorption (followed by desorption) tests, a majority of the Cs desorbed using relatively mild extractants. This suggests that Cs may become more strongly bound by SRS sediment with time. This same finding has been reported for Hanford and Chernobyl sediments. Goto (2001) conducted &gt;200 Cs sorption experiments with 5 SRS sediments of varying clay content. She showed a strong Cs-<math>K_d</math> dependency on Cs concentrations at environmental-relevant concentrations. The <math>K_d</math> values ranged from <math>226 \pm 51</math> to <math>21 \pm 7</math> mL/g at ambient pH levels; varying directly with clay content (Goto 2001; Table 5-3). Sediments with clay content &gt;10% had Cs <math>K_d</math> values &gt;139 mL/g. Those with clay content &lt;10% had <math>K_d</math> values of 73 to 15 mL/g. In distilled water, Cs <math>K_d</math> values were as high as 1500 mL/g, underscoring the importance of using appropriate background electrolytes when conducting sorption experiments. Grogan et al (29) measured Cs <math>K_d</math> values in 27 sediments collected from E-Area SRS. They used SRS groundwater as a background solution. Mean was <math>13 \pm 3.8</math> mL/g, ranging from 3.5 to 97 mL/g. The Upper Vadose Zone (dominated by clayey sediment) had a mean of <math>11.3 \pm 3.0</math> mL/g; the Lower Vadose Zone (dominated by sandy sediment) had a mean of <math>5.6 \pm 0.5</math> mL/g (Aquifer Zone 21.2 <math>\pm</math> 9.2 mL/g, but it included some clay lenses from the semi-permeable Tan Clay layer and bias the <math>K_d</math> values to be larger).</p> <p>There has not been any Na or K sorption studies conducted with SRS sediments. Estimates were set lower than Cs sorption values because Na and K are also monovalent cations in the Group 1A in the Periodic Table, but they are strongly hydrated, weakening their sorption bonds to sediments.</p>
Na, K	5	25	<p>Hoeffner (1985) reported that a SRS sandy sediment (9% clay) had a <math>Co K_d = 4.6</math> mL/g, pH ~4.7; SRS clayey sediment (23% clay) had a <math>Co K_d = 29</math> mL/g, pH ~4.7; <math>Co K_d</math> values in SRS sediments were independent of Co concentration between 1e-12 to 1e-6 M Co; <math>Co K_d</math> values in SRS sediments decreased in presence of high divalent cation concentrations but not in presence of high monovalent cation concentrations; strong pH dependency with a slight increase in <math>K_d</math> from pH 2 to 4.8 (background) then sharp increase in <math>K_d</math> as pH increases to pH 7 (<math>K_d = 20,000</math> mL/g), than as pH increased to 9.5 the <math>K_d</math> steadily decreased to ~20 mL/g (thus concrete pH <math>K_d = 30</math>). Oblath et al (1983) reported that SRS lysimeters studies calculated <math>K_d</math> values of 10 to 20 mL/g based on flow calculations. Grogan et al (29) measured Co <math>K_d</math> values in 27 sediments collected from E-Area SRS. Mean was <math>306 \pm 117</math> mL/g, ranging from 33 to 2710 mL/g. The Upper Vadose Zone (dominated by clayey sediment) had a mean of <math>154 \pm 37</math> mL/g; the Lower Vadose Zone had a mean of <math>54 \pm 3</math> mL/g; Aquifer Zone 535 <math>\pm</math></p>

Radio-nuclide	Sandy Sedi-ment	Clayey Sedi-ment	Comments/References <sup>(6)</sup>
At, I	0.3	0.9	264 mL/g (the high value reflect the presence of clay lenses from the semi-permeable Tan Clay layer and bias the $K_d$ values to be larger). Two important iodine studies have been conducted with iodine and SRS sediments in which a great deal was learned about iodine geochemistry on the SRS subsurface (39, 40). Schwehr et al. (39) reported that, not only iodide, but also iodate and organo-iodide existed in the SRS subsurface. This is an important finding because these latter species are known to sorb stronger to sediments than iodide, the assumed form that iodine was expected to exist as. They also reported that iodine sorbed at higher $K_d$ values, 2.5 mL/g (sandy sediment, this is the best measurement of a $K_d$ value we have under natural field conditions), when measured at ambient concentrations, 1e-8 M, than at commonly used elevated experimental values. Bruns et al. (40) further demonstrated Schwehr et al.'s (39) results and reported organo-I $K_d$ values greater than those of iodate values, which in turn were greater than comparable iodide values. Furthermore, for all three forms of iodine added, the $K_d$ values increased as the spiked iodine concentrations approached environmentally relevant concentrations. For iodide, the subsurface sediments had $K_d$ values ranging from 1.1 to 33.7 mL/g; for iodate, the $K_d$ values ranged from 2.4 to 60.9 mL/g. In summary of the 2009 iodine experimentation, the following results warrant increasing iodine sediment $K_d$ values: 1) the measurements of iodate and organo-iodine species in SRS aquifer groundwater (39) (previously it was assumed that the more mobile iodide species existed); 2) the <i>in situ</i> (Schwehr et al. 2009) and laboratory measurements of iodate and organo-iodine species having larger $K_d$ values than iodide; and 3) the observation that iodine $K_d$ value increase as the spike concentrations approach those of environmental relevant concentrations. All previous studies conducted at SRS incorrectly assumed iodine existed as iodide, the poorly sorbing species. Stone et al. (1985) reported iodide ( $I^-$ ) $K_d$ values based on column studies to be 0.6 mL/g, which was at the low range of $K_d$ values measured by the batch method, which ranged from 0.5 to 6.6 mL/g (texture of sediment is unknown). The column studies likely reflect non-equilibrium conditions and thus did not provide sufficient time for the iodide to sorb. Kaplan (2002) reported a similar $K_d$ of 0.6 mL/g at pH ~5 in an upland sandy sediment and 1.2 mL/g in a wetland sediment at pH 5. Hoeffner (1985) reported appreciably higher $K_d$ values in a sediment that contained 31% silt+clay content of 10, 5.35, and 3.62, mL/g for initial $I^-$ concentration of 5, 50 and 500 $\mu\text{g/L}$ . Iodide sorption to a clayey subsurface SRS sediment (no fulvic acid added) and SRS uncontaminated groundwater was (units of mL/g): $K_d = 0.2 \pm 0.2$ at pH 3.9, $K_d = 0.1 \pm 0.4$ at pH 5.3, and $0.2 \pm 0.1$ at pH 6.7 (24). Similar experimental setup, except to a sandy subsurface SRS sediment $K_d$ values were always ~0 mL/g between pH 3.9 and 6.7 (24). These latter studies had too much variability, making it impossible to discern whether the $K_d$ values were significantly different than 0 mL/g.
Ag	60	150	There has not been any Ag sorption studies conducted with SRS sediments. Consequently, literature values were used to select $K_d$ values for this table. In a survey of literature $K_d$ values, Thibault et al. (36) reported sand $K_d$ values of 20, 60, 75 and 200 mL/g and silt/clay Ag- $K_d$ values of 100, 170, 200, 200, and 300 mL/g.
Ni, Pd, Pt	7	30	Kaplan and Serkiz (2004) reported that SRS sandy sediment Ni $K_d = 7 \pm 2$ mL/g at pH 5.3; SRS clayey sediment Ni $K_d = 30 \pm 1$ mL/g at pH 5.3. Using 3 clayey sands (>19% clay) from the SRS, Neiheisel (1983) reported Ni $K_d$ values of 115, 116, and 120. The results from these two studies vary greatly. The lower, more conservative values will be used until additional work warrants using larger values.
Cu	50	70	Cu exists primarily in the +2 state through pH/Eh region of interest. Cu <sup>+</sup> exists only under reducing & pH >6. CuS formed under reducing conditions. In oxidizing conditions, above pH 7, Cu(OH) <sub>2</sub> dominates; below pH 7, Cu <sup>2+</sup> dominates. Did not find any $K_d$ values in literature in acidic or circum-neutral sediments. There have not been any $K_d$ values measured in SRS

Radio-nuclide	Sandy Sedi-ment	Clayey Sedi-ment	Comments/References <sup>(6)</sup>
Cd, Zn	15	30	<p>subsurface sediments. In a fine sand (pH 8.3; OM = 1.4%) Cu <math>Kd = 206</math> mL/g (Wong et al. 34); this value is probably the upper limit of the <math>Kd</math> we may expect in the SRS subsurface due to the elevated organic matter concentrations and pH. Buchter et al. (33) in a survey of 11 soils, reported that a soil ("Windsor": pH = 5.8, OM = 0.67%, silt+clay = 25%) similar to that of a clayey SRS sediment had a Cu <math>Kd</math> value of 77.1 mL/g. In the same study, the sediment most like a "sandy SRS sediment" ("Spodosol": pH 4.3; OM = 1.98%, silt+clay = 10%) had a Cu <math>Kd</math> value of 56 mL/g.</p> <p>Grogan et al (29) measured Cd <math>Kd</math> values in 27 sediments collected from E-Area SRS. Mean was <math>89 \pm 36</math> mL/g, ranging from 9 to 927 mL/g. The Upper Vadose Zone (dominated by clayey sediment) had a mean of <math>37 \pm 8</math> mL/g; the Lower Vadose Zone (dominated by sandy sediment) had a mean of <math>16 \pm 0.9</math> mL/g (Aquifer Zone 131 <math>\pm</math> 53 mL/g, but it included some clay lenses from the semi-permeable Tan Clay layer and bias the <math>Kd</math> values to be larger).</p> <p>Miller et al. (2009) measured <math>Kd</math> values in SRS sandy and clayey sediment of <math>4.26 \pm 0.24</math> mL/g and <math>9.05 \pm 0.61</math> mL/g, respectively. The latter represents the first Np <math>Kd</math> in a clayey sediment. Adding NOM resulted in increases in Np <math>Kd</math> values to 13 and 24 mL/g. In the presence of varying reductants, the <math>Kd</math> values increased between slightly between 13 and 24 mL/g. These slight increases presumably resulted from partial reduction of Np(V) to Np(IV), the stronger sorbing form of Np. An important finding in this study was that Np had little tendency to reduce under to Np(IV) even under the most strongly reducing conditions expected under natural SRS conditions. The only Np sorption study using SRS sediments found in the literature was Sheppard et al (1979). In this study, Np <math>Kd</math> values for a soil (pH = 5.1, cation exchange capacity = 2.5 meq/100 g, 3.6% silt, 0.5% clay, CaCO<sub>3</sub> = &lt;0.2 mg/kg) were 0.25 and 0.16 mL/g. This sediment is lower in clay content and pH than our assumed typical sediments for the "Sandy Sediment" or "Clayey Sediment". Therefore higher values were chosen herein. Np will exist primarily as NpO<sub>2</sub><sup>+</sup> (2f). It has been shown that Np: 1) sorbs moderately to iron oxides and clays, 2) does not compete favorably with dissolved Ca or other divalent ions, 3) sorption is strongly pH dependent, and 4) does not readily convert to Np(IV) under ambient groundwater conditions (2f). Due to lack of experimental data, extra conservatism is included in "Conservative" estimates.</p>
Np, Pa	3	9	<p>A great deal of Pu sorption studies has recently been completed by SRNL and Clemson University (10-19; 26, 27). In these papers the conceptual model for how Pu subsurface transport of Pu is believed to occur at SRS is described. These studies include batch equilibrium, kinetic, and 11 year field lysimeter studies containing sources of Pu of known oxidation state. Wet chemistry and spectroscopic methods (X-ray Absorption Spectroscopy) were conducted to determine Pu oxidation state on aqueous and solid phase samples. Briefly, the dominant Pu oxidation state in the aqueous phase was shown to be Pu(V) and on the solid phase Pu(IV), irrespective of what was the starting Pu oxidation of the solid or aqueous phases. (Note: Although most of Pu in the aqueous phase consists of Pu(V), only trace concentrations of Pu exist in the aqueous phase compared to the solid phase, which is primarily Pu(IV).) After 11 yr, Pu(IV) moved only a couple centimeters in the field, with &gt;95% remaining within 2 cm of the source material (10, 15). Sediment Pu concentration profiles were modeled using <math>Kd</math> sorption terms for a Pu(III/IV) and Pu(V/VI) and kinetic terms to describe the oxidation of Pu(III/IV) to Pu(V/VI) and a reduction term to describe the opposite reaction. Irrespective of what oxidation state Pu is added to SRS sediment, it quickly (within a day) is converted to Pu(IV) sorbed onto sediment (15). Most recently, aqueous Pu concentrations appear to be more controlled by solubility constraints than by adsorption (19). Powell et al. (2002) measured Pu(V) sorption to 4 end-member (extreme geological types) SRS sediments, two of which would be appropriate for consideration here, the "Subsurface Sandy" and "Subsurface Clayey" sediments. Sorption values in the "Subsurface Sandy" most representative of Pu(V) (<i>i.e.</i>,</p>
Pu(V/VI)	16	5000	<p>the "Subsurface Clayey" most representative of Pu(V) (<i>i.e.</i>, the "Subsurface Clayey" most representative of Pu(V) (<i>i.e.</i>,</p>

Radio-nuclide	Sandy Sedi-ment	Clayey Sedi-ment	Comments/References <sup>(6)</sup>
			before all of the Pu was reduced to Pu(IV) may be those measured after “1-day contact time”: at pH 5.3 the $K_d$ was 9 mL/g, at pH 5.72, the $K_d$ was 20 mL/g, at pH 5.94, the $K_d$ was 30 mL/g and at pH 5.90, the $K_d$ was 60 mL/g. The following are taken from the “33-day contact” Subsurface Sandy sediment and likely are more representative of Pu(IV) in the system: pH 5.41/ $K_d$ 4900, and pH 5.62/ $K_d$ 3100. Similarly, for the Subsurface Clayey sediment after 1 day contact ( $K_d$ units = mL/g): pH 4.81/ $K_d$ 2100, pH 5.82/ $K_d$ 6600, and pH 5.98/ $K_d$ 9000. For the “33-day contact” Subsurface Clayey sediment: pH 5.32/ $K_d$ 10,000, and pH 5.68/ $K_d$ 4700. It was shown through speciation studies that during the 33 days of time that the Pu(V) had in fact reduced to Pu(IV). Thus, the $K_d$ value in this case is not the true exchange Pu(V) $K_d$ value and it is clear that Pu(V) is unstable in the SRS subsurface. If the presence of both Pu(IV) and Pu(V) are not included in the transport model, it is more accurate to assume that all the Pu exists as Pu(IV) since >97% of the Pu exists as Pu(IV) (19). Prout’s (1958) frequently referenced research with Pu is purposely not applied here because of compromised experimental procedures. Furthermore, emphasis of the selection of data was placed on the most recent data, where controls of the Pu speciation were monitored and attempts were made to understand the differences between the sorption behaviors of the various Pu oxidation states.
Pu(III/IV)	300	6000	Powell et al. (2002) using a subsurface SRS sandy sediment and adding Pu(IV), reported a $K_d$ of 220 at pH 4.5 and 390 mL/g at pH 5.85. Using a SRS subsurface clay sediment and adding Pu(IV), they report $K_d$ values of 2100 mL/g at pH 4.81, 6600 mL/g at pH 5.82, and 9000 mL/g at pH 5.98. The “typical” sediment is assumed to have a pH of 5.5. (Also, see the Comments/References for Pu(V) in this table).
Pu(combo)	290	5950	Pu is a single geochemical parameter for Pu. It is a hybrid value of 95% of the Pu(III/IV) and 10% Pu(V/VI) measured $K_d$ values. Kaplan et al. (2004), in a laboratory experiment showed that after 50-hr that 99% of the Pu added as Pu(V) had converted to Pu(IV) in the sediment/water system. Demirkanli et al (2007) using computer simulation of a lysimeter study reported that during a 24 yr simulation that 99.99% of the Pu existed as Pu(III/IV). They reported that the short periods of time that Pu existed in the oxidized form, it moved appreciably faster than Pu in the reduced form. Finally, using X-ray adsorption spectroscopy, Kaplan et al. (28), did not detect any oxidized forms of Pu in SRS sediments that had been in field lysimeters for 11 years.
Th, Zr	900	2000	Tetravalent Cations: Kaplan and Serkiz (2004) reported that SRS sandy sediment had a Zr(IV) $K_d$ = 991 ± 352 mL/g at pH 5.3; SRS clayey sediment had a Zr(IV) $K_d$ = 1969 ± 561 mL/g at pH 5.3 (I). Kaplan and Serkiz (2004) reported that SRS sandy sediment had a Th(IV) $K_d$ = 245 ± 0 mL/g (the standard error is in fact zero) at pH 5.3; SRS clayey sediment Th(IV) $K_d$ = 99 ± 48 mL/g at pH 5.3 (I). The latter Th(IV) data appears suspect in that greater sorption to sand than clay is inconsistent with basic principles of surface chemistry. This latter value will drive the uncertainty high and the “Conservative” estimates low. Thibault et al. (1990) in their $K_d$ compilation of sorption values from throughout the world provide a very wide range of Th $K_d$ values, with almost all values being >10,000 mL/g, however, a few values were as low as 3.5 mL/g.
Pb, Po, Sn	2000	5000	Divalent Soft Metals: Bibler and Marson (7) reported that Pb $K_d$ values for a SRS burial ground sediment (TF1, 40-60 mesh) was generally >10,000 mL/g, a second burial ground sediment (TF2 40-60 mesh) was 63 to 925 mL/g, and a sediment from near the ETF (40-60 mesh) facility had Pb $K_d$ values generally >2,000,000 mL/g. It appears quite likely that all these experiments were conducted at concentrations above the solubility of Pb, and thus reflect precipitation more than adsorption; the experiments were conducted at an initial Pb concentration of 5 mg/L Pb <sup>2+</sup> . Furthermore, the <40-mesh fraction of the

Radio-nuclide	Sandy Sedi-ment	Clayey Sedi-ment	Comments/References <sup>(6)</sup>
Hg	800	1000	<p>sediment was not included in these experiments, thus greater sorption would likely have been measured with the entire sediment. In a compilation put together for groundwater modelers throughout the world, the estimated range of <math>K_d</math> values for sediments with a pH of 4 to 6.3 was 940 to 8,650 mL/g. Finally, these elements tend to have low solubility values. Solubility limits can easily be exceeded by these elements. Therefore it is especially important to consider using solubility constraints rather than <math>K_d</math> values when concentrations are slightly elevated for these elements.</p> <p>There has been two Hg<sup>2+</sup>-sorption study conducted with SRS sediments (Bibler and Marson (7); Kaplan and Iverson (36)). The study by Bibler and Marson (7) will not be discussed because they only used limited particle size fractions (40 to 60 mesh or 80 to 100 mesh sediment fractions) and they conducted their test using extremely high background ionic strength solutions, non-environmentally relevant levels, which would be expected to greatly influence sorption measurements. Kaplan and Iverson (36) measured Hg<sup>2+</sup> values of an SRS vadose zone sand and clay sediment samples, meant as end members of the types of sediments encountered at the SRS. The sand had <math>K_d</math> values ranging from 956 to 2452 mL/g, while the clay sample had <math>K_d</math> values 1296 to 8517 mL/g. <math>K_d</math> values measured in the clay sediment did not vary systematically with pH: at pH 3.1, 4.1, and 9.3 the Hg-<math>K_d</math> = 58, 1296 and 429 mL/g, respectively. Elevating Cl, a Hg complexing ligand known to reduce Hg sorption, concentrations by 0, 2, or 20 mg/L Cl, caused only marginal decreases in Hg <math>K_d</math>: 1296, 773, and 967 mL/g, respectively. Based on these data, Kaplan and Iverson (36) concluded that the mostly likely <math>K_d</math> for this system was 800 mL/g for the sand and 1000 mL/g for the clay. The corresponding reasonably conservative <math>K_d</math> values for the sand and clay were 600 and 700 mL/g, respectively.</p>
Ba, Ca, Ra, Sr	5	17	<p>Alkaline Earth Elements (Group IIA): Kaplan and Serkiz (2004) reported that SRS sandy sediment Sr <math>K_d</math> = <math>5 \pm 1</math> mL/g at pH 5.3; SRS clayey sediment Sr <math>K_d</math> = <math>17 \pm 0</math> mL/g at pH 5.3. Hoeffner (1985) reported SRS sandy sediment (9% clay) Sr <math>K_d</math> = 3 mL/g, pH ~4.7; SRS clayey sediment (23% clay) Sr <math>K_d</math> = 9 mL/g, pH ~4.7; very strong pH effect on Sr <math>K_d</math> values on SRS sediments: for sandy sediment (9% clay) between pH 2 to 4.8 (background) <math>K_d</math> slightly increased from 4 to 19, then increased sharply from pH 4.8 to 6.0-7.0, where the <math>K_d</math> became 2000 mL/g, then the <math>K_d</math> decreased gradually to 100 mL/g as the pH increased to pH 11 (2). Prout's work (1958) with Sr is purposely not applied here because of compromised experimental procedures. Sr sorption is almost entirely by cation exchange (25), and as such, is readily reversible upon changes in groundwater chemistry. Estimates in look-up table reflect this weak-sorption mechanism.</p>
Mo, Se, Te	1000	1000	<p>Selenate (SeO<sub>4</sub><sup>2-</sup>) sorbs strongly to SRS sediments between the pH values of 3.9 and 6.7 (24). With 0 mg/L C from fulvic acid added to SRS groundwater, selenate <math>K_d</math> values for a clayey subsurface SRS sediment were 1041±0.7 mL/g at pH 3.9; 1041±0.4 mL/g at pH 5.3, and 1041±0.3 mL/g at pH 6.7 (24). The authors remarked that there appeared to be an upper sorption limit reached yielded such similar <math>K_d</math> values as a function of pH. Under similar experimental conditions but using a subsurface sandy sediment, selenate <math>K_d</math> values were 1041±0 mL/g at pH 3.9, 1311±384 mL/g at pH 5.3, and 601±65 mL/g at pH 6.7 (24). The sandy sediment, but not the clayey sediment, showed the characteristic decrease in <math>K_d</math> values as the pH increased. Troubling, is that the sandy sediment also had larger <math>K_d</math> values than the clayey sediment.</p>
Mn	15	200	<p>Thibault et al. (1990) report Mn <math>K_d</math> values for sand textured sediments of 14, 18, 24, 29, 30, 50, 70, 71, 150, 2000 mL/g, and for clay sediments of 250, 2100, and 10,000 mL/g. In a highly weathered soil and low in organic matter, as we have ion the SRS, Willett and Bond (1995) reported <math>K_d</math> values at pH 5, 6, and 7 of 4, 5, and 9.5 mL/g. The increase Mn sorption with pH was attributed to the tendency for Mn to hydrolyze at elevated pH levels. Their soil had lower Fe-oxide concentrations than SRS sediments.</p>

Radio-nuclide	Sandy Sedi-ment	Clayey Sedi-ment	Comments/References <sup>(a)</sup>
As	100	200	Crapse et al. (37) measured in situ As $K_d$ values in D-Area, SRS, by collecting porewater/sediment paired samples along a pH gradient. The As $K_d$ values varied by 3 orders of magnitude along the transect and did not vary in a consistent manner with pH. At pH 5.5, the $K_d$ values varied from about 30 to 20,000 mL/g (Figure 45; Crapse et al. (37)). Also, note that Sb below can be considered a chemical analog.
Sb	2500	2500	Oxidizing: Sb(III) as $\text{HSbO}_2^0$ and $\text{Sb(OH)}_3^0$ . Sb sorption studies have been conducted with SRS burial ground sediments with deionized water or groundwater (2). They indicate Sb sorbs strongly to our sediment, with a near linear decrease in log $K_d$ values and pH. The decrease in sorption at the more basic pH levels may be a result of formation of anionic Sb complexes, such as $\text{Sb(OH)}_4^-$ and $\text{SbO}_2^-$ . Between pH 5 and 6, the five measured $K_d$ values were between 3000 and 4000 mL/g. At pH 10.5, the Sb $K_d$ value was 22 mL/g. SRS lysimeter studies indicate that a small amount of Sb is in a mobile anionic form (2). The literature indicates there have been very few Sb sorption studies conducted. Ames and Rai (38) reviewed Sb sorption and concluded that over the pH range of 4 to 8 that Sb exists as a neutral and complexed species. In high pH and high ionic strength systems, Sb $K_d$ values were very low, 0 to 2 mL/g (38). When Ca concentrations were high, such as in a concrete system, Sb appeared to coprecipitate with $\text{CaCO}_3$ , yielding $K_d$ values in the range of 17 to 122 mL/g. Beneath leaking high level waste tanks in Hanford, Sb was found to migrate rapidly through the subsurface sediment (at the same rate as Co and ruthenium) (38). The high mobility may be attributed to the tendency of Sb to form complex or hydrolyzed species which are neutral or negatively charged.
Re, Tc	0.6	1.8	Tc exists as the anion $\text{TcO}_4^-$ in oxidized systems, such as the vadose zone and the aquifer. Hoeffner (1985) reported correlation between clay content in SRS sediments and Tc $K_d$ : $<10\%$ clay $K_d=0.17$ mL/g, $\sim 10\%$ clay $K_d=0.14$ mL/g, $\sim 10\%$ clay $K_d=0.23$ mL/g, $11\%$ clay $K_d=0.10$ mL/g, $30\%$ clay $K_d=0.33$ mL/g, $43\%$ clay $K_d=1.31$ mL/g, $45\%$ clay $K_d=1.16$ mL/g. Kaplan (2005) reported $\text{TcO}_4^-$ sorption to an SRS sediment occurred only when the pH was $<4.3$ ; the $K_d$ values to this sandy subsurface sediment increased from 0 at pH 4.3 to $\sim 0.11$ at pH 3.7. Sorption studies with $\text{ReO}_4^-$ to a clayey subsurface SRS sediment in SRS groundwater as a function of pH all had a $K_d$ of $\sim 0$ mL/g: $-0.6 \pm 0.6$ mL/g at pH 3.9; $-0.3 \pm 0.1$ mL/g at pH 5.3; $-0.1 \pm 0.3$ mL/g at pH 6.7 (Kaplan and Serkiz 2006). Similar studies conducted with sandy subsurface SRS sediment showed no sorption between the pH of 3.9 and 6.7: $K_d = -0.4 \pm 0.3$ mL/g at pH 3.9, $K_d = -0.2 \pm 0.4$ mL/g at pH 5.3, and $K_d = 0 \pm 0.2$ mL/g at pH 6.7 (24). The variability in these latter studies was quite high due to the limited number of replicates, two. However, they indicate that Tc or Re sorption is either non-existent or very limited to SRS sediments. Kaplan et al. (2008a) measured Tc $K_d$ values in 26 sediments collected from E-Area SRS. The mean was $3.4 \pm 0.5$ mL/g and ranged from $-2.9$ to $11.2$ mL/g. The 95-percentile range was $2.4$ to $4.4$ mL/g. The Upper Vadose Zone and Lower Vadose Zone, which consist primarily of clayey and sandy sediments, respectively, didn't have significantly differently $K_d$ values, which is inconsistent with Hoeffner (1985). The recommended value originates from the median value of 47 Tc $K_d$ values, which includes the 26 $K_d$ values from E-Area reported by Kaplan et al. (2008a); the median value for clayey sediment = $1.8$ mL/g and for sandy sediment = $0.6$ mL/g (Kaplan 2009; SRNL-TR-2009-00019).
U	200	300	Johnson (1995) and Serkiz and Johnson (1994) conducted several field studies and laboratory studies to determine the processes controlling U sorption to SRS sediments. A portion of this work involved the collection of paired sediment-pore water samples from F-Area, within a U contaminated plume. Using the sequential extraction data (as defined by the sum of the concentrations of the first 6 extraction steps divided by the porewater U concentration in a saturated paste extract; see Johnson 1995): at pH 4.7 the $K_d$ was $87$ mL/g, at pH 4.75 the $K_d$ was $100$ mL/g, at pH 5.05 the $K_d$ was $37$ mL/g, and at pH

Radio-nuclide	Sandy Sedi-ment	Clayey Sedi-ment	Comments/References <sup>(a)</sup>
			<p>5.12 the <math>K_d</math> was 93 mL/g. The lack of trend with pH can be attributed to the fact that this was field data and reflects several different sediments. In an (ad)sorption test to a sandy subsurface F-Area sediment as a function of pH, at pH 4.82, 4.87, 5.01, and 5.04, the <math>K_d</math> values were 116, 153, 198, and 238 mL/g. At pH 5.5, the assumed background pH, the <math>K_d</math> is likely going to be greater than 238 mL/g (the <math>K_d</math> at pH 5.04) or 100 mL/g (the <math>K_d</math> measured at pH 4.75). Using all the U in the solid phase to calculate in situ <math>K_d</math> values resulted in <math>K_d</math> values that were 2000 to 10,000 mL/g (Serkiz and Johnson (1994); see Figure 4-12). This will clearly overestimate <math>K_d</math> values appropriate for use in reactive transport modeling. They reported <math>K_d</math> values of (presented as sample ID/pH/<math>K_d</math> (mL/g)): A-52/pH5.47/<math>K_d</math> 2,200, C-32/pH5.53/<math>K_d</math> &gt;6300, C-42/pH5.27/<math>K_d</math> &gt;14,000, F-42/pH5.2/<math>K_d</math> 34,000, F-52/pH5.91/<math>K_d</math> 5500, F-53/pH5.63/<math>K_d</math> 27,000. The data across the entire pH range of 3.0 to 6.8 suggest that U was solubility controlled in this field site. Additional work needs to be conducted to further understand this process to permit inclusion of solubility constraints, if appropriate, into PA modeling. Additional U sorption mechanistic experiments have been conducted with SRS sediments (8, 9). Bibler and Marson (1992) U sorption data could not be used for this review because it was conducted at pH 3.</p>
<p><sup>(a)</sup> References: (1) = Kaplan and Serkiz 2004 ; (2) = Hoeffner 1985; (3) = Oblath et al. 1983; (4) = Prout 1958 ; (7) = Bibler and Marson 1992 ; (8) = Johnson 1995; (9) = Bertsch et al. 1994 ; (10) = Kaplan et al. 2006a (11) = Powell et al. 2005 (12) = Serkiz et al. 2005 (13) = Powell et al. 2004 (14) = Kaplan et al. 2004 ; (15) =Fjeld et al. 2004 ; (16) = Powell et al. 2006; (17) = Kaplan et al. 2001; (18) = Kaplan and Wilhite 2001; (19) = Kaplan et al. 2006b; (20) = Sheppard et al. 1979; (21) = EPA 2004; (22) = Findley 1998; (23) = Goto 2001; (24) = Kaplan and Serkiz (2006); (25) = EPA 1999; (26) = Kaplan et al. 2001; (27) = Kaplan et al. 2004; (28) Kaplan et al. 2008c; (29) = Grogan et al. 2008; (30) = Roberts and Kaplan 2008; (31) = Crapse et al. 2004; (32) = Seaman et al. 1999; (33) = Buchter et al. 1989; (34) = Wong et al. 1993; (35) = Knox and Kaplan 2003; (36) = Thibault et al. 1990; (37) = Willett and Bond 1995; (38) = Ames and Rai = 1976; (39) = Schwehr et al. 2009; (41) = Miller et al. 2009; (42) = Lilley et al. 2009.</p>			

**Table 17.** Distribution Coefficients (*K<sub>d</sub>* values, mL/g): Oxidizing Cementitious Solids

Radio-nuclide	Young Cement 1 <sup>st</sup> Stage (pH ~12)	Moderately-aged Cement, 2 <sup>nd</sup> Stage (pH ~10.5)	Aged Cement 3 <sup>rd</sup> Stage (pH ~5.5)	Comments/References <sup>(a)</sup>
Ar, Kr, Rn	0	0	0	Until studies are conducted to prove otherwise (such as tritium (see below)), it will be necessary to assume their <i>K<sub>d</sub></i> values = 0 mL/g.
Re, Tc	0.8	0.8	0.5	TcO <sub>4</sub> <sup>-</sup> adsorption to cementitious material has been measured between 1 and 10 mL/g (1). Kaplan and Coates (24) measured TcO <sub>4</sub> <sup>-</sup> <i>K<sub>d</sub></i> values in Ca(OH) <sub>2</sub> -saturated and CaCO <sub>3</sub> -saturated solutions in ground, 40-yr old concrete, simulating 1 <sup>st</sup> /2 <sup>nd</sup> and 3 <sup>rd</sup> Stages, respectively. The measured <i>K<sub>d</sub></i> values were 0.8 and 1.4 mL/g, respectively. Lilley et al. (2009) measured TcO <sub>4</sub> <sup>-</sup> <i>K<sub>d</sub></i> : to 50 year old aged cement of 3.30 mL/g; to Vault 2 (25% slag) of 5.08 mL/g; and two Saltstone simulants of 4.77 & 2.75 mL/g (the latter three measurements were under oxidizing conditions).
<sup>3</sup> H	0	0	0	A great deal of recent research has been conducted using careful measurements of tritium sorption to cement (reviewed by Wieland and Van Loon 2003 and Tits et al. 2003). Through the use of batch sorption and through-diffusion experiments they have arrived at essentially the same <i>K<sub>d</sub></i> value, 0.8 ± 0.2 mL/g and 0.8 ± 0.1 mL/g, respectively. In Wieland and Van Loon's (2003) look-up table for cement <i>K<sub>d</sub></i> values, they suggest using a value of 1 mL/g for tritium (this value would be equivalent to a "Best" value in this table). However, there is also a great deal of data indicating that tritium really doesn't sorb and that experimental evidence indicating so is, in some cases, actually errors in mass balance (reviewed by Krupka et al. 2004). That is, during diffusion tests or batch sorption test, researchers incorrectly assign tritium existing in the concrete/cement pore water as "sorbed tritium" during their mass balance calculations ( <i>K<sub>d</sub></i> calculations).
Cl, Cr, F, N (nitrate, nitrite)	10	10	1	Based on diffusion studies with French sulfate-resistant cement Cl <i>K<sub>d</sub></i> values were 25 mL/g (2). Atkins and Glasser (3) also reported Cl sorption to cement, but it was not possible to calculate a <i>K<sub>d</sub></i> based on the data provided in the paper. Cl <i>K<sub>d</sub></i> to cement powder after 24 h contact time = 0.8 mL/g (4). (This latter value is not especially reliable considering compromised experimental technique.) Decreased <i>K<sub>d</sub></i> values in "Young Concrete" because of high concentration of aqueous salts resulting in anion exchange (desorption). CrO <sub>4</sub> <sup>2-</sup> immobilization as a result of carbonation (the natural process by which concrete becomes coated with CaCO <sub>3</sub> ) has been documented (5). (Note discussion below of iodine and astatine, which are also anions.)
At, I	8	15	4	Iodine assumed to be present as iodide (I <sup>-</sup> ). Iodide sorbed stronger to cement than Cs (1). I- <i>K<sub>d</sub></i> measured on 7 types of concrete samples increased gradually over 3-mo, then leveled off at 25 to 130 mL/g (1, 6). Iodide sorption to cement is highly reversible when Cl is added to aqueous phase, suggesting it adsorbed and was not precipitated (3). Increasing pH, decreased I <sup>-</sup> sorption (3);

Radio-nuclide	Young Cement 1 <sup>st</sup> Stage (pH ~12)	Moderately -aged Cement, 2 <sup>nd</sup> Stage (pH ~10.5)	Aged Cement 3 <sup>rd</sup> Stage (pH ~5.5)	Comments/References <sup>(a)</sup>
Inorganic C	3000	3000	300	therefore Stage 3 <i>Kd</i> values will be slightly greater than other stages). Iodide sorption on CSH varies with its C/S ratio, increasing towards high C/S ratios (3). Lowered <i>Kd</i> values in “Young Concrete” because of high concentration of aqueous salts. In 1 <sup>st</sup> Stage <i>Kd</i> values were decreased because high ionic strength likely resulted in anion exchange (desorption). Kaplan and Coates (24) measured I <i>Kd</i> values in Ca(OH)-saturated and CaCO <sub>3</sub> -saturated solutions in ground, 40-yr old concrete, simulating 1 <sup>st</sup> /2 <sup>nd</sup> and 3 <sup>rd</sup> Stages, respectively. The measured <i>Kd</i> values were 14.8 and 14.4 mL/g, respectively.
Inorganic C	3000	3000	300	<sup>14</sup> C chemistry is very complicated and is not well characterized by the <i>Kd</i> construct. It is influenced by carbon dioxide gas/water/solid phase equilibrium, isotopic exchange, adsorption, precipitation, and coprecipitation. To be conservative the role of gas phase and isotopic exchange (two very important processes for removing <sup>14</sup> C from groundwater) will not be considered. Inorganic C exists as an anion, CO <sub>3</sub> <sup>2-</sup> (1). Subsurface C chemistry in a cementitious environment is discussed by Dayal (7, 8) and how it has been applied to the SRS PAs by Kaplan (9). Roberts and Kaplan (30) found that <sup>14</sup> C-carbonate sorption to concrete was not a steady state process and that even after 6 months <sup>14</sup> C-carbonate sorption had not come to steady state. The cement used in this study was recovered from a boring of a SRS tank pad that was poured in 1972. Since 1972 it was exposed to the natural weathering elements. <i>Kd</i> values were 33.5 mL/g after 1 day and >2850 mL/g after 6 months. Allard et al, (1991) report <sup>14</sup> C-carbonate to cementitious materials was strongly kinetically driven: after 3 days the <i>Kd</i> was 3.7 mL/g and after 5 weeks the <i>Kd</i> was >10,000 mL/g.
Ac, Al, Am, Bk, Bi, Ce, Cf, Cm, Eu, Fe, Gd, Lu, Sm, Y	6000	6000	600	Trivalent cation <i>Kd</i> values for concrete exceed those for sediments (3). Am <i>Kd</i> > 10,000 mL/g (10). Am <i>Kd</i> value was 12,000 mL/g based on diffusion tests in cement (11). Am <i>Kd</i> values ranged from 2,500 to 35,000 mL/g for 7 fresh concrete blends (1, 6). Am <i>Kd</i> for 65-yr old concrete sample = 10,000 mL/g (1, 6). Fresh cement Am <i>Kd</i> = 2000 for 24-h contact time (12). Eu <i>Kd</i> = 2,400 mL/g for 24-h contact time (12). Very large <i>Kd</i> values may reflect precipitation reaction that occurred during the adsorption measurements. Kaplan and Coates (24) measured Am(III), Ce(III), and Y(III) <i>Kd</i> values in Ca(OH)-saturated and CaCO <sub>3</sub> -saturated solutions in ground, 40-yr old concrete, simulating 1 <sup>st</sup> /2 <sup>nd</sup> and 3 <sup>rd</sup> Stages, respectively. The measured Am(III) <i>Kd</i> values were 6031 and 4112 mL/g, respectively. The measured Ce(III) <i>Kd</i> values were 6003 and 4652 mL/g, respectively. Both sets of <i>Kd</i> values were quite similar. Y(III) <i>Kd</i> values were 4830 mL/g in Ca(OH)-saturated solution (for Stages 1&2), and 4738 mL/g in CaCO <sub>3</sub> -saturated solution (for Stage 3).
Ag, Cd, Co, Cu, Ni, Pd, Pt, Zn	4000	4000	400	Selected Monovalent and Divalent Transitions Metals: Using SRS materials, Kaplan and Coates (24) measured Cd(II) and Co(II) <i>Kd</i> values in Ca(OH)-saturated and CaCO <sub>3</sub> -saturated solutions in ground, 40-yr old concrete, simulating 1 <sup>st</sup> /2 <sup>nd</sup> and 3 <sup>rd</sup> Stages, respectively. The measured Cd(II) <i>Kd</i> values were 9907 mL/g and 3180 mL/g, respectively. The measured Co(II) <i>Kd</i> values were 4343 mL/g in Ca(OH)-saturated solutions and 3994 mL/g in CaCO <sub>3</sub> -saturated solutions. Three

Radio-nuclide	Young Cement 1 <sup>st</sup> Stage (pH ~12)	Moderately -aged Cement, 2 <sup>nd</sup> Stage (pH ~10.5)	Aged Cement 3 <sup>rd</sup> Stage (pH ~5.5)	Comments/References <sup>(a)</sup>
Ba, Ra	100	100	70	studies were found that included adsorption data for Ni onto cement/concrete. Hietanen et al (15) reported $Kd$ values that ranged from 500 to 3000 mL/g, Kato and Yanase (12) reported a Ni $Kd$ value of 1500 mL/g, and Pilkington and Stone (16) reported $Kd$ values that ranged from 500 to 3000 mL/g.
Sr, Ca	15	15	5	Bayliss et al. (11) and Berry et al. (13) measured Ra $Kd$ values onto ordinary Portland cement and as a function of Ra concentration. They reported $Kd$ that ranged from 50 to 530 mL/g. Jakubick et al. (14) reported Sr $Kd$ values of 0.8 to 1.6 mL/g for high density and normal density concretes, and 1.3 to 3 mL/g for the same concretes, but in lower ionic strength solutions. Ewart et al. (14) reported $Kd$ values between 1 and 4 mL/g. Kato and Yanase reported a Sr $Kd$ value of 56 mL/g for an experiment involving 24 h contact time, dried cement powder, pH 11 cement equilibrated water. We elected to disregard this value because it is an order-of-magnitude greater than those reported by other researchers and the nature of the solid phase was not clearly described by the author. In 1 <sup>st</sup> Stage $Kd$ values were decreased because high ionic strength likely results in competitive exchange (desorption). Kaplan and Coates (24) measured Sr $Kd$ values in Ca(OH)-saturated and CaCO <sub>3</sub> -saturated solutions in ground, 40-yr old concrete, simulating 1 <sup>st</sup> /2 <sup>nd</sup> and 3 <sup>rd</sup> Stages, respectively. The measured $Kd$ values were 28.1 and 39.1 mL/g, respectively.
Sn	4000	4000	2000	Sn exists in cementitious environments in the +4 state (17) and as such readily hydrolyses. Using sulfate resistant Portland cement, Sn $Kd$ values were >30,000 mL/g; this likely reflected some precipitation (17). Kaplan and Coates (24) measured Sn $Kd$ values in Ca(OH)-saturated and CaCO <sub>3</sub> -saturated solutions in ground, 40-yr old concrete, simulating 1 <sup>st</sup> /2 <sup>nd</sup> and 3 <sup>rd</sup> Stages, respectively. The measured $Kd$ values were 3900 and 3360 mL/g, respectively.
Cs, Fr, K, Rb, Tl	2	20	10	Cs $Kd$ values in hardened HTS cement discs, pH 13.3 were close to 3 mL/g (15). Wieland and Van Loon (17) reviewed Cs $Kd$ values onto various cementitious materials and they had a very narrow range: from 0.2 to 5.0 mL/g. In 1 <sup>st</sup> Stage $Kd$ values were decreased because high ionic strength likely results in competitive exchange (desorption). This has been shown experimentally (17). Kaplan and Coates (24) measured Cs <sup>+</sup> $Kd$ values in Ca(OH)-saturated and CaCO <sub>3</sub> -saturated solutions in ground, 40-yr old concrete, simulating 1 <sup>st</sup> /2 <sup>nd</sup> and 3 <sup>rd</sup> Stages, respectively. The measured $Kd$ values were 21 and 17.6 mL/g, respectively.
Na	0.5	1	0.5	Sodium is in the 1A group of elements with Cs, Fr, Tl, and K, but it would be expected to sorb less strongly due to its strong energy of hydration. Reduced $Kd$ values in half with respect to those of the other 1A group of elements.
Nb	1000	1000	500	Krupka and Serne (18) review Nb $Kd$ values and concluded that there was a great deal of variability related in Nb sorption data to cementitious materials. They reported $Kd$ ranges of 11 to 69,000 mL/g (from studies that had problems with the blanks, <i>i.e.</i> , the blanks indicated Nb sorbed to the glassware). We defer to their best values (1000 mL/g) and add conservatism to these values.

Radio-nuclide	Young Cement 1 <sup>st</sup> Stage (pH ~12)	Moderately -aged Cement, 2 <sup>nd</sup> Stage (pH ~10.5)	Aged Cement 3 <sup>rd</sup> Stage (pH ~5.5)	Comments/References <sup>(a)</sup>
Np, Pa	10,000	10,000	5,000	Neptunium sorption to aged cement samples were conducted by Miller et al. (2009). They used an ICP-MS which permitted them much lower detection limits than conventional radiometric analytical methods and as a result, much lower $Kd$ values were measured. They added Np(V) at varying concentrations to ground 50 year old cement samples and measured constant aqueous Np concentration at 1e-12 M, indicating solubility controls. Six triple Np $Kd$ values were measure with ground aged concrete, all were >100,000 mL/g. Previous measurements by Kaplan and Coates (24) measured lower $Kd$ values, but were running up against the analytical limits of the instruments. These radionuclides are assumed to exist in the +5 oxidation state. Np sorption test to 7 different 65-yr old cements using cement pore water reached steady state after 30 days, $Kd$ values ranged from 1500 to 9500 mL/g ( $I, \phi$ ). As is the case with all large $Kd$ values, these values may reflect some precipitation occurring during the adsorption measurement. Kaplan and Coates (24) measured $NpO_2^-$ and $PaO_2^-$ $Kd$ values in Ca(OH)-saturated and $CaCO_3$ -saturated solutions in ground, 40-yr old concrete, simulating 1 <sup>st</sup> /2 <sup>nd</sup> and 3 <sup>rd</sup> Stages, respectively. The measured $NpO_2^-$ $Kd$ values were 1652 and 1318 mL/g, respectively. The measured $PaO_2^-$ $Kd$ values were 1630 and 1074 mL/g, respectively.
Mo, Se, Te,	300	300	150	Twenty-seven cementitious formulations (varying water/solid, silica fume %, and clay concentration) were used to measure selenate ( $SeO_3^{2-}$ ) $Kd$ values from an alkaline solution (Johnson et al. 2000). $Kd$ values ranged from 250 to 930 mL/g. Sorption was irreversible. At high selenate ( $SeO_4^{2-}$ ) concentrations, sorption to ettringite, monosulfate, calcium-silicate-hydrate (all mineral constituents of concrete) resulted in selenate substitutes for sulfate (23). Selenite $Kd$ values measured in sulfate resistant Portland cement ranged from 30 to 100 mL/g (17). It is not clear why these latter $Kd$ values were so much lower than those reported by Johnson et al (2000). This variability in results requires that conservative values in table be lowered.
Mn	100	100	10	Taken from Bradbury and Sarott 1995
As, Sb	1000	1000	100	Phosphate, an analogue for $AsO_4^{3-}$ , is known to be very strongly bound to concret.
Hg, Pb, Po	300	300	100	Soft divalent cations : Bayliss et al. (1991) conducted a series of sorption experiments with Pb and crushed sulfate resisting Portland cement and ordinary Portland cement/blast furnace slag pastes with an Eh of +50 to -500 mV. The main findings were that sorption was concentration and cement composition dependent. Data strongly suggested solubility controls on Pb aqueous concentrations. Bradbury and Sarott (1995) suggested $Kd$ values of 500, 500, & 500 mL/g for these three stages, respectively. Using aged cementitious materials, Kaplan and Coates (2007) measured Hg $Kd$ values between 289 and 568 mL/g.
Pu(III/IV), Pu(combo) Th, Zr	10,000	10,000	2000	Concrete containing reducing agents (blast furnace slag, BFS) did not have greater Pu $Kd$ values than those that did not contain BFS. High $Kd$ values are attributed more to low solubility of Pu in high pH systems, than to adsorption/absorption processes. Using three 65-yr-old crushed concrete

Radio-nuclide	Young Cement 1 <sup>st</sup> Stage (pH ~12)	Moderately -aged Cement, 2 <sup>nd</sup> Stage (pH ~10.5)	Aged Cement 3 <sup>rd</sup> Stage (pH ~5.5)	Comments/References <sup>(a)</sup>
Pu(V/VI)	1000	1000	100	<p>samples and seven fresh concrete samples, Th-<i>Kd</i> values were 2,500 to 5,500 mL/g (1, 6). Th- <i>Kd</i> values were consistently less than Am <i>Kd</i> values, greater than U- <i>Kd</i> values, and very similar to Np and Pu <i>Kd</i> values (1, 6). Pu- <i>Kd</i> values ranged from 1,000 to 12,000 mL/g (1, 6). Using a sulfate resistant Portland cement, Th <i>Kd</i> values were measured to be 100,000 mL/g (17). Kaplan and Coates (24) measured Pu <i>Kd</i> values added as Pu(VI) but likely reduced to Pu(IV) in Ca(OH)-saturated and CaCO<sub>3</sub>-saturated solutions in ground, 40-yr old concrete, simulating 1<sup>st</sup>/2<sup>nd</sup> and 3<sup>rd</sup> Stages, respectively. The measured <i>Kd</i> values were 99,700 and 92,200 mL/g, respectively.</p> <p>Pu(V/VI) would likely not remain in this oxidation state for long, even under normal oxidizing conditions, before it would reduce to Pu(IV). These values are provided for models requiring separate reduced Pu (Pu(III/IV)) and oxidized Pu (Pu(V/VI)) species. Experimentally these would be difficult to measure and assure that reduced Pu species didn't form.</p>
U	250	250	70	<p>U(VI)- <i>Kd</i> values for 7 types of cement were 350 to 13,000 mL/g; median = 1400 mL/g (1, 6). Kaplan and Coates (24) measured U <i>Kd</i> values in Ca(OH)-saturated and CaCO<sub>3</sub>-saturated solutions in ground, 40-yr old concrete, simulating 1<sup>st</sup>/2<sup>nd</sup> and 3<sup>rd</sup> Stages, respectively. The measured <i>Kd</i> values were 259 and 165 mL/g, respectively.</p>
<p><sup>(a)</sup> References: (1) = Allard et al. 1984; (2) = Sarott et al. 1992 ; (3) = Atkins and Glasser 1992 ; (4) = Brodda 1988 ; (5) = Macias et al. 1997; (6) = Høglund et al. 1985 ; (7) = Dayal and Reardon 1992; (8) = Dayal et al. 1989; (9) = Kaplan 2005; (10) = Ewart et al. 1988; (11) = Bayliss et al. 1991; (12) = Kato and Yanase 1993; (14) = Ewart et al. 1986; (15) = Sarott et al. 1992; (16) = Pilkington and Stone 1990; (17) = Wieland and Van Loon 2003; (18) = Krupka and Serne 1998; (19) = Bradbury and Sarott 1995; (20) = Tits et al. 2003; (21) = Krupka et al. 2004; (22) = Johnson et al. 2000; (23) = Baur and Johnson 2003; (24) = Kaplan and Coates 2007.</p> <p><sup>(b)</sup> The age of each of the stages is facility specific because it depends on the amount of water that passes through the cementitious material (see Section 4.2).</p> <p><sup>(c)</sup> Inorganic carbon geochemistry is very complicated. The use of only the <i>Kd</i> value without the associated solubility value in a cementitious environment will greatly overestimate the true mobility of C through this environment.</p>				

Table 18. Distribution Coefficients ( $Kd$  values, mL/g): Reducing Cementitious Solids

Radio-nuclide	Young Cement 1 <sup>st</sup> Stage (pH ~12)	Moderately-aged Cement, 2 <sup>nd</sup> Stage (pH ~10.5)	Aged Cement 3 <sup>rd</sup> Stage (pH ~5.5)	Comments/References <sup>(a)</sup>
<sup>3</sup> H, Ar, As, Ba, C, Ca, Cl, Cs, F, Fr, K, Kr, Mn, Mo, N, Na, Nb, Ni, Pu(V/VI), Ra, Rb, Rn, Sb, Se, Sr, Te, Tl	5000	5000	1000	(Same values as reported in Table 17 for Oxidizing Cementitious Solids)
Ag, Cd, Co, Cu, Hg, Pb, Pd, Pt, Zn	5000	5000	1000	Selected transitions monovalent and divalent metals: Kaplan and Coates (3) measured Cd and Co $Kd$ values in Ca(OH)-saturated and CaCO <sub>3</sub> -saturated solutions in ground, SRS reducing grout, simulating 1 <sup>st</sup> /2 <sup>nd</sup> and 3 <sup>rd</sup> Stages, respectively. The measured Cd $Kd$ values were 297,000 and 17,500 mL/g, respectively. The measured Co $Kd$ values were 15,000 and 6,500 mL/g, respectively. It is likely the sulfides are forming strong bonds to these transition metals, perhaps forming sulfide precipitates.
Ac, Al, Am, Bi, Bk, Ce, Cf, Cm, Eu, Fe, Gd, Lu, Sm, Y	7000	7000	1000	Trivalent Cations: Kaplan and Coates (3) measured Am, Ce, and Y $Kd$ values in Ca(OH)-saturated and CaCO <sub>3</sub> -saturated solutions in ground, SRS reducing grout, simulating 1 <sup>st</sup> /2 <sup>nd</sup> and 3 <sup>rd</sup> Stages, respectively. The measured Am $Kd$ values were 42,900 and 17,000 mL/g, respectively. The measured Ce $Kd$ values were 104,000 and 4,560 mL/g, respectively. The measured Y $Kd$ values were 64,800 and 5,300 mL/g, respectively. It is likely the sulfides were forming strong bonds to multivalent cations, perhaps forming sulfide precipitates. Sorption to trivalent cations under reducing conditions and with reducing grout had higher $Kd$ values than under oxidizing conditions.
Po, Sn, Th, Zr	5000	5000	500	Tetravalent cations: Kaplan and Coates (3) measured Sn(IV) $Kd$ values in Ca(OH)-saturated and CaCO <sub>3</sub> -saturated solutions in ground, SRS reducing grout, simulating 1 <sup>st</sup> /2 <sup>nd</sup> and 3 <sup>rd</sup> Stages, respectively. The measured Sn $Kd$ values were 71,800 and 5,520 mL/g, respectively. It is likely the sulfides are forming strong bonds to these transition metals, perhaps forming sulfide precipitates.
Tc, Re	5000	5000	1000	Tc <sup>VI</sup> O <sub>4</sub> <sup>-</sup> gets reduced to Tc <sup>4+</sup> , which like other tetravalent cations sorbs strongly to surfaces. Lukens et al. (2005) conducted fundamental studies using SRS slag and grout mixtures. In their study, they added Tc(VII) to a reducing grout and using X-ray Absorption Spectroscopy, specifically, XANES, they observed the slow transformation of Tc(VII) to Tc <sup>VII</sup> O <sub>2</sub> -H <sub>2</sub> O to Tc <sup>IV</sup> S <sub>x</sub> . This process was monitored in the grout over a course of 45 months. The solubility of the Tc <sup>IV</sup> O <sub>2</sub> is low but that of Tc <sup>IV</sup> S <sub>x</sub> is extremely low, 10 <sup>-20</sup> molar in alkaline systems (2.4e-8 pCi/L <sup>99</sup> Tc; ref = (2), Table D.3-3). The high $Kd$ values selected for these conditions are to reflect the low solubility of Tc under these conditions. Lilley et al (2009) measured Tc <sup>VII</sup> O <sub>4</sub> <sup>-</sup> sorption to two SRS Saltstone simulants containing 45% slag, but did not reach steady state. In one he measured a $Kd$ of 18 in the other a $Kd$ of 3660 mL/g. They Additional information for why Tc sorption values are high in SRS-slag-containing cementitious materials see Page 157, Section 13.0.
Cr	1000	1000	1000	Bajt et al. (5) observed XAS spectra of the reduction of Cr(VI) in SRS reducing grout to Cr(III).

At, I	5	9	4	Rai et al (6) measured the solubility of Cr(III) at varying pH and ionic strengths and as varying solid phases.
Np, Pa	10,000	10,000	5000	Kaplan and Coates (3) measured iodide I <sup>-</sup> (iodide) <i>Kd</i> values in Ca(OH) <sub>2</sub> saturated and CaCO <sub>3</sub> -saturated solutions in ground, SRS reducing grout, simulating 1 <sup>st</sup> / <sub>2</sub> <sup>nd</sup> and 3 <sup>rd</sup> Stages, respectively. The measured I <sup>-</sup> <i>Kd</i> values were 6.2 and 11 mL/g, respectively. Electing to decrease <i>Kd</i> during 1 <sup>st</sup> stage because of high ionic strength that would promote anion exchange. Kaplan and Coates (3) measured Np(V) and Pa(V) (often considered chemical analogues) <i>Kd</i> values in Ca(OH) <sub>2</sub> -saturated and CaCO <sub>3</sub> -saturated solutions in ground, SRS reducing grout, simulating 1 <sup>st</sup> / <sub>2</sub> <sup>nd</sup> and 3 <sup>rd</sup> Stages, respectively. It is not clear whether each element underwent reduction to the +4 species, based on thermodynamic considerations alone, they would be expected to have been reduced. The Np <i>Kd</i> values in the Ca(OH) <sub>2</sub> solution were 3949 m/g and in the CaCO <sub>3</sub> solution was 2779 mL/g. ) The Pa <i>Kd</i> values in the Ca(OH) <sub>2</sub> solution was 9890 mL/g and in the CaCO <sub>3</sub> solution was 8049 mL/g. Kaplan et al. (4) using reducing DDA simulant Saltstone (25 wt-% slag) and Vault 2 concrete (10% slag) measured Np(V) <i>Kd</i> values that were all “greater than values”. Commutatively, the <i>Kd</i> values were >4218 mL/g. Lilley et al. (2009) measured 10 cementitious Np <i>Kd</i> values >1e6 mL/g, using varying types of solids (50 year old cement, two SRS Saltstone simulants, and Vault 2 Cement), and contact times of 1 or 4 days, and 3 NpO <sub>2</sub> concentrations. They demonstrated that solubility was controlling sorption. (See discussion in apparent solubility look-up tables.)
Pu	10,000	10,000	2000	Kaplan and Coates (3) measured Pu(VI) <i>Kd</i> values in Ca(OH) <sub>2</sub> -saturated and CaCO <sub>3</sub> -saturated solutions in ground, SRS reducing grout, simulating 1 <sup>st</sup> / <sub>2</sub> <sup>nd</sup> and 3 <sup>rd</sup> Stages, respectively. The Pu(VI) likely reduced to Pu(IV). The measured Pu <i>Kd</i> values were 5760 and 11055 mL/g, respectively. In the same study, Kaplan and Coates (3) also measured Sn (tin) sorption, also a tetravalent cation. It had a <i>Kd</i> of 71,762 mL/g in Ca(OH) <sub>2</sub> and 5520 mL/g in the CaCO <sub>3</sub> solutions. Using SRS DDA simulated Saltstone, Kaplan et al. (4) measured a <i>Kd</i> of 12,176 mL/g in Ca(OH) <sub>2</sub> saturated solution and a <i>Kd</i> of 165,570 mL/g in a CaCO <sub>3</sub> saturated solution. The first solution was design to simulate 1 <sup>st</sup> and 2 <sup>nd</sup> Stage aqueous conditions, whereas the second solution was to simulate the 3 <sup>rd</sup> stage. Pu(VI) was added but it likely reduced to Pu(IV) during the course of the measurement.
U	2500	2500	2500	Kaplan and Coates (3) measured U(VI) <i>Kd</i> values in Ca(OH) <sub>2</sub> -saturated and CaCO <sub>3</sub> -saturated solutions in ground, SRS reducing grout, simulating 1 <sup>st</sup> / <sub>2</sub> <sup>nd</sup> and 3 <sup>rd</sup> Stages, respectively. The U(VI) likely reduced to U(IV). The measured U <i>Kd</i> values were 2485 and 3182 mL/g, respectively.
<sup>(4)</sup> References: (1) = Lukens et al. 2005; (2) = MMES 1992; (3) = Kaplan and Coates 2007; (4) = Kaplan et al. 2008a; (5) = Bajt et al. (1993); (6) = Rai et al. (1987).				

Table 19. Apparent Solubility Concentration Limits (mol/L) for Oxidizing Cementitious Solids

Radio-nuclide	Young 1 <sup>st</sup> Stage (pH ~12)	Moderately-aged, (b) 2 <sup>nd</sup> Stage (pH ~10.5)	Aged (b) 3 <sup>rd</sup> Stage (pH ~5.5)	Comments/References <sup>(a)</sup>
<sup>3</sup> H, Ar, As, At, Cl, Cr, Cs, F, Fr, I, Kr, Mn, Mo, N, Na, Nb, Pu(V/VI) Rb, Re, Rn, Sb, Se, Tc, Te, Tl	NA	NA	NA	No solubility constraints are assumed to exist with these radionuclides. Ochs et al. (15) reported that SeO <sub>4</sub> <sup>2-</sup> may substitute for sulfate in ettringite, but more recent reports (3) indicate that this substitution on ettringite is quantitatively unimportant. Johnson et al. (2000) has also recently conducted some Se partitioning research with various cements.
C	10 <sup>-6</sup>	10 <sup>-4</sup>	10 <sup>-4</sup>	<sup>14</sup> C chemistry is influenced by carbon dioxide gas/water/solid phase equilibrium, isotopic exchange, adsorption, precipitation, aqueous chemistry, and coprecipitation. To be conservative the role of gas phase and isotopic exchange (two very important processes for removing <sup>14</sup> C from groundwater) will not be considered. For young concrete, assumed that Portlandite controls Ca to 10 <sup>-3</sup> M and CO <sub>3</sub> <sup>2-</sup> to 10 <sup>-6</sup> M (1). Ca concentrations are set by the solubility of calcite to "fix" the carbonate concentration. For moderately aged cement the Ca is controlled at 10 <sup>-2</sup> M by some undefined reactions (1). Subsurface C chemistry in a cementitious environment is discussed by Dayal (16, 17) and modeling gaseous C-14 in cementitious environments in the SRS subsurface has been discussed by Kaplan (18).
Ac, Al, Am, Bk, Bi, Ce, Cf, Cm, Eu, Fe, Gd, Lu, Sm, Y	10 <sup>-11</sup>	10 <sup>-8</sup>	10 <sup>-7</sup>	All +3 oxidation state: Young Concrete: Am solubility in concrete rinsate at pH 12 = 8e-11 M, at pH 13 = 1e-11 to 7e-12 M Am (2). Solid phase controlling solubility assumed to be Am(OH) <sub>3</sub> or Am(OH)CO <sub>3</sub> (2,4); Using a variety of cements and contact times of 100 days under oxidizing conditions measured Am solubility average was 1e-11 M (5). Experiments with sulfate resistant Portland cement consistently had Eu concentrations <1e-11 M. Time-resolved laser fluorescence spectroscopy (TRLFS) showed that Eu was incorporated within CSH and another fraction had properties suggesting it was within a structure like Eu(OH) <sub>3</sub> (11). Similarly, Cm was shown to be incorporated into the structure of calcium-silicate-hydrate (CSH) gels (6). Moderately Aged Concrete: Am solubility in concrete rinsate (no solid phase) at pH 10 to 11 was 1e-8 to 1.5e-10 M Am (2).
Ag, Co, Cd, Cu, Hg, Ni, Pb, Pd, Po, Pt,	10 <sup>-7</sup>	10 <sup>-7</sup>	10 <sup>-6</sup>	Solid phase assumed to control solubility is Co(OH) <sub>2</sub> (5, 6). Experiments with sulfate resistant Portland cement had Co solubility values of 5e-8 and 2e-7 M at pH 13.3 (6). The solubility of Co(OH) <sub>2</sub> was calculated to be 6.5e-5 M (6). Calculated values are considered less reliable than experimental values. Experiments and calculations have also been done with aged cement end members under alkaline cement conditions (2, 4, 7). Several experiments show solubility controls (6, 2, 4, 7). Solubility controls of Ni are shown by (8, 9, 10). Ni concentrations

Radio-nuclide	Young 1 <sup>st</sup> Stage (pH ~12)	Moderately-aged, (b) 2 <sup>nd</sup> Stage (pH ~10.5)	Aged (b) 3 <sup>rd</sup> Stage (pH ~5.5)	Comments/References <sup>(a)</sup>
Sn, Zn				consistently in range of 5e-8 to 2e-7 M regardless of the solid/liquid ratio (6).
Np, Pa	10 <sup>-13</sup>	10 <sup>-13</sup>	10 <sup>-7</sup>	Neptunium sorption to aged cement samples were conducted by Miller et al. (2009). They used an ICP-MS which permitted them much lower detection limits than conventional radiometric analytical methods and as a result, much lower <i>Kd</i> values were measured. They added Np(V) at varying concentrations to ground 50 year old cement samples and measured constant aqueous Np concentration at 1e-13 M, indicating solubility controls. Oxidation state of radionuclides is +5. Assume that NpO <sub>2</sub> <sup>+</sup> and PaO <sub>2</sub> <sup>+</sup> is the controlling solid. There is empirical data in Ewart et al. (2) that predicts much lower concentrations than thermodynamic predictions (2,4,7). Allard et al. (1984) added Np(V) to a variety of cements & measured solubility after 100 days of 4e-9 M. Solubility of Np(IV) is ~1e-8 M for pH 9.75 through pH 12.6 (3). Thus, according to Allard et al. (1984) and Ewart et al (1992) solubility of Np is about the same in concrete whether it is in +4 or +5 state. Miller et al (2009) had appreciably better detection limits than Ewart et al. (1992) and the former were working with aged material whereas the former were working with fresh materials.
Ra	10 <sup>-6</sup>	10 <sup>-6</sup>	10 <sup>-6</sup>	RaSO <sub>4</sub> is the controlling solid (1, 14). Bayliss et al. (1989) found no precipitation for Ra at ≥ 1e-7 M in concrete leachate. When appropriate, such as in the Saltstone Facility, it may be necessary to use sulfate controlling solubility phases, <i>i.e.</i> , BaSO <sub>4</sub> and SrSO <sub>4</sub> .
Ba, Ca, Sr	10 <sup>-5</sup>	10 <sup>-5</sup>	NA	SrCO <sub>3</sub> is solubility controlling phase. However, Sr may coprecipitate as (Ca,Sr)CO <sub>3</sub> which has an even lower solubility value (12). But solubility controls are only important at pH < 11, <i>i.e.</i> , in the absence of Ca(OH) <sub>2</sub> and high ratios of calcium-silicate-hydrate gel (12). Therefore, coprecipitation is unlikely in the paste matrix, but may occur at the cement/leachate interface. For this reason Atkins and Glasser (12) recommend a minimum Sr solubility of ~2e-5 M. This solubility value is likely to decrease even further if coprecipitation occurs (13). No solubility data is provided for “Aged Cement in the 3 <sup>rd</sup> Stage” because it is believed that it will likely not precipitate in this stage.
Pu(V/VI) Pu(III/IV), Pu(combo) Th, Zr	10 <sup>-12</sup>	10 <sup>-12</sup>	10 <sup>-7</sup>	Lilley et al (2009) measured Pu(V) <i>Kd</i> values in Vault 2 cement containing 25% slag and 2 Saltstone samples under reducing and oxidizing conditions. In both oxidizing and reducing conditions he measured 10 <sup>-12</sup> M solubility levels. One of the main reasons they were able to measure such low levels was because they used an ICP-MS rather than conventional radiometric analytical methods. Assumed solubility controlling phase are hydroxide/hydrous oxides for Th, Zr, Pu and hydroxycarbonates for Pb. The following is from (2) and was conducted by adding Th(IV) to water equilibrated with concrete and pH adjusted: solubility ranged from 1e-8 M to 4e-9 M as pH increased from 8.3 to 12.9. In essence, the solubility didn't change for Th. Sn exists in the tetravalent state, (Sn(IV), under the cementitious conditions and readily hydrolyses in the pH range >8. It sorbed to the same extent as Th(IV) to sulfate resistant Portland cement (2). Calculations of Pb, Pu, Th, and Zr solubility under cementitious conditions have been conducted (4, 7).
U(VI)	5 x 10 <sup>-6</sup>	5 x 10 <sup>-5</sup>	10 <sup>-6</sup>	Solubility controlling phases are likely U(VI) hydrous oxide [schoepite] and uranophase [calcium U(VI) silicate] (4, 7). Brady and Kozak (4) calculated a solubility of 1e-8 M U(VI).

<sup>(a)</sup> References: (1) = Krupka et al. 2004; (2) = Ewart et al. 1992; (3) = Baur and Johnson 2003; (4) = Brady and Kozak 1995; (5) Allard et al. 1984; (6) = Wieland & Van Loon 2003; (7) = Hietanen et al. 1984; (8) = Hietanen et al. 1984; (9) = Pilkington and Stone 1990; (10) = Atkins et al. 1993; (11) = Pointeau et al. 2001; (12) = Atkins and Glasser 1992; (13) = Smith and Walton 1991; (14) = Bayliss et al. 1989; (15) = Ochs et al. 2002; (16) = Dayal and Reardon 1992; (17)

Radio-nuclide	Young 1 <sup>st</sup> Stage (pH ~12)	Moderately-aged, (b) 2 <sup>nd</sup> Stage (pH ~10.5)	Aged (b) 3 <sup>rd</sup> Stage (pH ~5.5)	Comments/References <sup>(a)</sup>
				<p>= Dayal et al. 1989; (18) = Kaplan 2005; (19) = Kaplan and Coates 2007; (20) = Lilley et al. 2009; (21) = Miller et al. 2009; (22) = Lilley et al. 2009.</p> <p>(b) Making the same assumptions about the solid phase changes in the cementitious materials as Bradbury and Sarott (1995) and as described in Section 4.2, the solubility concentration limits values in the Aged Concrete (3<sup>rd</sup> Stage) were set to an order of magnitude higher (more soluble, more likely to be in the aqueous than the solid phase) than those in the Moderately Aged Concrete (2<sup>nd</sup> Stage). This same approach to assigning solubility concentration limits values to the 3<sup>rd</sup> Stage was used by Bradbury and Sarott (1995).</p>

Table 20. Apparent Solubility Concentration Limits (mol/L) for Reducing Cementitious Solids

Radio-nuclide	Young Cement 1 <sup>st</sup> Stage (pH ~12)	Moderately-aged Cement, 2 <sup>nd</sup> Stage (pH ~10.5)	Aged Cement 3 <sup>rd</sup> Stage (pH ~5.5)	Comments/References <sup>(a)</sup>
<sup>3</sup> H, Ac, Am, Ar, At, Ba, Bi, Bk, C, Ca, Cd, Cf, Cl, Cm, Co, Cs, Eu, Fr, Gd, I, Lu, Kr, Nb, Ni, Pb, Pd, Po, Pt, Ra, Rn, Se, Sm, Sn, Sr, Te, Tl, Th, Y, Zn, Zr,		These radionuclides are assumed to have the same apparent solubility values as for the Oxidizing Cementitious Solids (Table 19).		The solubility of a number of other metals would likely be further lowered in a concrete that contains blast furnace slag (BFS) because BFS greatly increases the concentration of sulfides (S <sup>2-</sup> ) in the porewater (J). Sulfide concentrations in BFS concrete porewater have been measured as high as 1100 mg/L (J). However, there has not been any experimental or theoretical work to substantiate the assertion that metal sulfides form and lower the solution concentrations of metals in this group below concentrations presented in Table 19).
Tc(IV), Re(IV)	10 <sup>-10</sup>	10 <sup>-10</sup>	10 <sup>-6</sup>	Bayliss et al. (2) adsorbed Tc onto Portland cement or concrete in an anoxic glove box with 0.05 M dithionite in 1.5 M NaCl for 28 days in 50:1 water:crushed cement: $K_d = 5000$ mL/g and measured Tc solution concentration was 1e-11 M. Assuming Tc <sub>2</sub> S <sub>7</sub> as the solubility controlling phase, MMES (1992; Appendix D) calculated that reducing grout used in the SRS saltstone program would maintain Tc at a concentration of 1.4e-20 M (2.4e-8 pCi/L). Allard (4) calculated that reducing concrete would maintain Tc at a concentration <1e-10 M. It is assumed that the SRS cementitious materials containing blast furnace slag remain reducing throughout all three stages. The 3 <sup>rd</sup> stage has a lower solubility only to permit some Tc to release into the environment due to oxidation of phase, not because the phase is believed to have change into a form that is more soluble (a way to release Tc into the aqueous phase). Additional information for why Tc sorption values are high in SRS-slag-containing cementitious materials see Page 157, Section 13.0, Appendix E: Spectroscopic Evidence of the Reduction of Tc(VII) to Tc(IV) by Cementitious Material Containing SRS Slag.
Cr	10 <sup>-7</sup>	10 <sup>-7</sup>	10 <sup>-6</sup>	Bajt et al. (10) observed XAS spectra of the reduction of Cr(VI) in SRS reducing grout to Cr(III). Rai et al (11) measured the solubility of Cr(III) at varying pH and ionic strengths and as varying solid phases.
Np(IV), Pa(IV)	10 <sup>-13</sup>	10 <sup>-13</sup>	10 <sup>-5</sup>	Lilley et al (2009) measured Np(V) Kd values in Vault 2 cement containing 25% slag and two SRS Saltstone samples under reducing and oxidizing conditions. In oxidizing conditions he measured 10 <sup>-12</sup> M solubility. Under reducing conditions, they measured 10 <sup>-13</sup> M solubility values. One of the main reasons they were able to measure such low levels was because they used an ICP-MS rather than conventional radiometric analytical methods. Under reducing conditions, both Np and Pa are reduced from +5 to +4. In the tetravalent form they would be expected to sorb very strongly or be insoluble. Assume that metal hydroxide is the controlling solid. The empirical laboratory data generated by Ewart et al. (1992) is much lower than thermodynamic predictions (2,4,7). Berry et al. 1988 reported that Pa sorbed very strongly, but due to experimental problems (sorption to glassware

Radio-nuclide	Young Cement 1 <sup>st</sup> Stage (pH ~12)	Moderately -aged Cement, 2 <sup>nd</sup> Stage (pH ~10.5)	Aged Cement 3 <sup>rd</sup> Stage (pH ~5.5)	Comments/References <sup>(a)</sup>
Pu(III/IV), Pu(combo)	10 <sup>-12</sup>	10 <sup>-12</sup>	10 <sup>-9</sup>	<p>and filters) was unable to come up with reliable cement sorption values. It is assumed that the cementitious materials remain reducing throughout all three stages.</p> <p>Lilley et al (2009) measured Pu(V) Kd values in Vault 2 cement containing 25% slag and 2 Saltstone samples under reducing and oxidizing conditions. In both oxidizing and reducing conditions he measured 10<sup>-12</sup> M solubility levels. The Pu(V) presumably quickly reduced to Pu(IV) (or perhaps less likely Pu(III)) in these experiments. Pu(IV) solubility measured by adding Pu(IV) spike into concrete rinsate under reducing conditions without solid phase and adjusting pH: from 9 to 11 the solubility was 1e-10 to 5e-11; essentially not changing (8). Assumed Pu(OH)<sub>4</sub> controlled solubility. Based on thermodynamic calculations, solubility limits under reducing cementitious conditions were estimated to be less than 10<sup>-9</sup> to 10<sup>-10</sup> M Pu (9). It is assumed that the cementitious materials remain reducing throughout all three stages. Lilley et al (2009) measured Pu(V) Kd values in Vault 2 cement containing 25% slag and 2 Saltstone samples under reducing and oxidizing conditions. In both oxidizing and reducing conditions he measured 10<sup>-12</sup> M solubility levels. Pu(combo) is a single geochemical parameter for Pu taking into account its many oxidation states. For this system, all Pu is assumed to exist in the +4 oxidation state.</p>
U	10 <sup>-6</sup>	10 <sup>-7</sup>	10 <sup>-7</sup>	<p>U(IV) solubility measured by adding U(IV) spike into concrete rinsate under reducing conditions without solid phase and adjusting pH: from 5 to 13 the solubility was 8e-7 to 2e-7; essentially not changing over that entire pH range (8). This wide pH range suggests that the solubility concentration limits does not change as a function of cement Stage. Assumed UO<sub>2</sub>(crystal) and UO<sub>2</sub>(amorph) were the solubility controlling phases. Based on thermodynamic calculations, solubility limits of U under reducing cementitious conditions were estimated to be less than 10<sup>-9</sup> to 10<sup>-10</sup> M U(IV) (9). It is assumed that the cementitious materials remain reducing throughout all three stages.</p>
<p><sup>(a)</sup> References: (1) = Angus and Glasser 1985; (2) = Bayliss et al. 1991; (3) = MMES 1992; (4) = Allard et al. 1984; (5) = Bajt et al. 1993; (6) = Macias et al. 1997; (7) = Rai and Szelmezcza 1990; (8) = Ewart et al. 1992; (9) = Brady and Kozak 1995; (10) = Bajt et al. 1993; (11) = Rai et al. 1987; (12) = Miller et al. 2009; (13) = Lilley et al. 2009;</p> <p><sup>(b)</sup> Discussion of the age of each of the stages is facility specific because it depends on the amount of water that passes through the cementitious material (see Section 11.0).</p>				

**Table 21.** Cellulose Degradation Product Correction Factors ( $f_{CDF}$ ).

Element	Correction Factor ( $f_{CDF}$ ) (unitless)	Species/Analog	Comments <sup>(a)</sup>	Ref. <sup>(b)</sup>
Ac	0.55	Ce(III) & Eu(III)	trivalent actinide	1
Ag	1	Ni(II)	Ag is a soft monovalent, and the analog is a hard divalent; hence not a good analog.	1
Al	0.55	Ce(III) & Eu(III)	Hard trivalent	1
Am	0.55	Ce(III) & Eu(III)	trivalent actinide	1
Ar	1	I(-1)		2
As	1	SeO <sub>4</sub> <sup>2-</sup>		2
At	1	I(-1)		1
Ba	1	Sr(II)		1
Bi	0.55	Ce(III) & Eu(III)	trivalent actinide	1
Bk	0.55	Ce(III) & Eu(III)	trivalent actinide	1
C	1	None		1
Ca	1	Sr(II)	divalent cation	1
Cd	1	Ni(II)		1
Ce	0.55	Ce(III)	trivalent actinide	1
Cf	0.55	Ce(III) & Eu(III)		1
Cl	1	I(-1)		2
Cm	0.55	Ce(III) & Eu(III)		1
Co	1	Ni(II)		1
Cr	1	SeO <sub>4</sub> <sup>2-</sup>		2
Cs	1	Cs(I)		1
Cu	1	Ni(II)		1
Eu	0.55	Eu(III)	trivalent lanthanide	1
F	1	I(-1)		2
Fe	0.55	Eu(III)	trivalent	1
Fr	1	Cs(I)		1
Gd	1	Ce(III) & Eu(III)	trivalent lanthanide	1
H	1	N/A		1
Hg	1	Ni(II)	<sup>(d)</sup>	1
I	1	I(-1)		2
K	1	Cs(II)	monovalent cation	1
Kr	1	N/A		1
Lu	0.55	Ce(III) & Eu(III)	trivalent lanthanide	1
Mn	1	SeO <sub>4</sub> <sup>2-</sup>		2
Mo	1	SeO <sub>4</sub> <sup>2-</sup>		2
N	1	I(-1)		2
Na	1	Cs(I)		1
Nb	1	SeO <sub>4</sub> <sup>2-</sup>		2
Ni	1	Ni(II)		1
Np	1	Cs(I)		1
Pa	1	Cs(I)		1
Pb	1	Ni(II)	<sup>(d)</sup>	1

Element	Correction Factor ( $f_{CDF}$ ) (unitless)	Species/Analog	Comments <sup>(a)</sup>	Ref. <sup>(b)</sup>
<b>Pd</b>	1	Ni(II)	<sup>(d)</sup>	1
<b>Po</b>	1	Ni(II)		1
<b>Pt</b>	1	Ni(II)	<sup>(d)</sup>	1
<b>Pu</b>	1	Th(IV)		1
<b>Ra</b>	1	Sr(II)		1
<b>Rb</b>	1	Cs(I)		1
<b>Re</b>	1	TcO <sub>4</sub> <sup>-</sup>		2
<b>Rn</b>	1	N/A		1
<b>Sb</b>	1	SeO <sub>4</sub> <sup>2-</sup>	Selenate is a poor analog	2
<b>Se</b>	1	SeO <sub>4</sub> <sup>2-</sup>		2
<b>Sm</b>	0.55	Ce(III) & Eu(III)	trivalent lanthanide	1
<b>Sn</b>	1	Ni(II)	<sup>(d)</sup>	1
<b>Sr</b>	1	Sr(II)		1
<b>Tc</b>	1	TcO <sub>4</sub> <sup>-</sup>		2
<b>Te</b>	1	SeO <sub>4</sub> <sup>2-</sup>	Assumed dominate phase TeO <sub>4</sub> <sup>2-</sup>	2
<b>Th</b>	1	Th(IV)		1
<b>Tl</b>	1	Cs(I)	<sup>(c)</sup>	1
<b>U</b>	1	Sr(II)		1
<b>Y</b>	0.55	Ce(III) & Eu(III)	trivalent cation	1
<b>Zn</b>	1	Ni(II)		1
<b>Zr</b>	1	Zr		1

<sup>(a)</sup> Comments provide basis for selection of analog for elements not listed in Kaplan (2007a) or Kaplan and Serkiz (2006) based on professional judgment

<sup>(b)</sup> 1 = Correction factor for element or analog given in Table 15 of Kaplan (2007a)

2 = Correction factor for element or analog given in Table 7 of Kaplan and Serkiz (2006)

<sup>(c)</sup> Monovalent cation except under strongly reducing conditions, where it becomes trivalent.

<sup>(d)</sup> No experimental data available for soft divalent cations; used Ni, a relatively hard divalent cation, as analog.

**Table 22.** Cementitious Leachate Impact Factors,  $f_{CementLeach}$  (Eq. 6).

Element	$f_{CementLeach}$ (Unitless)	Analog	Comments <sup>(a)</sup>
Ac	1.5	Eu	trivalent
Ag	3.2	Sr	Because Sr is not a good analog (Sr is a hard base and Ag is much softer), assumed half the impact factor
Al	1.5	Eu	trivalent
Am	1.5	Eu	trivalent
Ar	1	None	Inert
As	1.4	Se	Oxyanion
At	0.1	I	monovalent anion
Ba	3	Sr	hard divalent cation
Bi	1.5	Eu	trivalent
Bk	1.5	Eu	trivalent
C	5	C	
Ca	3	Sr	hard divalent cation
Cd	3	Sr	hard divalent cation
Ce	1.5	Eu	trivalent
Cf	1.5	Eu	trivalent
Cl	0.1	Cl	monovalent anion
Cm	1.5	Eu	trivalent
Co	3.2	Sr	Because Sr is not a good analog (Sr is a hard base and Co is much softer), assumed half the impact factor
Cr	1.4	Se	Oxyanion
Cs	1	Cs	hard monovalent cation
Cu	3.2	Sr	Because Sr is not a good analog (Sr is a hard base and Cu is much softer), assumed half the impact factor
Eu	1.5	Eu	trivalent
F	0.1	Cl	monovalent anion
Fe	1.5	Eu	trivalent
Fr	1	Cs	hard monovalent cation
Gd	1.5	Eu	trivalent
H	1	H	
Hg	3.2	Sr	Because Sr is not a good analog (Sr is a hard base and Hg is much softer), assumed half the impact factor
I	0.1	I	monovalent anion
K	1	Cs	hard monovalent cation
Kr	1	None	Inert
Lu	1.5	Eu	trivalent
Mo	1.4	Se	Oxyanion
Mn	1.4	Se	Oxyanion
N	0.1	I	monovalent anion
Na	1	Cs	hard monovalent cation
Nb	1.4	Se	Oxyanion
Ni	3.2	Sr	Because Sr is not a good analog (Sr is a hard base and Ni is much softer), assumed half the impact factor

Element	$f_{CementLeach}$ (Unitless)	Analog	Comments <sup>(a)</sup>
<b>Np</b>	1.5	Np	Assume $NpO_2^-$
<b>Pa</b>	1.5	Np	Assume $PaO_2^-$
<b>Pb</b>	3.2	Sr	Because Sr is not a good analog (Sr is a hard base and Pb is much softer), assumed half the impact factor
<b>Pd</b>	3.2	Sr	Because Sr is not a good analog (Sr is a hard base and Pd is much softer), assumed half the impact factor
<b>Po</b>	2	Pu	Tetravalent, Pu is only a marginal analog
<b>Pt</b>	3.2	Pu	Ni analog
<b>Pu</b>	2	Pu	Pu is Solubility controlled at pH >9
<b>Ra</b>	3	Sr	hard divalent cation
<b>Rb</b>	1	Cs	hard monovalent cation
<b>Re</b>	0.1	Tc	monovalent anion, $ReO_4^-$
<b>Rn</b>	1	None	Inert
<b>Sb</b>	1.4	Se	Oxyanion
<b>Se</b>	1.4	Se	Assumed dominate phase $SeO_4^{2-}$
<b>Sm</b>	1.5	Eu	trivalent
<b>Sn</b>	3	Sr	Sn is actually a soft divalent metal, whereas Sr is a hard metal therefore, not a good analog match
<b>Sr</b>	3	Sr	hard divalent cation
<b>Tc</b>	0.1	Tc	
<b>Te</b>	1.4	Se	Assumed dominate phase $TeO_4^{2-}$
<b>Th</b>	2	Pu	Pu is not a good analog, will assume
<b>Tl</b>	1	Cs	Cs is a hard monovalent cation; Tl is appreciably softer, not a good analog
<b>U</b>	3	Sr	hard divalent cation
<b>Y</b>	1.5	Eu	trivalent
<b>Zn</b>	3	Sr	hard divalent cation
<b>Zr</b>	2	Pu	Tetravalent, Pu is only a marginal analog

<sup>(a)</sup> All data in this table in based on experimentation conducted with offsite material (Cantrell et al. 2007). Cementitious Leachate Impact Factors are discussed in more detail in Section 4.1.4, in particular Table 2.

**Table 23.** *Kd* Values for Environments Impacted by CDP and Cementitious Leachate,  $Kd_{CDP\_CemLeach}$ .

<b>Rad</b>	<b>Correction Factor f(CDP) or f(ChemLech) for Best cement leachate with CDP Sand Kd</b>	<b>Correction Factor f(CDP) or f(ChemLech) for Best cement leachate with CDP Clay Kd</b>	<b>Best Cement Leachate with CDP Sand Kd</b>	<b>Best Cement Leachate with CDP Clay Kd</b>
	(unitless)	(unitless)	(mL/g)	(mL/g)
Ac	1.5	1.5	1650	12750
Ag	3.2	3.2	192	480
Al	1.5	1.5	1950	1950
Am	1.5	1.5	1650	12750
Ar	1	1	0	0
As	1	1	140	280
At	1	1	0.0	0.1
Ba	1	1	15	51
Bi	1.5	1.5	1650	12750
Bk	1.5	1.5	1650	12750
C	1	1	50	2000
Ca	1	1	15	51
Cd	3	3	45	90
Ce	1.5	1.5	1650	12750
Cf	1.5	1.5	1650	12750
Cl	1	1	0	0
Cm	1.5	1.5	1650	12750
Co	3.2	3.2	128	320
Cr	1	1	6	14
Cs	1	1	10	50
Cu	3.2	3.2	160	224
Eu	1.5	1.5	1650	12750
F	1	1	0	0
Fe	1.5	1.5	300	600
Fr	1	1	10	50
Gd	1.5	1.5	1650	12750
H	1	1	0	0
Hg	3.2	3.2	2560	3200
I	1	1	0.0	0.1
K	1	1	5	25
Kr	1	1	0	0
Lu	1.5	1.5	1650	12750
Mn	1	1	21	280
Mo	1	1	1400	1400
N	1	1	0	0
Na	1	1	5	25
Nb	0.2	1	0	0
Ni	3.2	3.2	22	96
Np	1.5	1.5	5	14
Pa	1.5	1.5	5	14

<b>Rad</b>	<b>Correction Factor f(CDP) or f(ChemLech) for Best cement leachate with CDP Sand Kd</b>	<b>Correction Factor f(CDP) or f(ChemLech) for Best cement leachate with CDP Clay Kd</b>	<b>Best Cement Leachate with CDP Sand Kd</b>	<b>Best Cement Leachate with CDP Clay Kd</b>
Pb	3.2	3.2	6400	16000
Pd	3.2	3.2	22	96
Po	2	2	4000	10000
Pt	3.2	3.2	22	96
Pu(combo)	2	2	580	11900
Pu(III/IV)	2	2	600	12000
Pu(V/VI)	1	1	32	10000
Ra	1	1	15	51
Rb	1	1	10	50
Re	1	1	0.1	0.2
Rn	1	1	0	0
Sb	1	1	3500	3500
Se	1	1	1400	1400
Sm	1.5	1.5	1650	12750
Sn	3	3	6000	15000
Sr	1	1	15	51
Tc	1	1	0.1	0.2
Te	1	1	1400	1400
Th	2	2	1800	4000
Tl	1	1	10	50
U	3	3	600	900
Y	1.5	1.5	1650	12750
Zn	3	3	45	90
Zr	2	2	1800	4000

## 7.0 FUTURE RESEARCH AND DATA NEEDS

In the process of collecting these input data for the PA modeling effort, several data needs were identified. The identification of data needs is part of the PA maintenance program which provides a vehicle to update PA calculations when new or improved data become available or when new information is learned that requires additional modeling scenarios to be conducted. The following is a list of the key areas that require additional research to gather new and improved data.

1. Reactive Transport Modeling: Although  $Kd$  and solubility concentration limits values are convenient for use in transport models, they are not robust parameters in that they represent rather limited ranges of geochemical conditions (Sections 3.1 and 3.3). For this reason, it is necessary to rely on site-specific and condition-specific experiments to provide insight into how the radionuclides interact with the solid phase. It is the express goal of the geochemistry research group within the PA to move towards a truly reactive transport model where important ancillary aqueous solutes, such as pH or dissolved organic carbon concentrations, can be modeled along with the radionuclide concentrations. Changes in the concentrations of these ancillary parameters are known to greatly influence the mobility of many radionuclides. The present PA attempts to estimate their impact by creating “Environments” of a class of aqueous chemistry, but a more elegant approach would be one in which the chemistry of the ancillary parameter was accounted for directly in the transport code. A good example of this type of geochemical modeling was recently completed for Eu (an analog for trivalent radionuclides) sorption to SRS sediments in the presence of varying pH and cellulose degradation products (more specifically, fulvic acid) (Kaplan et al. 2010). It is also the interest of the PA to incorporate more process-driven (mechanistic) approaches to describe the geochemistry in the PA. Important advances have been made towards this end with regards to Pu geochemistry and how it has been incorporated into performance assessment and special analysis calculations (Kaplan et al. 2001, 2004, 2006a, 2006b; 2008c; Fjeld et al. 2004; Powell et al. 2005, 2006). For example, Pu(V) reduction was found to occur under SRS vadose zone conditions. Similarly,  $^{14}\text{C}$ -carbonate sorption is better described using a kinetic model over months to years, rather than an instantaneous equilibrium  $Kd$  model. Additional work needs to be conducted to incorporate reactive transport modeling into the PA, including in cementitious environments.
2. Range and Distribution of Sorption Parameters for Cementitious Materials: Range and distributions of radionuclide  $Kd$  and solubility values with cementitious materials is needed. This needs to be measured using a wide range of cementitious materials, preferably prepared under field conditions where natural variability in mixing conditions will be sampled (Section 4.6).
3. C-14 Chemistry in Cementitious and Natural SRS Subsurface Environments: There is little information about inorganic C chemistry under natural SRS subsurface conditions. Given the importance of C-14 to risk calculations, additional attention should be directed at understanding how C-14 interacts with sediments at varying pH levels and in the

presence of natural organic matter. The latter is especially important for composite analyses or where cellulose degradation products may be present.

4. Colloids: The PA is presently modeling colloid facilitated transport of Pu and its approach is entirely empirical and based on two SRS field studies (Section 3.4.2). The conceptual and numerical models need to be improved based upon field and laboratory studies designed to develop a numerical model. Also, the role of strong pH gradients (such as at cement/soil interfaces) and cellulose degradation products (which is likely to be acidic and at the same time some dispersive properties) on colloid generation needs to be evaluated.
5. Kd Values for Cementitious Leachate Impacted Sediment Environments: Measure  $Kd$  values for key radionuclides under conditions simulating cementitious leachate sediment environments (Sections 4.2.4 and 4.2.5).
6. Kd Values for Cementitious Leachate Impacted and CDP-Impacted Sediment Environments: Measure  $Kd$  values for key radionuclides under conditions simulating both CDP- and cementitious leachate-impacted sediment environments (Section 4.2.6).
7. Technetium Interaction with Reducing Grout: The geochemistry describing the interaction of Tc with reducing grout/saltstone is extremely important to the PA. It is described here as a solubility controlled process, however, other reactions may also be important. Additional work needs to be conducted to more completely describe this system of reactions, including the reduction and oxidation kinetics of Tc(IV) and Tc(VII) conversions, and the influence of dissolved oxygen (in groundwater) on sulfide and sulfate conversions. Additional measurements of solubility concentration limits values are also required to determine variability associated between Saltstone batches. Tests must also be developed to determine good experimental protocols for determining the reduction capacity of a reducing cement/saltstone.
8. Degradation Rate of Cellulosic Materials: No site-specific work has been done to describe the degradation rate of cellulosic materials that is co-disposed with the radiological waste (Sections 3.4.1). Because soil microbes play an important role in cellulose degradation, it is especially necessary to conduct these studies under site-specific conditions.

## 8.0 REFERENCES

- Allard, B., L. Eliasson, S. Hoglund, and K. Andersson. 1984. Sorption of Cs, I and Actinides in Concrete Systems. SKB Technical Report SKB/KBS TR-84-15, SKB, Stockholm, Sweden.
- Allard, B., L. Hoglund, and K. Skagius. 1991. Adsorption of Radionuclides in Concrete. SKB Progress Report SKB/SFR 91/02, SKB Stockholm, Sweden.
- Allard, B., V. Moulin, L. Ballo, M. T. Tran, and D. Stammose. 1989. Americium Adsorption on Alumina in the Presence of Humic Materials. *Geoderma*. 44:181-187.
- Ames, L. L., and D. Rai. 1978. Radionuclide interactions with Rock and Soil Media. Volume I. EPA 520/6-78-007-A. U.S. Environmental Protection Agency, Office of Radiation Programs –Las Vegas, NV.
- Angus, M. J. and F. P. Glasser. 1985. The Chemical Environment in Cement Matrices. *Mat. Res. Soc. Symp. Proc.* 50:547–556.
- Atkins, M., and F. P. Glasser. 1992. Application of Portland Cement-Based Materials to Radioactive Waste Immobilization. *Waste Management*. 12:105–131.
- Atkins, M., F. P. Glasser, L. P. Moroni, and J. J. Jack. 1993. Thermodynamic Modeling of Blended Cements at Elevated Temperatures (50-90°C). DoE/HMIP/RP/94.011. UK Nirex Ltd., Harwell, UK.
- Atkinson, A., N. Everett, and R. Guppy. 1988. Evolution of pH in a Radwaste Repository: Internal Reactions Between Concrete Constituents. AERE-R12939, UKAEA, Harwell, UK.
- Baes, C. F., Jr., and R. E. Mesmer. 1976. *The Hydrolysis of Cations*. John Wiley and Sons, New York, NY.
- Bajt, S., S. B. Clark, S. R. Sutton, M. L. Rivers, and J. V. Smith. 1993. Synchrotron X-ray Microprobe Determination of Chromate Content using X-ray Absorption Near-edge Structure. *Analytical Chemistry*. 65:1800-1804.
- Baur, I., C. A. Johnson. 2003. Sorption of Selenite and Selenate to Cement Minerals. *Environ. Sci. Technol.* 37:3442-3447.
- Bayliss, S., F. T. Ewart, R. M. Howse, S. A. Lane, N. J. Pilkington, J. L. Smith-Briggs, and S. J. Williams. 1989. The Solubility and Sorption of Radium and Tin in a Cementitious Near-field Environment. *Mat. Res. Soc. Symp. Proc.* 127: 879-885.
- Bayliss, S., F. Ewart, R. Howse, J. Smith-Briggs, J. Thomason, and H. Willmott. 1988. The Solubility and Sorption of Lead-210 and Carbon-14 in a Near-Field Environment. – In:

- Scientific Basis for Nuclear Waste Management, Volume 11, p 33 (ed) M. Adted and R. Westerman. Material Research Society, Pittsburgh, PA.
- Bayliss, S., A. Haworth, R. McCrohon, A. D. Moreton, P. Oliver, N. J. Pilkington, A. J. Smith, and J. L. Smith-Briggs. 1991. Radioelement Behavior in a Cementitious Environment. In Scientific Basis for Nuclear Management XV, C. G. Sombret (ed) Materials Research Soc. Symposium Proceedings Vol. 257:641-648. Materials Research Society, Pittsburgh, PA.
- Berner, U. R. 1992. Evolution of Pore Water Chemistry during Degradation of Cement in a Radioactive Waste Repository Environment. *Waste Management*. 12: 201-215.
- Berry, J., J. Hobley, S. Lane, A. Littleboy, M. Nash, P. Oliver, J. Smith-Briggs, and S. Williams. 1988. The Solubility and sorption of Protactinium in the Near-Field and Far-Field Environment of a Radioactive Waste Repository. UK Nires Ltd Report NSS/R122, Harwell, UK.
- Bertsch, P. M., D. B. Hunter, S. R. Sutton, S. Bajt, and M. L. Rivers. 1994. In Situ Chemical Speciation of Uranium in Soils and Sediments by Micro X-ray Absorption Spectroscopy. *Environ. Sci. Technol.* 28:980-984.
- Bibler, J. P., and D. B. Marson. 1992. Behavior of Mercury, Lead, Cesium, and Uranyl Ions on Four SRS Soils. WSRC-RP-92-326. Westinghouse Savannah River Company, Aiken, SC.
- Bajt, S., S. B. Clark, S. R. Sutton, M. L. Rivers, and J. V. Smith. 1993. Synchrotron X-ray Microprobe Determination of Chromate Content Using X-ray Absorption Near-Edge Structure. *Anal. Chem.* 65: 1800-1804.
- Bower, H. 1991. Simple Derivation of the Retardation Equation and Application to Preferential Flow and Macrodispersion. *Ground Water*. 29:41-46.
- Bradbury, M. H., and F. A. Sarott. 1995. Sorption Databases for the Cementitious Near-field of a L/ILW Repository for Performance Assessment. PSI Bericht Nr. 95-06. Paul Scherrer Institut, Villigen, Switzerland.
- Brady, P. V., and M. W. Kozak. 1995. Geochemical Engineering of Low Level Radioactive Waste in Cementitious Environments. *Waste Management*. 15:293-301.
- Brodde, B. G. 1988. Leachability of Technetium from Concrete. *The Science of the Total Environment*. 69:319-345.
- Buice, J. M., R. K. Cauthen, R. R. Haddock, B. A. Martin, J. A. McNeil, J. L. Newman, and K. H. Rosenberger. 2005. Performance Objective Demonstration Document (PODD) for the Closure of Tank 19 and Tank 18 Savannah River Site. CBU-PIT-2005-00106, Rev. 1. Washington Savannah River Company, Aiken, SC.

- Buesseler, K. O., D. I. Kaplan, M. Dai, and S. Pike. 2009. Source Dependent and Source independent Controls on Plutonium Oxidation State and Colloid Associations in Groundwater. *Environ. Sci. Tech.* 43(5):1322–1328.
- Buchter, B., B. Davidoff, M. C. Amacher, C. Hinz, I. K. Iskandar, and H. M. Selim. 1989. Correlation of Freundlich  $K_d$  and  $n$  Retention Parameters with Soils and Elements. *Soil Sci.* 148: 370-379.
- Cantrell, K.J., J. M. Zachara, P. E. Dresel, K. M. Krupka, and R. J. Serne. 2007. Geochemical Processes Data package for the Vadose Zone in the Single-Shell Tank Waste Management Areas at the Hanford Site. PNNL-166663. Pacific Northwest National Laboratory, Richland, WA.
- Crapse, K. P., S. M. Serkiz, A. Pishko, P. C. McKinsey, R. L. Brigmon, E. P. Shine, C. Fliermans, and A. S. Knox. 2004. Monitored Natural Attenuation of Inorganic Contaminants Treatability Study Final Report. WSRC-TR-2004-00124, Rev. 0. Westinghouse Savannah River Company, Aiken, SC.
- Choppin G.R. 1989. Soluble Rare Earth and Actinide Species in Seawater. *Mar. Chem.* 28: 19-26.
- Collard, L. B., and R. A. Hiergesell. 2004 General Revision of Slit and Engineered Trench Limits. WSRC-TR-2004-00300. Westinghouse Savannah River Site, Aiken, SC.
- Dai, M., J. M. Kelley, and K. O. Buesseler. 2002. Sources and Migration of Plutonium in Groundwater at the Savannah River Site. *Environ. Sci. Technol.* 36:3690–3699.
- Davis, J.A. and D. B. Kent. 1990. Surface Complexation Modeling in Aqueous Geochemistry. In. *Review in Mineralogy: Mineral-Water Interface Geochemistry*, eds. M. F. Hochella and A. F. White, Mineralogy Society of America, Washington, DC, pp. 177-260.
- Davis, J. A., J. A. Coston, D. B. Kent, and C. C. Fuller. 1998. Application of the Surface Complexation Concept to Complex Mineral Assemblages. *Environ. Sci. Technol.* 32:2820–2828.
- Davis, J. A., D. E. Meece, M. Kohler, and G. P. Curtis. 2004. Approaches to Surface Complexation Modeling of Uranium(VI) Adsorption on Aquifer Sediments. *Geochem. Cosmochem.* 68:3621-3641.
- Dayal, R., H. Johnston, and Z. Zhou. 1989. Reactor Operating Waste Disposal Program, 1989 Progress Report. 89-226-K. Ontario Hydro, Ontario, Canada.
- Dayal, R., and E. J. Reardon. 1992. Cement-Based Engineered Barriers for Carbon-14. *Isolation. Waste Management* 12:189–200.

- Demirkanli, D. I., F. J. Molz, D. I. Kaplan, R. A. Fjeld, and S. M. Serkiz. 2007. Long-Term Vadose Zone Plutonium Transport at the Savannah River National Laboratory. *Vadose Zone J.* 6:344-352.
- Denham, M. E. 2009. Conceptual Model of Waste Release from the Contaminated Zone of Closed Radioactive Waste Tanks. WSRC-STI-2007-00544, Rev. 1. Savannah River National Laboratory, Aiken, SC.
- EPA. 1999. Understanding Variation in Partition Coefficient,  $K_d$ , Values. Volume II: Review of Geochemistry and Available  $K_d$  Values for Cadmium, Cesium, Chromium, Lead, Plutonium, Radon, Strontium, Thorium, Tritium, and Uranium. EPA 402-R-9-004B, US EPA, Washington, DC.
- EPA. 2004. Understanding Variation in Partition Coefficient,  $K_d$ , Values. Volume III: Review of Geochemistry and Available  $K_d$  Values for Americium, Arsenic, Curium, Iodine, Neptunium, Radium, and Technetium. EPA 402-R-04-002C, US EPA, Washington, DC.
- Ewart, F. T., J. L. Smith-Briggs, H. P. Thomason, and S. J. Williams. 1992. The Solubility of Actinides in a Cementitious Near-Field Environment. *Waste Management.* 12:241–252.
- Ewart, F. T., R. M. Howse, H. P. Thomason, S. J. Williams and J. E. Cross. 1986. The Solubility of Actinides in the Near-field, pp. 701-708. *Scientific Basis for Nuclear Waste Management IX*, ed. L. O. Werme. Materials Research Society Symposium Proceedings, Volume 50, Materials Research Society, Pittsburgh, PA.
- Ewart, R., S. Pugh, S. Wisbey, and D. Woodward. 1988. Chemical and Microbiological Effects in the Near-Field: Current Status. Report NSS/G103, U.K. Nirex Ltd., Harwell, United Kingdom.
- Fairhurst A.J., Warwick P., Richardson S. 1995. The Effect of pH on Europium-Mineral Interaction in the Presence of Humic Acid. *Radiochim. Acta.* 69: 103-111.
- Findley, M. 1998. Characterizing the Environment Availability of Trace Metals in Soils at the Savannah River Site. Masters' Degree Thesis, Clemson University, Clemson, SC.
- Fjeld, R. A., S. M. Serkiz, P. L. McGinnis, A. Elci, and D. I. Kaplan. 2004. Modeling the Effect of Surface-Mediated Reduction of Pu(V) to Pu(IV) on Plutonium Transport Behavior. *J. Contam. Hydrol.* 67:79-94.
- Goto, M. 2001. Development of a Quantitative Model for Binding Cesium to SRS Soils. Masters' Degree Thesis. Georgia Institute of Technology, Atlanta, GA.
- Grogan, K. P. 2009 Spatial Variability of Radionuclide Distribution Coefficients at the Savannah River Site and the Sub-surface Transport Implications. Master's Degree Thesis. Clemson University, Clemson, SC.

- Grogan, K. P., R. A. Fjeld, D. I. Kaplan, G. P. Shine, T. A. DeVol, and J. C. Seaman. 2008. Distribution of Sorption Coefficients ( $K_d$  Values) in the SRS Subsurface Environment. WSRC-STI-2008-00698. Washington Savannah River Company, Aiken, SC 29808.
- Grogan, K., R. A. Fjeld, D. I. Kaplan, T. DeVol, and J. D. Coates. 2010. Distributions of Radionuclide Sorption Coefficients ( $K_d$ ) in Subsurface Sediments and Their Implications to Transport. *Journal of Environmental Radioactivity*. (In Review).
- Herbelin, A. L., and J. C. Westall. 1999. FITEQL: A Computer Program for the Determination of Chemical Equilibrium Constants from Experimental Data. Version 4.0. Report 99-01, Chemistry Department, Oregon State University, Corvallis, OR.
- Hietanen, R., E. -L. Kamarainen, and M. Aluusua. 1984. Sorption of Cesium, Strontium, Iodine, Nickel and Carbon in Concrete. Nuclear Waste Commission of Finnish Power Companies, Report YJT 84-04, Helsinki, Finland.
- Hoeffner, S. L. 1985. Radionuclide Sorption on Savannah River Plant Burial Ground Soil A Summary and Interpretation of Laboratory Data. DP-1702. E.I. DuPont de Nemours & Co. Savannah River Laboratory, Aiken, SC.
- Hoglund, S., L. Eliasson, B. Allard, K. Andersson, and B. Torstenfelt. 1985. Sorption of some Fission Products and Actinides in Concrete Systems. *Mat. Res. Soc. Symp. Proc.* 50:683-690.
- Jenne, E. A. (Ed.) 1998. *Metal Adsorption by Geomedia*. Academic Press, San Diego.
- Johnson, E. A., M. J. Rudin, S. M. Steinberg, and W. H. Johnson. 2000. The Sorption of Selenite on Various Cement Formulations. *Waste Management*. 20:509-516.
- Johnson, W. H. 1995. Sorption Models for U, Cs, and Cd on Upper Atlantic Coastal Plain Soils. A Thesis Presented to the Academic Faculty at Georgia Institute of Technology. Atlanta, GA.
- Kaplan, D. I. 2002. Influence of Surface Charge of an Fe-oxide and an organic Matter Dominated Soil on Iodide and Perchnetate Sorption. *Radiochim. Acta.* 91:173-178.
- Kaplan, D. I. 2005. Estimate of Gaseous  $^{14}\text{C}$  Carbon Concentrations Emanating from the Intermediate-Level Vault Disposal Facility. WSRC-TR-2005-00222, Westinghouse Savannah River Company, Aiken, SC.
- Kaplan, D. I. 2006a. Geochemical Data Package for Performance Assessment Calculations Related to the Savannah River Site. WSRC-TR-2006-00004, Rev. 0. Washington Savannah River Company, Aiken, SC.
- Kaplan, D. I. 2006b. Dispersion of Savannah River Site Sediments as a Function of pH: Implications for Colloid-Facilitated Contaminant Transport. WSRC-STI-2006-00196. Washington Savannah River Company, Aiken, SC.

- Kaplan, D. I. 2007. Geochemical Data Package for Performance Assessment Calculations Related to the Savannah River Site. WSRC-TR-2006-00004, Rev. 1. Washington Savannah River Company, Aiken, SC.
- Kaplan, D. I. 2009. Tc and Pu Distribution Coefficients,  $K_d$  Values, for the Saltstone Facility Performance Assessment. SRNL-TR-2009-00019. Washington Savannah River Company, Aiken, SC.
- Kaplan, D. I., P. M. Bertsch, and D. C. Adriano. 1995. Facilitated Transport of Contaminant Metals Through an Acidified Aquifer. *Ground Water* 33:708-717.
- Kaplan, D. I., P. M. Bertsch, DE., D.C. Adriano, and K. A. Orlandini. 1994. Actinide Association with Groundwater Colloids in a Coastal Plain Aquifer. *Radiochimica Acta* 66/67:181–187.
- Kaplan, D. I., and J. T. Coates. 2007. Partitioning of Dissolved Radionuclides to Concrete under Scenarios Appropriate for Tank Closure Performance Assessments. WSRC-TR-2007-00640, Rev. 0. Washington Savannah River Company, Aiken, SC 29808.
- Kaplan, D. I., and C. Coffey. 2002. Distribution Coefficients ( $K_d$  Values) for Waste Resins Generated from the K L Disassembly Basin Facilities. WSRC-TR-2002-00349. Washington Savannah River Company, Aiken, SC.
- Kaplan, D. I., Coates, J. M., Siegfried, M, Roberts, K., Serkiz, S. 2008a. Saltstone and Radionuclide Interactions: Technetium Sorption and Desorption, Saltstone Reduction Capacity, and Radionuclide Sorption ( $K_d$ ) Value. SRNS-STI-2008-00045. Savannah River National Laboratory, Aiken, SC.
- Kaplan, D. I., D. I. Demirkanli, L. Gumapas, B. A. Powell, R. A. Fjeld, F. J. Molz, and S. M. Serkiz. 2006a. 11-Year Field Study of Pu Migration from Pu III, IV, and VI Sources. *Environ. Sci. Technol.* 40(2): 443-448.
- Kaplan, D. I., M. Duff, B. A. Powell, and M. E. Denham. 2008. Plutonium Oxidation State Transformations After 11 Years in Vadose Zone Sediments. *NLS Science Highlights*. March 26, 2008 pp. 1 – 3. <http://www.nsls.bnl.gov/newsroom/science/2008/03-342.htm> .
- Kaplan, D. I., T. L. Gervais, and K. M. Krupka. 1998. Uranium(VI) sorption to Sediments Under High pH and Ionic Strength Conditions. *Radiochimica Acta.* 80:201-211.
- Kaplan, D. I., K. P. Grogan, R. A. Fjeld, and J. C. Seaman. 2008b. Distribution of Technetium Sorption Coefficients ( $K_d$  Values) in the SRS Subsurface Environment. WSRC-STI-2008-00698, Rev. 1. Washington Savannah River Company, Aiken, SC 29808.
- Kaplan, D. I., and T. Hang. 2003. Estimated Duration of the Subsurface Reducing Environment Produced by the Z-Area Saltstone Disposal Facility. WSRC-RP-2003-00362, Rev. 2, Westinghouse Savannah River Company, Aiken, SC.

- Kaplan, D. I., and G. Iversen. 1999. Mercury- $K_d$  Values of Sediment Collected from the Ford Building Seepage Basin. WSRC-TR-99-00357, Westinghouse Savannah River Company, Aiken, SC.
- Kaplan, D. I. and M. R. Millings. 2006. Early Guidance for Assigning Distribution Parameters to Geochemical Input Terms to Stochastic Transport Models. WSRC-STI-2006-00019. Washington Savannah River Company, Aiken, SC.
- Kaplan, D. I., B. A. Powell, D. I. Demirkanli, R. A. Fjeld, F. J. Molz, S. M. Serkiz, and J. T. Coates. 2004. Enhanced Plutonium Mobility During Long-Term Transport Through an Unsaturated Subsurface Environment. *Environ. Sci. Technol.* 38:5053–5058
- Kaplan, D. I., B. A. Powell, M. C. Duff, D. I. Demirkanli, M. Denham, R. A. Fjeld, and F. J. Molz. 2007. Influence of Sources on Plutonium Mobility and Oxidation State Transformation in Vadose Zone Sediments. *Environ. Sci. Technol.* 41: 7417–7423.
- Kaplan, D. I., B. A. Powell, R. A. Fjeld, L. Gumapas, and J. T. Coates. 2006b. Influence of pH on Plutonium Desorption and Oxidation State in Sediment. *Environ. Sci. Technol.* 40(19): 5937-5942.
- Kaplan, D. I., and J. L. Myers. 2001. Long-Term Dynamics of Lead Solubility in a Cementitious Groundwater Environment. WSRC-TR-2000-00416, Westinghouse Savannah River Company, Aiken, SC.
- Kaplan, D. I., Serkiz, S. M., and J. Allison. 2010. Europium Sorption to Sediments in the Presence of Natural Organic Matter. *Applied Geol.* 25:224-232.
- Kaplan, D. I., S. M. Serkiz, R. A. Fjeld, and J. T. Coates. 2001. Influence of pH and Oxidation State on Plutonium Mobility through an SRS Sediment. WSRC-TR-2001-00472, Rev. 0, Westinghouse Savannah River Company, Aiken, SC.
- Kaplan, D. I., and S. M. Serkiz. 2000.  $^{129}\text{I}$  Iodine Desorption from Resin, Activated Carbon, and Filtercake Waste Generated from the F- and H-Area Water Treatment Units. WSRC-TR-2000-00308. Westinghouse Savannah River Company. Aiken, SC.
- Kaplan, D. I., and S. M. Serkiz. 2004. Influence of Dissolved Organic Carbon and pH on Contaminant Sorption to Sediment. WSRC-RP-2004-00593, Westinghouse Savannah River Company, Aiken, SC.
- Kaplan, D. I. and S. M. Serkiz. 2006b. Influence of Dissolved Organic Carbon and pH on Iodide, Perrhenate, and Selenate Sorption to Sediment. WSRC-STI-2006-00037. Washington Savannah River Company, Aiken, SC.
- Kaplan, D. I., S. M. Serkiz, and N. C. Bell. 1999. I-129 Desorption from SRS Water Treatment Media From the Effluent Treatment Facility and the F-Area Groundwater Treatment Facility. WSRC-TR-99-00270. Westinghouse Savannah River Company, Aiken, SC.

- Kaplan, D. I., and R. J. Serne. 2000. Geochemical Data Package for the Hanford Immobilized Low-Activity Tank Waste Performance assessment (ILAW PA). PNNL-13037, Rev. 1, Pacific Northwest National Laboratory, Aiken, SC.
- Kaplan, D. I. and E. Wilhite. 2001. Discovery of New Plutonium Chemistry and its Potential Effect on LLW Disposal at SRS. WSRC-RP-2000-00980, Westinghouse Savannah River Company, Aiken, SC.
- Kato, S., and Y. Yanase. 1993. Distribution Coefficients of Radionuclides in Concrete Waste for Coastal Soil and Concrete Powder. JAERI-M 93-113. Japan Atomic Energy Research Institute, Ibaraki-ken, Japan.
- Kent, D. B., V. S. Tripathi, N. B. Ball, J. O. Leckie, and M. D. Siegel. 1988. Surface-Complexation Modeling of Radionuclide Adsorption in Subsurface Environments. NUREG/CR-4807 and SAND86-7175. U.S. Nuclear Regulatory Commission, Washington, DC.
- Kersting, A. B., D. W. Efurud, D. L. Finnegan, D. J. Rokop, D. K. Smith, and J. L. Thompson. 1999. Migration of Plutonium in Groundwater at the Nevada Test Site. *Nature*. 397:56–59.
- Knox, A. S., and D. I. Kaplan. 2003. Phosphate Mineral Source Evaluation and Zone-of-Influence Estimates for Sediment Contaminant amendments at the TNX Outfall Delta operable Unit. WSRC-TR-2003-00579. Westinghouse Savannah River Co., Aiken, SC.
- Kretzschmar, R., and T. Schafer. 2006. Metal Retention and Transport on Colloidal Particles in the Environment. *Elements*. 1:205–210.
- Krupka, K. M., and R. J. Serne. 1998. Effects on Radionuclide Concentrations by Cement/Ground-water Interactions in Support of Performance Assessment of Low-level Radioactive Waste Disposal Facilities. NUREG/CR-6377, PNNL-11408.
- Krupka, K. M., R. J. Serne, and D. I. Kaplan. 2004. Geochemical Data Package for the 2005 Hanford Integrated Disposal Facility Performance Assessment. PNNL-13037, Rev. 2, Pacific Northwest National Laboratory, Richland, WA.
- Ledin A., Karisson S., Düker A., Allard B. 1994. The Adsorption of Europium to Colloidal Iron Oxy-hydroxides and Quartz – The Impact of pH and an Aquatic Fulvic Acid. *Radiochim. Acta*, vol.66/67, 213-220.
- Lilley, M. S., B. A. Powell, and D. I. Kaplan. 2009. Iodine, Neptunium, Plutonium, and Technetium Sorption to Saltstone Under Oxidizing Conditions. SRNL-STI-2009-00636. Savannah River National Laboratory, Aiken, SC.

- Lukens, W. W., J. J. Bucher, D. K. Shuh, and N. M. Edelstein. 2005. Evolution of Technetium Speciation in Reducing Grout. *Environ. Sci. Technol.* 39:8064-8070.
- Macias, A., A. Kindness, and F. P. Glasser. 1997. Impact of Carbon Dioxide on the Immobilization Potential of Cemented Wastes: Chromium. *Cement & Concrete Research.* 27:25-225.
- McCarthy, J. F., and C. Degueldre. 1993. Sampling and Characterization of Colloids and Particles in Groundwater for Studying Their Role in Contaminant Transport. In: J. Buffle and J. P. van Leeuwen (eds.) pp. 247-315. *Environmental Particles*. Boca Raton, Lewis Publishers.
- McCarthy, J. F., and J. M. Zachara. 1989. Subsurface Transport of Contaminants. *Environ. Sci. Technol.* 23:497-502.
- McDowell-Boyer, L. A. D. Yu, J. R. Cook, D. C. Kocher, E. L. Wilhite, H. Holmes-Burns, and K. E. Young. 2000. Radiological Performance Assessment for the E-Area Low-Level Waste Facility, WSRC-RP-94-218, Rev. 1. Westinghouse Savannah River Company, Aiken, SC.
- McIntyre, P.F., and E. L. Wilhite. 1987. Effect of Organics on Radionuclide Mobility in the SRP Burial Ground. DPST-87-762. Savannah River Laboratory. Aiken, SC.
- Mendenhall, W. and T. Sincich. 2003. *A Second Course in Statistics: Regression Analysis*. Pearson Education, Inc. p. 634.
- Miller, T. J., B. A. Powell, and D. I. Kaplan. 2009. Neptunium IV and V Sorption to End-Member Subsurface Sediments of the Savannah River Site. SRNL-STI-2009-00634. Savannah River National Laboratory, Aiken, SC.
- MMES (Martin Marietta Energy Systems, Inc., EG&G Idaho, Inc., Westinghouse Hanford Company, and Westinghouse Savannah River Company). 1992. Radiological Performance Assessment for the Z-Area Saltstone Disposal Facility, WSRC-RP-92-1360, Westinghouse Savannah River Company, Aiken, South Carolina.
- Neiheisel, J. 1983. Prediction Parameters of Radionuclide Retention of Low-Level Radioactive Waste Sites. EPA 520/1-83-025. Office of Radiation Programs, U.S. Environmental Protection Agency, Washington DC.
- Oblath, S. B., J. A. Stone, and J. R. Wiley. 1983. Special Wasteform Lysimeter Program at the Savannah River Laboratory. Proceedings of the Fifth Annual Participant's Information Meeting, DOE Low-Level Waste Management Program, CONF-8308106, p. 441. EG&G Idaho, Inc., Idaho Falls, ID.
- Ochs, M., B. Lothenbach, and E. Giffault. 2002. Uptake of Oxo-anions by Cements through Solid-solution Formation: Experimental Evidence and Modeling. *Radiochim. Acta* 90:639-645.

- Parson, R. 1982. Surface Properties of Oxides. *J. Electroanal. Chem.* 118:2-18.
- Perdue, E.M. and Gjessing, E.T. 1990. Dahlem Workshop Reports: Organic Acids in Aquatic Ecosystems. Wiley & Sons, New York.
- Phifer, M. A., K. P. Crapse, M. Millings, and M. G. Serrato. 2009. Closure Plan for the E-Area Low-Level Waste Facility. SRNL-RP-2009-00075. Savannah River National Laboratory, Aiken, SC.
- Phifer, M., M. R. Millings, and G. P. Flach. 2006. E-Area and Z-Area Hydraulic and Diffusional Material Properties Summary. SRNL-EST-2006-00016. Washington Savannah River Company, Aiken, SC.
- Pilkington, N., and N. Stone. 1990. The Solubility and Sorption of Nickel and Niobium under High pH Conditions. UK Nirex Ltd., Report NSS/R186, Harwell, UK.
- Poinreau, I., B. Piriou, M. Fedoroff, M. G. Barthes, N. Marmier, and F. Fromage. 2001. Sorption Mechanisms of  $\text{Eu}^{3+}$  on CSH Phases of Hydrated Cement. *J. Colloid Interface Sci.* 236:252-259.
- Powell, B. A., M. C. Duff, D. I. Kaplan, R. A. Fjeld, D. B. Hunter, P. M. Bertsch, J. T. Coates, P. Eng, M. Newville, M. L. Rivers, S. M. Serkiz, S. R. Sutton, I. R. Triay, and D. T. Vaniman. 2006. Plutonium Oxidation and Subsequent Reduction by Mn(IV) Minerals in Yucca Mountain Tuff. *Environ Sci. Technol.* 40(11):3508-3514.
- Powell, B. A., R. A. Fjeld, D. I. Kaplan, J. T. Coates, and S. M. Serkiz. 2004. Kinetics of  $^{239}\text{Pu}(\text{V})\text{O}_2^+$  Reduction by Synthetic Magnetite ( $\text{Fe}_3\text{O}_4$ ). *Environ. Sci. Technol.* 38:6016-6024.
- Powell, B. A., R. A. Fjeld, D. I. Kaplan, J. T. Coates, and S. M. Serkiz. 2005.  $\text{Pu}(\text{V})\text{O}_2^+$  Adsorption and Reduction by Synthetic Hematite ( $\alpha\text{-Fe}_2\text{O}_3$ ) and Goethite ( $\alpha\text{-FeOOH}$ ). *Environ. Sci. Technol.* 39:2107-2114.
- Powell, B. A., R. A. Fjeld, J. T. Coates, D. I. Kaplan, and S. M. Serkiz. 2002. Plutonium Oxidation State Geochemistry in the SRS Subsurface Environment. WSRC-TR-2003-00035, Rev. 0, Westinghouse Savannah River Company, Aiken, SC.
- Prout, W. E. 1958. Adsorption of Radioactive Wastes by Savannah River Plant Soil. *Soil Sci.* 86:13-17.
- Rai, D. and R. W. Szelmezcza. 1990. Aqueous Behavior of Chromium in Coal Fly Ash. *Journal of Environ. Qual.* 19:378-82.
- Rai D., Moore D.A., Felmy A. R., Choppin G. R., and Moore R.C. 2001. Thermodynamics of the  $\text{PuO}_2^+ - \text{Na}^+ - \text{OH}^- - \text{C}^- - \text{ClO}^- - \text{H}_2\text{O}$  system: Use of  $\text{NpO}^{2+}$  Pitzer parameters for  $\text{PuO}_2^+$ . *Radiochim. Acta.* 89:491-498.

- Rai, D., B. M. Sass, D. A. Moore, 1987. Chromium(III) Hydrolysis Constants and Solubility of Chromium(III) Hydroxide. *Inorganic Chemistry* 26: 345-349.
- Ramsay, J. D. F. 1988. The Role of Colloids in the Release of Radionuclides from Nuclear Waste. *Radiochim. Acta* 44/45:165-170.
- Reardon, E. J. 1992. Problems and Approaches to the Prediction of the Chemical Composition in Cement/Water Systems. *Waste Management*. 12:221-231.
- Roberts, K. A. and D. I. Kaplan. 2008. Carbon-14 Geochemistry at Savannah River Site. SRNL-STI-2008-00445. Savannah River National Laboratory, Aiken, SC.
- Roberts, K. A., and D. I. Kaplan. 2009. Reduction Capacity of Saltstone and Saltstone Components. SRNL-STI-2009-00637. Rev.0, Savannah River National Laboratory, Aiken, SC.
- Ryan, J.P. 1983. Groundwater Monitoring in the Savannah River Plant Low Level Waste Burial Ground. DPST-83-209. Westinghouse Savannah River Company. Aiken, SC.
- Sarott, F. A., M. H. Bradbury, P. Pandolfo, and P. Spieler. 1992. Diffusion and Adsorption Studies on Hardened Cement Paste and the Effect of Carbonation on Diffusion Rates. *Cement Concr. Res.* 22:439-444.
- Schindler, P. W., and G. Sposito. 1991. Surface Complexation at (Hydro)oxide Surfaces. pp 115–145. In *Interactions at the Soil Colloid-Soil Solution Interface*. G. H. Bolt, M. F. DeBoodt, M. H. B. Hayes, and M. B. McBride (eds.). Kluwer Academic Press.
- Seaman, J.C., P. M. Bertsch, and L. Schwallie. 1999. In Situ Cr(VI) Reduction Within coarse-Textured, Oxide-Coated Soil and Aquifer Systems Using Fe(II) Solutions. *Environ. Sci. Technol.* 33: 938-944.
- Serkiz, S. M., 2000. Recommended Partition Coefficient (*K<sub>d</sub>*) Values for Nuclide Partitioning in the Presence of Cellulose Degradation Products. WSRC-TR-2000-00262. Westinghouse Savannah River Company, Aiken, SC.
- Serkiz, S. M., and W. H. Johnson. 1994. Uranium Geochemistry in Soil and Groundwater at the F and H Seepage Basins. EPD-SGS-94-307. Westinghouse Savannah River Company, Aiken, SC.
- Serkiz, S. M., and D. I. Kaplan. 2006. Modeling the Influence of Dissolved Organic Carbon and pH on Cation Sorption to SRS Sediments. WSRC-RP-2005-01597. Westinghouse Savannah River Company. Aiken, SC.
- Serkiz S. M., Knaub D., and Lee C. 1999. Phase II Nuclide Partition Laboratory Study Influence of Cellulose Degradation Products On the Transport of Nuclides from SRS Shallow Land

- Burial Facilities. WSRC-TR-99-00298. Westinghouse Savannah River Company. Aiken, SC.
- Serkiz S. M., Knaub D., and Uhal H. 1998. Phase I Nuclide Partition Laboratory Study Influence of Cellulose Degradation Products On the Transport of Nuclides from SRS Shallow Land Burial Facilities. WSRC-TC-98-00460. Westinghouse Savannah River Company, Aiken, SC.
- Serkiz S. M. and Myers J.L. 1996. Additional Information for E-area Vault Performance Assessment, Appendix I "Suspect Soil Performance Analysis" – Results of Modeling the Effects of Organic Matter on the Mobility of Radionuclides as it Relates to the Disposal of Wood Products in E-Area Slit Trenches. WSRC-TR-98-00049. Westinghouse Savannah River Company. Aiken, SC.
- Serne, R.J., Conca, J.L., LeGore, V.L., Cantrell, K.J., Lindenmeier, C.W., Campbell, J.A., Amonette, J.E. and Wood, M.I. 1993. Solid-Waste Leach Characteristics and Contaminant-Sediment Interactions, Volume 1: Batch Leach and Adsorption Tests and Sediment Characterization. PNL-8889 Vol. 1. PNNL, Richland, WA.
- Sheppard, J. C., M. J. Campbell, J. A. Kittrick, and T. L. Hardt. 1979. Retention of Neptunium, Americium, and Curium, by Diffusible Soil Particles. *Environ. Sci. Technol.* 13:680–684.
- Sposito, G. 1984. *The Surface Chemistry of Soils*. Oxford University Press, New York.
- Sposito, G. 1989. *The Chemistry of Soils*. Oxford University Press, New York.
- Smith, R. W., and J. C. Walton. 1993. The role of Oxygen Diffusion in the release of Technetium from Reducing Cementitious Waste Forms. *Mat. Res. Soc. Symp. Proc.* Vol. 294. Materials Research Society, Warrendale, PA.
- Stone, J. A., S. B. Oblath, R. H. Hawkins, M. W. Grant, S. L. Hoeffner, and C. M. King. 1985. Waste Migration Studies at the Savannah River Plant Burial Ground. DP-MS-85-86, Westinghouse Savannah River Company, Aiken, SC.
- Strom, R. N., and D. W. Kaback. 1992. SRP Baseline Hydrogeologic Investigation: Aquifer Characterization, Groundwater Geochemistry of the Savannah River Site and Vicinity. WSRC-RP-92-450. Westinghouse Savannah River Company, Aiken, SC.
- Stumm W. and Morgan, J.J. 1981. *Aquatic Chemistry*. Wiley & Sons, New York.
- Thibault, D. M., M. I. Sheppard, and P. A. Smith. 1990. A Critical Compilation 2<sup>nd</sup> Review of Default Soil Soil/Liquid Partition Coefficients,  $K_d$ , For Use in Environmental Assessment. AECL-10125. White Shell Nuclear Research Establishment, Pinawa, Manitoba, Canada.
- Thurman, E.M. (1985). *Organic Geochemistry of Natural Waters*. Kluwer Academic, Hingham, MA.

- Tits, J., A. Jakob, E. Wieland, and P. Spieler. 2003. Diffusion of Tritiated Water and  $^{22}\text{Na}^+$  Through Non-Degraded Hardened Cement Pastes. *J. Contam. Hydrol.* 61:45–61.
- Valocchi, A.J. 1984. Validity of Equilibrium Assumption for Modeling Sorbing Solute Transport Through Homogeneous Soils. *Water Resour. Res.* 21:808–820.
- Van der Lee, J., E. Ledoux, G. De Marsily, A. Vinsot, H. van de Weerd, A. Liejnse, B. Harmand, E. Rodier, M. Sardin, J. Dodds, A. Hernandez Nenetex. 1997. Development of a Model for Radionuclide Transport by Colloids in the Geosphere. EUR 17480, Office for Official Publications of the European Communities, Luxembourg.
- Wang, F., J. Chen, and W. Forsling. 1997. Modeling Sorption of Trace Metals on Natural Sediments by Surface Complexation Model. *Environ. Sci. Technol.* 31:448-453.
- Westall, J. C. 1986. Reactions at the Oxide-Solution Interface: Chemical and Electrostatic Models. In *Geochemical Processes at Mineral Surfaces*. ACS Symposium Series 323, pp. 54-78. American Chemical Society, Washington, DC.
- Westall, J. C. 1994. Modeling of the Association of Metal Ions with Heterogeneous Environmental Sorbents. In *XVIII International Symposium on the Scientific Basis for Nuclear Waste Management*, pp. 1-12. Materials Research Society, Warrendale, PA.
- Westall, J.C., and J. Hohl. 1980. A comparison of Electrostatic Models for the Oxide Solution Interface. *Adv. Colloid. Interface Sci.* 12:265–294.
- Wieland, E., and L. R. Van Loon. 2003. Cementitious Near-Field Sorption Data Base for Performance Assessment of an ILW Repository in Opalinus Clay. PSI Bericht 03-06, Paul Scherrer Institut, Villigen, Switzerland.
- Willett, I. R., and Bond, W. J. 1995. Sorption of manganese, uranium, and radium by highly weathered soils. *Journal of Environmental Quality*, 24: 834-845.
- Wong, K.V., S. Sengupta, D. Dasgupta, E. L. Daly, Jr., N. Nemerow, and H. P. Gerrish. 1993. Heavy Metal Migration in Soil-leachate Systems. *BioCycle*. 24:30-33.
- WSRC (Washington Savannah River Company) 2008. E-Area Low-Level Waste Facility DOE 435.1 Performance Assessment Volume 1. WSRC-STI-2007-00306, Rev.0. Washington Savannah River Company, Aiken, SC.

**9.0 APPENDIX A: ADDITIONAL INFORMATION REGARDING CELLULOSE -  
DEGRADATION-PRODUCT CORRECTION FACTORS FOR  $K_d$  VALUES**

### 9.1 Selected Data Sets from Kaplan and Serkiz (2004) “Influence of Dissolved Organic Carbon and pH on Contaminant Sorption to Sediment”

Kaplan, D. I. and S. M. Serkiz. 2004. Influence of Dissolved Organic Carbon and pH on Contaminant Sorption to Sediment. WSRC-RP-2004-00593, Rev. 0, Westinghouse Savannah River Company, Aiken, SC. ([www.osti.gov/servlets/purl/835584-N20mx9/native/](http://www.osti.gov/servlets/purl/835584-N20mx9/native/))

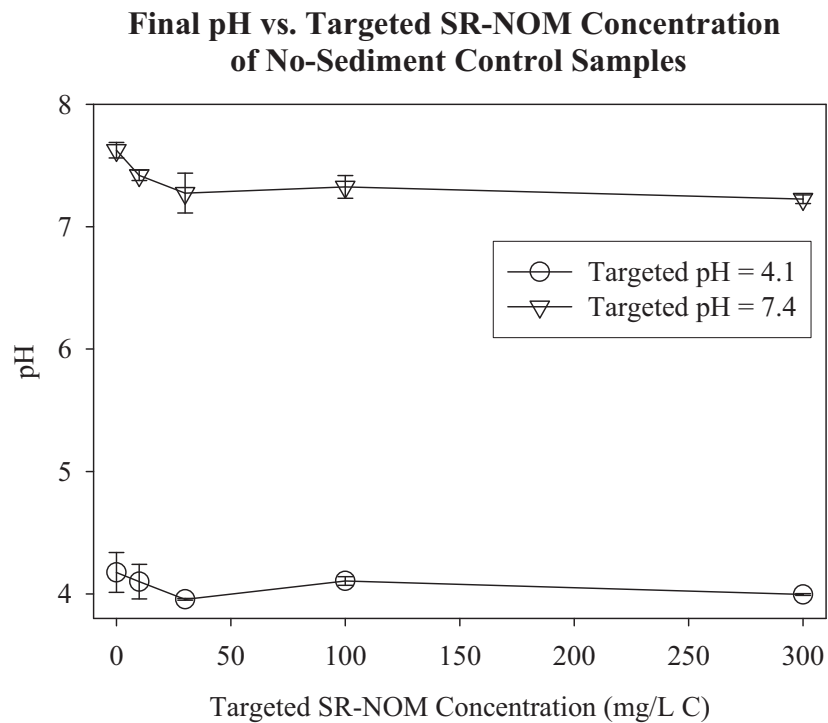


**Figure 24.** Final pH vs. targeted SR-NOM concentration of no-sediment control samples (2 observations for each mean and standard deviation).

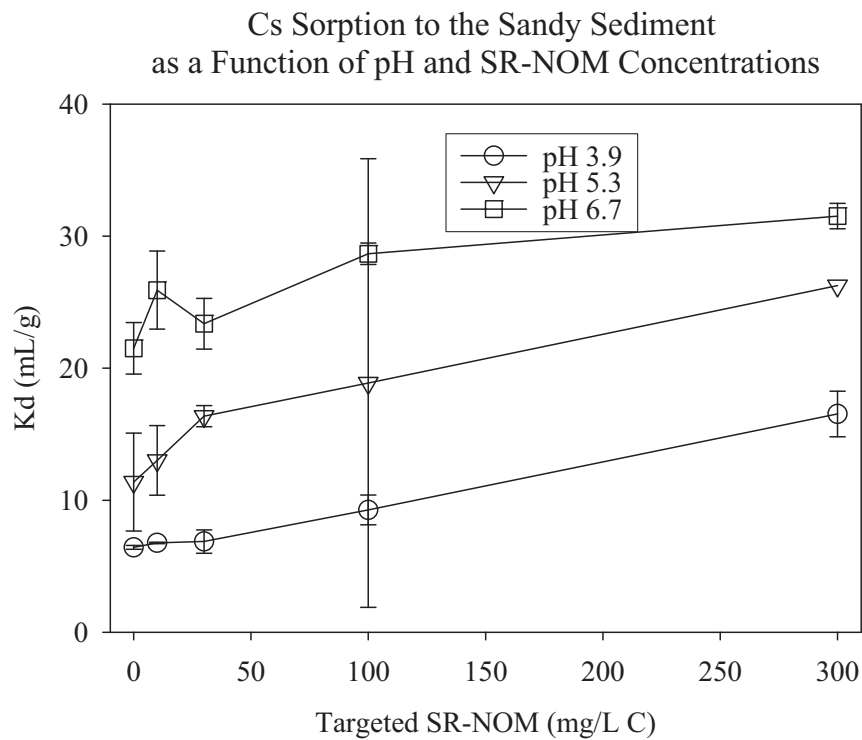
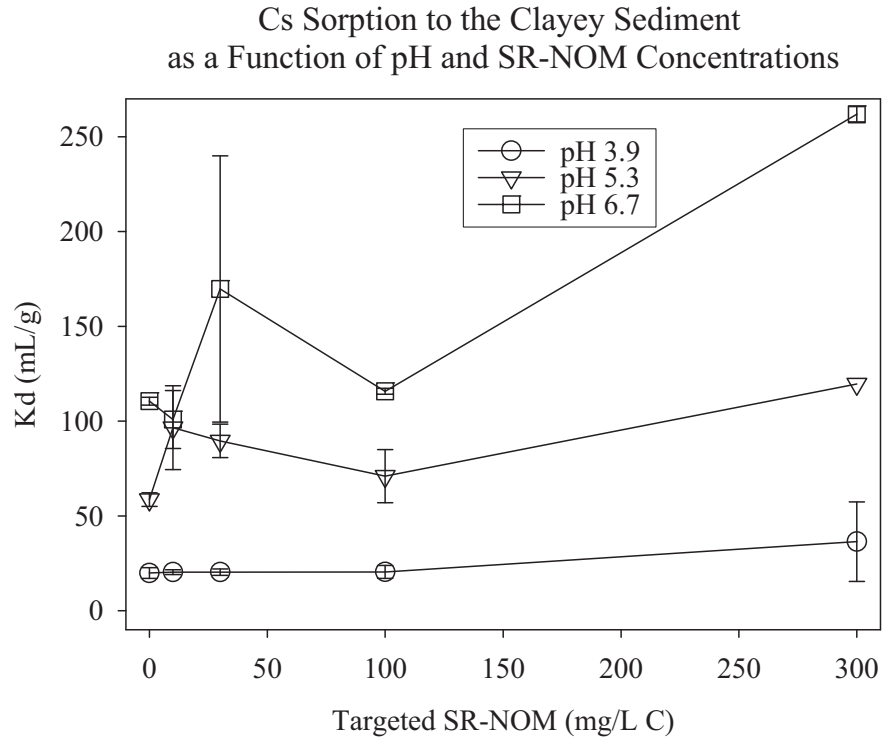


**Figure 25.** Cs  $K_d$  values as a function of pH and SR-NOM concentrations in clayey (top) and sandy (bottom) sediments.

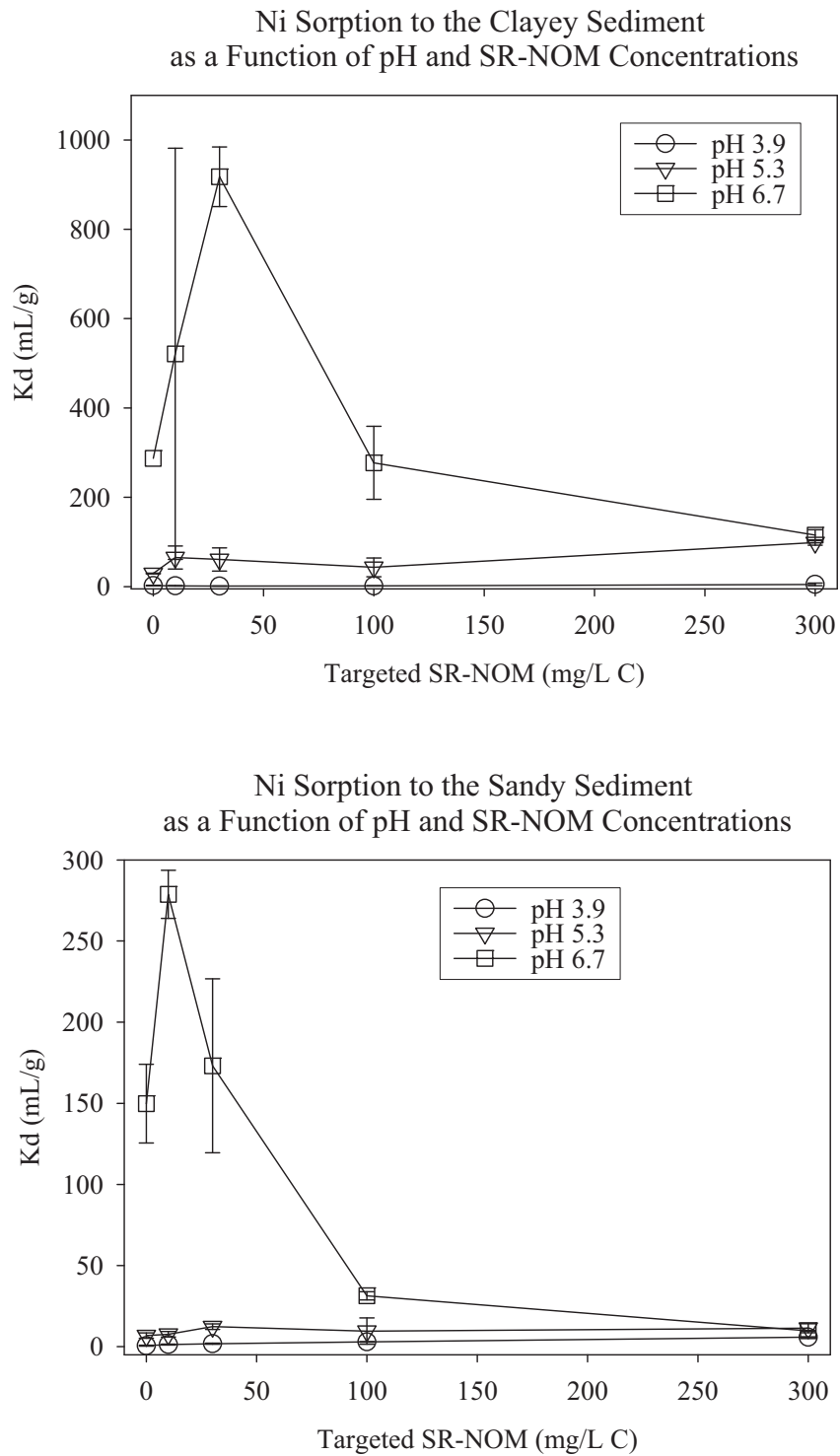


**Figure 26.** Ni  $K_d$  values as a function of pH and SR-NOM concentrations in clayey (top) and sandy (bottom) sediments.

**Table 24.** Ni *K $\alpha$*  Values (mL/g).

Target SR-NOM (mg/L C)	Clayey Sediment				Sandy Sediment							
	pH 3.9		pH 5.3		pH 6.7		pH 3.9		pH 5.3		pH 6.7	
	Avg.	Stdev.	Avg.	Stdev.	Avg.	Stdev.	Avg.	Stdev.	Avg.	Stdev.	Avg.	Stdev.
0	2.3	0.8	29.5	0.8	287.3	0.0	0.6	0.3	6.8	1.6	149.8	24.2
10	1.8	0.5	65.3	25.9	521.0	460.3	1.3	0.3	7.7	1.8	278.8	14.8
30	1.1	0.0	60.8	25.9	917.7	66.5	1.8	0.4	12.4	1.7	173.1	53.6
100	1.6	0.0	43.0	21.0	277.0	81.9	2.9	0.1	9.6	8.1	31.4	2.5
300	5.1	2.9	98.7	5.9	115.3	12.2	5.8	0.3	11.4	2.8	9.8	0.2
Avg.	2.4		59.4		423.7		2.5		9.6		128.6	
Stdev.	1.6		26.2		311.8		2.0		2.4		110.2	

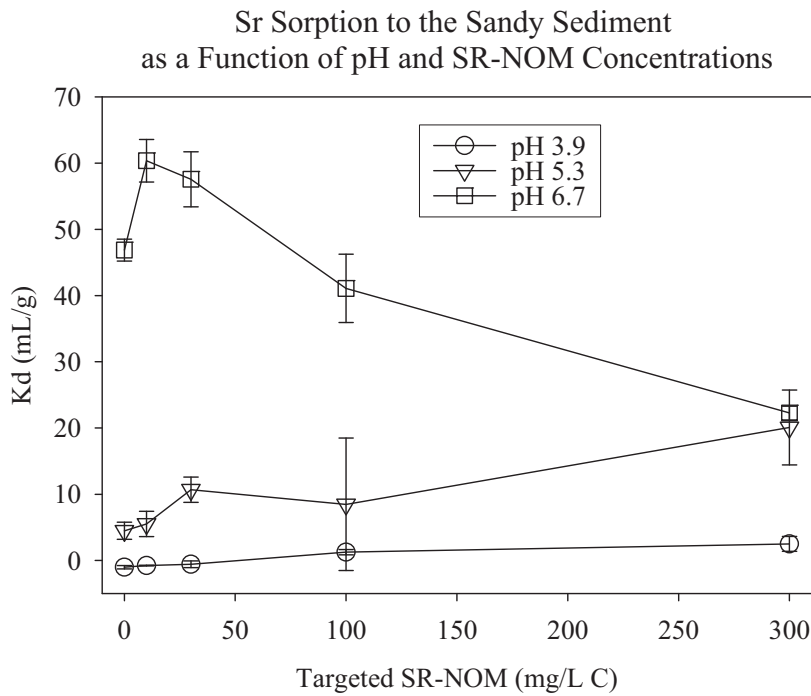
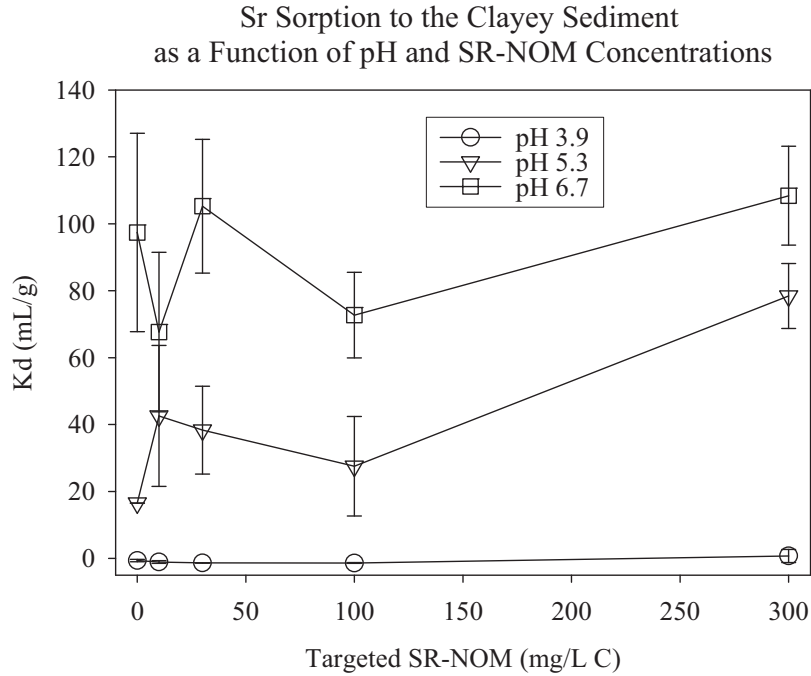


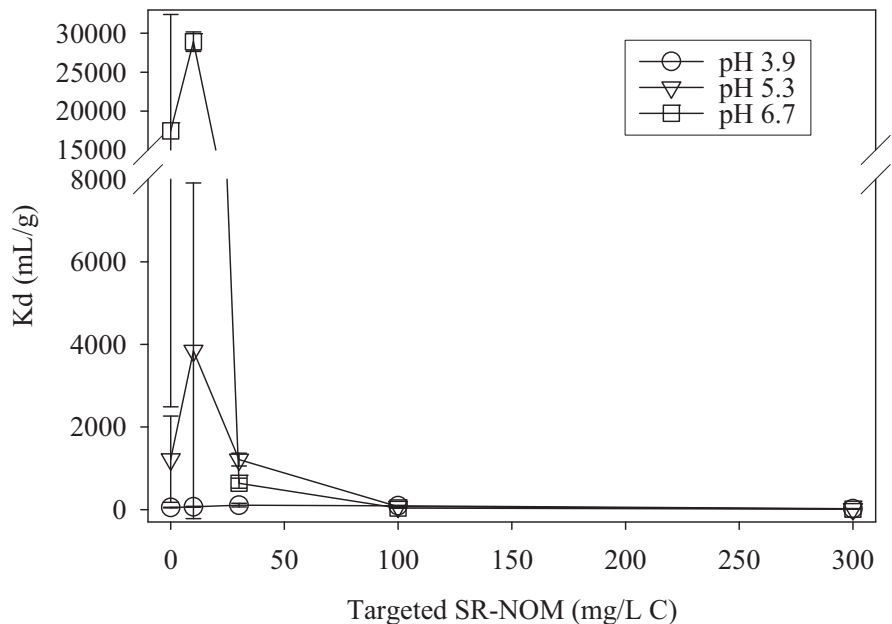
**Figure 27.** Sr  $K_d$  values as a function of pH and SR-NOM concentrations in clayey (top) and sandy (bottom) sediments.

**Table 25.** Sr *Kd* Values (mL/g).

Target SR- NOM (mg/L C)	Clayey Sediment						Sandy Sediment					
	pH 3.9		pH 5.3		pH 6.7		pH 3.9		pH 5.3		pH 6.7	
	Avg.	Stdev.	Avg.	Stdev.	Avg.	Stdev.	Avg.	Stdev.	Avg.	Stdev.	Avg.	Stdev.
0	-0.6 <sup>(a)</sup>	0.4	16.6	0.0	97.4	29.6	-1.0	0.3	4.5	1.3	46.9	1.7
10	-1.1	0.4	42.6	21.1	67.7	23.8	-0.8	0.0	5.5	1.9	60.4	3.2
30	-1.3	0.0	38.3	13.1	105.3	20.0	-0.6	0.5	10.7	1.9	57.6	4.2
100	-1.4	0.1	27.5	14.9	72.7	12.8	1.2	0.4	8.5	10.0	41.1	5.2
300	0.7	1.9	78.4	9.7	108.4	14.8	2.5	1.1	20.1	5.7	22.3	1.0
Avg	-0.7		40.7		90.3		0.3		9.8		45.6	
Stdev	0.9		23.4		18.9		1.5		6.2		15.2	

<sup>(a)</sup> Negative *Kd* values can be attributed to analytical error.

Ce Sorption to the Sandy Sediment  
as a Function of pH and SR-NOM Concentrations



Ce Sorption to the Sandy Sediment  
as a Function of pH and SR-NOM Concentrations

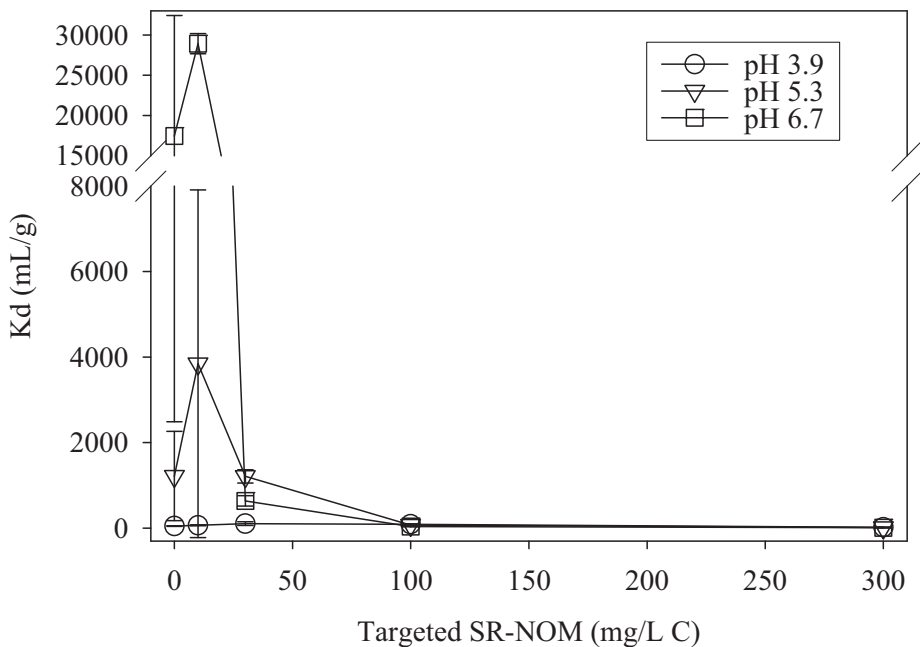


**Figure 28.** Ce  $K_d$  values as a function of pH and SR-NOM concentrations in clayey (top) and sandy (bottom) sediments (all  $K_d$  values >25,000 mL/g are greater-than values).

**Table 26.** Ce *Kd* Values (mL/g).

Target SR-NOM (mg/L C)	Clayey Sediment				Sandy Sediment							
	pH 3.9		pH 5.3		pH 6.7		pH 3.9		pH 5.3		pH 6.7	
	Avg.	Stdev.	Avg.	Stdev.	Avg.	Stdev.	Avg.	Stdev.	Avg.	Stdev.	Avg.	Stdev.
0	36	8	8687	4980	19343	9316	49	7	1220	1042	17450	14961
10	26	1	>28020	12	>29963	1934	68	12	3845	4067	>28918	1257
30	33	4	>22913	7242	>27481	1985	107	45	1210	157	638	122
100	40	4	4960	1690	7822	1694	92	9	69	22	37	3
300	71	27	361	180	105	14	21	4	14	3	10	0
Avg	41		12988		16943		67		1272		9411	
Stdev	18		11904		12777		34		1554		13213	

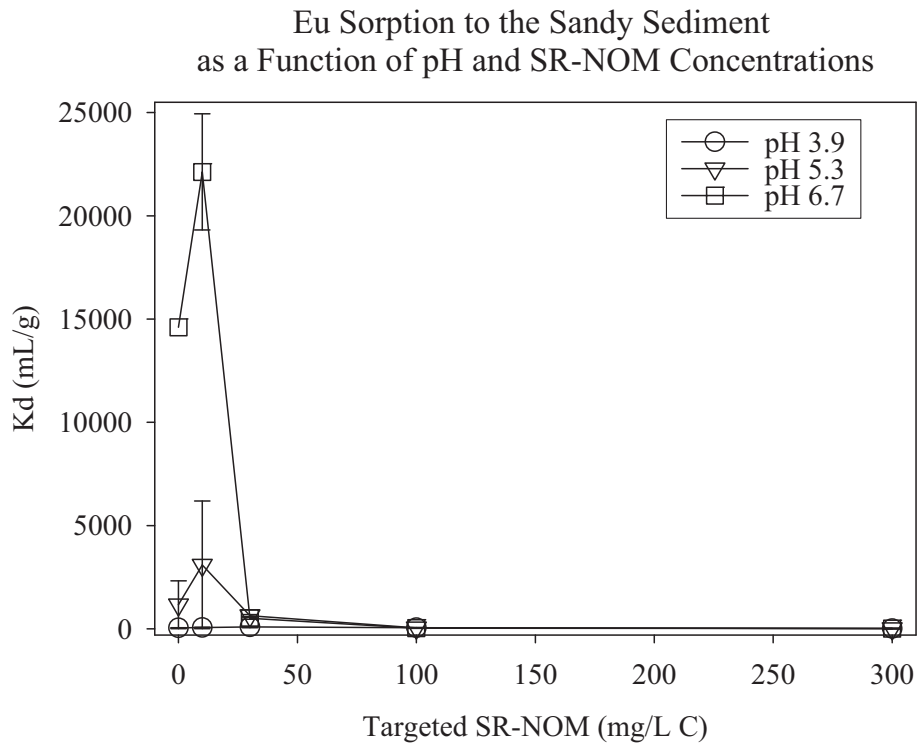
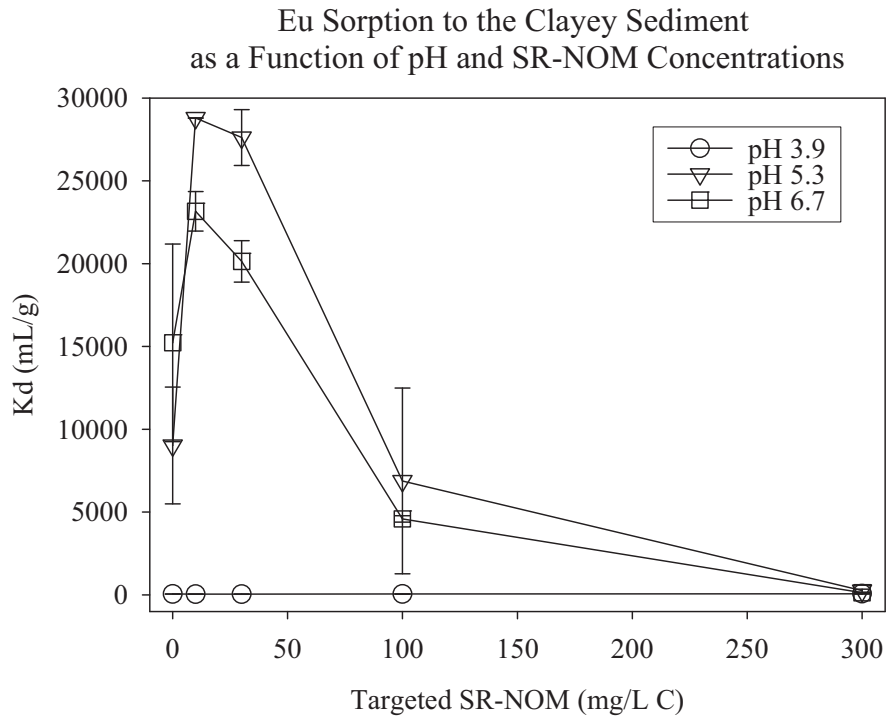


**Figure 29.** Eu  $K_d$  values as a function of pH and SR-NOM concentrations in clayey (top) and sandy (bottom) sediments (all  $K_d$  values >20,000 mL/g are greater-than values).

**Table 27.** Eu *Kd* Values (mL/g).

Target SR-NOM (mg/L C)	Clayey Sediment				Sandy Sediment							
	pH 3.9		pH 5.3		pH 6.7		pH 3.9		pH 5.3		pH 6.7	
	Avg.	Stdev.	Avg.	Stdev.	Avg.	Stdev.	Avg.	Stdev.	Avg.	Stdev.	Avg.	Stdev.
0	45	8	9020	3526	15218	5967	47	7	1168	1159	14602	20072
10	37	0	28787	12	23159	1194	65	11	3096	3094	22121	2812
30	40	4	27609	1686	20135	1252	97	38	641	52	516	53
100	47	4	6882	5606	4583	192	59	4	49	5	33	3
300	67	22	252	92	127	2	15	0	11	2	10	0
Avg	47.1		14510.0		12644.4		56.5		993.4		7456.5	
Stdev	11.6		12913.3		9936.8		29.6		1268.1		10305.9	

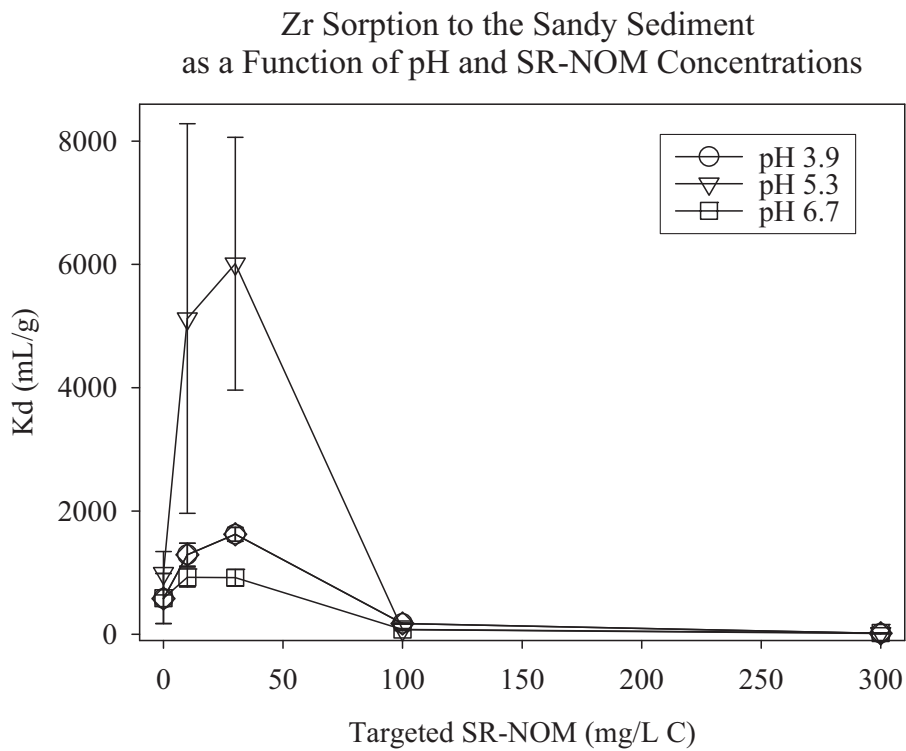
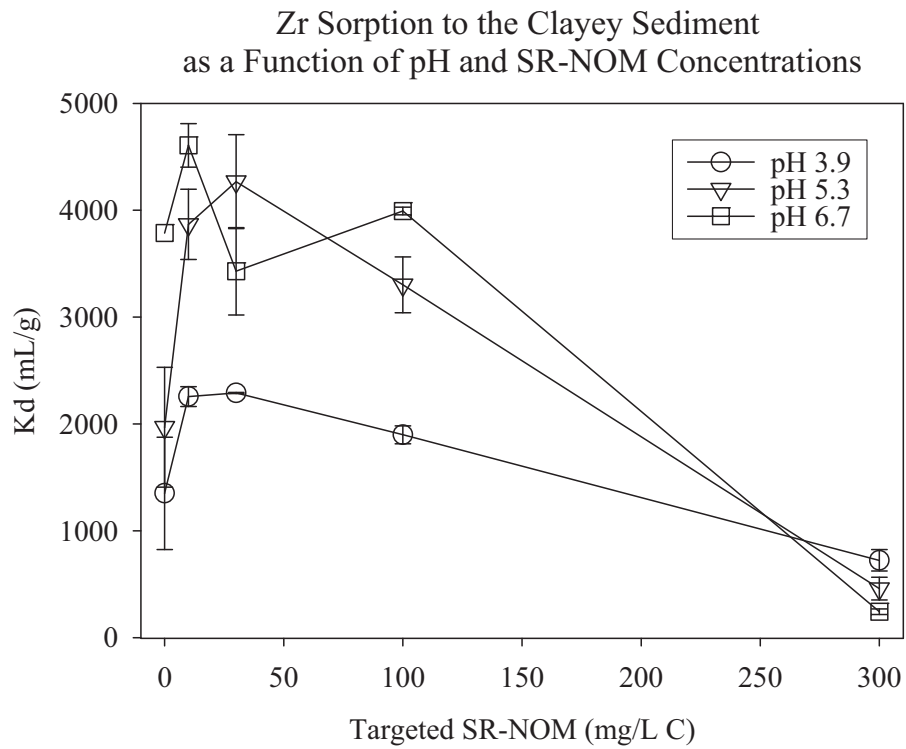


**Figure 30.** Zr  $K_d$  values as a function of pH and SR-NOM concentrations in clayey (top) and sandy (bottom) sediments.



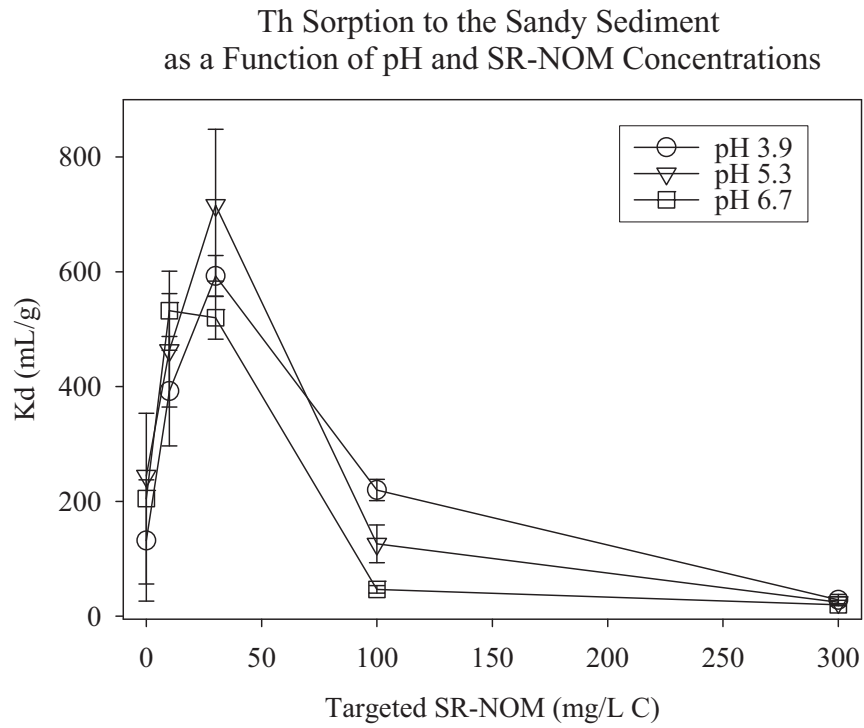
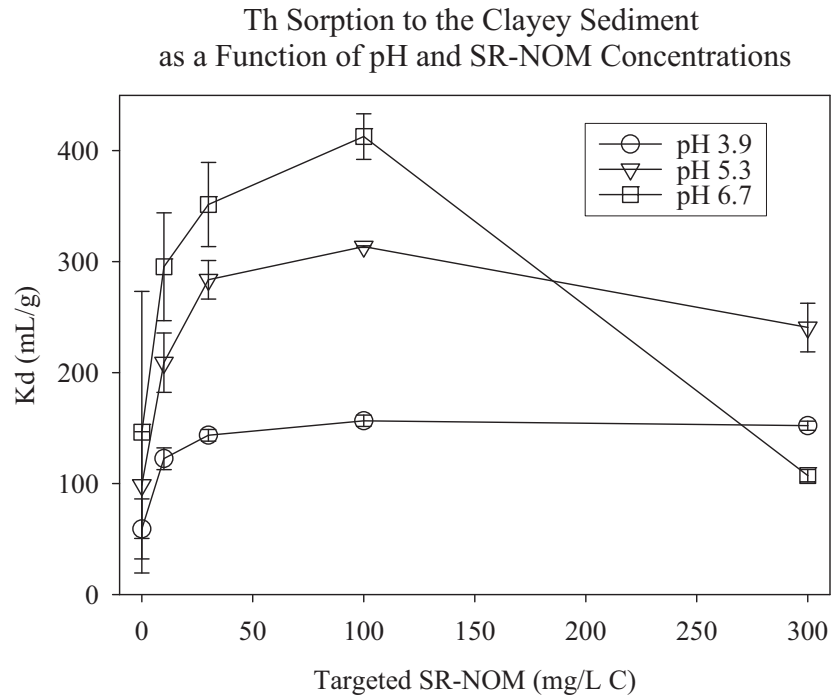


**Figure 31.** Th  $K_d$  values as a function of pH and SR-NOM concentrations in clayey (top) and sandy (bottom) sediments.

**Table 29.** Th *K<sub>d</sub>* Values (mL/g).

Target SR-NOM (mg/L C)	Clayey Sediment				Sandy Sediment							
	pH 3.9		pH 5.3		pH 6.7		pH 3.9		pH 5.3		pH 6.7	
	Avg.	Stdev.	Avg.	Stdev.	Avg.	Stdev.	Avg.	Stdev.	Avg.	Stdev.	Avg.	Stdev.
0	59	27	99	48	146	127	132	106	245	0	205	149
10	122	10	209	27	295	49	392	95	463	99	532	69
30	144	5	284	17	351	38	593	36	716	132	520	38
100	157	5	314	1	413	21	220	19	126	33	47	7
300	152	4	241	22	107	6	29	10	24	3	20	2
Avg	127		229		263		273		315		265	
Stdev	40		83		132		223		277		249	

**Table 30.** CDP Correction Factors Based on  $K_d$  Values Measured in the pH 3.9 or 5.3 Sandy Sediment System.

Val- ence	$0^{(a)}$ (mg/L C)	$K_d$ (mL/g)				CDP Correction Factors			
		10 (mg/L C)	20 (mg/L C)	95 (mg/L C)	222 <sup>(b)</sup> (mg/L C)	$K_d(10)/K_d(0)$	$K_d(20)/K_d(0)$	$K_d(95)/K_d(0)$	$K_d(222)/K_d(0)$
Cs	+1	11.4	13	18.9	17	1.14	1.14	1.66	1.49
Ni	+2	6.8	12.4	9.6	6	1.13	1.82	1.41	0.88
Sr	+2	4.5	10.7	8.5	2	1.22	2.38	1.89	0.44
Ce	+3	1220	3840	69	21	3.15	0.99	0.057	0.02
Eu	+3	1170	3100	49	15	2.65	0.55	0.042	0.01
Ce& Eu	+3					2.900 <sup>(c)</sup>	0.770	0.049	0.015
Th	+4	245	463	126	29	1.89	2.92	0.514	0.12
Zr	+4	990	5120	75	16	5.17	6.07	0.076	0.02

<sup>(a)</sup> DOC concentration represent those in the aqueous phase prior to coming into contact with sediment, i.e., the leachate DOC concentrations rather than the final concentrations after the system obtains steady state with the sediment.

<sup>(b)</sup> pH 3.9  $K_d$  data was used for the 222 mg/L C condition because elevated DOC levels commonly cause sediment pH to decrease. For example Johnson (1995) used the same sandy sediment as used in this study and observed that at 1 mg/L C from SR-NOM that the pH was 5.5; 30 mg/L C, the pH was 5.0, at 1000 mg/L C, the pH was 4.5.

<sup>(c)</sup> Ce & Eu average CDP Correction Factors.

**Table 31.** Cellulose-degradation-products Correction Factors,  $f_{CDP}$ , for  $Kd$  Values.

Radionuclides	10 mg/L C	20 mg/L C	95 mg/L C	222 mg/L C
Ac	2.9	0.77	0.049	0.015
Am	2.9	0.77	0.049	0.015
Cf	2.9	0.77	0.049	0.015
Cm	2.9	0.77	0.049	0.015
Cs	1.14	1.14	1.66	1.49
Eu	2.65	0.55	0.04	0.01
Ni	1.13	1.82	1.41	0.88
Np	1.14	1.14	1.66	1.49
Pa <sup>(a)</sup>	1.14	1.14	1.66	1.49
Pb	1.13	1.82	1.41	0.88
Pd	1.13	1.82	1.41	0.88
Po	1.13	1.82	1.41	0.88
Pu	1.89	2.92	0.51	0.12
Ra	1.22	2.38	1.89	0.44
Rb	1.14	1.14	1.66	1.49
Sn	1.13	1.82	1.41	0.88
Sr	1.22	2.38	1.89	0.44
Th	1.89	2.92	0.51	0.12
U	1.22	2.38	1.89	0.44
Zr	5.17	6.07	0.08	0.02

$F_{CDP}$  = defined in Equation 3 in this document; this table is taken from Serkiz and Kaplan (2006).  
<sup>(a)</sup> In Serkiz and Kaplan (2006), they assumed that Pa had an oxidation state of +4 ( $\text{Pa}^{+4}$ ), for this PA, it was assumed Pa had an oxidation state of +5 ( $\text{PaO}_2^+$ ). The values reported in this table are appropriate for Pa(V).

## **10.0 APPENDIX B: CEMENT LIFESPAN**

This discussion is based largely from results presented in Berner (1992). The total lifetime of the cement is somewhat arbitrarily defined by Berner (1992) as the cycle number where calcium-silicate-hydrate gel has dissolved completely. This is an arbitrary definition because this gel dissolves to form other solid phases, such as brucite [ $\text{Mg}(\text{OH})_2$ ], calcite ( $\text{CaCO}_3$ ), and gypsum ( $\text{CaSO}_4$ ) and silica ( $\text{SiO}_2$ ). However, the physical and chemical properties of the cement change appreciably after the calcium-silicate-hydrate gel has dissolved. Berner (1992) reported that between 5,000 and 10,000 exchange cycles were required to degrade completely the calcium-silicate-hydrate gel.

Perhaps the single most important porewater constituent influencing the “lifetime” of a cement is the concentration of carbonate in the groundwater (Berner 1992, Reardon 1992). For example, calculations conducted by Berner (1992) showed that a cement interacting with a high-carbonate (4.6 mM) infiltrating groundwater had a “lifetime” of 4480 cycles, whereas the same cement interacting with a low-carbonate (0 mM) infiltrating groundwater had a “lifetime” of 7450 cycles. The sediment pore water at SRS has a total inorganic carbon concentrations of about 0.2-mM (Strom and Kaback 1992). The reason SRS pore water is low in carbonate is that our surface soils contain little or no carbonate, the result of our soils being highly weathered and acidic.

The reason that groundwater carbonate concentrations are important is because the carbonate combines with the calcium released from the calcium-silicate-hydrate gel and forms calcite ( $\text{CaCO}_3$ ). The calcite acts as a sink, “sucking” calcium from the calcium-silicate-hydrate gel, thereby promoting the gel’s dissolution. Berner (1992) reported that nearly 83% of the total calcium-inventory could be reprecipitated during the 3<sup>rd</sup> Stage as calcite in the cement mixture (discussed below). This transformation to calcite approximately halved the calculated “lifetime” of the calcium-silicate-hydrate gel, compared to gel degradation in pure water, where no calcite was formed.

As an example, if we were to assume that the waste was held within 60-cm of the grout (as is the case for waste disposed as Components-in-Grout), the entire lifespan of the cement waste through a 50 cycle 1<sup>st</sup> Stage (Section 4.2.1), 500 cycle 2<sup>nd</sup> Stage (Section 4.2.2), and a 7000 cycle for the 3<sup>rd</sup> Stage (Section 4.2.3) would be 12,000 years, assuming an infiltration rate of 4-cm/yr for the first 750 years before the solid has started to physically degrade, and then 40-cm/yr thereafter.<sup>13</sup>

For example, a 2-ft thick layer of concrete buried at SRS may be expected to have a 750 yr 1<sup>st</sup> Stage, 750 yr 2<sup>nd</sup> Stage, and a 10,500 yr 3<sup>rd</sup> Stage, for a total life span of 12,000 yr.

<sup>13</sup> 1<sup>st</sup> Cycle: 50 cycles x 60-cm cement/cycle x 0.25 yr/cm = 750 yr

2<sup>nd</sup> Cycle : 500 cycles x 60-cm cement/cycle x 0.025 yr/cm = 750 yr

3<sup>rd</sup> Cycle : 7500 cycles x 60-cm cement/cycle x 0.025 yr/cm = 10500 yr.

These infiltration rates of 4- and 40-cm/yr were taken from the E-Area LLW PA (McDowell-Boyer et al. 2000). For the first 1050 yrs, the concrete is assumed to be physically intact. The greater infiltration rate was assumed to account for the concrete crumbling into particles that were about the same size as the surrounding sediment.

**11.0 APPENDIX C: INFLUENCE OF CEMENTITIOUS LEACHATE ON  
SEDIMENT BUFFERING CAPACITY**

## Influence of Cementitious Leachate on Sediment Buffering Capacity

### Input:

porosity of concrete = 0.18  
porosity of clayey sediment = 0.5  
pH of effluent is 12.8  
bulk density of sediment = 1.4 g/cm<sup>3</sup>

pH of effluent is 12.8 and there are 50 pore volumes in this stage.

pH + pOH = 14  
12.8 + pOH = 14  
pOH = 1.2  
[OH<sup>-</sup>] = 10<sup>-1.2</sup> = 0.063 mol/L = 63 mmol/L = meq<sub>(-)</sub>/L

50 pore volumes x 0.18 m<sup>3</sup>/P.V. = 9 m<sup>3</sup> pore water  
Total # meq<sub>(-)</sub> from concrete:

$$(9 \text{ m}^3 \text{ porewater}) \times (63 \text{ meq}_{(-)}/\text{L}) (1000\text{L}/1\text{m}^3) = 5.7\text{e}5 \text{ meq}_{(-)}/\text{m}^3 \text{ concrete} \quad [1]$$

Then using the titration data for the clayey sediment in Figure 32 and extrapolating to pH 12.8 with a linear line (using SigmaPlot to draw a line from pH 5.5 to 12.8), we get the slope:

$$149 \text{ pH}/\text{meq}_{(+)}/\text{g sediment} = 0.149 \text{ pH}/\text{meq}_{(+)}/\text{kg sediment} \quad [2]$$

which states that for every meq of positive charge per kg of sediment neutralized by OH<sup>-</sup>, we can expect the pH to go up by 0.149 pH units.

How many equivalents can 1 m<sup>3</sup> sediment buffer?

1 m<sup>3</sup> sediment contains 1400 kg sediment

Sediment buffering capacity is 0.0073 meq/g = 7.3 meq/kg buffering capacity, based on Figure 32 and the following pointed extrapolated from the figure (pH 4.53 & 0 meq/g) and (pH 12.5 & 0.058 meq/g)<sup>14</sup>.

$$1\text{-m}^3 \text{ sediment can buffer: } 1400 \text{ kg sed.} \times 7.3 \text{ meq}/\text{kg} = 10,222 \text{ meq OH in leachate} \quad [3]$$

1-m<sup>3</sup> concrete creates 0.18 m<sup>3</sup> water at pH 12.8 during Stage I. Total volume = 9 m<sup>3</sup> porewater.

$$\frac{5.7\text{e}5 \text{ meq eluted from concrete during Stage 1}}{10,220 \text{ meq OH} - /\text{m}^3} = 55.8 \text{ m}^3 \quad [4]$$

---

<sup>14</sup> (0.058-0)/(12.5-4.5) = 0.058/8 = 0.0073 meq/g

Thus, a 1 m<sup>3</sup> block of concrete sitting on the top of a clayey sediment would release enough OH<sup>-</sup> after 50 pore volumes to neutralize the buffering capacity of the sediment down to a depth of 55.8 m, i.e., it would neutralize 55.8 m<sup>3</sup> of sediment.

*Caveat:* This calculation does not include a water balance. It is simply an equivalence (OH<sup>-</sup>/H<sub>2</sub>O<sup>+</sup>) balance. In fact, because the porosity of cement is less than that of sediment, it is physically impossible for 50 pore volumes to neutralize 55.8 m<sup>3</sup> of sediment (porosity of concrete = 0.18 and the porosity of clayey sediment = 0.5, the void space in the sediment is almost 2.8 times greater than that of the concrete). This is not especially important because eventually, water would move the hydroxides down to the empty pore volumes. For this calculation, mass balance and not time is of interest.

**Conclusion:** Hydroxides from cementitious materials would likely overwhelm the buffering capacity of the SRS subsurface sediments, resulting in an increase in the aqueous phase ionic strength, dominated by hydroxides and Ca<sup>2+</sup>. In this calculation, a 1 m high cementitious slab altered the buffering capacity all the way down to the water table during the early stages of concrete aging (Stage I). Once this high pH front reached the aquifer it would likely be rapidly diluted, and would have negligible influence on radionuclide sorption.

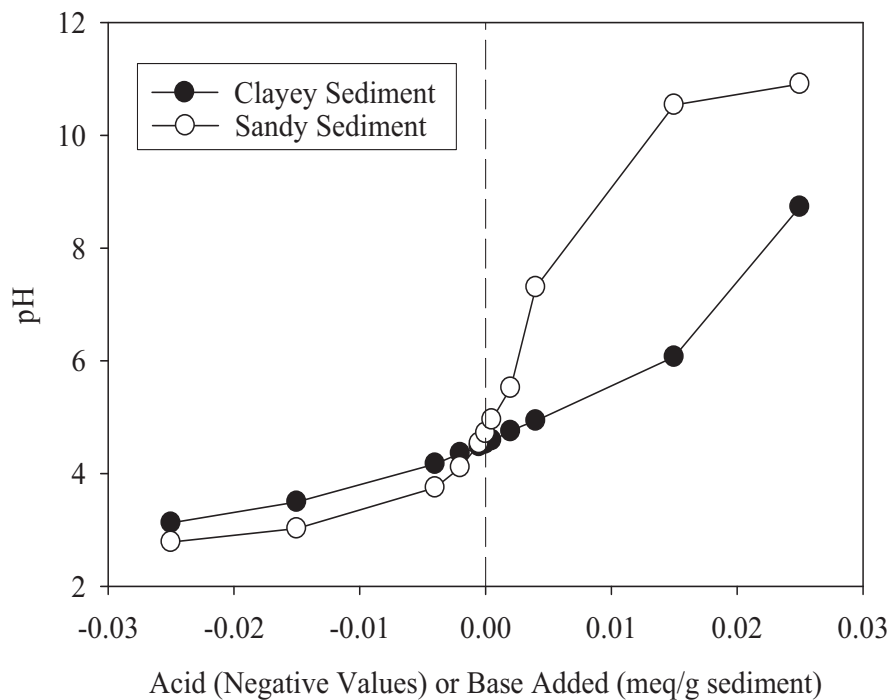


**Figure 32.** Titration of two sediments collected from the SRS subsurface environment (4-g soil: 25 mL aqueous; constant ionic strength = 0.01 M, 0.02 M NaCl, distilled water, and 0.005 M NaCl).

**12.0 APPENDIX D: ADDITIONAL INFORMATION REGARDING RANGE  
AND DISTRIBUTION OF  $K_d$  VALUES IN SRS SUBSURFACE  
SEDIMENTS**

## 12.1 Selected Data Sets from Grogan et al. (2008) “Distribution of Sorption Coefficients ( $K_d$ Values) in the SRS Subsurface Environment”

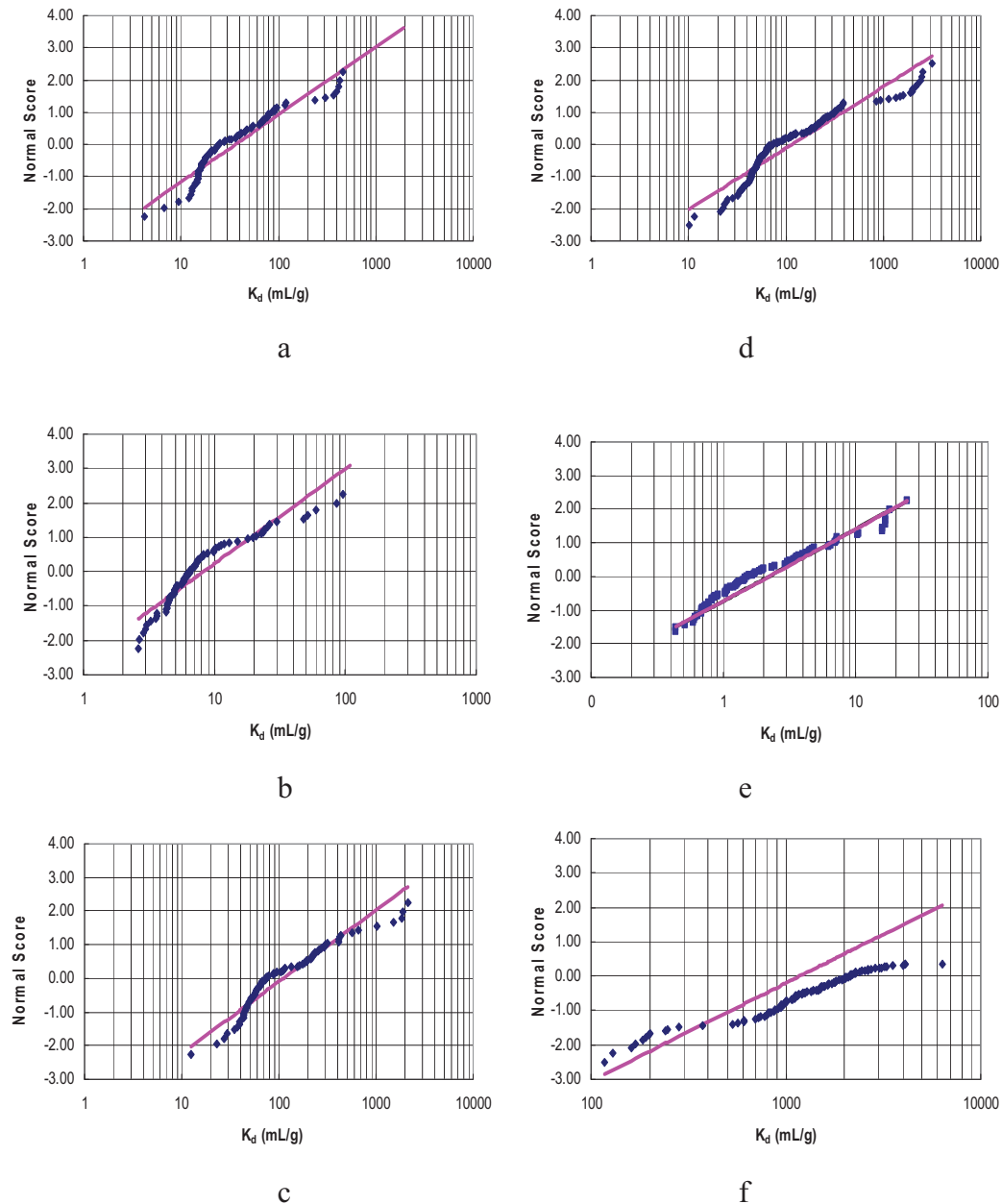


Figure 33. Log-normal fit of  $K_d$  values for a)  $^{109}\text{Cd}$ , b)  $^{137}\text{Cs}$ , c)  $^{57}\text{Co}$ , d)  $^{60}\text{Co}$ , e)  $^{85}\text{Sr}$ , and f)  $^{88}\text{Y}$  (Grogan et al. 2009).

*This data largely shows, with the exception perhaps of Y, that the 81  $K_d$  values (27 sediments x 3 replicates) followed a log-normal distribution. The Y data statistically did not adhere to either a normal or log normal distribution.*

**Table 32.** Summary Statistics of *Kd* Values (Grogan et al. 2008).

<b>Distributions of Isotope Median <i>Kd</i> Values</b>		<b>Co-57</b>	<b>Cd-109</b>	<b>Hg-203</b>	<b>Sr-85</b>	<b>Cs-137</b>	<b>Co-60</b>	<b>Average</b>
<b>Upper Vadose</b>								
Distribution	Normal	Normal	Normal	Not Normal	Normal	Not Normal	Not Normal	
Mean	159.7	37.4	22.7	1.49	11.26	10.76	40.6	
Lower 95%	68.9	18.6	9	0.5	4.14	4.11	17.5	
Upper 95%	250.4	56.2	33	2.47	18.38	17.41	63.5	
delta 95%	181.5	37.6	27.4	1.97	14.24	13.3	46.0	
<b>Lower Vadose</b>								
Distribution	Normal	Normal	Normal	Normal	Normal	Normal	Normal	
Mean	54.5	16.3	13.5	0.41	5.62	5.03	15.9	
Lower 95%	47.3	14.3	9.1	0.17	4.53	4.27	13.3	
Upper 95%	61.8	18.4	17.9	0.65	6.71	5.78	18.5	
delta 95%	14.5	4.1	8.8	0.48	2.18	1.51	5.3	
<b>Aquifer</b>								
Distribution	Not Normal	Not Normal	Normal	Normal	Normal	Not Normal	Not Normal	
Mean	457.1	131.3	20.9	6.97	21.2	20.4	109.6	
Lower 95%	-16.9	12.4	10.5	2.1	-0.3	-0.1	1.3	
Upper 95%	931.1	250.1	31.2	11.84	42.7	40.8	218.0	
delta 95%	948	237.7	20.7	9.74	43	40.9	216.7	

**Continuation of Table 33. Distribution Test Results and 95-Percentile Ranges for Tc Kd Values**

Distributions of Log(e) of Isotope Median Kd Values		Co-57	Cd-109	Hg-203	Sr-85	Cs-137	Co-60
<b>Upper Vadose</b>							
Distribution	Log-norm	Log-norm	Log-norm	Log-norm	Log-norm	Log-norm	Log-norm
<b>Lower Vadose</b>							
Distribution	Log-norm	Log-norm	Not log-n	Not log-n	Not log-n	Log-norm	Log-norm
<b>Aquifer</b>							
Distribution	Log-norm	Log-norm	Not log-n	Log-norm	Log-norm	Log-norm	Log-norm

**Conclusions**

- 1 Ranking of zone by variance: Aquifer >> Upper Vadose > Lower Vadose
- 2 95% range in Upper = 1X Mean; 95% range in Lower Vadose = 0.3X Mean; 95% range in Aquifer zone = 2X mean
- 3 Ranking of zone by Kd: Aquifer :: Upper Vadose > Lower Vadose
- 4 Ranking of isotopes by Kd: Co-57 >> Cd > Hg > Cs = Co-60 > Sr
- 5 Same Kd ranking for all three layers.

## 12.2 Distribution of Tc $K_d$ Values in an SRS Borehole

Kaplan, D. I., K. P. Grogan, R. A. Fjeld, J. C. Seaman. 2008b. Distribution of Technetium Sorption Coefficients ( $K_d$  Values) in the SRS Subsurface Environment. WSRC-STI-2008-00698, Rev. 1. Washington Savannah River Company, Aiken, SC 29808.

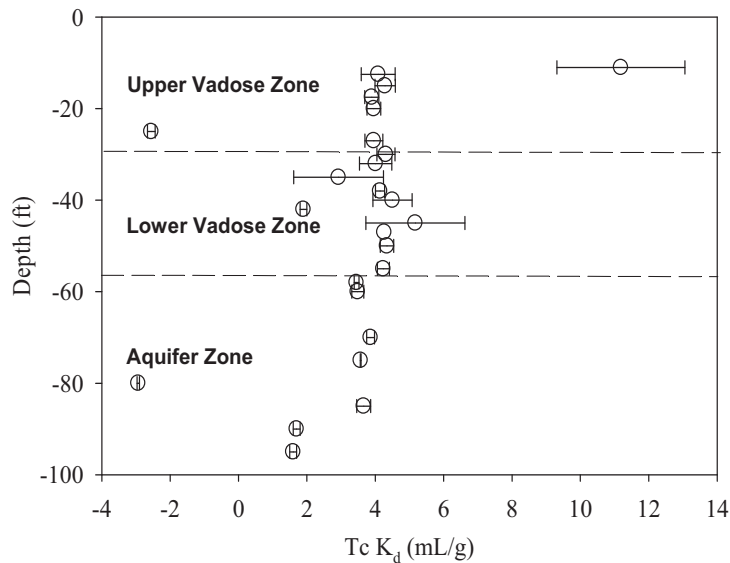


**Figure 34.** Average Tc  $K_d$  (mL/g) vs. depth below ground surface (0 ft) in Upper Vadose, Lower Vadose and Aquifer Zone.

*This Tc  $K_d$  data is statistically described below in Figure 35.*

**Figure 35.** Normal quantile plot, outlier box plot, and distribution functions for Tc *K<sub>d</sub>*s for the entire core, Upper Vadose Zone, Lower Vadose Zone, and Aquifer (Kaplan et al. 2008b).

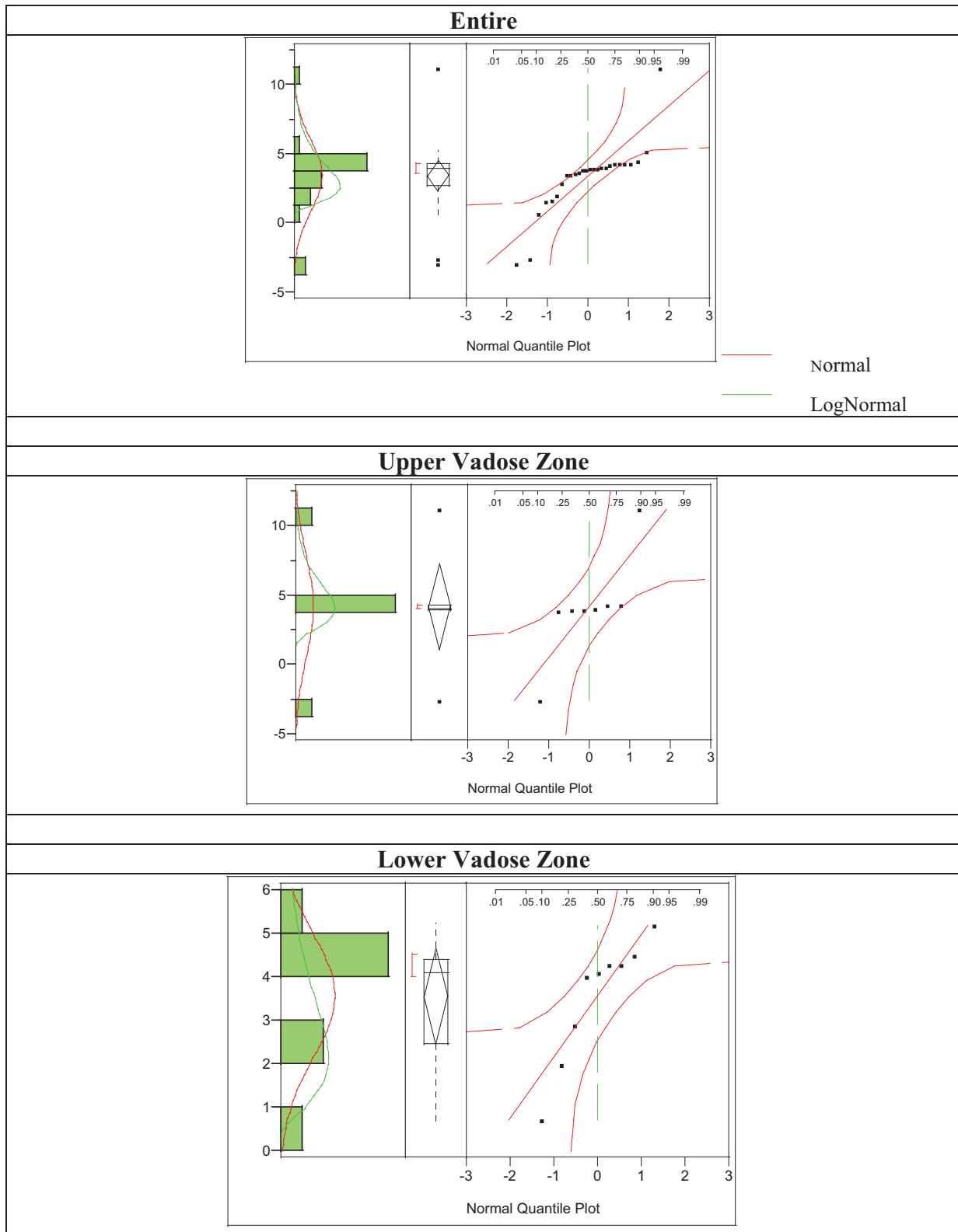


**Figure 35 (Continuation).** Normal Quantile Plot, Outlier Box Plot, and Distribution Functions for  $T_c K_d$  Values for the Entire Core, Upper Vadose Zone, Lower Vadose Zone, and Aquifer.

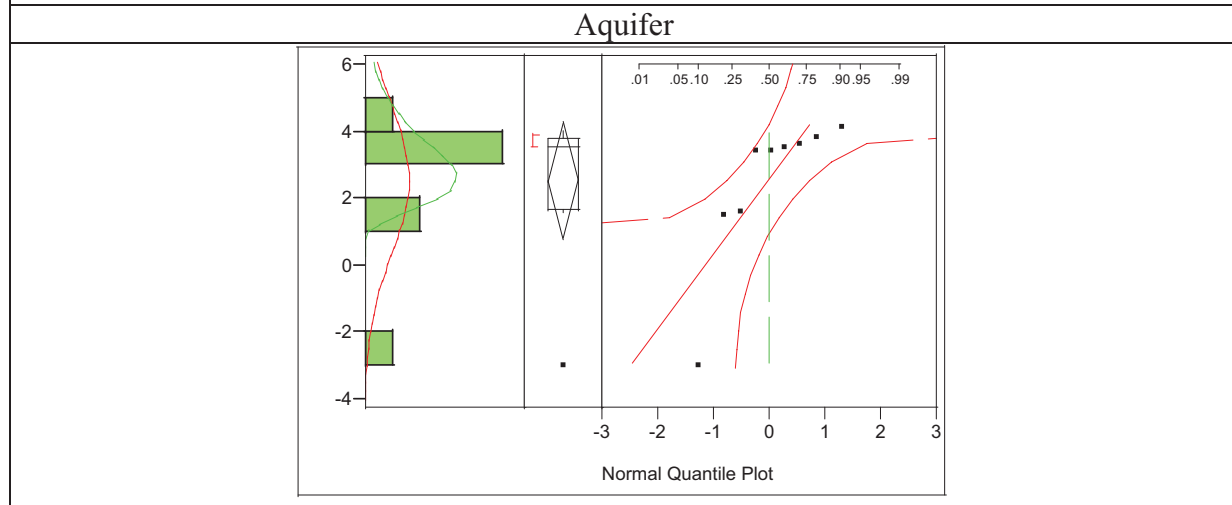


Table 33. Distribution Test Results and 95-Percentile Ranges for  $T_c K_d$  Values

Data Set	Kurtosis	Skewness	Shapiro-Wilk Value			Visual <sup>(b)</sup>	95-percentile	
			W-statistic	p-value	Conclusion		Lower	Upper
Entire	-0.01	4.55	0.73	<.0001	Not Normal	Normal	2.4	4.6
Upper Vadose Zone	0.19	3.49	0.77	0.015	Not Normal	Normal	1.1	7.2
Lower Vadose Zone	-1.20	0.79	0.83	0.040	Not Normal	Log-Normal	2.4	4.6
Aquifer Zone	-2.15	4.92	0.52	<.0001	Not Normal	Log-Normal	0.5	5.1

<sup>(a)</sup> The p-values are the probability that we can reject the null hypothesis stating that the data are from the normal distribution. Small p values indicate we must reject the null hypothesis. For example, a p-value of 0.015 indicates that the null hypothesis can be rejected at the 99.5% confidence level.

<sup>(b)</sup> Visual tests were conducted by simply looking at distributions presented in Figure 35.

### Distributions of $T_c K_d$ Values

The distribution functions of the entire  $T_c K_d$  data set, as well as subsets of the Upper Vadose, Lower Vadose and Aquifer Zones are presented in Figure 35. The data presented in Figure 34 were used to generate these distribution functions. To help understand the large amount of data presented in Figure 35, a more detailed discussion will be presented of the entire dataset (top plot in Figure 35) to provide an example of interpretation. On the left of each plot

included in Figure 35 is the distribution function, where the y-axis is the  $Kd$  value and the (unlabelled) x-axis is the number of observations. Drawn over the figures are fits to the normal distribution in red and log-normal distribution in green. In the case of the entire dataset, neither fitted line is a good fit; they both under estimate the number of observations in the central  $Kd$  grouping and the extreme  $Kd$  groupings. To the right of the distribution function, is a plot describing key statistical moments: the middle of the diamond identifies the mean and the horizontal lines identify the 25 and 75 percentiles. The dots outside the diamonds, identify Tc  $Kd$  values that are outliers, i.e.,  $>5$  standard deviations from the mean. For the entire dataset, three outliers are identified, 11.2 mL/g (11 ft depth), -2.6 mL/g (25 ft depth), and -2.9 mL/g (80 ft depth) (Figure 34). The normal quantile plot is presented on the right. There are 26 dots on this plot representing each Tc  $Kd$  value. The red straight line identifies where the data would lie if they were normally distributed and the red arching lines identify the 95% confidence limits from this red line. Comparing the position of the dots to the red line, it can be seen that the dots do not form a straight line: instead they appear to form two lines, suggesting two separate populations. The zone that these  $Kd$  values (dots) originate from can be extrapolated from the three other normal quantile lots for the Upper Vadose Zone, Lower Vadose Zone and Aquifer Zone. For example, several of the data points forming the horizontal cluster of points (i.e., those points between 0.25 and 0.90 percentiles), appear to originate in the Upper Vadose and the Aquifer Zones, whereas the data between the 0.25 to 0.05 percentiles (the data forming the sloping cluster of points) originate from the Lower Vadose and Aquifer Zones. Finally, the normal quantile plot for the entire data set shows the disproportional importance that the three extreme points have on fitting the dataset distribution. Dropping these three points results in a better fit to a log-normal distribution, but we believe the  $Kd$  values are real and hold important information about the true Tc  $Kd$  value distribution. As such, these values should be included in the statistical description.

The Upper Vadose Zone included eight  $Kd$  values and had a range of values that were almost identical to the range for the entire data set; Upper Vadose Zone – 13.8 mL/g, and for the entire dataset – 14.1 mL/g (Figure 35). The normal and log-normal fits to the distribution functions were poor. The reason for this can be readily seen in the normal quantile plot (plots furthest to the right in Figure 35) which shows the two extreme values and the remaining six values forming a line almost perpendicular to the red line identifying a normal distribution. Of the three subsurface zones, the Lower Vadose Zone showed the closest conformity to a normal or log-normal distribution, the former being slightly better than the latter. It also had the lowest range of values, from 0.7 to 5.2 mL/g. Finally, the normal and log-normal distributions could not be fitted to the Aquifer Zone  $Kd$  values. The normal quantile plot shows poor agreement between the ideal distribution and the actual measured  $Kd$  values in this zone.

A statistical test, the Shapiro-Wilk test, was conducted to test the null hypothesis that the data is from the Normal distribution (Table 33). The low probability values shown in Table 33 means that the null hypothesis should be rejected, meaning the distribution is not normal. The Tc  $Kd$  values were log-transformed (dropping the two negative values, for which there are no logarithmic values, from consideration) to test whether the dataset was log-normally distributed. Again, the Shapiro-Wilk statistic for these log transformed distributions indicated that they were not from the log transformed distribution (data not presented). It appears that the use of between 8 to 26  $Kd$  values does not provide enough power for this statistical test. However, it should be

noted that the Shapiro-Wilk test is sensitive to even small deviations from normality, thus limiting the value of this statistic test for this application (Mendenhall and Sincich, 2003).

The skewness and kurtosis (Table 33) are two terms that are used to describe a population's distribution. A positive kurtosis indicates a distribution curve with a longer tail than a normal distribution, whereas a negative kurtosis indicated a distribution curve that is flatter than normal. A kurtosis absolute value of  $>\pm 3$ , i.e.,  $>|3|$ , is considered significant. The kurtosis of the entire data set and the Upper Vadose Zone data set were 4.55 and 3.49 (Table 33), indicating that these two data set have longer tails than a normal distribution. The Lower Vadose Zone and Aquifer Zone had kurtosis values within the range of  $\pm 3$ . A skewness value  $>|3|$ , is considered significant and indicates that the data is not symmetrical. Furthermore, a negative skewness indicates tailing of the curve to the left, whereas a positive skewness indicates tailing of the curve to the right. The skewness values for all the data sets were small, the largest (absolute) skewness value was for the Aquifer Zone, -2.15, that had a tail towards the negative values (Table 33).

Given the limited number of values, between 8 and 26, and the highly sensitive nature of the statistical approach (Shapiro-Wilk test), it was decided to evaluate distributions based on visual inspection (Figure 35). This was done by visually inspecting the  $Kd$  distribution curves and then evaluate whether the data best fitted a log normal or normal distribution; particular attention was directed at the normal quantile plots in Figure 35. The entire dataset and the Upper Vadose Zone  $Kd$  values appeared to best fit normal distributions, whereas the Lower Vadose Zone and Aquifer Zone appeared to best fit log-normal distributions.

Also included in Table 33 is the 95 percentile range of each of the data sets. Most notable about this data is that it does not include a  $Kd$  value of 0 mL/g (or negative  $Kd$  values). Perhaps not apparent is why the entire dataset had a lower 95 percentile range than the Upper Vadose and Aquifer Zones. This occurred because the entire dataset tended to have more data centered on the mean and had more degrees of freedom than these two subsets of the data. The 95 percentile ranges for each dataset were (units of mL/g): - 2.2 for the entire dataset, 6.1 for the Upper Vadose Zone, 2.2 for the Lower Vadose Zone and 4.6 for the Aquifer Zone. The 95 percentile ranges for Tc  $Kd$  values can be expressed in terms of multiples of the mean (2.5 mL/g): Upper Vadose Zone - 3x mean, Lower Vadose Zone - 1x mean, and Aquifer Zone - 2x mean. Grogan et al. (2008) estimated that the range for  $\text{Am}^{3+}$ ,  $\text{Ca}^{2+}$ ,  $\text{Cs}^+$ ,  $\text{Ce}^{3+}$ ,  $\text{Co}^{2+}$ ,  $\text{Hg}^{2+}$ ,  $\text{Sr}^{2+}$ ,  $\text{Sn}^{2+}$ , and  $\text{Y}^{3+}$ , were: Upper Vadose Zone 1x mean, Lower Vadose Zone 0.5x mean, and Aquifer Zone - 2x mean. It is unexpected that Grogan et al (2008) values for metals are similar to those for the anion  $\text{TcO}_4^-$ , with the exception of the Upper Vadose Zone. Processes that control sorption of metals and anions are quite different and for this reason their range of  $Kd$  values were expected to differ.

**13.0 APPENDIX E: SPECTROSCOPIC EVIDENCE OF THE REDUCTION OF Tc(VII) TO Tc(IV) BY CEMENTITIOUS MATERIAL CONTAINING SRS SLAG**

### **Spectroscopic Evidence of the Reduction of Tc(VII) to Tc(IV) by Cementitious Material Containing SRS Slag**

$\text{Tc}^{\text{VII}}\text{O}_4^-$  gets reduced to  $\text{Tc}^{4+}$ , which like other tetravalent cations sorbs strongly to surfaces. Lukens et al. (2005) conducted fundamental studies using SRS slag and grout mixtures. In their study, they added Tc(VII) to a reducing grout and using X-ray Absorption Spectroscopy, specifically, XANES, they observed the slow transformation of Tc(VII) to  $\text{Tc}^{\text{VII}}\text{O}_2\text{-H}_2\text{O}$  to  $\text{Tc}^{\text{IV}}\text{S}_x$ . This process was monitored in the grout over a course of 45 months. The solubility of the  $\text{Tc}^{\text{IV}}\text{O}_2$  is low but that of  $\text{Tc}^{\text{IV}}\text{S}_x$  is extremely low,  $10^{-20}$  molar in alkaline systems (2.4e-8 pCi/L  $^{99}\text{Tc}$ ; ref = (2), *Table D.3-3*). The high  $Kd$  values selected for these conditions are to reflect the low solubility of Tc under these conditions.

Using identical analytical techniques, Bajt et al. (1993) demonstrated that an SRS slag-containing cementitious waste form contained reduced Cr(III), whereas the same cementitious material with out the slag contained the chrome in the higher hexavalent oxidation state, Cr(VI).

Bajt, S., S. B. Clark, S. R. Sutton, M. L. Rivers, and J. V. Smith. 1993. Synchrontron X-ray Microprobe Determination of Chromate Content Using X-ray Absorption Near-Edge Structure. *Canal. Chem.* 65: 1800-1804.

Lukens, W. W., J. J. Bucher, D. K. Shuh, and N. M. Edelstein. 2005. Evolution of Technetium Speciation in Reducing Grout. *Environ. Sci. Technol.* 39:8064-8070.

## Evolution of Technetium Speciation in Reducing Grout

WAYNE W. LUKENS,\* JEROME I. BUCHER,  
DAVID K. SHUH, AND  
NORMAN M. EDELSTEIN

Actinide Chemistry Group, Chemical Sciences Division,  
Lawrence Berkeley National Laboratory,  
Berkeley, California 94720

Cementitious waste forms (CWFs) are an important component of the strategy to stabilize nuclear waste resulting from plutonium production by the U. S. Department of Energy. Technetium ( $^{99}\text{Tc}$ ) is an abundant fission product of particular concern in CWFs because of the high solubility and mobility of Tc(VII), pertechnetate ( $\text{TcO}_4^-$ ), the stable form of technetium in aerobic environments. CWFs can more effectively stabilize  $^{99}\text{Tc}$  if they contain additives that chemically reduce mobile  $\text{TcO}_4^-$  to immobile Tc(IV) species. The  $^{99}\text{Tc}$  leach rate of reducing CWFs that contain Tc(IV) is much lower than that for CWFs that contain  $\text{TcO}_4^-$ . Previous X-ray absorption fine structure studies showed that Tc(IV) species were oxidized to  $\text{TcO}_4^-$  in reducing grout samples prepared on a laboratory scale. Whether the oxidizer was atmospheric  $\text{O}_2$  or  $\text{NO}_3^-$  in the waste simulant was not determined. In actual CWFs, rapid oxidation of Tc(IV) by  $\text{NO}_3^-$  would be of concern, whereas oxidation by atmospheric  $\text{O}_2$  would be of less concern due to the slow diffusion and reaction of  $\text{O}_2$  with the reducing CWF. To address this uncertainty, two series of reducing grouts were prepared using  $\text{TcO}_4^-$  containing waste simulants with and without  $\text{NO}_3^-$ . In the first series of samples, referred to as "permeable samples", the  $\text{TcO}_4^-$  was completely reduced using  $\text{Na}_2\text{S}$ , and the samples were sealed in cuvettes made of polystyrene, which has a relatively large  $\text{O}_2$  diffusion coefficient. In these samples, all of the technetium was initially present as a Tc(IV) sulfide compound,  $\text{TcS}_x$ , which was characterized by extended X-ray absorption fine structure (EXAFS) spectroscopy. The EXAFS data is consistent with a structure consisting of triangular clusters of Tc(IV) centers linked together through a combination of disulfide and sulfide bridges as in  $\text{MoS}_3$ . From the EXAFS model, the stoichiometry of  $\text{TcS}_x$  is  $\text{Tc}_3\text{S}_{10}$ , which is presumably the compound generally referred to as " $\text{Tc}_3\text{S}_7$ ". The  $\text{TcS}_x$  initially present in the permeable samples was steadily oxidized over 4 years. In the second series of samples, called "impermeable samples", the  $\text{TcO}_4^-$  was not initially completely reduced, and the grout samples were sealed in cuvettes made of poly(methyl methacrylate), which has a small  $\text{O}_2$  diffusion coefficient. In the impermeable samples, the remaining  $\text{TcO}_4^-$  continued to be reduced, presumably by blast furnace slag in the grout, as the samples aged. When the impermeable samples were opened and exposed to

atmosphere, the lower-valent technetium species were rapidly oxidized to  $\text{TcO}_4^-$ .

### Introduction

Remediation of the U. S. Department of Energy (DOE) sites used for plutonium production is one of the most expensive and complex remediation projects in the U. S. An important component of this effort is the use of grout-based cementitious waste forms (CWFs) at the Savannah River Site to solidify and stabilize the low-activity waste stream and to stabilize the waste residues in high-level tanks (1–4). The effectiveness of these measures to prevent the migration of radionuclides is described by performance assessments that depend on the leach rates of the radionuclides (1, 3, 5, 6).  $^{99}\text{Tc}$  is one of the radionuclides of greatest concern for leaching from CWFs because of the high mobility and lack of sorption of Tc(VII), pertechnetate ( $\text{TcO}_4^-$ ), the stable form of technetium under aerobic conditions (6,7).

For soluble contaminants such as  $\text{TcO}_4^-$  or  $\text{NO}_3^-$ , leach rates from CWFs can be modeled using an effective diffusion coefficient,  $D_{\text{eff}} = D_m/N_m$ , where  $D_m$  is the diffusion coefficient of the contaminant in water and  $N_m$  is the MacMullin number, a characteristic of a porous solid that is identical for solutes such as gases or anions that are highly soluble and not adsorbed by the matrix (8). The MacMullin number is generally defined as the tortuosity of the pore system divided by the porosity of the matrix. Since porosity and tortuosity are not available for most CWFs, the MacMullin number will be employed as an empirical parameter derived from  $D_{\text{eff}(\text{NO}_3^-)}$  in these systems. This definition for the effective diffusion coefficient assumes that the CWF behaves similarly to soil media and the distribution coefficient between the solute and the solid phase is negligible, which is true for  $\text{TcO}_4^-$ ,  $\text{NO}_3^-$ , and  $\text{O}_2$  but not for Tc(IV) as discussed below. Among CWFs similar to the one described here, the MacMullin numbers, derived from  $D_{\text{eff}(\text{NO}_3^-)}$ , are 11 800 (9), 3100 (9), 3100 (2), 2200 (3), 510 (3), and 300 (7).  $D_{\text{eff}(\text{NO}_3^-)}$  and  $D_{\text{eff}(\text{TcO}_4^-)}$  are similar because their molar diffusion coefficients are almost identical,  $1.53 \times 10^{-5}$  and  $1.48 \times 10^{-5} \text{ cm}^2 \text{ s}^{-1}$ , respectively (10, 11).

Tc leachability can be greatly decreased by reducing soluble  $\text{TcO}_4^-$  to Tc(IV) species by the addition of blast furnace slag (BFS) or other reductants to the grout. The  $D_{\text{eff}(\text{Tc})}$  values of reducing grouts are much smaller than those in ordinary CWFs because Tc(IV) has low solubility and is readily adsorbed by the grout matrix (7, 12). Reducing conditions are used in actual CWFs to create more effective waste forms (4, 12).

A previous research study showed that although  $\text{TcO}_4^-$  was reduced to Tc(IV) in reducing grouts; the degree of reduction varied with experimental conditions (13). Often,  $\text{TcO}_4^-$  was initially reduced to Tc(IV) but later oxidized. Two species,  $\text{NO}_3^-$  and  $\text{O}_2$ , are present in large quantities in or around CWFs and are potentially capable of oxidizing Tc(IV) to  $\text{TcO}_4^-$ . (The relevant reduction potentials are listed in Table 1.) Whether  $\text{NO}_3^-$  or  $\text{O}_2$  is responsible for oxidizing Tc(IV) has a profound effect on the behavior of technetium in CWFs. If  $\text{NO}_3^-$  is chiefly responsible for the oxidation, then Tc(IV) would be oxidized throughout the entire CWF, increasing the leachability of  $^{99}\text{Tc}$  throughout the entire volume of the waste. In this scenario, the rate of oxidation of Tc(IV) to  $\text{TcO}_4^-$  depends only on the reaction rate and the concentration of the reactants.

Oxidation by  $\text{O}_2$  is more complicated: Diffusion of  $\text{O}_2$  into the CWF forms an oxidized surface region with a greater

\* Corresponding author phone: (510)486-4305; fax: (510)486-5596; e-mail: wwlukens@lbl.gov.

**TABLE 1. Reduction Potentials at pH 14 for Selected Electrochemically Active Species in Reducing Grout (17, 14)**

reaction	potential (V)
$\text{SO}_4^{2-} + 2\text{e}^- + 2\text{H}^+ \rightarrow \text{SO}_2^{2-} + \text{H}_2\text{O}$	-0.93
$\text{S}_2\text{O}_8^{2-} + 4\text{e}^- + 6\text{H}^+ \rightarrow 2\text{S} + 3\text{H}_2\text{O}$	-0.77
$\text{SO}_3^{2-} + 4\text{e}^- + 6\text{H}^+ \rightarrow \text{S} + 3\text{H}_2\text{O}$	-0.66
$2\text{SO}_3^{2-} + 4\text{e}^- + 6\text{H}^+ \rightarrow \text{S}_2\text{O}_3^{2-} + 3\text{H}_2\text{O}$	-0.58
$\text{S} + 2\text{e}^- \rightarrow \text{S}^{2-}$	-0.51
$\text{TcO}_4^- + 3\text{e}^- + 4\text{H}^+ \rightarrow \text{TcO}_2 \cdot 2\text{H}_2\text{O}$	-0.36
$\text{NO}_3^- + 2\text{e}^- + 2\text{H}^+ \rightarrow \text{NO}_2^- + \text{H}_2\text{O}$	0.01
$\text{O}_2 + 4\text{e}^- + 4\text{H}^+ \rightarrow 2\text{H}_2\text{O}$	0.40

technetium leachability, similar to that of  $\text{NO}_3^-$  (15). However, the leachability of Tc in the bulk of the CWF remains unchanged. As shown by Smith and Walton, the thickness of the oxidized region depends on the rate of  $\text{O}_2$  diffusion and the reductive capacity of the CWF (15). Through the use of typical parameters for reducing CWFs, the thickness of the oxidized region is small compared to the dimensions of the CWF contemplated for use at the Savannah River at times comparable to the half-life of  $^{99}\text{Tc}$ , so oxidation by  $\text{O}_2$  is of less concern than oxidation by  $\text{NO}_3^-$ .

Therefore, the primary issue raised by the rapid oxidation of Tc(IV) observed in the previous study was the possibility that  $\text{NO}_3^-$  rather than  $\text{O}_2$  was responsible. In this paper, the evolution of  $^{99}\text{Tc}$  speciation in a series of grout samples in containers with very different  $\text{O}_2$  permeabilities and prepared with and without  $\text{NO}_3^-$  was followed over 4 years using X-ray absorption fine structure (XAFS) to determine whether  $\text{NO}_3^-$  or  $\text{O}_2$  was responsible for oxidizing Tc(IV) species in these grout samples.

### Experimental Section

**Procedures.** *Caution:*  $^{99}\text{Tc}$  is a  $\beta$ -emitter ( $E_{\text{max}} = 294 \text{ keV}$ ,  $\tau_{1/2} = 2 \times 10^5 \text{ years}$ ). All operations were carried out in a radiochemical laboratory equipped for handling this isotope. Tc, as  $\text{NH}_4^{99}\text{TcO}_4$ , was obtained from Oak Ridge National Laboratory and was purified as previously described (16). Where available, the standard deviation of measured and calculated values are included in parentheses following the value and are in the same units as the last digit.

All operations were carried out in air. Water was deionized, passed through an activated carbon cartridge to remove organic material, and then distilled. All other chemicals were used as received except for  $\text{Na}_2\text{S}_2\text{O}_3$ , which was dehydrated at  $120^\circ\text{C}$  for 12 h prior to use. The grout samples are similar to those previously used for the study of chromium reduction in reducing grout samples (17) and are similar to the CWF used to immobilize low-activity waste at the Savannah River Site, in that the waste simulant is similar in composition to the Savannah River high-level tank supernate, the dry grout

components are those used at the Savannah River, and the cement-to-water ratio is similar. The dry grout components consisted of 46% type F fly ash, 46% BFS, and 8% Portland cement (17). Two series of grout samples were prepared and are assumed to have a density of  $1.7 \text{ g cm}^{-3}$  (6). The cuvettes used to contain the samples were standard semi-microcuvettes with interior dimensions of  $1.0 \times 0.4 \times 4.5 \text{ cm}^3$ . To obtain XAFS spectra, the amount of Tc in the waste surrogates is approximately 300 times greater than that in actual waste. The increased Tc concentration has little effect on the grout chemistry, because Tc is a minor component of the grout.

**Attempted Reduction of Per technetate by Alkaline Thiosulfate.**  $\text{TcO}_4^-$  (0.01 mmol, 0.10 mL, 0.106 M  $\text{NaTcO}_4$ ) was added to  $\text{Na}_2\text{S}_2\text{O}_3$  (0.14 mmol, 1 mL, 0.14 M  $\text{Na}_2\text{S}_2\text{O}_3$  in 1.8 M NaOH). No reaction occurred upon mixing. After 14 days, the solution remained colorless.

**Preparation of Permeable Grout Samples.** Samples were prepared using waste simulants (17) with and without  $\text{NO}_3^-$  and  $\text{NO}_2^-$  as shown in Table 2. To the waste simulant was added  $\text{TcO}_4^-$  (0.02 mmol, 0.1 mL, 0.2 M  $\text{NaTcO}_4$ ), which was then reduced with  $\text{Na}_2\text{S}$  (0.29 mmol, 0.1 mL, 2.9 M) in 1 M LiOH, forming a very dark solution with a black precipitate. The dry grout components were added, forming a slurry that was placed in a polystyrene (PS) cuvette, which was capped and closed with vinyl tape. These samples will be referred to as "permeable samples" since  $\text{O}_2$  has a large diffusion coefficient of  $2.3 \times 10^{-7} \text{ cm}^2 \text{ s}^{-1}$  in PS (18, 19). The final composition of the waste solution after addition of the  $\text{TcO}_4^-$  and  $\text{Na}_2\text{S}$  solutions is listed in Table 2.

**Preparation of Impermeable Grout Samples.** The second series of samples was prepared analogously to the first, but the waste simulant was greatly simplified to distinguish the effect of  $\text{NO}_3^-$  upon Tc speciation. To the waste simulant were added  $\text{TcO}_4^-$  (0.012 mmol, 0.30 mL, 0.039 M  $\text{NaTcO}_4$ ) and 0.065 mL of same  $\text{Na}_2\text{S}$  solution as above, which had oxidized due to the diffusion of  $\text{O}_2$  through the polypropylene (PP) bottle containing the solution. (PP has a large  $\text{O}_2$  diffusion coefficient,  $1.6 \times 10^{-7} \text{ cm}^2 \text{ s}^{-1}$  (20).) The dry grout components were added, forming a slurry that was placed in a poly(methyl methacrylate) (PMMA) cuvette that was sealed with epoxy. These samples will be referred to as "impermeable samples" since  $\text{O}_2$  has a diffusion coefficient of  $2.3 \times 10^{-9} \text{ cm}^2 \text{ s}^{-1}$  in PMMA (21). The final composition of the waste solution after addition of the  $\text{TcO}_4^-$  and oxidized  $\text{Na}_2\text{S}$  solutions is given in Table 2. Samples A and C were opened after 26 months and placed in loosely capped jars that were fully opened weekly. Sample B remained sealed.

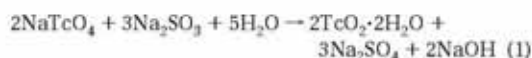
The oxidized  $\text{Na}_2\text{S}$  solution was analyzed for  $\text{S}^{2-}$ ,  $\text{SO}_3^{2-}$ , and  $\text{S}_2\text{O}_3^{2-}$  by iodometric titration (22) 6 years after the oxidized solution was used, and it was found to contain 1.44 M  $\text{S}_2\text{O}_3^{2-}$ , 0.03 M  $\text{SO}_3^{2-}$ , and no  $\text{S}^{2-}$ . When it was used, it must have contained more  $\text{SO}_3^{2-}$ , because  $\text{SO}_3^{2-}$  reduces  $\text{TcO}_4^-$  to

**TABLE 2. Composition of Cement Samples**

sample	Tc (mg)	solution (mL)	final solution composition	dry grout mixture (g)
<b>Permeable Samples</b>				
1	2	1.5	1.61 M $\text{NaNO}_2$ , 0.93 M NaOH, 0.49 M $\text{NaNO}_2$ , 0.14 M $\text{NaAl(OH)}_4$ , 0.14 M $\text{Na}_2\text{CO}_3$ , 0.12 M $\text{Na}_2\text{SO}_4$ , 0.02 M NaCl, 0.02 M $\text{Na}_2\text{C}_2\text{O}_4$ , 0.007 M $\text{Na}_3\text{PO}_4$ , 0.19 M $\text{Na}_2\text{S}$ , 0.066 M LiOH	3
2	2	1.5	as sample 1, but no $\text{NaNO}_2$ , $\text{NaNO}_2$	3
3	2	0.95	as sample 1, but 0.04 M $\text{Na}_2\text{PO}_4$	1.5
4	2	0.95	as sample 2, but 0.04 M $\text{Na}_2\text{PO}_4$	1.5
<b>Impermeable Samples</b>				
A	1.2	0.66	1.8 M NaOH, 1.8 M NaCl, 0.12 M $\text{Na}_2\text{S}_2\text{O}_3$ , 0.001 M $\text{Na}_2\text{SO}_3$ , 0.1 M LiOH*	1.0
B	1.2	0.66	1.8 M NaOH, 1.8 M $\text{NaNO}_3$ , 0.12 M $\text{Na}_2\text{S}_2\text{O}_3$ , 0.001 M $\text{Na}_2\text{SO}_3$ , 0.1 M LiOH*	1.0
C	1.2	0.66	1.8 M NaOH, 1.8 M $\text{NaNO}_2$ , 0.12 M $\text{Na}_2\text{S}_2\text{O}_3$ , 0.001 M $\text{Na}_2\text{SO}_3$ , 0.1 M LiOH*	1.0

\* The concentrations of  $\text{Na}_2\text{SO}_3$  and  $\text{Na}_2\text{S}_2\text{O}_3$  are inferred from the speciation of technetium.

$\text{TcO}_2 \cdot 2\text{H}_2\text{O}$  (23) and  $\text{S}_2\text{O}_3^{2-}$  does not react with  $\text{TcO}_4^-$  under these conditions (see above). The composition was estimated to be 0.1 M  $\text{NaSO}_3$  and 1.4 M  $\text{S}_2\text{O}_3^{2-}$  from the initial Tc speciation in the samples based on the assumption that  $\text{SO}_3^{2-}$  reacted quantitatively with  $\text{TcO}_4^-$ , as shown in eq 1. Reduction of  $\text{TcO}_4^-$  to  $\text{TcS}_2$  is assumed to react with BFS as previously observed (13). The PP bottle (6.9 cm high, 3.3 cm diameter, 0.1 cm thick) containing the  $\text{Na}_2\text{S}$  solution allowed the diffusion of 0.1 mmol  $\text{O}_2$  day $^{-1}$ . Given the initial amount of  $\text{Na}_2\text{S}$  (36 mmol), oxidation to  $\text{Na}_2\text{S}_2\text{O}_3$  would have occurred in 1 year, assuming that  $\text{O}_2$  diffusion was rate-limiting. Since the impermeable samples were prepared 15 months after the  $\text{Na}_2\text{S}$  solution was prepared, it is unlikely that the solution still contained  $\text{Na}_2\text{S}$ .



**Determination of the Reductive Capacity of BFS.** The reductive capacity of the BFS was determined using two techniques. In the first (24), the BFS (~0.5 g) was slurried in 5–10 mL of  $\text{H}_2\text{O}$  to which was added 25.0 mL of 0.059 M  $(\text{NH}_4)_2\text{Ce}(\text{SO}_4)_2 \cdot 2\text{H}_2\text{O}$  in 2 M  $\text{H}_2\text{SO}_4$ . After 1 h, the solution was titrated with freshly prepared 0.050 M  $(\text{NH}_4)_2\text{Fe}(\text{SO}_4)_2 \cdot 6\text{H}_2\text{O}$  in 0.75 M  $\text{H}_2\text{SO}_4$ . The end point was determined using 0.25 mL of 0.025 M Fe(II) tris-(1,10-phenanthroline) complex (25, 26). The reductive capacity of the BFS sample was 0.82(1) mequiv  $\text{g}^{-1}$  as determined from the difference in the volume of Fe(II) solution needed to titrate 25.0 mL of the Ce(IV) solution alone and with the BFS.

The reductive capacity of BFS was also estimated from its  $\text{S}^{2-}$  content, 0.57(1) wt %, determined using ASTM C144 section 15.2 (27). The reductive capacity of the  $\text{S}^{2-}$  depends on which species is formed upon oxidation. If  $\text{S}^{2-}$  is oxidized to  $\text{SO}_4^{2-}$ , then the reductive capacity is 1.42(2) mequiv  $\text{g}^{-1}$ , and if  $\text{S}^{2-}$  is oxidized to  $\text{S}_2\text{O}_3^{2-}$ , then the reductive capacity is 0.71(1) mequiv  $\text{g}^{-1}$ . Because the final oxidation state of the sulfur species formed during oxidation by Ce(IV) or  $\text{O}_2$  is unknown and because ASTM C144 is susceptible to loss of  $\text{H}_2\text{S}$ , the reductive capacity of 0.82(1) mequiv  $\text{g}^{-1}$  was used as the reductive potential of BFS.

Determination of the reductive capacity of BFS using Cr(VI) as the oxidizer has also been reported and gives much smaller values, which presumably reflect the reductive capacity of Fe(II) rather than  $\text{S}^{2-}$  in the BFS (6, 28).

**XAFS Spectroscopy.** XAFS spectra were acquired in fluorescence mode at the Stanford Synchrotron Radiation Laboratory (SSRL) at beamlines 4-1 and 11-2. Samples were oriented at 45° relative to both the photon beam and the fluorescence detector, and the photon beam probed the "side" (nonoptical face) of the cuvette rather than the "front" or optical face. Extended X-ray absorption fine structure (EXAFS) data analysis was performed by standard procedures (29) using the programs ifeffit (30) and Athena/Artemis (31); theoretical EXAFS phases and amplitudes were calculated using FEFF7 (32) as previously described (16); details are given in the Supporting Information.

## Results

**Initial Technetium Speciation.** A prerequisite for investigating the behavior of Tc in grout is identifying which species are present. While  $\text{TcO}_4^-$  obviously will be present under oxidizing conditions (33), the species present under reducing conditions are less obvious. The hydrous Tc(IV) oxide,  $\text{TcO}_2 \cdot 2\text{H}_2\text{O}$ , results from the reduction of  $\text{TcO}_4^-$  in the absence of other ligands both in solution and in grout samples (13, 23). In addition,  $\text{S}^{2-}$ , either CaS in BFS or added as  $\text{Na}_2\text{S}$ , reduces  $\text{TcO}_4^-$  to a lower-valent technetium sulfide species thought to be similar to  $\text{TcS}_2$  (13). Interestingly, the reaction of  $\text{S}^{2-}$  with  $\text{TcO}_4^-$  in alkaline solution produces  $\text{Tc}_2\text{S}_7$  (34), the Tc

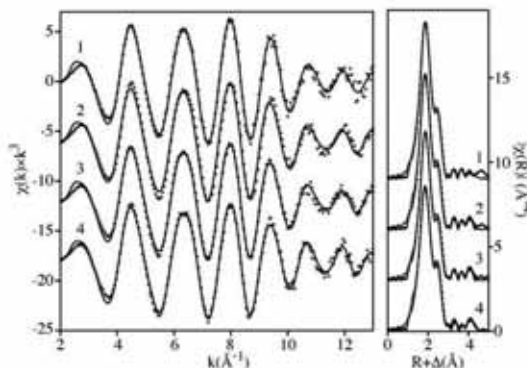


**FIGURE 1.** Tc K-edge EXAFS spectra (left panel) and their Fourier Transforms (right panel) of the technetium species initially present in grout samples prepared by reducing the  $\text{TcO}_4^-$  with excess sodium sulfide. Data are shown as dots, and fits are shown as lines. (Fit range:  $2 < k < 13.3 \text{ \AA}^{-1}$ ;  $1 < R < 4.5 \text{ \AA}$ ). Sample numbers are indicated next to the traces.

species generally thought to be present in reducing CWFs (15, 34). While these results seem contradictory, the inconsistency is due to the Tc(VII) oxidation state implied by the stoichiometry  $\text{Tc}_2\text{S}_7$ . If  $\text{Tc}_2\text{S}_7$  is actually a lower-valent disulfide complex, then no contradiction exists. Although  $\text{Tc}_2\text{S}_7$  is generally assumed to contain Tc(VII), this assumption has never been examined (11).

To identify the species present in reducing grouts, the Tc K-edge EXAFS spectra of the permeable samples were examined 1 week after they were prepared and are shown in Figure 1. The parameters derived by fitting the spectra are listed in Table 3. Only these samples contained a single Tc species, referred to as  $\text{TcS}_2$ . All other samples, including these samples examined 1 year later, contained multiple species.

The proposed structure of  $\text{TcS}_2$  can be described by considering the first two and last three coordination shells separately. The first two coordination shells consist of approximately seven S neighbors at 2.37 Å and two Tc neighbors at 2.77 Å, similar to  $\text{Mo}_3(\mu^3\text{-S})(\text{S}_2)_2^{2-}$ , shown in Figure 2, in which each Mo center has seven S and two Mo neighbors at 2.44 and 2.72 Å, respectively (35). The  $\text{Mo}_3(\mu^3\text{-S})(\mu\text{-S})_2$  core of this complex, without the apical  $\text{S}^{2-}$ , forms the building block of the proposed  $\text{MoS}_3$  structure (36), which has an EXAFS spectrum similar to that of  $\text{TcS}_2$  (37). In  $\text{MoS}_3$ , each Mo center has approximately six S neighbors at 2.44 Å and two Mo neighbors at 2.75 Å. These similarities strongly suggest that the  $\text{TcS}_2$  structure contains the same triangular core,  $\text{Tc}_3(\mu^3\text{-S})(\mu\text{-S})_2\text{S}_6$ , as shown in Figure 3. More importantly, the 2.77 Å Tc–Tc distance is typical of triangular complexes composed of seven-coordinate metal centers; analogous triangular complexes with six-coordinate metal centers have substantially shorter metal–metal distances (38).

The last three coordination shells give rise to the small features at higher  $R$  in the Fourier transform. The uncertainty in the assignments of these last shells is greater than that for the first two shells except for the S atoms at 4.5 Å, which must be present in the  $\text{Tc}_3(\mu^3\text{-S})(\text{S}_2)_2\text{S}_6$  core. In addition to the S neighbors, each Tc has an additional Tc neighbor at either 3.8 Å ( $\sim 1/3$  of the Tc centers) or 4.3 Å ( $\sim 2/3$  of the Tc centers). The different Tc–Tc distances suggest that different ligands bridge the Tc centers. Because the presence of seven first shell S neighbors requires that two S atoms bridge adjacent triangular clusters, possible identities of the bridging ligands are either two bridging  $\text{S}^{2-}$  (or  $\text{HS}^-$ ) ligands or an edge-bound  $\text{S}_2^{2-}$ .

TABLE 3. Initial Tc Coordination Environment in the Permeable Samples<sup>a</sup>

scattering atom		sample				all data <sup>c</sup>
		1 <sup>b</sup>	2	3	4	
S	$N^d$	7.3(5)	7.6(6)	7.0(5)	7.4(6)	7.4(2)
	$R$ (Å) <sup>e</sup>	2.379(5)	2.376(6)	2.381(5)	2.380(5)	2.378(2)
	$\sigma^2$ (Å <sup>2</sup> ) <sup>f</sup>	0.0111(7)	0.0118(9)	0.0113(7)	0.0121(8)	0.0117(3)
Tc	$N^d$	1.9(4)	1.8(5)	1.6(4)	1.7(4)	1.8(2)
	$R$ (Å) <sup>e</sup>	2.771(4)	2.771(5)	2.779(5)	2.776(5)	2.774(2)
	$\sigma^2$ (Å <sup>2</sup> ) <sup>f</sup>	0.007(1)	0.007(1)	0.007(1)	0.007(1)	0.0071(5)
Tc	$N^d$	0.3 <sup>g</sup>	0.4 <sup>g</sup>	0.3 <sup>g</sup>	0.3 <sup>g</sup>	0.4 <sup>g</sup>
	$R$ (Å) <sup>e</sup>	3.80(4)	3.83(3)	3.83(3)	3.86(3)	3.84(1)
	$\sigma^2$ (Å <sup>2</sup> ) <sup>f</sup>	0.007 <sup>g</sup>	0.005 <sup>g</sup>	0.004 <sup>g</sup>	0.004 <sup>g</sup>	0.006 <sup>g</sup>
Tc	$N^d$	0.7(2)	0.6(2)	0.7(2)	0.7(1)	0.6(1)
	$R$ (Å) <sup>e</sup>	4.30(3)	4.28(2)	4.29(2)	4.30(3)	4.30(1)
	$\sigma^2$ (Å <sup>2</sup> ) <sup>f</sup>	0.006(2)	0.005(2)	0.004(1)	0.004(2)	0.006(1)
S	$N^d$	11(11)	6(6)	6(6)	6(5)	5(2)
	$R$ (Å) <sup>e</sup>	4.48(3)	4.47(3)	4.48(3)	4.49(3)	4.47(1)
	$\sigma^2$ (Å <sup>2</sup> ) <sup>f</sup>	0.02(1)	0.02(1)	0.01(1)	0.01(1)	0.012(4)
$\Delta E_0^h$		0.4(7)	0.8(8)	0.6(7)	0.5(8)	0.7(3)
$R^i$		0.078	0.096	0.082	0.085	0.102

<sup>a</sup> The number in parentheses is the standard deviation of the parameter obtained by fitting the EXAFS data. In comparison to crystallographic data,  $N$  differs by up to 25%, and in  $R$  by 0.5%. <sup>b</sup> The best model for the EXAFS spectrum of sample 1 did not include the Tc shells at 3.82 and 4.31 Å, but this model is included for comparison with the other samples. <sup>c</sup> All data were fit simultaneously using a single set of parameters. <sup>d</sup>  $N$  is the number of neighboring atoms. <sup>e</sup>  $R$  is the distance from the scattering atom to the technetium center. <sup>f</sup>  $\sigma^2$  is the Debye-Waller parameter, the amount of disorder in the distance to the neighboring atoms. <sup>g</sup> Parameter determined from the corresponding parameter in the following shell. <sup>h</sup>  $\Delta E_0$  was identical for all shells;  $S_0$  was 0.9 in all cases. <sup>i</sup>  $R$  factor =  $(\sum(\gamma(\text{data}) - \gamma(\text{fit}))^2 / \sum(\gamma(\text{data}))^2)^{1/2}$ .

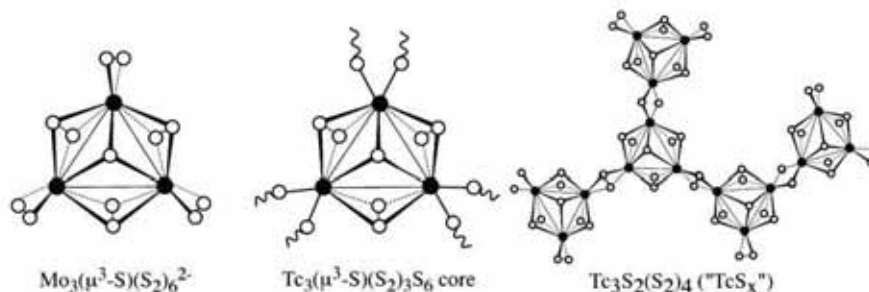


FIGURE 2. Structures of  $\text{Mo}_3(\mu^3\text{-S})(\text{S}_2)_6^{2-}$ , the  $\text{Tc}_3(\mu^3\text{-S})(\text{S}_2)_3\text{S}_6$  core that forms the building block of  $\text{TcS}_x$ , and a portion of proposed structure of  $\text{TcS}_x$ . Metal atoms are illustrated by solid circles; sulfur atoms are depicted by open circles.

The Tc–Tc distance of two Tc centers symmetrically bridged by an edge-bound  $\text{S}_2^{2-}$  would be  $\sim 4.3$  Å. In a  $\text{S}_2^{2-}$ -bridged Cu complex (39), the Cu–Cu distance is 4.03 Å, but the Tc–S bonds in  $\text{TcS}_x$  are 0.1 Å longer than the Cu–S bonds. Moreover, the S–S distance of the  $\text{S}_2^{2-}$  bridge, determined from the Tc–Tc and Tc–S distances, is 2.0 Å, typical of a bridging  $\text{S}_2^{2-}$  (35, 39). Therefore, the 4.3 Å Tc–Tc distance is assigned to two Tc centers symmetrically bridged by  $\text{S}_2^{2-}$ .

The 3.8 Å Tc–Tc distance could result from either two  $\text{S}^{2-}$  or  $\text{HS}^-$  bridges. If the Tc and S atoms are coplanar, then the Tc–S–Tc angle is  $109^\circ$ . Although few families of complexes exist in which the geometries of these ligands can be compared directly, a M–S–M angle of  $109^\circ$  is more typical of  $\text{S}^{2-}$  than of  $\text{HS}^-$ , which generally has M–(SH)–M angles of  $\sim 100^\circ$  (40–42). Therefore, the 3.8 Å Tc–Tc distance is assigned to two Tc centers symmetrically bridged by two  $\text{S}^{2-}$ . Overall, the EXAFS data is consistent with a  $\text{TcS}_x$  structure composed of triangular  $\text{Tc}_3(\mu^3\text{-S})(\mu\text{-S}_2)_3$  clusters linked by either  $\text{S}_2^{2-}$  or two  $\text{S}^{2-}$  ligands as shown in Figure 3.

Although the assignments of the last two Tc scattering shells in the EXAFS spectrum of  $\text{TcS}_x$  are less certain than the assignments of the other three shells, the resulting model provides the best fit to the data. In addition, the resulting bond distances can be interpreted in a chemically meaningful and reasonable manner. For these reasons, the model that

best describes the EXAFS spectrum of  $\text{TcS}_x$  is the one given in Table 3 and shown in Figure 3. Overall, the proposed structure of  $\text{TcS}_x$  is similar to that proposed for  $\text{MoS}_3$  by Weber et al., with the main difference that the Tc centers in  $\text{TcS}_x$  are seven-coordinate while the Mo centers in  $\text{MoS}_3$  are six-coordinate (36).

The proposed structure of  $\text{TcS}_x$  has a stoichiometry of  $\text{Tc}_3\text{S}_2(\text{S}_2)_4$  or  $\text{Tc}_3\text{S}_{10}$ , which is almost identical to the stoichiometry of  $\text{TcS}_{2.2}$  determined for “ $\text{Tc}_2\text{S}_7$ ” (34). Since the conditions used to prepare grout samples are analogous to those used to prepare  $\text{Tc}_2\text{S}_7$ , it seems likely that  $\text{TcS}_x$  and  $\text{Tc}_2\text{S}_7$  are the same compound. (In other words,  $\text{Tc}_2\text{S}_7$  is actually  $\text{Tc}_3\text{S}_{10}$ .) However, from the proposed structure,  $\text{TcS}_x$  is a Tc(IV) compound, which is consistent with its Tc K-edge absorption energy, 6.5 eV below that of  $\text{TcO}_4^-$  (16). Consequently, the species initially present in reducing-agent-containing grouts,  $\text{TcS}_x$ , appears to be identical to  $\text{Tc}_2\text{S}_7$  as previously suggested (15, 34), but the technetium centers in  $\text{TcS}_x$  are most likely Tc(IV), in agreement with the previous XAFS study (13).

**Evolution of Technetium Speciation Determined by XANES Spectroscopy.** The Tc speciation was determined by least-squares fitting of the XANES spectra using the XANES spectra of  $\text{TcO}_2 \cdot 2\text{H}_2\text{O}$ ,  $\text{TcO}_4^-$ , and  $\text{TcS}_x$  as components (43).

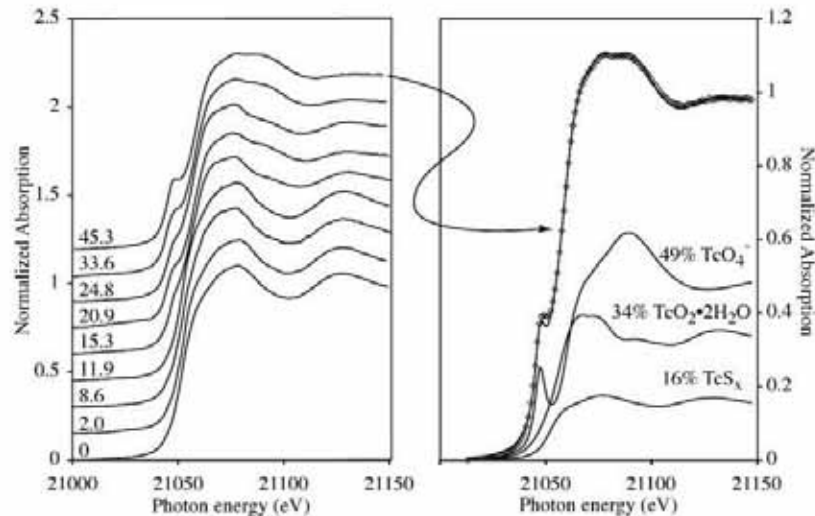


FIGURE 3. Evolution of the Tc K-edge XANES spectra of sample 4 as a function of age (left panel). The age of cement (in months) is given next to the corresponding spectrum. Deconvolution of the XANES spectrum of a 45 month old sample including the XANES spectra of the standards (right panel). Data are shown as dots, and the least-squares fit is shown as a line.

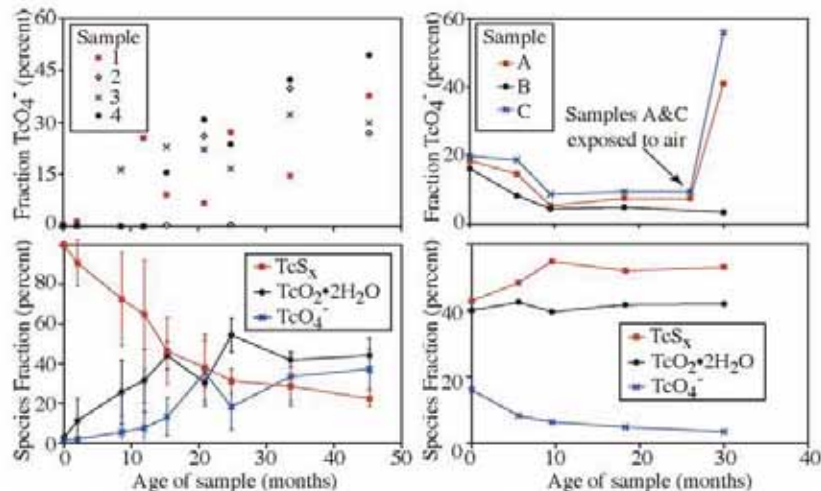


FIGURE 4. Evolution of the fraction of Tc present as  $\text{TcO}_4^-$  as a function of age in the permeable samples (upper left panel) and in the impermeable samples (upper right panel). The arrow indicates when samples A and C were opened at 26 months. Evolution of Tc speciation in the permeable samples averaged over all samples (lower left panel) and in the impermeable sample B (lower right panel), which contained  $\text{NO}_3^-$  but remained sealed. The error bars in the plot of the Tc speciation in the permeable sample reflect the variation in speciation among the samples.

The results for the evolution of Tc speciation in the permeable and impermeable samples are addressed separately.

**Permeable Samples.** The Tc speciation was initially identical in all samples since they contained only  $\text{Tc}_5\text{S}_{10}$ . As the samples aged, their XANES spectra evolved as shown in Figure 3. The mole fraction of  $\text{TcO}_4^-$  in these samples is shown in Figure 4. The scatter of the data shown in Figure 4 is much greater than the standard deviation of the speciation measurement as discussed below. While this large degree of scatter produces a large uncertainty in the rate of oxidation of Tc(IV), Figure 4 shows that  $\text{NO}_3^-$  does not play the major role in oxidizing Tc(IV) because the degree of oxidation of all samples is approximately equivalent despite the fact that samples 2 and 4 do not contain  $\text{NO}_3^-$ . However, the large degree of scatter precludes the conclusion that  $\text{NO}_3^-$  plays no role in the oxidation of Tc(IV).

**Impermeable Samples.** Unlike the permeable samples, ~20% of the  $\text{TcO}_4^-$  in the impermeable samples was not

reduced to Tc(IV) at the beginning of the experiment because the  $\text{Na}_2\text{S}$  solution had oxidized to  $\text{Na}_2\text{S}_2\text{O}_3$ , which does not react with  $\text{TcO}_4^-$  under these conditions. In addition, the observations that the alkaline  $\text{Na}_2\text{S}$  solution oxidized almost quantitatively to  $\text{S}_2\text{O}_3^{2-}$  and that the  $\text{S}_2\text{O}_3^{2-}$  was not further oxidized to  $\text{SO}_4^{2-}$  strongly suggest that  $\text{S}_2\text{O}_3^{2-}$  does not contribute to the reductive potential of these samples. Although  $\text{S}_2\text{O}_3^{2-}$  is not thermodynamically stable with respect to oxidation to  $\text{SO}_4^{2-}$ , it oxidizes very slowly under alkaline conditions (44).

As the samples aged, the amount of  $\text{TcO}_4^-$  decreased, as shown in Figure 4, presumably from its reaction with the BFS in the grout (13). The large increase in the amount of  $\text{TcO}_4^-$  observed in samples A and C at 26 months is due to exposure of these samples to atmosphere; sample B remained sealed. Assuming that the fraction of  $\text{TcO}_4^-$  in these samples is the same at 26 months as at 18 months, the fraction of  $\text{TcO}_4^-$  present in samples A and C increased by 34% and

46%, respectively, during the 4 months that they were exposed to air. In contrast to the permeable samples, little scatter exists in the fraction of  $\text{TcO}_4^-$  until samples A and C were exposed to air. As in the permeable samples, the presence of  $\text{NO}_3^-$  has no observable effect on the speciation.

## Discussion

The data from both series of samples show that  $\text{Tc}_2\text{S}_{10}$  in grout is unstable towards oxidation. Since the presence of  $\text{NO}_3^-$  had no significant effect on the rate of Tc oxidation in these samples,  $\text{O}_2$  is the likely oxidizer. In addition, oxidation by  $\text{O}_2$  rather than by  $\text{NO}_3^-$  can explain the scatter observed in the permeable samples.

The scatter in the data in Figure 4 is believed to result from a spatial variation in the amount of  $\text{O}_2$  diffusing into the samples, which produces different degrees of Tc oxidation in different areas of the samples. Since the regions probed by the X-ray beam were chosen arbitrarily, such spatial inhomogeneity of the Tc speciation would produce the scatter shown in Figure 4. Although the  $\text{O}_2$  diffusion into the samples was originally thought to result from air leaking through the caps of the PS cuvettes, XANES spectra obtained at intervals from the top of the samples to the bottom show that this is not the case; instead, Tc speciation varies somewhat along the length of the cuvette (Figure S2). The source of the variation in the rate of  $\text{O}_2$  diffusion is believed to be the ridged walls of the cuvette through which the XAFS spectra were obtained because  $\text{O}_2$  would diffuse more quickly through the thinner areas between the ridges.

The premise that  $\text{O}_2$  is the actual oxidizer is strongly supported by the results from the impermeable samples shown in Figure 4. Although Tc speciation evolved and the areas probed by XANES were arbitrarily chosen, little scatter exists in the Tc speciation of the impermeable samples. Because  $\text{O}_2$  cannot readily diffuse through PMMA, Tc speciation should not vary with position, as observed. However, the most dramatic evidence for  $\text{O}_2$  oxidation is the increase in the amount of  $\text{TcO}_4^-$  in these samples upon exposure to atmosphere.

The oxidation of the impermeable samples after removal from the cuvettes should occur at all of surfaces of the sample. Consequently, the XAFS experiment examines a layer of oxidized grout on a sample consisting mainly of reduced grout, based on the reasonable assumption that reducing grout oxidizes by the shrinking core mechanism (15). The thickness of the oxidized region can be determined from the fraction of oxidized Tc observed in fluorescence. The relationship between the fluorescence,  $I_d$ , from a surface layer of thickness  $d$  to the total fluorescence,  $I_{\text{tot}}$ , is given by eq 2, where  $\mu_i$  and  $\mu_f$  are the X-ray absorption coefficients of the sample at the incident and fluorescent photon energies, 5.2 and  $7.5 \text{ cm}^{-1}$  respectively, and  $\phi$  and  $\theta$  are the angles of the incident and fluorescent photons with respect to the sample,  $45^\circ$  in both cases. Equation 2 is obtained from the fluorescence yield from a surface layer derived previously in the context of EXAFS fluorescence self-absorption (45–47). The 40% increase in the  $\text{TcO}_4^-$  content of samples A and C upon air exposure corresponds to the formation of the oxidized layer, which is 0.28 mm thick according to eq 2 ( $I_d/I_{\text{tot}} = 0.4$ ).

$$\frac{I_d}{I_{\text{tot}}} = 1 - \exp\left[-\left(\frac{\mu_i}{\sin \phi} + \frac{\mu_f}{\sin \theta}\right)d\right] \quad (2)$$

The thickness of the oxidized layer determined by XAFS can be compared to the thickness of the oxidized region determined from the shrinking core model of Smith and Walton (15). The difference between the model employed here and the Smith and Walton model is that here the effective diffusion coefficient of  $\text{O}_2$ ,  $D_{\text{eff}(\text{O}_2)}$ , is determined from the

MacMullin number and the diffusion coefficient of  $\text{O}_2$  in  $\text{H}_2\text{O}$ :  $D_{\text{eff}(\text{O}_2)} = D_{m(\text{O}_2)}/N_m$ . The rate of growth of the oxidized layer of thickness  $d$  is given by eq 3 where  $t$  is time (in seconds),  $C_{\text{O}_2}$  is the concentration of  $\text{O}_2$  in  $\text{H}_2\text{O}$  ( $2.7 \times 10^{-7} \text{ mol cm}^{-3}$ ),  $D_{m(\text{O}_2)}$  is the diffusion coefficient of  $\text{O}_2$  in  $\text{H}_2\text{O}$  ( $2.0 \times 10^{-5} \text{ cm}^2 \text{ s}^{-1}$ ), and  $C_{\text{red}}$  is the concentration of reducing equivalents in the sample ( $3.3 \times 10^{-4} \text{ mol cm}^{-3}$  for a CWF with a density of  $1.7 \text{ g cm}^{-3}$  composed of 27% BFS with a measured reducing capacity of  $0.82 \text{ mequiv g}^{-1}$  plus  $0.013 \text{ mequiv}$  due to  $\text{SO}_3^{2-}$  in the oxidized  $\text{Na}_2\text{S}$  solution; all other grout components are assumed to have a negligible reducing capacity). Through the use of eq 3, the growth of a 0.028-cm-thick oxidized layer in 120 days corresponds to a  $N_m$  of 1500, which is within the range reported for similar CWFs albeit at the low end. Therefore, the thickness of the oxidized layer determined from the XANES experiment is consistent with the thickness of the oxidized layer anticipated from the shrinking core model. All of these results indicate that the oxidation of Tc(IV) species in these grout samples is due to  $\text{O}_2$  and that  $\text{NO}_3^-$  has no observable effect on the speciation of Tc in these samples. While these results do not show that  $\text{NO}_3^-$  is unreactive toward Tc(IV) in reducing grouts, this reaction occurs too slowly to be observed in this study.

$$d = \sqrt{\frac{8C_{\text{O}_2}tD_{m(\text{O}_2)}}{N_m C_{\text{red}}}} \quad (3)$$

## Acknowledgments

The authors thank Corwin Booth for helpful discussions about least-squares fitting of the XAFS and for the use of the code "fites", Daniel Kaplan for helpful discussions about the reducing potential of BFS, and Christine Langton for providing pulverized fly ash, BFS, and Portland cement. This work was supported by the Environmental Management Science Program of the U. S. DOE Office of Science, Biological and Environmental Research, Environmental Remediation Sciences Division and was performed at the Lawrence Berkeley National Laboratory, which is operated by the U. S. DOE under Contract No. DE-AC03-76SF0098. Portions of this research were carried out at the Stanford Synchrotron Radiation Laboratory, a national user facility operated by Stanford University on behalf of the U. S. Department of Energy, Office of Basic Energy Sciences.

## Supporting Information Available

Detailed description of EXAFS data analysis and model selection criteria, composition of sample A used to determine the X-ray absorption coefficients, detailed results from fitting the XANES data shown in Figure 4, plots of the evolution of the XANES spectra of sample B and an example of a XANES fit for sample B, the derivation of eq 2, and the derivation of the shrinking core model used to obtain eq 3. This information is available free of charge via the Internet at <http://pubs.acs.org>.

## Literature Cited

- Oblath, S. B. *Relative Release Rates of Nitrate, Tc, Cs, and Sr from Saltstone*; DPST-84-620; Savannah River Laboratory: Aiken, SC, 1984.
- Oblath, S. B. Leaching from solidified waste forms under saturated and unsaturated conditions. *Environ. Sci. Technol.* **1989**, *23*, 1098–1102.
- Serne, R. J.; Lokken, R. O.; Criscenti, L. J. Characterization of grouted low-level waste to support performance assessment. *Waste Manage.* **1992**, *12*, 271–287.
- National Research Council. *Research Needs for High-Level Waste Stored in Tanks and Bins at U. S. Department of Energy Sites*; National Academy Press: Washington, DC, 2001.
- Seltz, R. R.; Walton, J. C.; Dicke, C. A.; Cook, J. R. Near-field performance assessment for the Saltstone disposal facility. *Mater. Res. Soc. Symp. Proc.* **1993**, *294*, 731–736.

- (6) Kaplan, D. I.; Hang, T. *Estimated Duration of the Subsurface Reducing Environment Produced by the Z-Area Saltstone Disposal Facility (U)*, revision 2; WSRC-RP-2003-00362; Westinghouse Savannah River Company: Aiken, SC, 2003.
- (7) Gillam, T. M.; Spence, R. D.; Bostick, W. D.; Shoemaker, J. L. Solidification/stabilization of technetium in cement-based grouts. *J. Hazard. Mater.* **1990**, *24*, 189–197.
- (8) MacMullin, R.; Muccini, G. Characteristics of porous beds and structures. *AIChE J.* **1956**, *2*, 393–403.
- (9) Langton, C. A. Slag-based saltstone formulations. *Mater. Res. Soc. Symp. Proc.* **1988**, *112*, 61–70.
- (10) Yeh, B. S.; Wills, G. B. Diffusion coefficient of sodium nitrate in aqueous solution at 25 °C as a function of concentration from 0.1 to 1.0 M. *J. Chem. Eng. Data* **1970**, *15*, 187–189.
- (11) Bard, J. A.; Rand, M. H.; Anderegg, G.; Wanner, H. *Chemical Thermodynamics of Technetium*; Elsevier Science: Amsterdam, 1999.
- (12) Langton, C. A. *Challenging Applications for Hydrated and Chemically Reacted Ceramics*; DP-MS-88-163; Savannah River Laboratory: Aiken, SC, 1988.
- (13) Allen, P. G.; Stiemering, G. S.; Shuh, D. K.; Bucher, J. J.; Edelstein, N. M.; Langton, C. A.; Clark, S. B.; Reich, T.; Denecke, M. A. Technetium speciation in cement waste forms determined by X-ray absorption fine structure spectroscopy. *Radiochim. Acta* **1997**, *76*, 77–86.
- (14) Zhdanov, S. I. In *Encyclopedia of Electrochemistry of the Elements*; Bard, A., Ed.; Marcel Dekker: New York, 1975; Vol. IV.
- (15) Smith, R. W.; Walton, J. C. The role of oxygen diffusion in the release of technetium from reducing cementitious waste forms. *Mater. Res. Soc. Symp. Proc.* **1993**, *294*, 247–253.
- (16) Lukens, W. W.; Bucher, J. J.; Edelstein, N. M.; Shuh, D. K. Products of pertechnetate radiolysis in highly alkaline solution: Structure of  $\text{TeO}_2 \cdot x\text{H}_2\text{O}$ . *Environ. Sci. Technol.* **2002**, *36*, 1124–1129.
- (17) Bajt, S.; Clark, S. B.; Sutton, S. R.; Rivers, M. L.; Smith, J. V. Synchrotron X-ray microprobe determination of chromate content using X-ray absorption near-edge structure. *Anal. Chem.* **1993**, *65*, 1800.
- (18) Kneas, K. A.; Demas, J. N.; Nguyen, B.; Lockhart, A.; Xu, W.; DeGraff, B. A. Method for measuring oxygen diffusion coefficients of polymer films by luminescence quenching. *Anal. Chem.* **2002**, *74*, 1111–1118.
- (19) Gao, Y.; Ogilby, P. R. A new technique to quantify oxygen diffusion in polymer films. *Macromolecules* **1992**, *25*, 4962–4966.
- (20) Alba, S.; Ohashi, M.; Huang, S. Rapid determination of oxygen permeability of polymer membranes. *Ind. Eng. Chem. Fundam.* **1968**, *7*, 497–502.
- (21) Hormats, E. I.; Unterleitner, F. C. Measurement of the diffusion of oxygen in polymers by phosphorescent quenching. *J. Phys. Chem.* **1965**, *69*, 3677–3681.
- (22) Karchmer, J. H.; Dunahoe, J. W. Rapid determination of sulfides, thiosulfates, and sulfites in refinery spent caustic solutions. *Anal. Chem.* **1948**, *20*, 915–919.
- (23) Burgl, H.-B.; Anderegg, G.; Blauenstein, P. Preparation, characterization, and crystal, molecular and electronic structure of  $(\text{H}_2\text{EDTA})^{4-}\text{Te}(\mu\text{-O})_2\text{Te}(\text{H}_2\text{EDTA}) \cdot 5\text{H}_2\text{O}$ . A 2.33-Å distance which may represent a  $\sigma^2\pi^2\delta^2$  bond. *Inorg. Chem.* **1981**, *20*, 3829–3834.
- (24) Angus, M. J.; Glasser, F. P. The chemical environment in cement matrices. *Mater. Res. Soc. Symp. Proc.* **1985**, *50*, 547–556.
- (25) Walden, G. H.; Hammett, L. P.; Chapman, R. P. A reversible oxidation indicator of high potential especially adapted to oxidimetric titrations. *J. Am. Chem. Soc.* **1931**, *53*, 3908.
- (26) Smeller, J. A. Automatic titration of cerium. *Am. Lab. News* **1999**, (October), 6–8.
- (27) ASTM International. *Standard Test Methods for Chemical Analysis of Hydraulic Cement*; ASTM C144; ASTM International: West Conshohocken, PA.
- (28) Lee, W.; Batchelor, B. Reductive capacity of natural reductants. *Environ. Sci. Technol.* **2003**, *37*, 535–541.
- (29) Koningsberger, D. C.; Prins, R. *X-Ray Absorption: Principles, Applications, Techniques of EXAFS, SEXAFS, and XANES*; John Wiley & Sons: New York, 1988.
- (30) Newville, M. IFEFFIT: Interactive XAFS analysis and FEFF fitting. *J. Synchrotron Radiat.* **2001**, *8*, 322–324.
- (31) Ravel, B. ATHENA and ARTEMIS interactive graphical data analysis using IFEFFIT. *Phys. Scr.* **2005**, *115*, 1007–1010.
- (32) Rehr, J. J.; Albers, R. C.; Zabinsky, S. I. High-order multiple-scattering calculations of X-ray-absorption fine structure. *Phys. Rev. Lett.* **1992**, *69*, 3397–3400.
- (33) Colton, R. *The Chemistry of Technetium and Rhenium*; Interscience Publishers: New York, 1965.
- (34) Lee, S. Y.; Bondietti, E. A. Technetium behavior in sulfide and ferrous iron solutions. *Mater. Res. Soc. Symp. Proc.* **1983**, *15*, 315–322.
- (35) Müller, A.; Pohl, S.; M., D.; Cohen, J. P.; Bennett, J. M.; Kirchner, R. M. Crystal structure of  $(\text{NH}_4)_2[\text{Mo}_2\text{S}(\text{S}_2)_4]$  containing the novel isolated cluster  $[\text{Mo}_2\text{S}_3]^{2-}$ . *Z. Naturforsch., B: Chem. Sci.* **1979**, *34*, 434–436.
- (36) Weber, T.; Muijsers, J. C.; Niemantsverdriet, J. W. Structure of amorphous  $\text{MoS}_2$ . *J. Phys. Chem.* **1995**, *99*, 9194–9200.
- (37) Cramer, S. P.; Llang, K. S.; Jacobson, A. J.; Chang, C. H.; Chianelli, R. R. EXAFS studies of amorphous molybdenum and tungsten trisulfides and triselenides. *Inorg. Chem.* **1984**, *23*, 1215–1221.
- (38) Müller, A.; Jostes, R.; Cotton, F. A. Trinuclear clusters of the early transition elements. *Angew. Chem., Int. Ed. Engl.* **1980**, *19*, 875–882.
- (39) Fujisawa, K.; Moro-oka, Y.; Kitajima, N. Formation of a  $\mu\text{-}\eta^2\text{-}\eta^2$ -disulfide dinuclear copper(II) complex by thermal decomposition of a thiolate complex via C–S bond cleavage. *J. Chem. Soc., Chem. Commun.* **1994**, 623–624.
- (40) Muetting, A. M.; Boyle, P.; Pignolet, L. H. Reaction of  $\text{H}_2\text{S}$  with phosphine complexes of Rh(I) and Ir(I). Crystal and molecular structure of  $[\text{RhCl}(\text{H})(\mu\text{-SH})(\text{PPh}_3)_2]_2 \cdot 2\text{CH}_2\text{Cl}_2$  and  $[\text{IrCl}(\text{H})(\text{SH})(\text{CO})(\text{PPh}_3)_2]$ . *Inorg. Chem.* **1984**, *23*, 44–48.
- (41) Bianchini, C.; Mealli, C.; Mell, A.; Sabat, M. Reversible double addition of  $\text{H}_2$  on a bis( $\mu$ -sulfido) binuclear rhodium complex. *Inorg. Chem.* **1986**, *25*, 4617–4618.
- (42) Pleus, R. J.; Waden, H.; Saak, W.; Haase, D.; Pohl, S. Preparation of the first sulfur containing cobalt and nickel complexes stabilized by the macrocyclic cyclam ligand: Observation of S–H bond activation. *J. Chem. Soc., Dalton Trans.* **1999**, 2601–2610.
- (43) Ressler, T.; Wong, J.; Roos, J.; Smith, I. L. Quantitative speciation of Mn-bearing particulates emitted from autos burning (methylcyclopentadienyl)manganese tricarbonyl-added gasolines using XANES spectroscopy. *Environ. Sci. Technol.* **2000**, *34*, 950–958.
- (44) Rolla, E.; Chakrabarti, C. L. Kinetics of decomposition of tetrathionate, trithionate, and thiosulfate in alkaline media. *Environ. Sci. Technol.* **1982**, *16*, 852–857.
- (45) Goulon, J.; Goulon-Ginet, C.; Cortes, R.; Dubois, J. M. On experimental attenuation factors of the amplitude of the EXAFS oscillations in absorption, reflectivity and luminescence measurements. *J. Phys.* **1982**, *43*, 539–548.
- (46) Tröger, L.; Arvanitis, D.; Baberschke, K.; Michali, H.; Grimm, U.; Zschech, E. Full correction of the self-absorption in soft-fluorescence extended X-ray-absorption fine structure. *Phys. Rev. B* **1992**, *46*, 3283–3289.
- (47) Booth, C. H.; Bridges, F. Improved self-absorption correction for fluorescence measurements of extended X-ray absorption fine structure. *Phys. Scr.* **2005**, *115*, 202–204.

Received for review January 24, 2005. Revised manuscript received July 13, 2005. Accepted August 5, 2005.

ES050155C

**14.0 APPENDIX F: TOTAL ORGANIC CARBON CONCENTRATIONS IN  
THE OLD LOW LEVEL WASTE BURIAL GROUNDS**

**Table 34.** Total organic carbon concentrations is well near and beneath the Low Level Waste Burial Ground. (Data from McIntyre and Wilhite 1987; DPST-87-762). Data used to established concentration to use in CDP concentrations in E-Area applications.

Well ID	Oct 1982	Mar 1984	Jun 1984	Sept 1984	Jun 1985	From Figure 4 DPST-83-209
	----- (mg/L) -----					
A-1	3.7	0.5 <sup>(a)</sup>	0.5			
A-3	0	3.2	0.5	0.5		
A-5	0	0.5	0.5			
A-7		0.5	0.5			
A-9		0.5	0.5			
A-11	0	0.5	0.5			
A-19	0	0.5	0.5			
A-21	0	0.5	0.5			
A-23	5.6	1.6	1.2			
A-32	5.2	0.5	2			
A-34	0.4	0.5	0.5			
A-36	4	5.6	0.5	0.5		
C-1	0	1				
C-3	0	1.8	3		38.8	Potentially impacted by decon. station (p. 7) <sup>(b)</sup>
C-5	0	0.5	2.6	25.3	11.2	
C-7	0	3.8	3.8	11.4		
C-9	6	0.5	1.3	2.2		
C-11	11	0.5		0.5		
C-13	0	0.5	0.5			
C-15	0	5.6	0.5	0.5		Potentially impacted by solvent plume
C-17	20.9	0.5	0.5			Potentially impacted by solvent plume
C-19	0	1	2.2			
C-21	18	2.8	0.5	0.5		
C-23	0	6.5	1.4	0.5		
C-30	12.1	0.5	0.5			
C-32	0	3.7	3.9			
C-34	8	1.3	1.6			
C-36	3	0.5	0.5			
E-1	10.1	2.4	1.9			
E-3	11.9	2.4	0.5	14	8.1	
E-5	3.9	3.5	0.5	0.5		
E-7	5	2.5	0.5	0.5		

Well ID	Oct 1982	Mar 1984	Jun 1984	Sept 1984	Jun 1985	From Figure 4 DPST-83-209
E-9	10	3.4	2.7			
E-13	4.3	0.5	0.5			Potentially impacted by solvent plume
E-15			2	0.5	8.1	
E-17	0.4	0.5	6.9	0.5		Potentially impacted by solvent plume
E-19	0.2	1.5	1.2			Potentially impacted by solvent plume
E-21	10	0.5	0.5			
E-23	3.3	1.1	0.5	0.5		
E-30	3	0.5	0.5	0.5		
E-32	0	1.5	8.5	0.5		
E-34	0	0.5	0.5			
E-36	25	0.5	0.5			
G-1	0	2.5	0.5	0.5		
G-3	0	2.1	0.5	0.5		
G-5	0	2.2	0.5	0.5		
G-7	45	61.4	65.6		30.3	
G-9	9	2.9	0.5	0.5		
G-13	0	6.2	0.5	0.5		Potentially impacted by solvent plume
G-15	0	0.5	0.5			Potentially impacted by solvent plume
G-17	0	0.5	0.5			Potentially impacted by solvent plume
G-19	4	0.5	0.5			Potentially impacted by solvent plume
G-21	225	400	317		946	Potentially impacted by solvent plume
G-23	0	0.5	0.5			
G-28	0	1.5	0.5	1		
G-30	4	1.8	0.5	0.5		
G-32	0	1.7	18	11.2	14.3	
G-34	0	0.5	0.5			
G-36	4	0.5	0.5			
I-1	16	5.4	4.2			
I-3		5.5	2.4			
I-5	6	21.5	364		334	Potentially impacted by solvent plume
I-7	8	30	26		64.5	Potentially impacted by solvent plume
I-9	3	5.4	0.5	0.5		Potentially impacted by solvent plume
I-13	1	0.5	0.5			Potentially impacted by solvent plume
I-15	0	0.5	0.5			Potentially impacted by solvent plume
I-17	1.6	0.5	0.5	75.1		Potentially impacted by solvent plume
<b>AVE</b>	<b>5.0</b>	<b>2.9</b>	<b>2.9</b>	<b>3.2</b>	<b>12.0</b>	<b>Grand Average = 5.2</b>

<sup>(a)</sup> All values in table entered in as "0.5" are actually <0.1 values.

<sup>(b)</sup> Data in gray were not used to generate averages. They are data that may have been impacted by either the solvent plume (i.e., the well is located near or in the solvent plume) or its near the decontamination station. The averages were generated to provide an estimate of the total organic carbon generated from the cellulosic material disposed in the trenches.

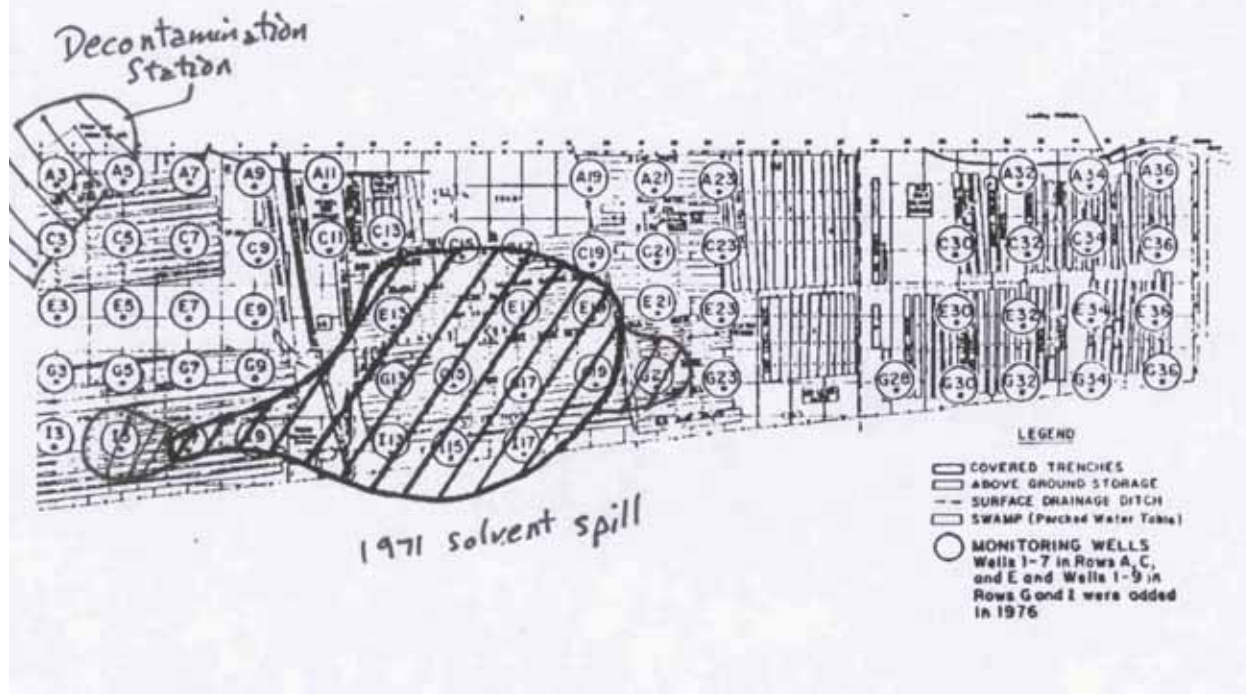


**Figure 36.** Map of wells used to collect total organic carbon data at LLW Burial Ground. Outline shows plumes from 1971 solvent spill and plume generated near decontamination station.



**DISTRIBUTION**

## Savannah River Site

B. T. Butcher	773-43A, Rm. 211
L. B. Collard	773-43A, Rm. 207
K. P. Crapse	773-41A, Rm. 114
D. A. Crowley	773-43A, Rm. 216
M. E. Denham	773-42A, Rm. 218
G. P. Flach	773-42A, Rm. 211
W. T. Goldston	705-3C, Rm. 105
J. C. Griffin	773A, Rm. A-231
L. L. Hamm	773-42A, Rm. 145
R. A. Hiergesell	773-42A, Rm. 251
G. K. Humphreys	705-3C, Rm. 206
D. I. Kaplan (3 copies)	773-43A, Rm. 215
C. A. Langton	773-43A, Rm. 211
M. H. Layton	705-1C, Rm. 14
S. L. Marra	773A, Rm. A-230
M. A. Phifer	773-42A, Rm. 252
K. A. Roberts	773-43A, Rm. 225
K. H. Rosenberger	705-1C, Rm. 16
R. R. Seitz	773-43A, Rm. 213
R. F. Swingle	773-42A, Rm. 122
G. A. Taylor	773-41A, Rm. 156
E. L. Wilhite	773-43A, Rm. 214
RPA File (2 copies)	773-43A, Rm. 213

Pacific Northwest National Laboratory, PO Box 999, Richland WA 99352

K. J. Cantrell	MS-81
R. J. Serne	P7-22
K. M. Krupka	MS-81

Clemson University, Environmental Engineering and Earth Sciences, 372 Computer Court, L.G.  
Rich Environmental Laboratory, Anderson, SC 29625

T. DeVol  
R. A. Fjeld  
B. A. Powell